Testing and Multiphysics Modelling of the Shear Behaviour of Rock-Cemented Paste Backfill Interface

Submitted by

Kun Fang

Under the supervision of

Dr. Mamadou Fall

Thesis submitted to the University of Ottawa
in partial fulfillment of the requirements for the
Doctorate in Philosophy degree in Civil Engineering

Department of Civil Engineering
Faculty of Engineering
University of Ottawa

To my parents, wife and child

Abstract

Cemented paste backfill (CPB) is an innovative technology developed in the mining industry during the last few decades. It has been adopted worldwide by many underground mines for its tremendous advantages: (1) mining space is stabilized by pumping cemented paste backfill into the underground cavities created by mining activity, which is critical to the safety of mine workers; (2) the consumption of tailings (which is stored at the ground surface and is a major source of acid mine drainage (AMD)) is beneficial for environmental protection and community safety; (3) due to the supporting effect of the CPB structure on underground cavities, the recovery ratio is significantly increased; and (4) CPB structures can also carry heavy equipment when mining the adjacent orebody, facilitating mining operations.

How to design a safe and cost-effective CPB structure is a key task or challenge for mining engineers and researchers. Mechanical stability is one of the most important design criteria. This stability is mainly a function of the uniaxial compressive strength (UCS) of CPB body and the shear strength/behaviour of the CPB–rock interface. Given the lower friction angle and adhesion of the CPB–rock interface (in comparison with the friction angle and cohesion of CPB body), a thorough understanding of the shear strength/behaviour of the interface is critical for a cost-effective geotechnical design of underground CPB structures. However, only limited studies have been conducted to date on the shear performance of the CPB–rock interface, and no studies have taken into consideration the effects of different factors (e.g., temperature, sulphate ions, self-weight or surface morphology) on the shear behaviour of the CPB–rock interface. Moreover, no multiphysics interface model is currently available that incorporates the aforementioned factors to describe and predict the CPB–rock interface shear behaviour. This research gap was therefore addressed in this PhD study.

In this PhD research, a series of laboratory tests were conducted assessing the effects of sulphate content, temperature, curing stress, drainage condition and interface roughness on the shear strength/behaviour of the interface between CPB and rock. The results obtained so far indicated that sulphate and temperature can either positively or negatively affect the shear strength of the CPB–rock interface, depending on the initial sulphate contents and curing time. In terms of the effect of temperature, the shear strength and shear strength properties generally increased with temperature. However, high temperature ($\geq$ 35°C) resulted in an adverse effect on the shear strength because of the crossover effect. In addition, higher curing stress benefitted to the shear strength acquisition of the interface and, due to the increased effective stress and matrix suction, the drained condition increased shear strength as well. As for the effect of surface morphology, the shear strength of the CPB–rock interface rose with surface roughness. Furthermore, chemo-elastic as well as coupled thermo-chemo-mechanical cohesive zone models (CZMs),

which take the sulphate attack and temperature-induced acceleration in the cement hydration into consideration, are also developed to simulate the shear strength and behaviour of the CPB–rock interface. The proposed models can well capture the shear behaviour of the interface under different loading conditions. Besides, they also numerically attest to the importance of the shear resistance of the CPB-rock interface in controlling stress distribution in CPB structures.

The results obtained from experimental tests, numerical modelling and simulations concerning the shear behaviour of the CPB–rock interface under different multiphysics conditions provided useful information for understanding and more effectively assessing the shear strength and behaviour of the interface between a CPB structure and rock mass, which is critical for the design of safer and more cost-effective CPB structures.

ACKNOWLEDGEMENT

The work presented in this thesis was conducted under the supervision of Dr. Mamadou Fall. Taking this chance, I would like to express my sincere and heartfelt gratitude and respect to my supervisor, Dr. Mamadou Fall. Without his endless guidance, support and encouragement, this thesis would never be completed. The spirit of his perseverance, passion and devotion to research will inspire me all the time, both in my academic and personal life!

My sincere appreciation is extended to late Dr. Erman Evgin, Dr. Sai Vanapalli from University of Ottawa, Dr. Mehdi Pouragha from Carleton University, Dr. Patrice Rivard from Unversity of Sherbrooke and Dr. Othman Nasir from University of New Brunswick for their invaluable feedbacks on my PhD manuscript. Besides, Dr. Liang Cui is sincerely acknowledged for his help during my Ph.D. program.

Thanks are also extended to Mr. Jean Claude Célestin, the technical officer of the geotechnical engineering laboratory at the University of Ottawa. I also want to thank my colleagues, Sada Haruna, Dr. Gongda Lu, Dr. Guanlong Guo, Jianxiong Yang, Dr. Imad Alainachi, Dr. Anis Roshani, Mukhtar Abukhettala, Hoda Mohammad Pour, and Mohammad Salah for all their support, encouragement, and persistent friendship in the past few years.

The Chinese people are gratefully acknowledged for their financial support. It is because of the tax they paid that I can then finish my Ph.D. program.

Lastly, special appreciation goes to my families, especially my parents and my wife. I wish to deeply thank my parents for their unconditional support and tremendous patience during all the past years. And my wife, thank you very much for being so considerate, so nice and so not stereotyped. My baby girl, I wish you an enjoyable, healthy and peaceful life.

Contents

List of Figures

List of Tables

List of Symbols and Abbreviations

C_w	Tailings percentage
σ_v	Vertical stress
$\sigma_{v'}$	Effective vertical stress
γ	Unit weight of the CPB
ϕ'	Effective friction angle of the CPB-rock interface
k_a	Active ratio of the lateral stress to the vertical stress
ϕ	Friction angle of CPB
S_j	Frictional force
C_j	Lateral compressive force
L'	Length of the stope
B'	Width of the stope
K_{cj}	Coefficient of the lateral pressure
σ_n	Normal stress
φ_b	Basic friction angle
τ_p	Peak shear stress
c	Adhesion
K_H	Hydraulic conductivity
K_T	Thermal conductivity
Z_2	Surface parameter
L	Number of the discrete points
(x_i, y_i)	Coordinates of a discrete point
w/c	water-to-cement ratio
σ_h	Horizontal pressure
α	Inclined angle of the CPB structure
t_e	Chronological curing age of interface samples
ξ_u	Ultimate degree of cement hydration
κ	Time parameter

ς	Shape parameter
ϑ_{FA}	Weight proportion of fly ash
ϑ_s	Weight proportion of slag
χ	Sulphate content
δ_i^0	Critical relative displacement ($i = 1, 2$ refers to Modes I and II)
δ_i^f	Final relative displacement
δ_m	Relative displacement of the mixed-mode
δ_m^0	Critical displacement of the mixed-mode
δ_m^f	Final displacement of the mixed-mode
P_n	Penalty stiffness
K_p	Normal stiffness
K_τ	Shear stiffness
d_i	Damage parameter
σ_{1c}	Maximum tensile stress
τ_{2c}	Peak shear stress
n_τ	Coefficient between the shear and normal stiffness
ν	Poisson's ratio
σ_{res}	Residual strength of the interface
G_{I}	Strain energy release rate of Mode I
G_{II}	Strain energy release rate of Mode II
$G_{\mathrm{I\,c}}$	Critical energy release rate of Mode I
$G_{\mathrm{II\,c}}$	Critical energy release rate of Mode II
$K_{\mathrm{I\,c}}$	Fracture toughness of Mode I
$K_{\mathrm{II\,c}}$	Fracture toughness of Mode II
K	Elastic stiffness
α'	Crack angle
a	Length of the crack
R	Radius of semi-circular samples

t	Thickness of semi-circular samples
S	Half distance between the two supporting points
P	Normal peak load
$Y_{\mathrm{I}}, Y_{\mathrm{II}}$	Geometry factors
T_c	Curing temperature
T_r	Reference temperature
CPB	Cemented paste backfill
AMD	Acid mine drainage
UCS	Uniaxial compressive strength
SCB	Simi-circular bending test
CB	Chevron bending test
CCNBD	Cracked chevron notched Brazilian disc test
SR	Short rod test
DST	Direct shear test
CZM	Cohesive zone model
TSF	Tailings storage facility
CHB	Cemented hydraulic backfill
CRB	Cemented rock backfill
PCI	Portland cement Type I
VCR	Vertical crater retreat
C-S-H	Calcium silicate hydrate
CH	Calcium hydroxide
PWP	Pore water pressure
XRD	X-ray diffraction
JRC	Joint roughness coefficient
JCS	Compressive strength
TSL	Traction separation law
GDP	Gross domestic product
NT	Natural tailings
ST	Silica tailings
LVDT	Linear variable differential transformer
EC	Electrical conductivity
TG	Thermo-gravimetric
DTG	Differential thermo-gravimetric

C_3A	Tricalcium aluminate
MIP	Mercury intrusion porosimetry
VWC	Volumetric water content
C_2S	Dicalcium silicate
C_3S	Tricalcium silicate
RMS	Root mean square roughness index
CLA	Arithmetical mean deviation roughness index
MSV	Mean square value roughness index
R_p	Ratio between the true length of profile to its projected length
ITZ	Interfacial transition zone

Chapter 1 Introduction

1.1 Background

The extraction of economically significant minerals from the earth's crust is an important objective of mining activity. However, whether in metal mines or in non-metallic mines, the extensive exploitation of mineral resources will inevitably result in the creation of huge underground voids. Meanwhile, a large quantity of waste would be produced during the mining operation and mineral processing (Bull and Fall, 2020a,b). In Australia, for example, 10 million cubic meters of underground voids are generated annually as a result of mining, while in Canada, the annual production of waste is approximately 500 million metric tons (Grice, 2001). Hence, how to manage the mine waste environment-friendly and cost-effectively is a significant problem for mining engineers.

Mine waste management techniques include surface and underground disposals. The surface management mainly refers to constructing tailings storage facilities (TSFs, e.g., embankments and dams) or piling waste at the ground surface (solid waste, e.g., gangue). However, both of them pose huge threats to the environment and nearby communities (Buckby et al., 2003; Fall et al., 2009; Huang et al., 2011; Roshani et al. 2017; Xiao et al. 2020). Take a dam failure as an example, the failure of a tailings dam happened in Shanxi, China 2008, caused catastrophic damages with a leakage of 26.8 million cubic tailings and 281 fatalities (Sun et al., 2012). In contrast, the underground management of waste comprises three main types of mine cemented backfill, namely the cemented hydraulic, rock and paste backfills. Cemented hydraulic backfill (CHB) is a mixture of mill tailings and cement (with a solid percentage of 60%~75%), while cemented rock backfill (CRB) is usually a mixture of waste rock, tailings and a small percentage of cement (Amaratunga and Yaschyshyn, 1997). However, due to the potential serious geotechnical hazards posed by CHB (e.g., failure of backfill barricade) and its higher cost, the use of CHB has been increasingly restricted. In contrast, cemented paste backfill (CPB) has become more and more popular in underground mining operations during the last three decades (Brackebusch, 1994; Guo et al. 2020; Hassani and Archibal, 1998; Belem et al., 2006).

CPB is a cementitious material produced by mixing thickened tailings (with a solid percentage of 70%-85%), binder (3%-7%, mostly) and water in paste backfill plant, which is commonly built on the ground surface of mines. The obtained CPB mixture is transported to the underground void through pipes by pumping or gravity. The underground disposal of tailings can not only reduce the cost of constructing tailings storage facilities on the ground surface, but also improve the recovery ratio due to the supporting CPB structures. In addition, the mining structure/space is also stabilized, which is critical to the safety of mine workers (Yilmaz et al., 2004; Benzaazoua et al., 2004; Cui and Fall, 2016).

1.2 Problem statement

The mechanical stability of underground backfill structures is vital to the safety of mine workers and the production of mines, therefore, a better understanding and effectively assessing of the stability of CPB structure play a key role in CPB design. Although the interface was usually regarded as the weak face in interlaminar structures, most of the previous studies conducted on CPB mainly focused on the uniaxial compressive strength (UCS) of CPB (Kesimal et al., 2005; Ercikdi et al., 2009; Simms and Grabinsky, 2009), and only a limited number of studies have been conducted on the shear strength/behaviour of the interface between CPB and surrounding rock mass (Aubertin et al., 2003; Nasir and Fall, 2008; Fall and Nasir, 2010; Koupouli et al., 2016). In addition to the priority in safety, how to reduce the investment cost is another concern in CPB design (Yilmaz and Fall, 2017). Given that the arching effect (which is closely related to the shear behaviour between CPB and surrounding rock mass) in CPB can considerably decrease the vertical stress in CPB structure, the utilization of the arching effect can then lower the strength requirement (Helinski et al., 2010). This allows reducing the dosage of cement in CPB preparation, the cost of which takes up to 75% of the CPB cost. Because the cost can be mitigated to 42% when the cement content drops from 9 wt.% to 3 wt.% (De Souza et al., 2003; Fall and Benzaazoua, 2003), it is thus important to investigate the shear behaviour of the CPB-rock interface from the perspective of interests. It is well known that the evolution of the mechanical strength of cementitious material (e.g., CPB) is determined by the cement hydration, which is sensitive to multiphysical conditions or factors (thermal, chemical, mechanical and hydraulic conditions), to which the CPB structures and rock-CPB interfaces are subjected in the field. However, no studies have taken into account the effects of the multiphysical factors, such as thermal, chemical (sulphate ions), mechanical (curing stress) or surface morphology, on the shear behaviour of the CPB–rock interface. Moreover, no multiphysical model is currently available that integrates the aforementioned factors to elucidate and predict the CPB–rock interface shear behaviour. There is a need to address this research and technology gap for the reasons mentioned above. Therefore, in order to provide a cost-effective and safer design of CPB structures, a series of laboratory tests are conducted in this PhD study to investigate the effects of interface roughness, temperature, sulphate ions, curing stress and drainage condition on the shear performance of the CPB-rock interface. In addition, some CZMs are also developed to predict the shear capacity of the CPB-rock interface.

1.3. Research objectives

The main objectives of this research are to probe into the shear strength/behaviour of CPB-rock interface under different thermal, chemical, hydraulic, and mechanical conditions. In addition, multiphysical models are developed as well to describe and predict the shear capacity of the CPB-rock interface. The findings in this PhD study are dedicated to a better understanding of the shear performance of the CPB-rock interface, which is critical for the design of safer and more cost-effective CPB structures. The specific objectives of this research are summarized as follows:

1 To introduce CPB performance properties, the interactions between CPB and the adjacent or surrounding rock mass, as well as a review of the existing studies on the CPB-rock interface.

2 To investigate the effects of various multiphysical loading factors on the shear strength/behaviour of CPB-rock interface at the experimental level. This objective includes the following sub-objectives:

2.1 The effect of chemical factor (different sulphate contents) on the shear strength/behaviour of the CPB-rock interface cured for short-term;

2.2 The effect of the thermal factor (different curing temperatures) on the shear strength/behaviour of the CPB-rock interface;

2.3 The effect of the sulphate attack on the long-term shear resistance of the CPB-rock interface;

2.4 The effect of the mechanical factor (curing stress) on the shear properties of the CPB-rock interface;

2.5 The effect of the hydraulic factor (drainage condition) on the shear performance of the CPB-rock interface;

2.6 The effect of the surface morphology (different roughness) on the shear behaviour of the CPB-rock interface.

3 To develop multiphysical models to describe and predict the shear behaviour of the interface between CPB and rock. This objective includes the following two sub-objectives:

3.1 The development of a chemo-elastic CZM for the assessment and prediction of the shear behaviour of CPB-rock interface;

3.2 The development of a coupled thermo-chemo-mechanical CZM to illustrate the shear behaviour of the CPB-rock interface (considering the beneficial effect of the temperature on the cement hydration).

4 To provide technical information and tools for the sake of a better understanding of the shear behaviour of the interface between CPB and rock.

1.4. Research approach and methods

Two main methods, namely experimental investigation and numerical modelling/simulation are adopted to explain the effects of the aforementioned factors on the shear strength/behaviour of the CPB-rock interface in this PhD research. The specific research methodology is schematically shown in Figure 1.1.

As can be seen from the figure, the theoretical and technical background of CPB is firstly introduced. Besides, the interaction function between the CPB and the adjacent rock mass is emphasized. Subsequently, a comprehensive literature review of previous studies on CPB-rock interface behaviours is provided.

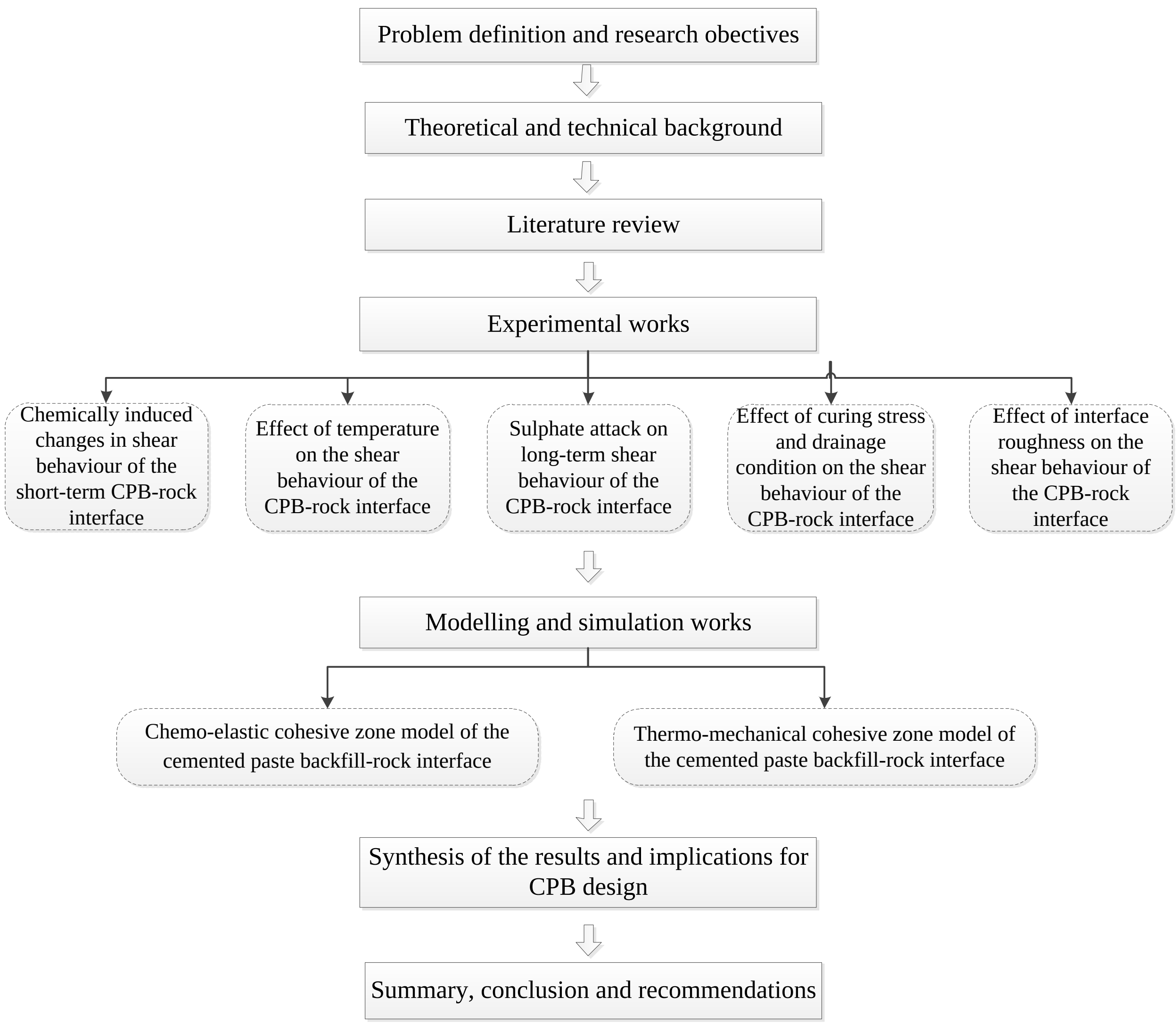

Figure 1.1 Research methodology

The experimental work in this PhD research consisted of five experimental series, which deal with the study of the effects of thermal (T, temperature), hydraulic (H, drainage condition), mechanical (M, curing stress), chemical (C, sulphate content) conditions as well as the rock surface morphological condition (interface roughness) on the shear strength/behaviour of the CPB-rock interface, respectively. Two test sets are conducted to interpret the influence of the sulphate content (C) on the shear behaviour of the interface. The first one concerns the chemically induced change in the shear behaviour of the short-term CPB-rock interface (1 day, 3 and 7 days), while the other focuses on the sulphate attack on the shear behaviour of the long-term CPB-rock interface (28 days, 90 and 150 days). For these two test sets, interface samples with different sulphate contents of 0 ppm, 5000 ppm, 15000 ppm and 25000 ppm are produced by mixing certain amounts of ferrous sulphate heptahydrate ($FeSO_4$▪$7H_2O$), silica tailings, Portland cement Type I (PCI) and distilled water. In contrast, one test is conducted to study the effect of temperature (T) on the shear behaviour of the CPB-rock interface, and the samples are cured at three different temperatures (2°C, 20°C, and 35°C). The tests concerning the effects of the hydraulic and mechanical factors (H&M) refer to the test conducted on samples cured with three different levels of curing stress (0 kPa, 50 kPa, and 150 kPa) under drained and undrained conditions. The uOttawa Backfill Curing System is adopted in this test to ensure the interface samples are cured under different drainage conditions. To address the effect of roughness on the shear behaviour of the CPB-rock interface, samples with three kinds of interface roughness (R0, R1 and R2) are produced. Regardless of the influencing factors to which the interface samples were subjected, all of them are hence arranged for direct shear test once being cured.

The numerical modelling and simulation works herein comprise the development of two multiphysics CZM models and the application of these models to simulate the interface shear behaviour. The first model is a chemo-elastic CZM, whereas the second one is a coupled thermo-chemo-mechanical CZM of CPB-rock interface. To evaluate the failure of CPB-rock interface from the perspective of fracture propagation, the key issue is to determine the evolution of the fracture toughness of the interface. Thereafter, by using the fracture toughness and other parameters, the shear strength/behaviour of CPB-rock interface under different loading conditions can be simulated with CZM. The developed CZMs are implemented in a finite element code, COMSOL Multiphysics, and then validated against experimental data obtained experimentally.

1.5. Tasks and organization of the thesis

The manuscript of this PhD thesis is organized into seven chapters which are shown in Figure 1.2 below. It should be noted that because the main results of the chapters are presented in technical papers, some information is repeated in the thesis.

Chapter 1 provides a general introduction of this PhD study, which includes problem statements, objectives and research methods used in this research.

Chapter 2 presents the background information of CPB and the interaction between CPB and the surrounding rock mass. It emphasizes the importance of the shear strength/behaviour of the CPB-rock interface in the assessment of the stability of CPB structures.

Chapter 3, 4 and 5 are structured into a paper-based thesis format. Each technical paper includes an introduction, demonstration on the material/methods, results and discussion, and conclusion.

Chapter 3 is mainly a comprehensive literature review of the existing studies on the shear behaviour between CPB and rock, including laboratory tests and mathematical modelling.

Chapter 4 focuses on the effects of multiphysical factors on the shear strength/behaviour of the CPB-rock interface, and it consists of five technical papers, as a result of five tests series. Section 4.2 presents the effect of the chemical factor (C) on the shear behaviour of the CPB-rock interface (**Technical paper 2**), namely the chemically induced change in the shear behaviour of the short-term CPB-rock interface. Section 4.3 discusses the effect of the thermal factor (T) on the shear behaviour of the CPB-rock interface (**Technical paper 3)**. The effect of hydraulic and mechanical factors (H&M) on the shear performance of the CPB-rock interface is described in section 4.4 (**Technical paper 5)**, while the sulphate attack (C) on the shear behaviour of the long-term cured interface samples is presented in section 4.5 (**Technical paper 4).** The effect of surface morphology on the shear performance of CPB-rock interface is shown in section 4.6 (**Technical paper 6).**

Chapter 5 presents the numerical simulation of failure of CPB-rock interface by developing two CZM models. First, a chemo-elasto CZM model that integrates the effect of sulphate ions on the cement hydration is developed in section 5.2. Then, section 5.3 shows a coupled thermo-chemo-mechanical CZM to encapsulate the shear behaviour of interface samples cured at different temperatures.

In chapter 6, the results obtained in this study are synthesized to provide insights into the interaction behaviour between CPB and adjacent rock mass under different multiphysics conditions. The findings are critical for the design of a safer and cost-effective CPB structures.

Chapter 7 presents the main conclusions and recommendations for future research.

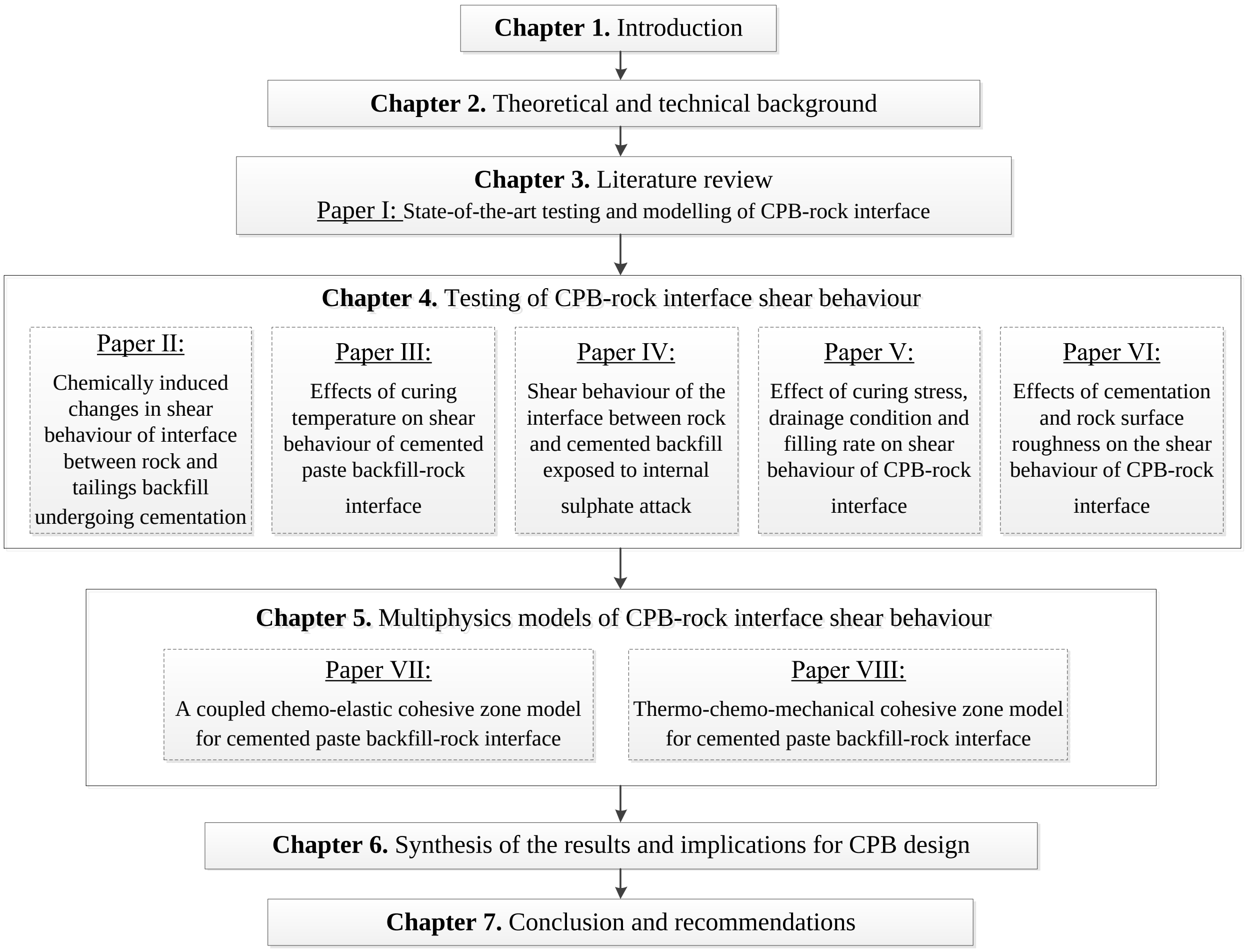

Figure 1.2 Tasks and organization of the proposal

1.6. References

Amaratunga LM, Yaschyshyn DN (1997) Development of a high modulus paste fill using fine gold mill tailings. Geotechnical and Geological Engineering 15:205-219.

Aubertin M, Li L, Arnoldi S, Belem T, Bussière B, Benzaazoua M, Simon R (2003) Interaction between backfill and rock mass in narrow stopes. Soil and rock America 1:1157-1164.

Belem T, El Aatar O, Bussière B, Benzaazoua M, Fall M, Yilmaz E (2006). Characterisation of self-weight consolidated paste backfill. Proceedings of the Ninth International Seminar on Paste and Thickened, At Limerick, Ireland, April 3-7, pp. 333-345., Volume: 9

Benzaazoua M, Fall M, Belem T (2004) A contribution to understanding the hardening process of cemented pastefill. Miner. Eng. 17(2):141-152.

Brackebusch FW (1994) Basic of paste backfill system. Miner. Eng., 46:1175-1178.

Buckby T, Black S, Coleman ML, Hodson ME (2003) Fe-sulphate-rich evaporative mineral precipitates from the Rio Tinto, southwest Spain. Mineral. Mag. 67:263-278.

Bull, AJ, Fall M (2020a) Thermally induced changes in metalloid leachability of cemented paste backfill that contains blast furnace slag. Minerals Engineering 156, 106520

Bull AJ, Fall M (2020b) Curing temperature dependency of the release of arsenic from cemented paste backfill made with Portland cement. Journal of Environmental Management 269, 110772

Cui L, Fall M (2016). Mechanical and thermal properties of cemented tailings materials at early ages: Influence of initial temperature, curing stress and drainage conditions. Construction and Building Materials 125, 553-563.

De Souza E, Archibald JF, Dirige APE (2003) Economics and perspectives of underground backfill practices in Canadian mining. In: 105th annual general meeting of the Canadian institute of mining, Metallurgy and Petroleum, Montreal, Canada, 15p.

Ercikdi B, Kesimal A, Cihangir F, Deveci H, Alp I (2009) Cemented paste backfill of sulphide-rich tailings: Importance of binder type and dosage. Cement and Concrete Composites 31(4):268-274.

Fall M, Benzaazoua M (2003) Advances in predicting performance properties and cost of paste backfill. In: Proceedings on tailings and mine waste'03, Vail, USA, 73–85.

Fall M, Célestin JC, Han FS (2009). Suitability of bentonite-paste tailings mixtures as engineering barrier material for mine waste containment facilities. Minerals Engineering 22 (9-10), 840-848.

Fall M, Célestin J, Sen HF (2010). Potential use of densified polymer-pastefill mixture as waste containment barrier materials. Waste Management 30 (12), 2570-2578.

Fall M, Nasir O (2010) Mechanical behaviour of the interface between cemented tailings backfill and retaining structures under shear loads. Geotech. Geol. Eng. 28(6):779-790.

Grice T (2001) Recent mine developments in Australia. Proceeding of the 7th international symposium on mining with backfill (MINEFILL). p.351-7.

Guo S, Fall M, Haruna S (2020). Interface shear behavior of cementing underground mine backfill. International Journal of Geomechanics 20 (12), 04020230

Hassani F, Archibal J (1998) Mine backfill. Canadian Institute of Mine, Metallury and Petroleum, Canada.

Helinski M, Fahey M, Fourie A (2010) Behavior of cemented paste backfill in two mine stopes: Measurements and modeling. Journal of Geotechnical and Geoenvironmental Engineering, 137(2):171-182.

Huang Y, Zhang JX, Zhang Q, Nie SJ (2011) Backfilling technology of substituting waste and fly ash for coal underground in china coal mining area. Environmental Engineering & Management Journal (EEMJ), 10(6):769-775.

Kesimal A, Yilmaz E, Ercikdi B, Alp I, Deveci H (2005) Effect of properties of tailings and binder on the short-and long-term strength and stability of cemented paste backfill. Materials Letters 59(28):3703-3709.

Koupouli NJF, Belem T, Rivard P, Effenguet H (2016) Direct shear tests on cemented paste backfill-rock wall and cemented paste backfill-backfill interfaces. J. Rock. Mech. Geotech. Eng. 8(4):472-479.

Nasir O, Fall M (2008) Shear behaviour of cemented pastefill-rock interfaces. Eng. Geol. 101(3):146-153.

Roshani A, Fall M, Kennedy K (2017). A column study of the hydro-mechanical behavior of mature fine tailings under atmospheric drying. International Journal of Mining Science and Technology 27 (2), 203-209

Simms P, Grabinsky M (2009) Direct measurement of matrix suction in triaxial tests on early-age cemented paste backfill. Canadian Geotechnical Journal 46(1):93-101.

Sun EJ, Zhang XK, Li ZX (2012) The internet of things (IOT) and cloud computing (CC) based tailings dam monitoring and pre-alarm system in mines. Safety science 50(4):811-815.

Xiao, B., Fall, M., Roshani, A. (2020) Towards understanding the rheological properties of slag-cemented paste backfill. International Journal of Mining, Reclamation and Environment, 1-23

Yilmaz E, Kesimal A, Ercidi B (2004) Strength development of paste backfill simples at long term using different binders. Proceedings of 8th symposium MineFill04, China.

Yilmaz E, Fall M (2017) Paste tailings management: Springer.

Chapter 2 Theoretical and Technical Background

2.1 Introduction

A review of the fundamental theoretical and technical background on mining and CPB is provided in this chapter, including typical mining methods with CPB (section 2.2), preparation and backfilling process of CPB (section 2.3), mechanical response of CPB under multiphysical loading conditions (from perspectives of experimental tests and numerical simulation, section 2.4). Finally, the potential effects of multiphysical loading conditions on the shear performance of the CPB-rock interface and the importance of the interaction between CPB and surrounding rock mass to the stability assessment of CPB structures are introduced in section 2.5.

2.2 Typical mining methods with CPB

There are many mining methods/technologies employed to extract orebody from underground. Some common ones include block caving, sublevel caving, room and pillar, longwall, vertical crater retreat, cut and fill, sublevel stoping mining method and so on. The choice of the mining method is closely related to the geology of the deposit and the degree of ground support necessary to make the method productive and safe. In the following section, the mining methods with CPB are introduced, which include vertical crater retreat, cut and fill, as well as sublevel stoping mining method. In comparison to other mining methods, the obvious advantage of mining methods with CPB is that they can prevent the occurrence of ground surface subsidence. Besides, the disposal of tailings stored on the ground surface is beneficial to the environmental protection.

2.2.1 Vertical crater retreat mining method

Vertical crater retreat (VCR) mining method is originally developed by the Canadian mining company INCO, and nowadays it is mainly used by mines with steeply dipping ore and host rock (Hustrulid et al., 2001). Figure 2.1 shows the layout of vertical crater retreat mining method and from the figure, it can be seen that VCR is based on the crater blasting technique. The blasting is performed from bottom to the top and part of the blasted ore remains in the stope to support the structure temporarily. It can also be observed from Figure 2.1(b) that after the blasted ore accumulated in the stope is moved, a barricade will be constructed at the drawpoint. The prepared CPB is then backfilled into the stope to support the structure permanently, which facilitates the extraction of the adjacent ore body.

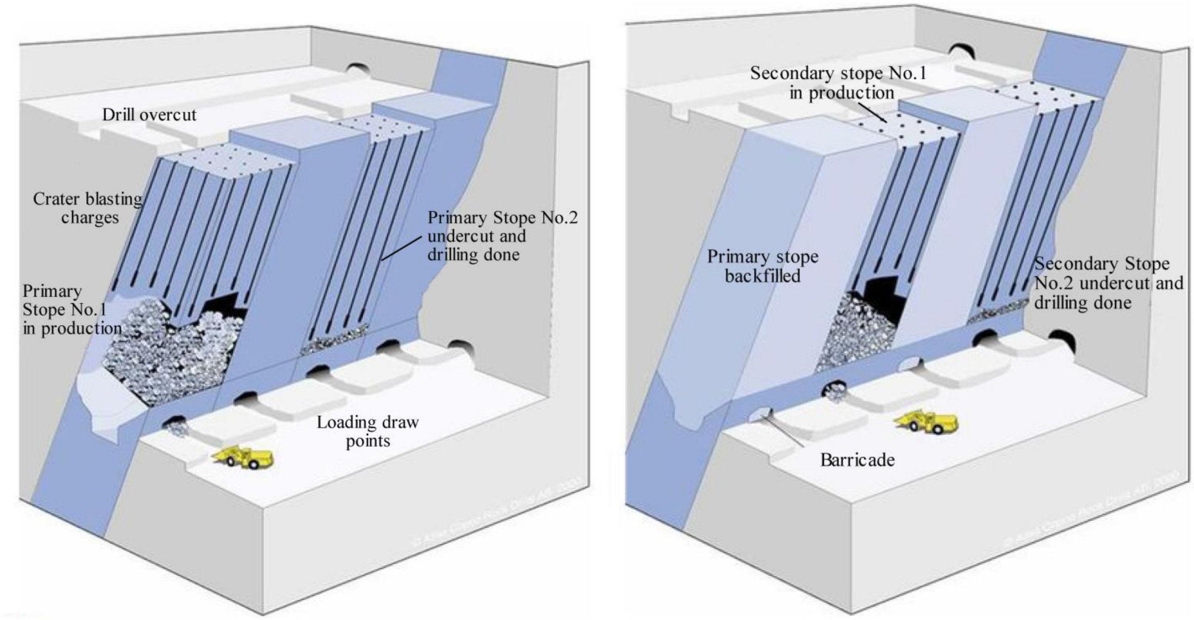

(a) Exploitation of primary stopes (b) Recovery of secondary stopes

Figure 2.1 Layout of vertical crater retreat (Adopted from Atlas Copco, 2007)

2.2.2 Cut and fill mining method

Like the VCR, cut and fill is also an ideal mining method for mines with steeply dipping ore, it is generally referred to as a small-scale mining method. The layout of the cut and fill mining method is shown in Figure 2.2. From the figure, it can be seen that mining is carried out in horizontal slices along the orebody and the bottom slice is mined first. A barricade is constructed after the bottom slice is completely extracted, and CPB will then be pumped into the space through the pipeline. The fill mass can serve both to support the surrounding wall, and as a work platform for mining the upper slice, which is shown in Figure 2.2. To improve the productivity, more production levels can be developed, thereafter, the excavation work can be executed in parallel. Even though cut and fill mining is regarded as a low productivity mining method, the advantage is high selectivity with good ore recovery and low dilution (Adopted from Atlas Copco, 2007).

2.2.3 Sublevel stoping mining method

Sublevel stoping is a commonly used method in large-scale mining, which is versatile and productive for mining large orebody with a steep dip and a regular shape. This mining method is similar to the vertical crater retreat and Figure 2.3 shows the distribution of primary and secondary stopes. As it can be seen from the figure, the orebody is divided into primary and secondary stopes, where the primary stopes are mined first. The secondary stopes are left as pillars until the adjacent primary stopes have been mined.

After that, the primary stopes are backfilled with CPB to prevent sidewalls from caving in when exploiting the secondary stopes.

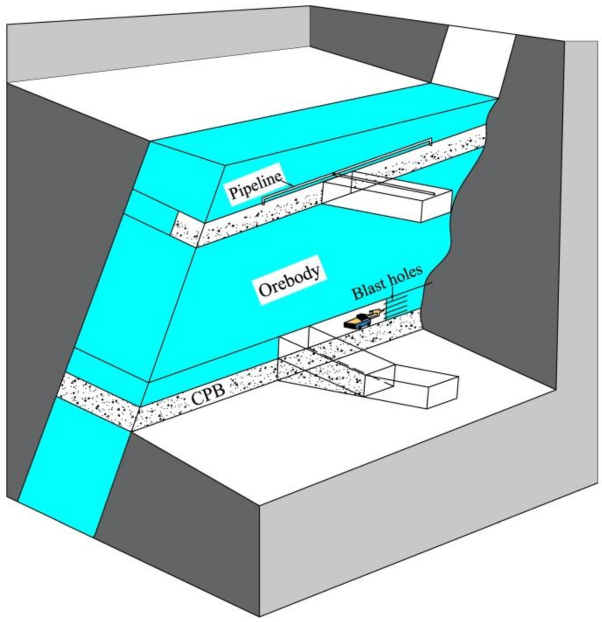

Figure 2.2 Layout of cut and fill mining method

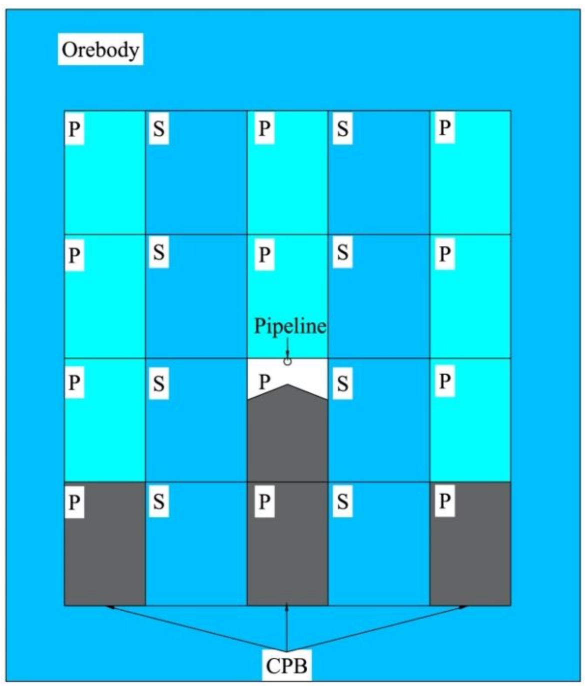

Figure 2.3 Distribution of primary and secondary stopes of sublevel stoping mining method

2.3 Background information on CPB

To design a CPB structure in a mine, a wide scope of knowledge and various operations are required, such as (i) how to determine the mix recipe of CPB for the sake of obtaining the optimum mechanical strength; (ii) the CPB preparation; (iii) the rheological properties of CPB with different mix recipes; (iv) the evolution of the mechanical properties of CPB with time; (v) the arching effect in CPB structure; (vi) backfilling strategy; (vii) the design of the barricade. Figure 2.4 illustrates the key research topics in CPB design, and some of them will be elaborated in the following section.

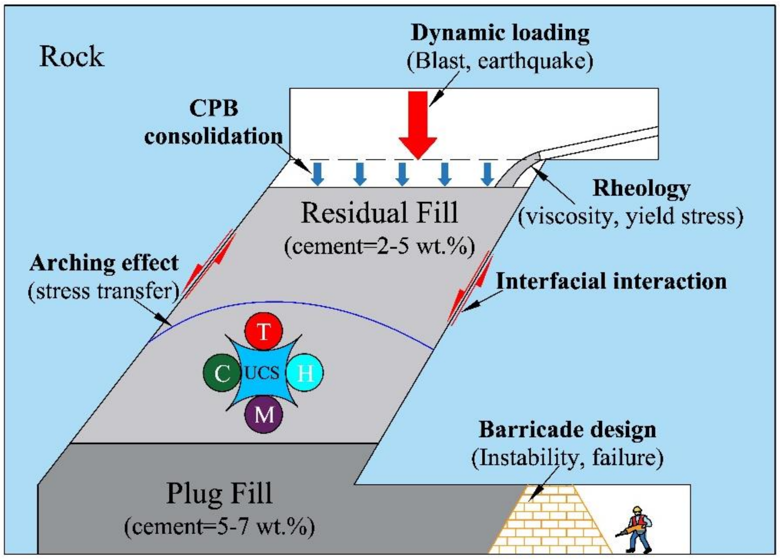

Figure 2.4 Research topics involved in CPB design

2.3.1 Mix design

The optimization of the CPB mix design is critical for the practicability and safety of CPB structures. On the one hand, the mix design determines the cost of the technology, which is a key factor to the application. On the other hand, some properties, such as strength and, transportability, which are influenced by the mix design, are important to the CPB performance (Fall and Samb 2009; Fall et al., 2008; Jiang et al., 2017).

CPB is a mixture of thickened tailings (with a solid percentage of 70%-85%), binder (3-7 wt.%, usually) and water (15%-25%), which is shown in Figure 2.5. In the Canadian mining industry, the most common type of binder used in CPB is Portland cement Type I (PCI). In this PhD research, all samples are produced with PCI. Generally, the usage of binder usually makes up 75% of the cost of CPB, which accounts for 10%-20% of the total cost of mining operations (Grice, 2001). Hence, the ultimate goal is to meet the required strength of CPB structures with a minimum usage of binder.

Tailings is a main component of CPB which is an inevitable product of mineral processing (almost 95-98% of the feed ore). In Canada, there are approximately 500 million tons of tailings and waste rock being produced annually (Amaratunga and Yaschyshyn, 1997). The inappropriate disposal of tailings poses an environmental threat (e.g. the release/mobility of heavy metals) by contaminating the water source and the soil (Aldhafeeri et al., 2016; Yilmaz and Fall, 2017).

Water content of CPB is another important factor that determines the rheology of the mixture. On the one hand, the low water content of the mixture reduces the flow ability (can be assessed by slump test) of the mixture, which impedes the rate of material transfer and reduces the efficiency of backfilling (Huynh et al., 2006). On the other hand, the higher water content of the mixture means CPB can be easily transported to underground stopes (Brackebusch, 1994; Grabinsky et al., 2002; Orejarena and Fall, 2011; Jiang and Fall, 2017). However, excess water prolongs the curing time and reduces the strength as well as the durability of CPB. In this PhD research, CPB with a water-cement ratio of 7.35 is produced.

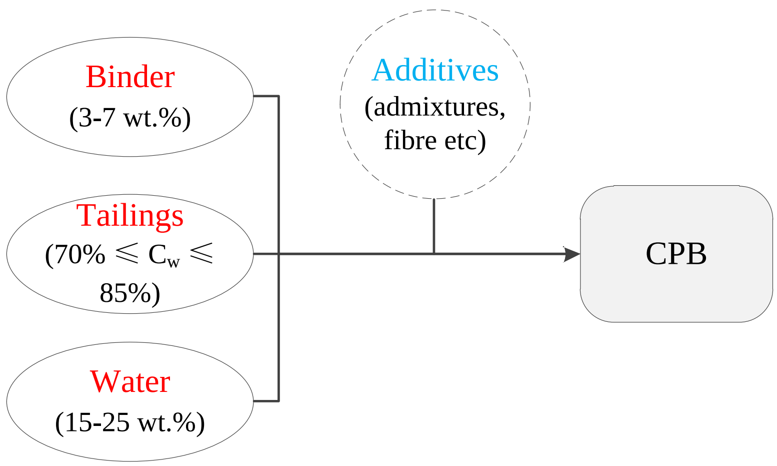

Figure 2.5 Components of CPB

2.3.2 Backfill preparation

The production of CPB includes several processes, such as thickening of the tailings, filtering, mixing and transporting. The processes are schematically shown in Figure 2.6. The following section will introduce the production of CPB elaborately.

2.3.2.1 Paste thickening

Tailings obtained from milling processes have a low solid concentration, which usually ranges from 35% to 60%. This kind of tailings cannot be used for CPB preparation until the solid concentration is increased to higher than 75% (Ghirian, 2016). As a result, a thickener is generally required to dewater the tailings before the mixing process begins. There are two types of thickeners nowadays, namely conventional paste thickener and deep-cone paste thickener. Compared with conventional paste thickener, the deep-cone paste thickener is a highly accepted technology in the mining industry owing to its capability of dewatering tailings to a higher solid concentration (Slottee and Johnson, 2009).

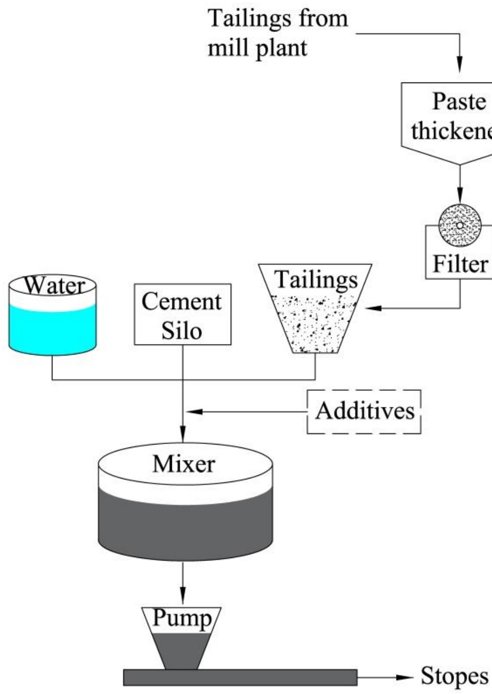

Figure 2.6 Production of cemented paste

2.3.2.2 Paste filtering

Filtering is a process to decrease the number of ultrafine particles (i.e., particles less than 5 μm in size) in tailings. Wilson and Calverd (2011) found that the existence of a large amount of ultrafine particles in tailings necessitates the usage of the binder in order to reach a target strength. Consequently, the higher consumption of binder increased the cost of CPB method, which was against the principle of economic activity.

There are many different kinds of filters, such as vacuum disc filters, drum filters and belt filters. Due to the large filtration area and comparatively low cost, the vacuum disc filter is widely adopted in the mining industry.

2.3.2.3 Mixing process

Mixing is one of the most important stages in producing a high-quality cemented paste. When the mix design as described in section 2.3.1 is determined, the components are mixed by a mixer with either a batch of or continuous processes. Compared to the continuous system, one obvious advantage of the batch system is its easier controlling process. As for the mixer, three common ones are screw mixer, paddle mixer and ploughshare mixer. Usually, the traditional screw mixer is used for the continuous system while the high-intensity screw and paddle mixers can be operated in both batch and continuous modes.

An interesting phenomenon is that some mechanical properties of CPB structures, e.g., mechanical strength, elastic modulus, are relevant to the mixer adopted to some degree. For example, Dirige and Archibald (2014) found that the strength and elastic modulus of CPB produced by ploughshare mixer are both higher than that produced by the screw mixer.

2.3.3 Transporting system

The transporting system is used to deliver fresh CPB produced from the backfill plant at the ground surface to underground stopes. The paste is a non-Newtonian fluid, hence, to overcome the resistance between the paste and pipeline, a pump is adopted to push the paste forward. The flow ability of cemented paste is characterized by its rheological behaviour (Peng et al., 2019), which is significantly affected by the cement content, temperature and elapsed time (Wu et al., 2013). Fresh CPB with poor flow ability not only affects efficiency in pumping to stopes, but can also result in pipe clogging which is associated with significant financial ramifications for mines. To prevent this kind of condition from happening, the pressure generated by the pump should be greater than the yield stress of CPB. Furthermore, the collaboration of the velocity, density of CPB and diameter of the pipe is also beneficial to the optimization of the transporting system (Landriault et al., 1997). The industry's rule of thumb is that the fresh CPB with a yield stress less than 250 kPa can be delivered to the underground openings at a rate of 35 m^3/h through 125 mm diameter pipes (Yilmaz and Guresci, 2017).

2.3.4 Backfill filling process

Prior to the mining operation, overcut and undercut are usually developed to delineate the planned stope. Once the ore body is extracted, a barricade should be constructed at the bottom access (drawpoint), subsequently, fresh CPB is then pumped into the stope through the pipeline which is set at the overcut (as shown in Figure 2.4). Even though the volume of the stope is variable, which is depending on the ore body geometry, the height of the stope can vary from 25 m to 200 m (Yilmaz and Fall, 2017; Lu and Fal 2017). Therefore, the huge CPB structure created by a consistent backfilling operation leads to significant horizontal stress on the barricade. In order to ensure the stability of the barricade, two methods are commonly adopted. The first one is to backfill the stope separately. In other words, a small amount of fresh CPB (with 5-7 wt.% cement content, the backfilling height is usually up to 7 m) is pumped to the stope at first to form a small backfilling body, which is also known as plug fill. The rest of the space will not be backfilled until the plug fill reaches a target stiffness and strength, the residual fill (with a cement content of 2-5 wt.%) then being completed. One disadvantage of this method is the extended cycle time of the backfilling process. Another technique is to increase the cement content of the CPB in the equivalent plug fill location. The higher cement content corresponds to active cement hydration, which in turn shortens the cycle time. However, the obvious drawback of this method is the increased preliminary investment.

2.4 Physical and mechanical properties of CPB

The performance or mechanical stability of CPB structures is determined by many factors, particularly the physical and mechanical properties of CPB. In the following section, a detailed description of the effect of key factors on the properties of CPB, especially the mechanical strength, will be introduced.

2.4.1 Laboratory works on the physical and mechanical properties of CPB

2.4.1.1 Physical properties and strength of CPB

Many physical properties, such as porosity, density, and water content, are important to the design and stability assessment of CPB structures. The factors affecting properties of CPB can be classified into two kinds: intrinsic and extrinsic factors. Some typical intrinsic factors include tailings properties (e.g., particle size distribution, mineralogy), binder properties (e.g., binder type, dosage), and mixing properties (e.g., water-to-cement ratio, solid ratio). In contrast, curing temperature, drainage condition, curing pressure and so on are regarded as extrinsic factors (Ghirian and Fall, 2016a).

Mechanical stability is the most important design criteria of CPB structures and it is generally evaluated from the uniaxial compressive strength (UCS) and shear strength of CPB (Fall et al., 2007). Previous investigations on mechanical properties of CPB mainly focused on the development of UCS, and it is found that the UCS of CPB values mostly varies between 0.2 MPa and 4 MPa (Klein and Simon, 2006; Pokharel and Fall, 2011; Peyronnard and Benzaazoua, 2011). The UCS of CPB is dependent on many factors, such as tailings mineralogy, sulphate content, binder type and content, curing temperature (Fall and Nasir, 2010). The presence of large amounts of sulphide minerals has a negative effect on the CPB strength due to two mechanisms, the first one being the inhibition effect of sulphate on binder hydration, and the other one being the physical damage caused by the excessive amounts of expansive minerals (Benzaazoua et al., 2002; Kesimal et al., 2004; Fall and Benzaaoua, 2005). However, for a given curing time, the existence of lower sulphate content increases the UCS of CPB due to the refinement of the pore structure by abundant (not excessive) expansive minerals (Fall et al., 2004; Fall and Pokharel, 2010; Li and Fall, 2018). Binder type and content also have a significant role in the UCS development of CPB. Binder type, such as PCI, slag, fly ash, can deliver different strengths to CPB. For example, Benzaazoua et al. (2002) found out that the ordinary Portland cement and the mixture of Portland cement and fly ash are appropriate for sulphate-rich tailings. Furthermore, higher binder content generally corresponds to higher UCS of CPB (Benzaazoua et al., 2004). Moreover, curing temperature is an important external factor which affects the short-term and long-term UCS of CPB significantly (Fall et al., 2007, 2010). With the increase in curing temperature, the rate of cement hydration is accelerated. The enhanced cement hydration increases the amounts of cement hydration products (e.g., C-S-H and CH), which lead to finer pore structure and higher cohesion in CPB (Fall et al., 2010). Fall et al. (2005) investigated the effect of tailings fineness on the short-term strength of CPB and found out the CPB with a fines content of 25-30 wt.% are more likely to exhibit higher strength. Similarly, Ercikdi et al. (2013) found that long-term CPB with coarse tailings (16-27.7 wt.%) tends to show higher strength compared with samples prepared with medium tailings (49.7-51 wt.%). In addition to the aforementioned factors, curing stress, drainage conditions are also critical for the UCS evolution of CPB (Ghirian and Fall, 2015, 2016b). As for the shear properties of CPB, many studies have also been conducted so far (Belem et al., 2000; Rankine and Sivakugan, 2007; Veenstra, 2013). Belem et al. (2000) found out the evolution of friction angle of CPB depends on the binder type and content. The higher cement content decreases the friction angle of CPB. Besides, with the increase in curing time, the friction angle also shows a decreasing trend, regardless of cement content (Rankine and Sivakugan, 2007), this was also found in the studies conducted by Veenstra (Veenstra, 2013). The cohesion of CPB is a time-dependent property that normally develops through cementation. Hence, the evolution of cohesion is mainly determined by the curing time, cement type and content (Fall et al., 2007; Veenstra, 2013).

2.4.1.2 Coupled THMC processes and its effect on the mechanical strength of CPB

The effect of thermal (T), hydraulic (H), mechanical (M) and chemical (C) processes on the evolution of mechanical strength of CPB structures is an important issue to consider in the geotechnical design and the stability assessment of CPB structures. The interaction between these multiphysics processes is shown in Figure 2. 7.

The thermal characteristics of CPB mainly refer to the thermal conductivity and temperature of CPB as well as the heat transfer between the CPB and the surrounding media. The thermal conductivity of CPB is influenced by the tailings mineralogy (e.g., quartz) and fine content. Many previous studies concluded that the increase in quartz content increases the thermal conductivity of tailings (Côté and Konrad, 2005; Célestin and Fall, 2009; Ghirian and Fall, 2013). This is because the thermal conductivity of quartz (7.7 W/m°C) is higher than that of many other materials (for example, the thermal conductivity of feldspar is 2.25 W/m°C). Besides, the increase in fine content of tailings also increases the thermal conductivity, as a result of the higher density of CPB (Célestin and Fall, 2009). In contrast, the temperature decreases the thermal conductivity because the increased temperature accelerates the rate of cement hydration, which in turn consumes a larger amount of water. The desaturation resulted in a replacement of water by air in the CPB pores. Since the thermal conductivity of water is about 25 times that of air (Abdul-Hussain et al. 2012), then the thermal conductivity of CPB is subsequently decreased. The temperature of CPB is to a large extent dependent on the geographical location and depth of the mine as well as on the cement hydration. However, the heat produced by the cement hydration is the major source of the heat in CPB, which can increase the temperature up to 50°C or a higher value (Fall et al., 2010; Thompson et al., 2012).

Heat exchanges between the CPB mass and the surrounding rock mass and/or the air in the mine take place, once the CPB is placed in the mine opening.

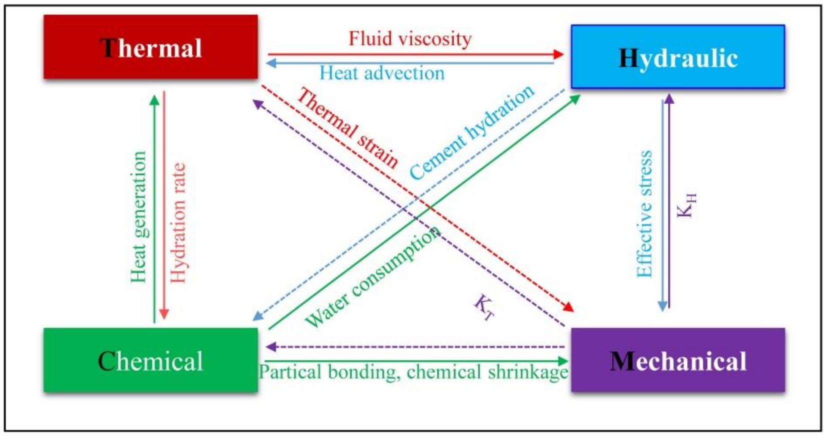

Figure 2.7 Interactions between multiphysics processes (K_H: hydraulic conductivity; K_T: thermal conductivity)

Changes in the thermal factor or process can also bring about variation in other processes, as shown in Figure 2.7. The increase in temperature decreases the viscosity of the water, which enhances the flow ability of water in CPB. This in turn affects the water drainage ability of the backfill mass. Vice versa, the flow ability of water in CPB cured under lower temperature is reduced. Besides, the temperature is also a significant influencing factor in the surface evaporation rate (Ghirian and Fall, 2013). As for the effect of the thermal factor on the mechanical property, it is mainly characterized by the mechanical deformation due to the thermal expansion or contraction (Cui and Fall, 2015). Another important relation between the thermal factor and other physical factors or processes is the effect of thermal processes (heat) on the chemical process in CPB, which mainly referred to the cement hydration. In other words, the rate of the cement hydration in CPB is temperature-dependent, and the increase in temperature is generally associated with a faster hydration rate (Schindler, 2004; Poole et al., 2007).

The primary hydraulic properties of CPB include hydraulic conductivity and pore water pressure (PWP, positive or negative) in CPB. A depiction of the evolution of hydraulic conductivity and PWP is essential for a reliable assessment of the stability of CPB structures. The hydraulic conductivity can be classified into two states, namely the saturated and unsaturated condition. Saturated hydraulic conductivity is necessary to examine the consolidation behaviour, water drainage ability and transportability as well as the durability of CPB. To date, many studies have been dedicated to study the evolution of saturated hydraulic conductivity and its influential factors (Godbout and Bussière 2007; Pokharel and Fall 2013; Ghirian and Fall 2013). The column experiment conducted by Ghirian and Fall (2013) indicated that the saturated hydraulic conductivity decreases with curing time, and the saturated hydraulic conductivity value in CPB is not uniformly distributed in a CPB mass. Another test performed by Ghirian and Fall (2015) reported that at any curing time, the application of the curing stress reduces the saturated hydraulic conductivity significantly. This is a result of the particle rearrangement and the porosity reduction in CPB due to the stress. However, the possibility of the occurrence of the physical damage caused by excessively high stress (80% of the UCS) increases the saturated hydraulic conductivity (Fall et al.2009), as a result of the generation of microcracks (mechanical damage) in CPB. As for the evolution of unsaturated hydraulic conductivity, only a limited number of studies have been conducted. Abdul-Hussain and Fall (2011) observed that a higher binder content lead to a slightly lower unsaturated hydraulic conductivity for a given suction. This is because the higher binder content corresponds to more products generated by binder hydration, which in turn leads to a finer pore structure in CPB. In addition, the development of PWP affected the magnitude of the effective stress in CPB which is an important mechanical parameter in porous media. One of the main factors that can influence the evolution of PWP is the sulphate content, and an increase in initial sulphate content reduces the suction in CPB (Li and Fall, 2016). Other factors such as binder content, binder type, curing temperature and drainage condition also affect the development of PWP (Wu et al., 2014; Ghirian and Fall, 2016b).

The evolution of hydraulic process has strong effects on other multiphysical factors or processes through the following mechanisms: (i) the change in hydraulic conductivity and the water content in CPB causes variations in the thermal conductivity (Cui and Fall, 2015). Besides, the dissipation of the heat with water drainage also affects the temperature in CPB; (ii) the water drainage in CPB leads to an increase in effective stress, as a result of the reduction in PWP. The higher effective stress then contributes to the strength acquisition (Le Roux et al., 2005; Ghirian and Fall, 2014); (iii) the coating of unhydrated binder particles with initial products of binder hydration (e.g., ettringite) inhibits pore water from diffusing inward to have access to the unhydrated particles. Consequently, this process decreases the rate and degree of the binder hydration (Nawy, 2008; Kumar et al., 2009).

The mechanical processes include strength, deformation behaviour and stress of CPB. As shown in Figure 2.7, the change in mechanical processes also affects other physical properties inevitably. The thermal conductivity of a porous medium is related to its porosity, which can be reduced by a higher curing stresses. As a result of the decreased thermal conductivity, the rate of heat dissipation is reduced. Similarly, the hydraulic conductivity also decreases with a decreasing porosity. High curing stress can result in the production of a larger quantity of cement hydration products. i.e. it affects the chemical process (Ghirian and Fall, 2016a,b).

The chemical process of CPB usually refers to the cement or binder hydration which is significantly affected by the sulphate content and curing temperature, as explained previously. Some techniques to measure and monitor the chemical process in CPB include pore water chemistry measurement, cement dissolution analyses, thermal analyses, XRD analyses and electrical conductivity monitoring (Thottarath, 2010; Ghirian and Fall, 2013, 2014; Li and Fall, 2016). The chemical process in CPB can significantly affect the thermo-hydro-mechanical properties, as shown in Figure 2.7. As the chemical reaction proceeds, the resulting hydration products, such as C-S-H, CH, ettringite and gypsum, not only change the microstructure in CPB (thereby leading to changes in thermal and hydraulic conductivity), but also affect the mechanical strength of CPB (Fall et al., 2009; Fall and Pokharel, 2010; Yilmaz et al., 2015). Besides, given the binder hydration is an exothermic reaction, the heat released by the reaction affects the temperature in CPB. Moreover, the binder hydration also consumes water, which not only decreases the degree of saturation, but also increases the effective stress in CPB (Ghirian and Fall, 2013).

2.4.2 Numerical modelling of the mechanical properties or behaviour of CPB

There have been tremendous contributions from previous studies on the understanding of the mechanical behaviour of CPB under various loading conditions, although many of them were experimental investigations. However, it is extremely hard to conduct laboratory tests that simultaneously consider more than two multphysics factors or processes, or all THMC processes. Therefore, studying the mechanical properties of CPB from the perspective of numerical modelling is important for the assessment and prediction of the stability of CPB structures. To date, much work has been done to describe the mechanical behaviour of CPB (Pierce, 2001; Helinski et al., 2007; Wu et al. 2013; Hughes, 2014; Cui and Fall, 2016b; Lu and Fall, 2016; Cui and Fall, 2019). For example, Pierce (2001) analyzed the stability of CPB mass with Mohr-Coulomb criterion. One major shortcoming of the study was the assumption by the authors that the mechanical properties of CPB were constant and failed to consider the effect of cement hydration on the evolution of the mechanical properties. Nevertheless, Helinski (2007) took the cement hydration into consideration when simulating the consolidation behaviour of CPB. By adopting a piece-wise function to control the pre- and post-peak stress, Hughes (2014) depicted the strain-softening behaviour of CPB. Wu et al. (2014) developed a thermo-hydro-chemical (THC) model to predict the PWP and temperature changes with the progression of the binder hydration. In addition, Cui and Fall (2016a) proposed an evolutive elasto-plastic model to address the effects of the cement hydration on the evolution of mechanical properties of CPB. They also developed a coupled thermo-hydro-mechanical-chemical (THMC) model to predict the THMC behaviour of CPB as well as a multiphysical consolidation model for CPB. Moreover, a coupled chemo-viscoplastic cap model was proposed to simulate the behaviour of CPB under blast loading (Lu and Fall, 2016).

2.5 Interaction between CPB and the adjacent rock mass

As mentioned previously, the mechanical stability is one of the most important design criteria of CPB structures. Most of the previous studies assumed that the UCS and the shear strength of CPB are the two main factors that determine the mechanical stability of CPB structures, and only limited investigations deal with the mechanical behaviour of the interface between CPB and surrounding rock mass, as shown in Figure 2.8. The interface behaviour is critical in the evaluation of the mechanical stability of CPB structures. For instance, Nasir and Fall (2008) found out that the shear properties (e.g., adhesion, friction angle) of the CPB-rock interface are lower than those of CPB body. These lower properties indicated that the CPB-rock interface is a weak plane at which a failure of the CPB structure may occur. Hence, the shear performance of the interface is important when assessing the stability of the CPB structures. Besides, the interaction between CPB and adjacent rock mass also resulted in the occurrence of the arching effect, which sustained the weight of overlying strata to a high extent (Marston, 1930). Moreover, the shear properties of the CPB-rock interface may vary when being exposed to different loading conditions (Figure 2.8). Therefore, a full understanding of the interaction of CPB and the adjacent rock mass is extremely important for cost-effective and safe design of CPB structures.

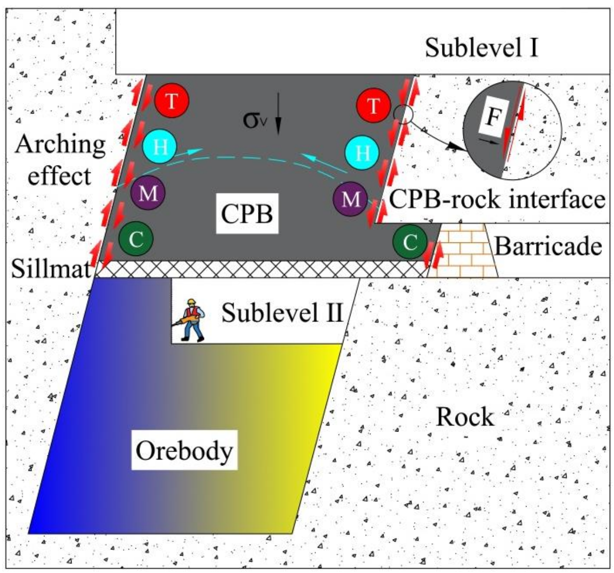

Figure 2.8 Interaction between CPB and adjacent rock mass

2.5.1 Arching effect

The arching effect, as shown in Figure 2.8, is induced by the load transfer along the interface between the CPB and the surrounding rock mass. It has been introduced in different ways to analyze wall pressure in silos (Blight, 1986), vertical stress and supporting requirements above tunnels (Iglesia et al., 1999) and earth pressure on retaining walls in trenches (Spangler and Handy, 1984; Take and Valsangkar, 2001). When the arching effect occurs, a large part of the weight of the CPB above the arching structure will be transferred to the CPB-rock interface, under which circumstance, the vertical stress on the sillmat and the barricade (on which the vertical stress will be transferred to horizontal pressure by multiplying the active ratio of the lateral stress to vertical stress) becomes much lower than the weight of the overlying CPB mass. Figure 2.9 represents a three-dimensional backfilled stope, and the calculation of the effective stress is described below.

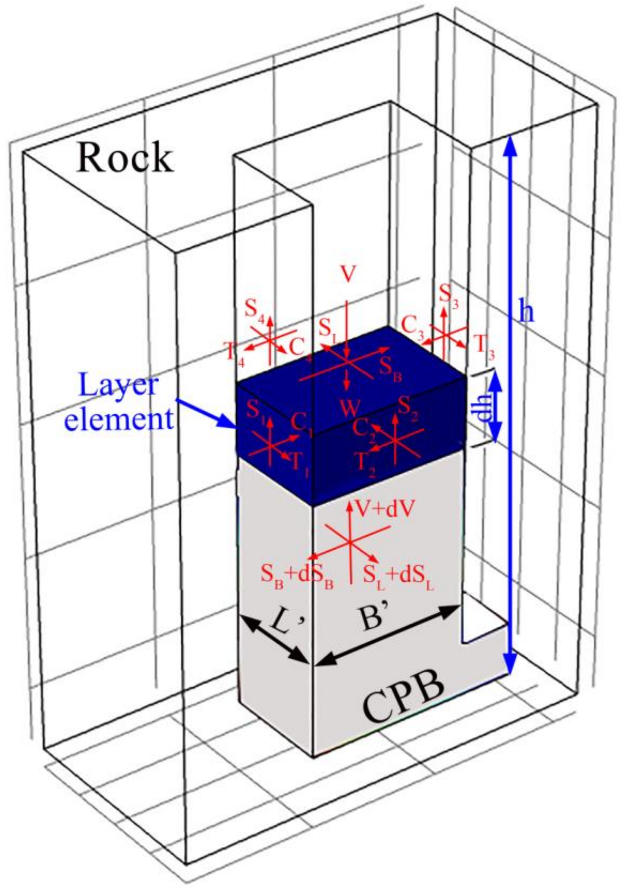

Figure 2.9 Three-dimensional representation of vertical backfilled stope

It is well known that the CPB body placed in the stope area, especially in the early age, is much softer than that of the surrounding rock. With the passage of time, the cement hydration consumes large amount of water. As a result, some cement hydration products are generated. However, the volume of the cement hydration products is smaller than that of the water consumed (Cui and Fall, 2016). The consolidation therefore takes place inside CPB structure, which then induces some load transfer from CPB to surrounding rock due to the frictional force (as shown in Figutre 2.8) at the interface. The frictional force S_j (j =1-4) is a function of lateral compressive force C_j (with Coulomb criterion):

$$\begin{cases} S_j = (\frac{C_j}{L'\times dh}\tan\phi_j^{'} + c_j)\times L'\times dh \quad For\ j=1,3 \\ S_j = (\frac{C_j}{B'\times dh}\tan\phi_j^{'} + c_j)\times B'\times dh \quad For\ j=2,4 \end{cases} \tag{2-1}$$

where $\phi_j^{'}$ and c_j are the frictional angle and adhesion at the interface, L' and B' are the length and width of the stope area. The lateral compressive force C_j is expressed as:

$$\begin{cases} C_j = K_{cj}\sigma_v L'\times dh \quad For\ j=1,3 \\ C_j = K_{cj}\sigma_v B'\times dh \quad For\ j=2,4 \end{cases} \tag{2-2}$$

Where σ_v is the vertical stress, K_{cj} is the coefficient of lateral pressure. To determine the coefficient of lateral pressure in CPB, Li et al. (2005) simulated the vertical stress distribution inside CPB with K_0 (at rest) and K_a (active) respectively, and it was found that the results obtained with K_a are in good agreement with data recorded in the field. Herein, the active ratio of the lateral stress to vertical stress K_a is adopted. Therefore, the shearing force at the interface is:

$$\begin{cases} S_j = (K_a\sigma_v \tan\phi_j^{'} + c_j)\times L'\times dh \quad For\ j=1,3 \\ S_j = (K_a\sigma_v \tan\phi_j^{'} + c_j)\times B'\times dh \quad For\ j=2,4 \end{cases} \tag{2-3}$$

According to the physical and moment equilibrium equations, the effective stress inside CPB is then formulated as (the coefficient of lateral pressure, friction angle, and adhesion are assumed as constants at different interfaces):

$$\sigma_v = \frac{\left[\gamma(B'^{-1}+L'^{-1})^{-1} - 2c(1+2\tan(\phi'/2-45^{\circ})\times\tan\phi')\right]\left[1-\exp(-2K_a h(B'^{-1}+L'^{-1})\tan\phi')\right]}{2K_a\tan\phi'} \tag{2-4}$$

where γ is the unit weight of CPB, and h is the height of the CPB. From the equation, it can be concluded that the occurrence of the arching effect is dependent on the width and depth of the opening, the interface friction angle and the active ratio of the lateral stress to the vertical stress. Readers who are interested in the derivation are referred to representative papers written by Aubertin et al. (2003) and Li et al. (2005).

The arching effect has also been observed by the in-situ measurement of stress and pore water pressure in CPB during the filling operation (Helinski et al., 2010). For example, the total overburden pressure at the bottom of the stope is initially estimated as 836 kPa, but the measured stress is only 190 kPa. Besides, the decreasing trend of stress during the period when filling is also suspended indicates the effect of the arching effect (caused by self-desiccation) on the reduction of the vertical stress.

The reduced vertical stress in CPB means considering the arching effect can decrease the amount of cement used for sillmat, plug fill and the barricade as well as the residual fill, which can effectively reduce the cost of CPB design (Grice, 2001).

2.5.2 Coupled THMC processes on the CPB-rock interface

The shear properties of the CPB-rock interface are affected by multiphysics processes that take place at the interface, as shown in Figure 2.10 (e.g., thermal, mechanical, hydraulic and chemical factors), which is in the same vein as the effects of coupled THMC effects on the mechanical properties of CPB body. Specifically, the temperature will change the rate of self-desiccation of CPB and the hydraulic conductivity (Cui and Fall, 2018), thereby affecting the mechanical properties of CPB. Besides, the higher temperature can also lead to the presence of crossover effect in cementitious material, which subsequently reduces the mechanical strength (Alexander and Taplin, 1962; Kjellsen et al., 1991; Escalante-Garcia and Sharp, 2001). Most significantly, temperature plays an important role in controlling the rate of the cement hydration. In contrast, the change in microstructure and water content of CPB will in turn influence the thermal conductivity and effective stress respectively. Moreover, the different amount of products generated by cement hydration can not only affect the pore structure within CPB, but also change the hydraulic and thermal conductivity of CPB. On the other hand, the existence of sulphate can negatively or positively affect the mechanical strength of the CPB, depending on the concentration of the sulphate content and curing time. In addition, the higher concentration of sulphate content can result in the formation of C-S-H gel, a lower quality C-S-H with a weaker binding ability (Jelenić et al., 1977; Divet and Randriambololona, 1998; Barbarulo, 2002; Pokharel and Fall, 2011). Moreover, the water drainage (hydraulic factor) can affect the effective stress and by extension, the shear characteristics of the interface.

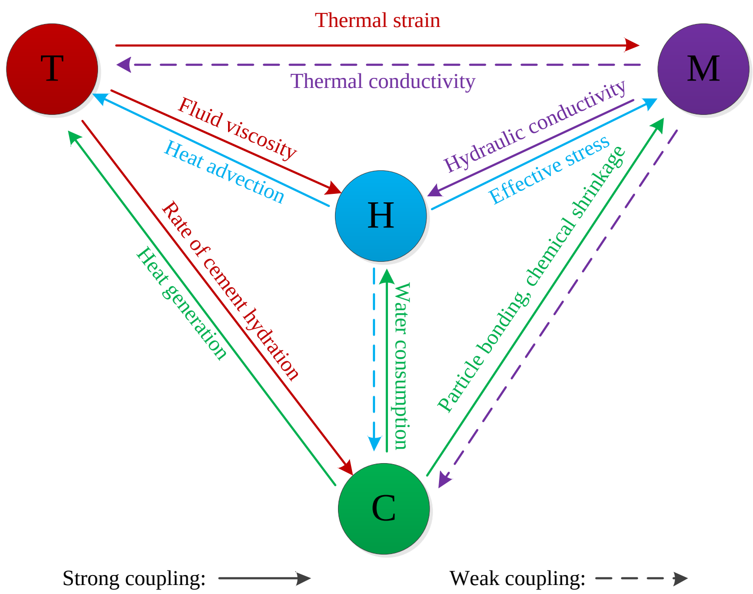

Figure 2.10 Effects of multiphysics processes on shear characteristics of CPB-rock interface

To date, only limited studies on CPB-rock interface have been conducted, and none of them has experimentally investigated the effects of multiphysics factors, such as temperature (T), sulphate (C), curing stress (M) and drainage (H), on the shear characteristics of the CPB-rock interface. Moreover, there is currently no multiphysics model developed to describe and predict these shear behaviour of the interface.

2.6 Conclusion

Theoretical and technical background information on CPB has been summarized in this chapter. Besides, the coupled effects of THMC process on the mechanical properties of CPB, the importance of the interaction between CPB and the surrounding rock mass to the stability of CPB structures are also introduced. However, the previous studies on CPB have never addressed the shear performance of CPB-rock interface under multiphysics conditions. In addition, the numerical models for describing the failure of CPB-rock interface remain unknown. Therefore, to reliably assess the stability of CPB structures, laboratory tests and numerical simulations on the shear performance of the CPB-rock interface under different thermal, mechanical and chemical conditions are conducted in this PhD research.

2.7 References

Abdul-Hussain N, Fall M (2011) Unsaturated hydraulic properties of cemented tailings backfill that contains sodium silicate. Eng. Geol. 123(4):288–301

Abdul-Hussain N, M Fall (2012) Thermo-hydro-mechanical behaviour of sodium silicate-cemented paste tailings in column experiments. Tunnelling and Underground Space Technology 29:85-93.

Aldhafeeri Z, Fall M, Pokharel M, Pouramini Z (2016). Temperature dependence of the reactivity of cemented paste backfill. Applied geochemistry 72, 10-19.
Alexander K, Taplin J (1962) Concrete strength, paste strength, cement hydration, and the maturity rule. Australian Journal of Applied Science 13(4):277-284.
Amaratunga LM, Yaschyshyn DN (1997) Development of a high modulus paste fill using fine gold mill tailings. Geotechnical and Geological Engineering 15:205-219.
Atlas Copco (2007) Mining methods in underground mining. Second edition.
Aubertin M, Li L, Arnoldi S, Belem T, Bussière B, Benzaazoua M, Simon R (2003) Interaction between backfill and rock mass in narrow stopes. Soil and rock America, 1:1157-1164.
Barbarulo R (2002) Comportement des matériaux cimentaires: actions des sulfates et de la température. Dissertation, École Normale Supérieure de Cachan, France – Université Laval, Canada; [in French]
Belem T, Benzaazoua M, Bussière B (2000) Mechanical behaviour of cemented paste backfill. In: Proceedings of the Canadian geotechnical society conference geotechnical engineering at the Dawn of the Third Millennium 15–18 October, Montréal, vol. l, p 373–380.
Belem T, El Aatar O, Bussière B, Benzaazoua M, Fall M, Yilmaz E (2006) Characterization of self-weight consolidated paste backfill. Proceedings of 9th International Seminar on Paste and Thickened Tailings – Paste'06, Limerick, Ireland. 3–7:333–345.
Belem T, Benzaazoua M (2008) Design and application of underground mine paste backfill technology. Geotechnical and Geological Engineering 26(2):147-174.
Benzaazoua M, Belem T, Bussiere B (2002) Chemical factors that influence the performance of mine sulphidic paste backfill, Cement Concrete Research 32(7):1133–1144.
Benzaazoua M, Fall M, Belem T (2004) A contribution to understanding the hardening process of cemented pastefill. Minerals Engineering 17(2):141-52.
Blight GE (1986) Pressure exerted by materials stored in silos. Part I: coarse materials. Géotechnique, 36(1):33-46.
Brackebusch FW (1994) Basics of paste backfill systems. Miner. Eng. 46(10):1175–1178.
Célestin J, Fall M (2009) Thermal conductivity of cemented paste backfill material and factors affecting it. Int. J. Min. Reclam. Environ. 23(4):274–290.
Côté J, Konrad JM (2005) A generalized thermal conductivity model for soils. Canadian Geotechnical Journal 42(2):443-458.
Cui L, Fall M (2015) A coupled thermo–hydro-mechanical–chemical model for underground cemented tailings backfill. Tunnelling and Underground Space Technology 50:396–414.
Cui L, Fall M (2016a) An evolutive elasto-plastic model for cemented paste backfill, Comput. Geotech. 71:19–29.
Cui, L., Fall, M. (2016b). Multiphysics model for consolidation behaviour of cemented paste backfill. ACSE International Journal of Geomechanics 17(3): 23p; 04016077-23.
Cui L, Fall M (2018). Modeling of self-desiccation in a cemented backfill structure. International journal for numerical and analytical methods in geomechanics 42(3): 558-583.
Cui L, Fall M (2019). Mathematical modelling of cemented tailings backfill: a review. International Journal of Mining, Reclamation and Environment 33 (6), 389-408.
Dirige APE, Archibald JF (2014) Investigation of the influence of homogeneous mixing on the strength behaviour of paste backfill. Can. Geotech. J.
Divet L, Randriambololona R (1998) Delayed ettringite formation: the effect of temperature and basicity on the interaction of sulphate and CSH phase, Cem. Concr. Res. 28(3):357-363.
Ercikdi B, Baki H, İzki M (2013) Effect of desliming of sulphide-rich mill tailings on the long-term strength of cemented paste backfill. J. Environ. Manage. 115:5–13
Escalante-Garcia JI, Sharp JH (2001) The microstructure and mechanical properties of blended cements hydrated at various temperatures. Cem. Concr. Res. 31(5):695–702.
Fall M, Benzaazoua M, Ouellet S (2004) Effect of tailings of paste backfill properties. In: International symposium Mine Fill 2004, Beijing, 19–21 September 2004
Fall M, Benzaazoua M, Ouellet S (2005) Experimental characterization of the effect of tailings fineness and density on the quality of cemented paste backfill. Miner. Eng. 18(1):41–44
Fall M, Benzaazoua M, Saa EG (2008) Mix proportioning of underground cemented tailings backfill. Tunnelling and Underground Space Technology 28(1):80–90.
Fall M, Samb S.S. (2009). Effect of high temperature on strength and microstructural properties of cemented paste backfill. Fire Safety Journal 44 (4), 642-651
Fall M, Celestin J, Pokharel M, Touré M, (2010) A contribution to understanding the effects of curing temperature on the mechanical properties of mine cemented tailings backfill. Engineering Geology 114(3-4):397–413.

Fall M, Pokharel M (2010) Coupled effects of sulphate and temperature on the strength development of cemented tailings backfills: Portland cement-paste backfill. Cement & Concrete Composites 32(10):819-828.
Fall M, Nasir O (2010) Predicting the temperature and strength development within cemented paste backfill structures. Proceedings of the thirteenth international seminar on paste and thickened tailings, Publisher: Australian Centre for Geomechanics, pp: 125-136
Fall M, Belem T, Samb S, Benzaazoua M (2007) Experimental characterization of the stress-strain behaviour of cemented paste backfill in compression. J. Mater. Sci. 42(11):3914–3992
Fall M, Adrien D, Celestin J, Pokharel M, Toure M (2009) Saturated hydraulic conductivity of cemented paste backfill. Miner. Eng. 22:1307–1317
Ghirian A, Fall M (2013) Coupled thermo-hydro-mechanical–chemical behaviour of cemented paste backfill in column experiments. Part I: physical, hydraulic and thermal processes and characteristics. Eng. Geol. 164:195–207.
Ghirian A and Fall M (2014) Coupled thermo-hydro-mechanical-chemical behaviour of cemented paste backfill in column experiments. Part II: mechanical, chemical and microstructural processes and characteristics. Eng. Geol. 170: 11-23.
Ghirian A, Fall M (2015) Coupled behaviour of cemented paste backfill at early ages. Geotech. Geol. Eng. 33(5):1141–1166
Ghirian A (2016) Coupled thermo-hydro-mechanical-chemical (THMC) processes in cemented tailings backfill structures and implications for their engineering design. Ph.D. thesis, University of Ottawa.
Ghirian A, Fall M (2016a) Properties of cemented paste backfill. In Paste Tailings Management (Eds Yilmaz and Fall), Springer, pp 59-109.
Ghirian A, Fall M (2016b) Strength evolution and deformation behaviour of cemented paste backfill at early ages: effect of curing stress, filling strategy and drainage. Int. J. Min. Sci. Technol. 26(5):809–817
Godbout J, Bussière B (2007) Evolution of cemented paste backfill saturated hydraulic conductivity at early curing time. In: Proceedings of 60th Canadian geotechnical conference and the 8th Joint CGS/IAH-CNC groundwater conference, 21–24 October 2007, Ottawa, p 2230–2236
Grabinsky MW, Theriault J, Welch D (2002) An overview of paste and thickened tailings disposal on surface. In: Proceedings of the symposium sur l'environnement et les mines: Defis et perspectives. Rouyn-Noranda, Canada, 8 p
Grice T (2001) Recent mine developments in Australia. Proceeding of the 7th international symposium on mining with backfill (minefill), 351–357.
Helinski M, Fourie A, Fahey M, Ismail M (2007) Assessment of the self-desiccation process in cemented mine backfills. Can. Geotech. J. 44(10):1148–56.
Helinski M, Fahey M, Fourie A (2010) Behaviour of cemented paste backfill in two mine stopes: Measurements and modelling. Journal of Geotechnical and Geoenvironmental Engineering 137(2):171-182.
Hughes PB (2014) Design guidelines: underhand cut and fill cemented paste backfill sill beams. PhD thesis, University of British Columbia, Vancouver.
Hustrulid WA, Bullock RL, Bullock RC (2001) Underground mining methods: Engineering fundamentals and international case studies: SME.
Huynh L, Beattie DA, Fornasiero D, Ralston J (2006) Effect of polyphosphate and naphthalene sulfonate formaldehyde condensate on the rheological properties of dewatered tailings and cemented paste backfill. Miner. Eng. 19:28–36.
Iglesia GR, Einstein HH, Whitman RV (1999) Determination of vertical loading on underground structures based on an arching evolution concept. Geo-Engineering for Underground Facilities, Fernandez, C., Bauer, R. A. (eds.). Geo-Institute of ASCE, pp. 495-506.
Jiang H, Fall M (2017). Yield stress and strength of saline cemented tailings in sub-zero environments: Portland cement paste backfill. International Journal of Mineral Processing 160, 68-75.
Jiang H, Fall M, Cui L (2017). Freezing behaviour of cemented paste backfill material in column experiments. Construction and Building Materials 147, 837-846.
Jelenić I, Panović A, Halle R, Gaćeša T (1977) Effect of gypsum on the hydration and strength development of commercial Portland cements containing alkali sulfates. Cement and Concrete Research 7(3):239-245.
Kesimal A, Yilmaz E, Erikdi B, (2004) Evaluation of Paste Backfill Mixtures Consisting of Sulphide-rich Mill Tailings and Varying Cement Contents. Cement Concrete Research 34(10):1817-1822.
Kjellsen KO, Detwiler RJ, Gjorv OE (1991) Development of microstructures in plain cement pastes hydrated at different temperatures. Cem. Concr. Res. 21(1):179–189.

Klein K, Simon D (2006) Effect of specimen composition on the strength development in cemented paste backfill. Canadian Geotechnical Journal (43):310–24.
Kumar M, Singh N, Singh N (2009) Effect of water proofing admixture on the hydration of Portland cement. Ind. J. Chem. Technol. 16:499-506.
Landriault DA, Verburg R, Cincilla W, Welch D (1997) Paste technology for underground backfill and surface tailings disposal applications. Short course notes, Canadian Institute of Mining and Metallurgy, Vancouver, British Columbia, Canada, 120.
Le Roux K, Bawden WF, Grabinsky MF (2005) Field properties of cemented paste backfill at the Golden Giant mine. Trans. Inst. Min. Metall. Sect. A Min. Technol. 114:65–80.
Li L, Aubertin M (2008) An improved analytical solution to estimate the stress state in subvertical backfilled stopes. Canadian Geotechnical Journal 45(10):1487-1496.
Li W, Fall M (2016) Sulphate effect on the early age strength and self-desiccation of cemented paste backfill. Construct. Build. Mater. 106:295–304.
Li W, Fall M (2018). Strength and self-desiccation of slag-cemented paste backfill at early ages: link to initial sulphate concentration. Cement and Concrete Composites 89, 160-168.
Lu G, Fall M (2017) Modelling blast wave propagation in a subsurfacegeotechnical structure made of an evolutive porous material. Mechanics of Materials 108: 21-39
Lu G, Fall M (2016) A coupled chemo-viscoplastic cap model for simulating the behaviour of hydrating cemented tailings backfill under blast loading. International journal for numerical and analytical methods in geomechanics 40(8):1123-1149.
Marston A (1930) The theory of external loads on closed conduits in the light of latest experiments. Highway research board proceedings, Ames Iowa.
Nasir O, Fall M (2008) Shear behaviour of cemented pastefill-rock interfaces. Eng. Geol. 101(3):146-153.
Nawy EG (2008) Concrete Construction Engineering Handbook, seconded. CRC Press, Boca Raton, FL, USA.
Orejarena L, Fall M (2011). Artificial neural network based modeling of the coupled effect of sulphate and temperature on the strength of cemented paste backfill. Canadian Journal of Civil Engineering 38 (1), 100-109.
Peng XP, Fall M, Haruna S (2019). Sulphate induced changes of rheological properties of cemented paste backfill. Minerals Engineering 141, 105849.
Peyronnard O, Benzaazoua M (2011) Estimation of the cementitious properties of various industrial by-products for applications requiring low mechanical strength. Resources, Conservation and Recycling 56:22–23.
Pierce ME (2001) Stability analysis of paste backfill exposures at Brunswick mine. In: 2nd International FLAC symposium, Lyon, France, 147–56.
Pokharel M, Fall M (2011) Coupled thermo-chemical effects on the strength development on Slag-Paste backfill materials. ASCE Journal of Materials in Civil Engineering 23(5):511–525.
Pokharel M, Fall M (2013) Combined influence of sulphate and temperature on the saturated hydraulic conductivity of hardened cemented paste backfill. Cem. Concr. Compos. 38:21–28
Poole JL, Riding KA, Folliard KJ, Juenger MC, Schindler AK (2007) Methods for calculating activation energy for Portland cement. ACI Mater. J. 104:303–311.
Rankine R, Sivakugan N (2007) Geotechnical properties of cemented paste backfill from Cannington Mine, Australia. Geotech. Geol. Eng. 25:383–393.
Schindler AK (2004) Effect of temperature on hydration of cementitious materials. ACI Material Journal, 101(1):72–81.
Slottee JS, Johnson JL (2009) Paste thickener design and operation selected to achieve downstream requirements. In: The 12th international seminar on paste and thickened tailings, Viña del Mar, Chile, 69–76
Spangler MG, Handy RL (1984) Soil Engineering. Harper and Row.
Take WA, Valsangkar AJ (2001) Earth pressures on unyielding retaining walls of narrow backfill width. Canadian Geotechnical Journal 38:1220-1230.
Thompson BD, Bawden WF, Grabinsky MW (2012) In-situ measurements of cemented paste backfill at the Cayeli Mine, Canadian Geotechnical journal 49(7):755-772.
Thottarath S (2010) Electromagnetic characterization of cemented paste backfill in the field and laboratory. Master thesis, University of Toronto.
Veenstra RL (2013) A design procedure for determining the in situ stresses of early age cemented paste backfill. PhD thesis, University of Toronto, 275
Wilson S, Calverd J (2011) Benefits of paste aggregate backfill. In: The 10th international symposium on mining with backfill, Cape Town, 1–8.

Wu D, Fall M, Cai SJ (2013) Coupling temperature, cement hydration and rheological behaviour of fresh cemented paste backfill, Minerals Engineering 42:76–87.
Wu D, Fall M, Cai SJ (2014) Numerical modelling of thermally and hydraulically coupled processes in hydrating cemented tailings backfill columns. Int. J. Min. Reclam. Environ. 28(3):173–199.
Yilmaz E, Fall M (2017) Introduction to paste tailings management Paste Tailings Management (pp. 1-5): Springer.
Yilmaz E, Guresci M (2017) Design and characterization of underground paste backfill Paste Tailings Management (pp. 111-143): Springer.
Yilmaz E, Belem T, Bussière B, Mbonimpa M, Benzaazoua M (2015) Curing time effect on consolidation behaviour of cemented paste backfill containing different cement types and contents. Constr. Build. Mater. 75:99–111.

Chapter 3 Cemented paste backfill and progress in testing and modelling of the interface between cemented paste backfill and rock: Literature Review (Paper I)

Kun Fang, Mamadou Fall

Abstract

To address environmental issues and geotechnical hazards caused by mining operations, cemented paste backfill (CPB) is a mining method adopted by the mining industry worldwide. This review introduces three main processes in the CPB design and summarizes their recent progress. Moreover, the priority of this review is to retrospect on the shear properties of the CPB-rock interface under the influence of multiphysical factors. These factors include mechanical (curing stress), chemical (e.g., cement hydration, sulphate attack), thermal (e.g., the heat generated by the cement hydration, geothermal gradients, thermal load from the environment), hydraulic (drainage condition) and interface morphology (surface roughness). Such testing and modelling are essential for the reliable and cost-effective design of CPB structures.

3.1 Introduction

Minerals and metals are the building blocks of modern society, the extraction of which contributes significantly to the world economy. For example, the mining industry in Canada (with a contribution of $97 billion to the total value of the gross domestic product) took up 19% of its goods export in 2017 (Mining Association of Canada, 2019). However, together with precious minerals, a large number of waste rocks are excavated during the mining operation. Besides, the mineral processing and hydrometallurgical techniques produce a considerable amount of tailings. Take one copper mine as an example, the amount of waste and tailings produced by each process is illustrated in Figure 3.1. In general, the waste-to-product ratio is 100:1 in volume (Dudeney et al., 2013), and to date, more than 1150 million tonnes of metals have been generated (Lu and Wang, 2012; Edraki et al., 2014). Hence, the accumulated amount of tailings produced is massive. Moreover, the amount of tailings is still increasing by at least 10 billion tonnes per year worldwide (Jones and Boger, 2012; Adiansyah et al., 2015). Given the large volume of tailings produced in the mining industry, how to manage or dispose of tailings in an environment-friendly and cost-effective way has been a heated issue in the mining community.

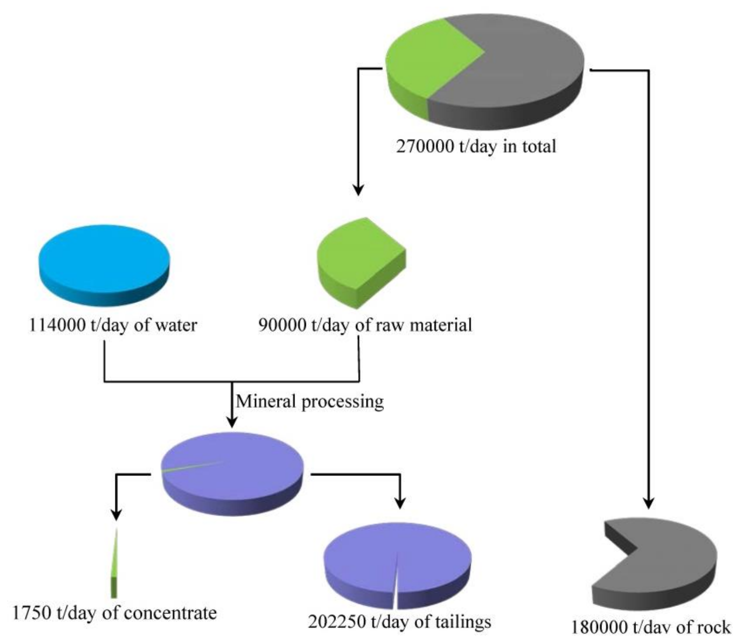

Figure 3.1 Production of waste rock and tailings by mineral processing (take a copper mine as an example)

Despite many frameworks in terms of sustainable approach to tailings management, practically, there are two methods, namely direct and indirect disposal (Adiansyah et al., 2015). Direct disposal, including riverine and marine disposal, refers to discharging tailings to rivers, lakes and ocean directly. Due to the irreversible impact and unsustainability on environmental control, direct disposal is barely put into practice, except in some countries such as Indonesia and Papua New Guinea (Rusdinar et al., 2013; Angela et al., 2013). Compared with direct disposal, indirect disposal, typically discharging tailings into storage facilities, such as embankments, dams and dykes, is regarded as a convenient approach (Qi and Fourie, 2019). Nevertheless, the increasing public awareness of environmental protection has made tailings dams less practical because of its intrinsic drawbacks. First of all, traditional surface management of tailings, especially the oxidation of chemical components (e.g., pyrite), is the main trigger of acid mine drainage. The presence of acid mine drainage will pollute water resources, which makes water unsuitable for domestic and agricultural uses. Even worse, biotic impairment will occur due to the toxicity of the heavy metal leaching (Buckby et al., 2003; Skousen et al., 2017). In addition, the construction of tailings dams occupies a large area of land. For instance, there are currently more than 12000 tailings ponds in China, and the total area of land affected by tailings disposal is up to 2000 hectares (Wang et al., 2017). Another example is that more than 130 km^2 land was affected by the tailings slurry impoundment in Alberta (Canada) in 2011 (Wang et al., 2014). Apart from the environmental issue, tailings dam failure, which is usually caused by a high percentage of water in slurry (Fourie, 2009), poses significant threats to the safety of local communities (Alainachi and Fall, 2020). Up to now, more than 272 cases of tailings dam failure have taken place worldwide since 1917, and Figure 3.2 lists the tailings dam failures happened from 2009 to 2019 (Lottermoser, 2010; WISE Uranium Project, 2019), among which, the tailings dam failure that happened on 25th January 2019 in Brazil led to a catastrophic consequence (Porsani et al., 2019). The tailings wave devastated the mine's loading station and its administrative area, and then it travelled approximately 7 km downhill until reaching Rio Paraopeba. It brought about 249 fatalities, and more than 21 individuals were reported missing.

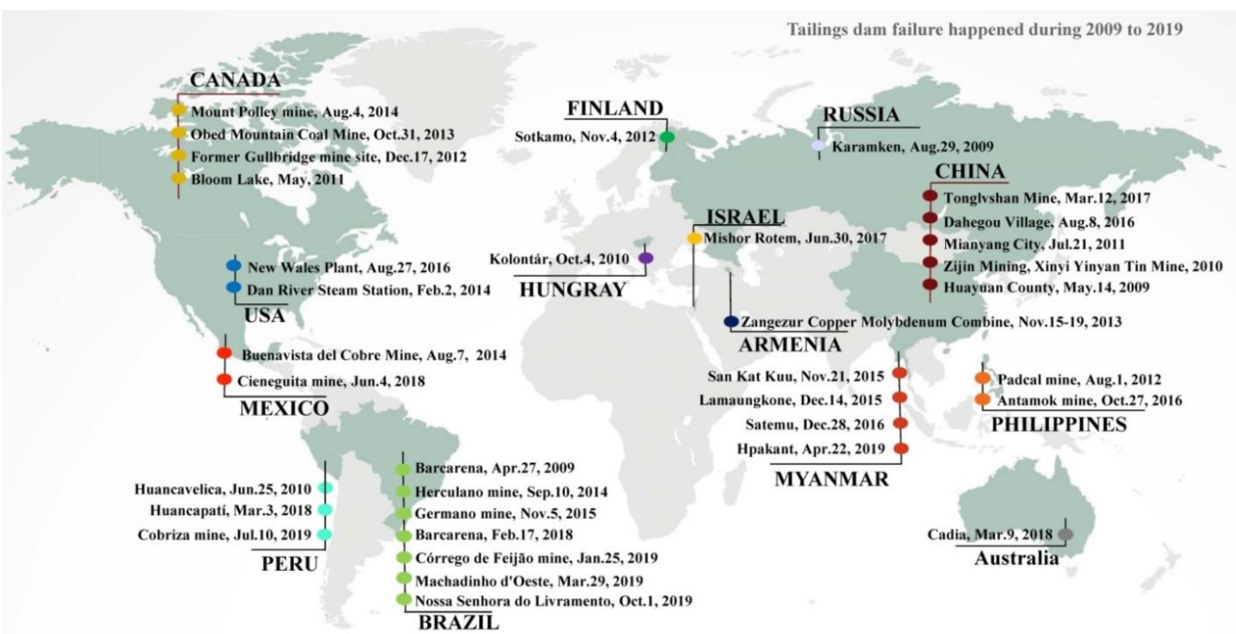

Figure 3.2 Tailings dam failures happened from 2009 to 2019 (The data is updated to Dec. 2019, which is collected from WISE Uranium Project (2019))

Given the above-mentioned reasons, the appearance of cemented paste backfill (CPB, which not only can dispose of the tailings, at the same time, it requires no tailings dam to be built), has the potential to manage the tailings safely, substantially and environment-friendly. Actually, the mine backfill method had been initially proposed for waste management, and then it was known as rockfill in the 1930s. Thereafter, in the 1960s, it was found that the addition of cement to rockfill improved the ground support effect. CPB was not proposed until the mid-1970s, and it was first put into practice at the Bad Grund Mine (Germany) in 1979 (Hustrulid et al., 2001). After being successfully applied in several mines in Canada and Australia in the 1990s, CPB was then regarded as one of the three mine backfill methods (Rankine and Sivakugan, 2007). In the past few decades, CPB has been increasingly adopted by many mines worldwide due to its economic and environmental advantages. The benefits of CPB include but are not confined to (I) minimizing the negative effect of tailings accumulation on the environment; (II) eliminating the risk of tailings dam failure on individuals and society; (III) providing ground support and ensuring the stability of underground structures; (IV) improving the recovery ratio and reducing ore dilution; (V) ensuring the safety of mine workers; (VI) working as a platform and carrying heavy equipment (Yilmaz et al., 2004; Fall et al., 2005; Deb et al., 2017). One major disadvantage of CPB is that the operational cost accounts for 20% of the whole mining expenditure (75% of the CPB expenditure is attributed to the consumption of cement) (Edraki et al., 2014; Jiang et al., 2019). Therefore, how to design stable CPB structures in the most cost-effective manner and then to decrease the investment cost of CPB is one of the key goals of CPB research. To achieve this goal, the understanding of the CPB technology (CPB mix design, transport and mechanical stability) and CPB-rock interface shear behaviour is critical.

The objectives of this manuscript are to:

(i) Provide technical background on CPB technology, including preparation and transport of CPB as well as key properties that define the mechanical stability of CPB.

(ii) Povide a comprehensive review of the progress achieved in understanding and characterizing the CPB-rock interface shear behaviour and properties, from perspectives of both laboratory tests and mathematical modelling.

(iii) Discuss the potential effects of multiphysical loading conditions or factors on the shear performance of the CPB-rock interface and the importance of considering these factors in the assessment of CPB-rock interface behaviour.

3.2 CPB: preparation, transport and mechanical stability

From the preparation of CPB at the ground surface to the transportation and the curing of CPB underground, many processes are involved. Therefore, diversified knowledge is required, including CPB mix design, CPB pipe transport and the mechanical stability or strength of CPB. The three topics mentioned above are introduced briefly below, and interested readers can obtain more detailed information from the studies listed in Table 3.1.

Table 3.1 Studies on CPB mix design, transport and mechanical strength

Research interest	Influencing factors	References
CPB mix design	Tailings and its particle size distribution	Landriault, 2001; Kesimal et al., 2003; Fall et al., 2005; Ercikdi et al., 2013; Ke et al., 2015; Sun et al., 2016; Deb et al., 2017
	Water to cement ratio	Belem and Benzaazoua, 2008; Lin and Meyer, 2009; Monteiro and Mehta, 2014
	Binder type and content	Fall and Benzaazoua, 2005; Ouellet et al. 2006; Celestin and Fall, 2009; Cihangir et al., 2012; Yilmaz 2015;
CPB pipe transport (rheological property of CPB)	Tailings and binder	Westerholm et al., 2008; Niroshan et al., 2018; Mehdipour and Khayat, 2018; Deng et al., 2018;
	Mixing water	Brackebusch, 1994; Johnson et al., 2000; Yu et al., 2018
	Additives and curing conditions	Huynh et al., 2006; Jiang et al., 2016; Ouattara et al., 2017; Marchon et al., 2018; Sada and Fall, 2019
Evolution of mechanical strength of CPB	Binder type and content, Water to cement ratio	Pierce,1997; Belem et al., 2000; Fall et al., 2005; Kesimal et al., 2005; Rankine and Sivakugan, 2007; Fall et al., 2008
	Additives and curing conditions	Kesimal et al., 2004; Fall and Benzaazoua, 2005; le Roux et al., 2005; Fall and Pokharel, 2010; Fall et al., 2010; Veenstra, 2013; Ghirian and Fall, 2013; Li and Fall, 2016; Ghirian and Fall, 2016; Haruna and Fall (2020)

3.2.1 CPB mix design

CPB is prepared as a free-flowing mixture of thickened tailings (with a solid percentage of 70%~85%), binder (Portland cement, blast furnace slag and/or fly ash, commonly 3%~7%) and water. Sometimes, crushed rock is also mixed with tailings to change its particle size distribution. The determination of the recipe is known as CPB mix design, and each of the three main components (i.e., tailings, binder, water) plays an important role in the properties of CPB. For example, the particle size distribution of tailings is related to its specific surface area, which determines the adsorption ability of water molecules. Generally, to avoid slurry separation in transportation, the proportion of fine particles (< 20 um) must be higher than 15 wt% (Landriault, 2001). It was also found that with regard to the uniaxial compressive strength (UCS) of CPB, the optimum proportion of fine particles ranges from 30 wt% to 45 wt% (Fall et al., 2005). Different materials, such as fly ash, slag and cement, can be used as a binder to produce CPB. Among which, cement, especially portland cement Type I (PCI), is the most widely used binder. The amount of cement used not only determines the investment cost, as mentioned above, but also affects the amount of calcium silicate hydrate (C-S-H, a major product of cement hydration), thereby influencing the mechanical strength of CPB (Fall et al., 2010). In some mines located in the eastern part of Canada, they use a mixture of PCI and slag or fly ash as a binder to reduce the cost, and the addition of slag can even improve the mechanical strength of CPB. Interested readers can refer to representative papers listed in Table 3.1 for details. It is well-known that the rate and degree of cement hydration are determined by many factors, which are also discussed in section 2.3. In addition, to ensure the flowability of CPB, the water to cement ratio (w/c) should range from 2.7 to 20.2 (Belem and Benzaazoua, 2008). Water is a necessary component when it comes to the cement hydration as well, and the lack of water leads to uncompleted cement hydration. According to the estimation equation, the cement hydration degree will equal to 1 as long as the w/c is higher than 6.258 (Kjellsen et al., 1991; Wu et al., 2014).

3.2.2 CPB pipe transport

After the preparation of CPB at the ground surface, the homogeneous paste is usually transported to mine cavities (stope) underground through pipes by pumping or gravity. Therefore, the rheological property of CPB is also an important characteristic which requires further investigation. Generally, yield stress, which can be determined by the vane shear or slump test, and viscosity (can be determined by using a viscometer) are properties to evaluate the transportability of CPB (Nguyen and Boger, 1985; Haruna and Fall, 2020; Ali et al., 2021). There are many factors affecting the rheological property of CPB, including solid content, amount and pH value of water, chemical additive and external conditions, etc. (Jiang and Fall, 2017). Specifically, because of the hydrodynamic and granulovirus effect, higher solid content corresponds to higher viscosity (Niroshan et al., 2018; Deng et al., 2018). In addition, the shape and the particle size distribution also affect the rheological properties of CPB. This is because (i) the particle shape influences the "elbow" position (Westerholm et al., 2008); (ii) the increase in the proportion of fine particles increases the specific surface area of solids, thereby decreasing the amount of water at the surface of particles (Mehdipour and Khayat, 2018). The rheological property varies with mixing water through the following two mechanisms: (i) water content – the increasing amount of water (working as a lubricant in the mixture) benefits the improvement of the flowability (Brackebusch, 1994); (ii) pH value of water – the pH of water affects the evolution of zeta potential, which can change the interaction between particles and then affect the shear stress (Johnson et al., 2000). Moreover, the additive and external conditions also affect the flowability of CPB. For example, superplasticizers can improve the rheology of CPB by increasing the electrostatic repulsive force among particles (Huynh et al., 2006; Ouattara et al., 2017; Marchon et al., 2018; Haruna and Fall, 2020). In contrast, the rise of temperature can increase the yield stresss and viscosity of CPB by changing the rate of cement hydration (Jiang et al., 2016; Sada and Fall, 2019).

3.2.3 Mechanical stability

One important function of CPB is to provide ground support, therefore, mechanical stability is one of the most important design criteria of CPB structures (Fall et al., 2007; Fang and Fall, 2020). Regarding the mechanical stability of CPB, the UCS and the shear strength of CPB are often utilized to evaluate its mechanical stability (Yilmaz and Fall, 2017). For example, in terms of the shear strength of CPB, many studies have been conducted to investigate the effects of binder type and content and the degree of cement hydration on the shear strength properties (Belem et al., 2000; Le Roux et al., 2002; Rankine and Sivakugan, 2007; Veenstra, 2013; Ghirian and Fall, 2013). As for the UCS of CPB, it varies with different purposes. For the structure with the sole goal of tailings disposal, the UCS should range from 150 kPa to 300 kPa so as to avoid liquefaction. However, when CPB plays as a ground support, it should have a UCS of up to 4 MPa (Grice, 1998). To sum up, the evolution of the UCS of CPB is up to many factors, such as binder type and content, w/c ratio, additives, curing time and temperature, as well as curing stress (Fall et al., 2005; Kesimal et al., 2005; Li and Fall, 2016; Ghirian and Fall, 2016).

Including the UCS and the shear strength of CPB, another key factor that affects the mechanical stability of underground CPB structures is the shear strength and behaviour of the interface between CPB and the surrounding rock mass, as illustrated in Figure 3.3 (Nasir and Fall, 2008). Nasir and Fall (2008) found out that the shear strength properties (e.g., adhesion, friction angle) of the CPB-rock interface (smooth rock surface) are lower than those of the CPB body. These lower properties indicated that the CPB-rock interface can be a weak plane at which a failure of the CPB structure may occur. Hence, the shear performance of the interface is important when assessing the stability of the CPB structures. Besides, the interaction between CPB and the adjacent rock mass also resulted in the occurrence of the arching effect, which sustained the weight of overlying strata to a high extent (Marston, 1930). The appearance of the arching effect can decrease the amount of the cement used, thereby decreasing the cost of the CPB design. After the placement of CPB underground, the CPB-rock interface is generally subject to complex multiphysics (thermal (T), hydraulic (H), mechanical (M) and chemical (C)) processes. The variation in these processes results in a different rate and degree of cement hydration. Correspondingly, the mechanical response of the interface varies. Therefore, studying the shear behaviour of the CPB-rock interface under different loading conditions is critical to a safer and cost-effective design of CPB structures.

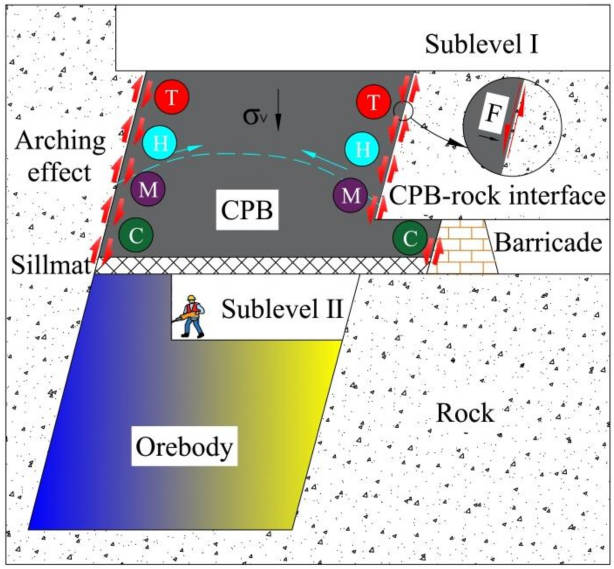

Figure 3.3 Interaction between CPB and adjacent rock mass

3.3 Laboratory tests on the CPB-rock interface

A number of laboratory tests have been conducted on the mechanical properties of the CPB-rock interface. A detailed review of the tests on the CPB-rock interface is presented in this section. As mentioned above, the shear performance of the CPB-rock interface is mainly affected by: (i) curing stress (M); (ii) cement hydration, sulphate attack (C); (iii) heat generated by the cement hydration, geothermal gradients, thermal load from the environment (T); (iv) drainage condition (H); and (v) interface roughness (surface morphology).

3.3.1 Mechanical process

The mechanical processes or factors on the CPB-rock interface mainly include CPB-rock interface curing stress, and normal stress applied to the interface during shearing. As a result of the difference in the geotechnical condition of various mines, the size of orebody varies from each other. This means the lateral pressure on the CPB-rock interface (as a result of self-weight) evolves with the backfill height. In other words, the CPB material at the interface is subjected to variable curing stresses in the field. Hence, assessing the effect of curing stress on the CPB-rock interface is essential to describe the CPB-rock interface in the field. To the best of the author's knowledge, no studies have considered the effect of the curing stress when investigating the shear performance of the CPB-rock interface. All the previous studies on CPB-rock interface shear characteristics were conducted on CPBs cured under stress-free conditions. These studies considered only the normal stress applied to the CPB-rock interface during its shearing. For example, Nasir and Fall (2008) conducted a series of direct shear tests on the CPB-rock samples cured with no stress. The research found out the shear strength of the CPB-rock interface increases with normal stress. Besides, the shear failure envelopes of the interface follow the Mohr-Coulomb criterion. The evolution of the shear strength of the CPB-rock interface (cured for 1day, 3, 7 and 28 days) is shown in Figure 3.4. Moreover, although cured under similar stress-free conditions, the shear strength of the CPB material is found to be greater than that of the CPB-rock interface.

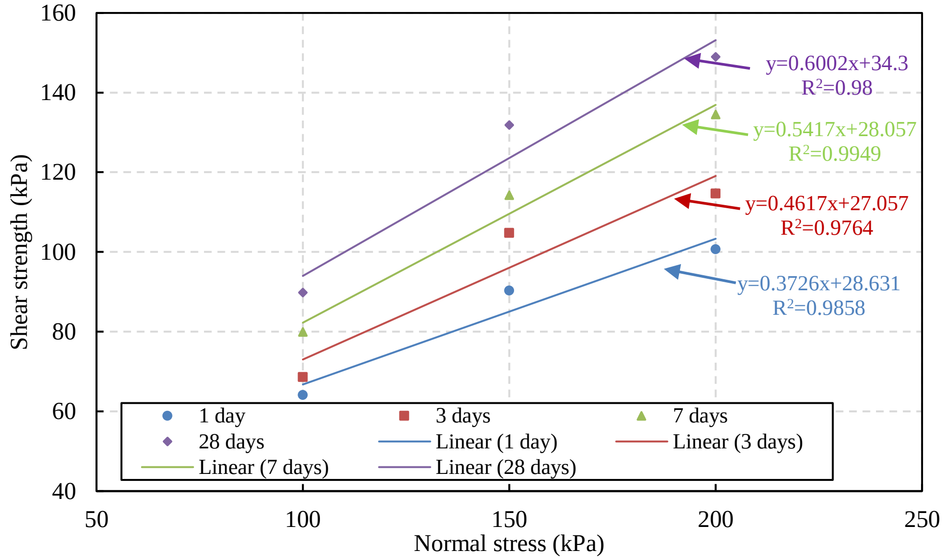

Figure 3.4 Evolution of the shear strength of the CPB-rock interface with normal stress (data from Nasir and Fall 2008)

3.3.2 Chemical process

The chemical process here mainly refers to the cement hydration that occurs in the cementitious material as well as the sulphate attack or effect on cement hydration due to the existence of sulphate ions in CPB. As for the effect of the degree of cement hydration on the shear strength of the CPB-rock interface, studies were conducted on the CPB-limestone and the CPB-concrete interface (Nasir and Fall, 2008, Fall and Nasir, 2010). The evolution of the shear strength of the CPB-limestone with time is shown in Figure 3.4. It can be observed from the figure that the shear strength of the CPB-rock interface increases with the curing time, as a result of the increased degree of the cement hydration. Moreover, Koupouli et al. (2016) prepared some interface samples, and the cement content was designed as 2.3%, 5.3% and 8.2%. The results show that the shear strength of the CPB-rock interface is much more dependent on the binder content than on the curing time. Besides, they also adopt the Mohr-Coulomb criterion to describe the failure envelopes of the interface.

The chemical factor considered by previous studies mainly limits to the degree of the cement hydration. Actually, apart from the cement hydration, there are many sources of sulphate ions in CPB systems (Fall and Benzaazoua, 2005), which also affect the shear properties of the CPB-rock interface. Based on the effect of sulphate ions on UCS of CPB, it potentially influences the shear strength of the CPB-rock interface as well. For now, no studies have been conducted on this knowledge gap.

3.3.3 Thermal process

The thermal characteristics of the CPB-rock interface can be classified into two categories, namely intrinsic properties and external thermal factors. A typical intrinsic property is the thermal conductivity of CPB, while the external thermal factor mainly refers to the thermal condition at the CPB-rock interface, such as the curing temperature and the initial CPB temperature. There are three major heat resources contributing to the thermal condition at the CPB-rock interface: (1) geographical location. The temperature in shallow orebodies is closely related to the seasonal changes of the climate; (2) cement hydration. The exothermic process of cement hydration is a significant heat source for CPB; and (3) geothermal gradients. As the depth of mine varies, the geothermal gradient also leads to the variations of environmental and backfill temperature. As for the thermal conductivity, it is determined by many factors, such as tailings mineralogy, porosity and the degree of saturation (Celestin and Fall, 2009). For example, tailings with higher conductive minerals (e.g., quartz) tend to have higher thermal conductivity (Côté and Konrad, 2005). However, no studies have been conducted on the effects of the thermal factor, particulayly temperature, on the shear properties of the CPB-rock interface so far.

3.3.4 Hydraulic processes

The primary hydraulic properties of the CPB-rock interface include the hydraulic conductivity and the pore water pressure, which are mainly determined by the water saturation and the drainage conditions of the interface. For most laboratory tests, the saturation degree of samples varies with the passage of time. Initially, the sample is fully saturated, however, with the ongoing cement hydration (which consumes a large amount of water), the sample becomes unsaturated. The drainage ability of CPB, inevitably, is determined by such factors as the geometry of the stope, the type of the surrounding rock mass (permeability), the drawpoint location, etc. (EI Mkadmi et al., 2014; Helinski et al., 2010; Yilmaz et al., 2015). Even though the effect of the drainage conditions on the strength of CPB has been investigated by Yilmaz et al., (2009), and Ghirian and Fall (2016), no studies have probed into the shear strength/behaviour of the CPB-rock interface cured under different drainage conditions.

3.3.5 Interface morphology

Most of the samples being tested by previous studies are characterized by a smooth surface, but in reality, the roughness of the CPB-rock interface is determined by the morphology of the surrounding rock. In order to visually characterize the effects of roughness on the shear strength of geomaterials, the joint roughness coefficient (JRC) was proposed by Barton and Choubey (1977). Specifically, the JRC (which was assigned from 0 to 20, with 0 referring to the smoothest profile and 20 to the roughest) was presented by ten standard profiles with different roughness, as shown in Figure 3.5. Then, Manaras et al. (2011) produced two hundred CPB-rock interface samples with five different JRC (0, 3, 11, 15 and 19) to investigate the strength behaviour and failure mechanisms of the CPB-rock interface. They found out that the shear strength derived from Barton's equation (Barton and Choubey, 1977; Li and Zhang, 2015) was lower compared to measured samples. To remedy the difference, they proposed a revised version of Barton's equation to predict the shear strength of the CPB-rock interface. The newly proposed equation considering the adhesion of the CPB-rock interface is expressed as:

$$\tau_p = c + \sigma_n \cdot tan[\varphi_{\mathrm{b}} + JRC \times log_{10}(\frac{JCS}{\sigma_n})] \tag{3-1}$$

where τ_p, c, and JCS are the peak shear stress, the adhesion and the compressive strength of the interface, respectively; σ_n is the applied normal stress, φ_{b} is the basic friction angle.

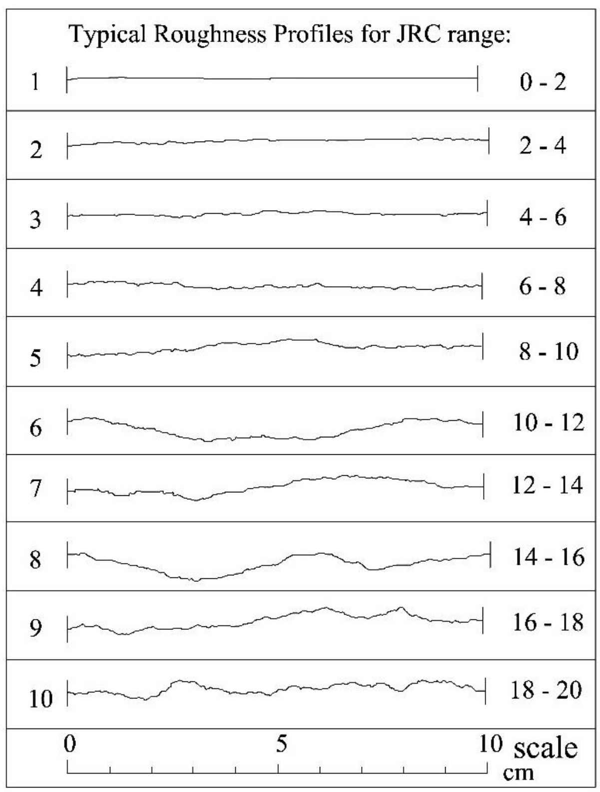

Figure 3.5 Roughness profiles and their JRC values (Barton and Choubey, 1977)

The effect of the rock surface roughness on the shear characteristics of the CPB-rock interface has been ignored in the previous studies, although it is important for a thorough evaluation of the geomechanical stability of CPB structures in the practice.

3.4 Mathematical modelling of the CPB-rock interface

Cohesive zone model (CZM) is effective in simulating the fracture initiation and propagation in interlaminar structures. It was initially proposed by Barenblatt (1959, 1962) and Dugdale (1960) with the Barenblatt-Dugdale (BD) model. The CZM can not only address the stiffness degradation due to the fracture propagation, but also resolve the mesh-sensitivity problem posed by employing nonlocal damage functions (Xie and Waas, 2006). To describe the softening behaviour of sandwich structures, the determination of the traction separation laws (TSLs, such as exponential and polynomial TSL, trapezoidal TSL, bilinear TSL etc.) is a key factor (Needleman, 1987, 1990; Tvergaard and Hutchinson, 1992; Geubelle and Baylor; 1998). For example, Camanho et al. (2003) adopted the bilinear TSL to simulate the delamination in fibre-reinforced composites. For geomaterials, CZM was also used to predict the interfacial fracture between concrete and fibre reinforced polymer (Park et al., 2015). Besides, Mu and Vandanbossche (2017) also used CZM to describe the debonding between concrete and asphalt. However, no studies have demonstrated the shear performance of the CPB-rock interface with CZMs.

There are only a few analytical and numerical studies focusing on the shear properties of the CPB-rock interface (Li and Aubertin, 2008; Fahey et al., 2009; Helinski et al., 2010; Cui and Fall, 2017). An analytical solution based on the arching theory has been developed to evaluate the earth pressure in the three-dimensional backfilled opening (Li and Aubertin, 2008). The effects of the stope size and the friction angle are included to estimate the effective vertical stress, as shown in the following equation:

$$\sigma_v^{'} = \frac{\gamma B}{2k_a \tan\varphi}\left[1-\exp(\frac{-2k_a H \tan\varphi}{B})\right] \tag{3-1}$$

where $\sigma_v^{'}$ is the effective vertical stress, k_a is the active ratio of the lateral stress to the vertical stress, γ is the unit weight of CPB, B and H are the width and height of the CPB structure, φ is the friction angle of the interface.

Fahey et al. (2009) adopted the Mohr-Coulomb model to numerically investigate the effects of the stope size (i.e. the ratio between height and diameter) and the mechanical parameters (e.g., Poisson's ratio, Young's modulus) on the arching effect in CPB. However, they assume the material properties (e.g., adhesion, interface friction angle, Poisson's ratio, Young's modulus) keep constant during the process, although these properties are closely associated with cement hydration. Besides, they only take the mechanical process into consideration, neglecting the influence of multiphysical factors on the material properties and the consolidation behaviour. Helinski et al. (2010) simulated the stress in CPB with Minefill-2D and compared the results with the field measurements. They found out that the arching effect can significantly decrease the pressure in CPB. It is worth mentioning that an integrated multiphysics model was developed by Cui and Fall (2017). To formulate the interface model, the relative displacement is decomposed into elastic and plastic parts, and the Drucker-Prager yield criterion is adopted to describe the initial yield surface of the interface. The time-dependent elastoplastic mechanical behaviour of the CPB-rock interface is fully considered in the developed model. However, most of the interface parameters are derived according to the friction angle and the cohesion of the CPB body, such as the friction angle, the adhesion and the dilation angle of the interface. Besides, the chemical process mentioned in the study only refers to the effect of cement hydration, thereby neglecting the potential influence caused by the sulphate ions in CPB. A detailed summary of the existing numerical simulations of the CPB-rock interface is provided in Table 3.2.

Table 3.2 Summary of existing numerical simulation of CPB-rock interface

Constitutive model	Source	Remarks
Mohr-Coulomb	Fahey et al. (2009)	(1) Stope shape and size are considered; (2) CPB with different material parameters (e.g., adhesion, interface friction angle, Poisson's ratio, Young's modulus) are considered; (3) Drainage conditions and filling rate are simulated; (4) Effects of cement hydration on material parameters are ignored.
Shear yield model Mohr-Coulomb	Helinski et al. (2010)	(1) The change in stiffness due to cement hydration is considered; (2) The reduction in permeability of CPB because of the increasing amount of cement hydration products is considered; (3) The net volume loss as a result of cement hydration is considered; (4) The influence of multiphysics processes on the cement hydration is neglected.
Evolutive elastoplastic model	Cui and Fall (2017)	(1) The effects of multiphysics processes on shear properties of CPB-rock interface are considered; (2) The material parameters are not constant; (3) Most of the interface parameters (e.g., friction angle, adhesion and dilation angle) are derived from the friction angle and the cohesion of CPB. (4) The change in material parameters with time only refers to the effects of cement hydration, neglecting the potential influence of the sulphate ions.

3.5 Coupled THMC processes of the CPB-rock interface

THMC processes are one of the most prominent phenomena in geotechnical and environmental engineering (Ogata et al., 2018; Kolditz et al., 2018). As introduced by previous studies (Ghirian and Fall, 2013, 2014; Cui and Fall, 2015), the CPB behaviour is governed by fully coupled thermo-hydro-mechanical-chemical (THMC) processes. Similarly, the shear performance and the shear properties of the

CPB-rock interface are affected by the coupled multiphysical processes. The interplays between these factors are illustrated in Figure 3.6.

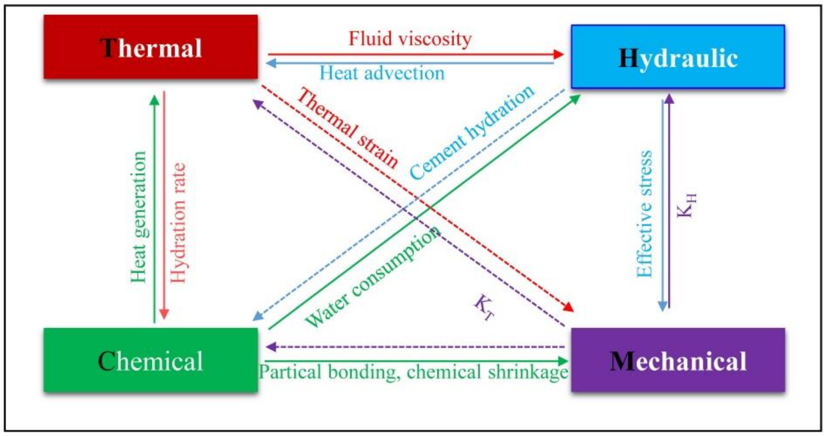

Figure 3.6 Coupled effects of thermal, hydraulic, mechanical, and chemical factors

From the figure, it can be observed that the interactions between the mechanical process and other physics are: (1) M→M: higher overlying stress leads to the reduction in the porosity as well as the refinement of the microstructure of CPB. In addition, it can be beneficial to the increase in the effective stress; (2) M→T: the evolution of the microstructure as well as higher stress-induced water drainage result in a reduction in the thermal conductivity (Celestin and Fall, 2009); (3) M→H: Similarly, finer pore structure decreases the hydraulic conductivity as well; (4) M→C: the reduced thermal conductivity decreases the rate of the heat dissipation in CPB. This results in higher temperature within CPB, which in turn accelerates the rate of the cement hydration, thereby increasing the adhesion and the friction angle of the CPB. Moreover, higher stress can slightly speed up the cement hydration, thereby increasing the adhesion and the friction angle of the CPB. In terms of thermal process, the variation in the temperature within CPB can also have tremendous effects on other processes, such as: (1) T→C: the rate of the cement hydration is temperature-dependent. In other words, a reasonable increase in the temperature can accelerate the rate of the cement hydration. As a result, more C-S-H is generated, thereby benefiting the increase in the adhesion and the friction angle. However, excessively high temperature results in a crossover effect in cementitious materials and consequently leads to a reduction in mechanical parameters (Kjellsen et al., 1991); (2) T→H: a higher temperature corresponds to higher hydraulic conductivity. Meanwhile, it contributes to the evaporation and the consumption of the capillary water, hence leading to an intense self-desiccation. The temperature-induced self-desiccation then benefits to the increase in the matrix suction, thereby increasing the mechanical resistance of CPB. Moreover, the progression of the chemical reaction influences the properties of CPB with the following mechanisms: (1) C→C: the cement hydration is an exothermic process, and the heat generated by it in turn boosts the rate of the cement hydration; (2) C→M: the mechanical strength of CPB generally increases with time due to the progress of binder hydration. However, due to the competition between the strength-decreasing and increasing factors, the existence of the sulphate ions in CPB system can negatively or positively influence the strength of CPB; (3) C→H: the consumption of the capillary pore water by the cement hydration not only leads to a reduction in saturation (increasing the matrix suction), but also contributes to the increase in effective stress. On the other hand, the precipitation of expansive products of the cement hydration, e.g., ettringite and gypsum, will refine or coarsen the capillary pore structure in CPB. Consequently, the change in the microstructure of CPB results in the change of hydraulic conductivity in CPB; (4) C→T: as mentioned above, the reduced thermal conductivity decreases the rate of heat dissipation. The heat generated by cement hydration raises the temperature in CPB. The influence of hydraulic factor on other processes can be concluded as: (1) H→C: the change in the hydraulic conductivity affects the progress of the cement hydration; (2) H→M: the reduction in the amount of water leads to an increase in the effective stress, and this can increase the mechanical strength of CPB.

The sophisticated interaction between the THMC processes indicates the importance of the studies focusing on the effects of the coupled multiphysics processes on the shear properties of the CPB-rock interface. However, most of the existing laboratory and numerical studies on the CPB-rock interface have ignored the effects of these multiphical factors and their coupling on the shear behaviour of the CPB-rock interface.

3.6 Conclusions

The existing laboratory studies and mathematical modelling of the CPB-rock interface as well as the technology of CPB are discussed in this literature review. The previous studies show that the shear performance of the CPB-rock interface plays an important role in the assessment of the stability of CPB structures, and the shear resistance and behaviour of the interface are significantly affected by multiphysics factors. From the literature review, it can be drawn that:

(1) No studies have been conducted to assess the effects of thermal (temperature), chemical (sulphate ions), hydraulic (drainage condition), mechanical (curing stress) and surface morphology (interface roughness) factors on the shear characteristics of the CPB-rock interface. Besides, there is currently no multiphysical model for the CPB-rock interface that can incorporate the aforementioned factors while exploring the shear behaviour of the interface.

(2) The existing laboratory tests only describe the shear strength/behaviour of the CPB-rock interface (cured with no pressure, only taking the effect of the cement hydration into consideration). Besides, the shear failure envelopes of the interface follow the Mohr-Coulomb failure criterion.

(3) The existing mathematical modelling of the CPB-rock interface cannot describe the shear strength/behaviour of the CPB-rock interface comprehensively since they miss taking the sulphate attack and the crossover effect into consideration.

(4) Therefore, a thorough understanding of the shear properties of the CPB-rock interface under various loading conditions is important to safer and cost-effective design of CPB structures. And the major purpose of this PhD research is to experimentally investigate the mechanical responses of CPB-rock interface to different multiphysical loading factors, as well as to develop multiphysical models to describe the shear performance of the CPB-rock interface.

3.7 References

Adiansyah JS, Rosano M, Vink S, Keir G (2015) A framework for a sustainable approach to mine tailings management: disposal strategies. J. Clean. Prod. 108:1050-1062.

Alainachi I, Fall M (2020) Chemically induced changes in the geotechnical response of cementing paste backfill in shaking table test. Journal of Rock Mechanics and Geotechnical Engineering, https://doi.org/10.1016/j.jrmge.2020.11.002

Ali G, Fall M, Alainachi I. (2021) Time-and temperature-dependence of rheological properties of cemented tailings backfill with sodium silicate. Journal of Materials in Civil Engineering 33 (3): 04020498

Angela BM, Simpsona SL, Jarolimeka CV, Junga R, Waworuntub J, Batterham G (2013) Trace metals associated with deep-sea tailings placement at the Batu Hijau copperegold mine, Sumbawa, Indonesia. Mar. Pollut. Bull. 73:306-313.

Barenblatt GI (1959) The formation of equilibrium cracks during brittle fracture. General ideas and hypotheses. Axially-symmetric cracks. Journal of Applied Mathematics and Mechanics 23:622–636.

Barenblatt GI (1962) The mathematical theory of equilibrium cracks in brittle fracture. Advances in applied mechanics 7:55–129.

Barton N, Choubey V (1977) The shear strength of rock joints in theory and practice. Rock mechanics 10(1):1-54.

Belem T, Benzaazoua M (2008) Design and application of underground mine paste backfill technology. Geotech. Geol. Eng. 26:147-174.

Belem T, Benzaazoua M, Bussière B (2000) Mechanical behaviour of cemented paste backfill. In: Proceedings of the Canadian geotechnical society conference geotechnical engineering at the Dawn of the Third Millennium 15–18 October, Montréal, vol. l, 373-380

Brackebusch FW (1994) Basics of paste backfill systems. Miner. Eng. 46(10):1175-1178.

Buckby T, Black S, Coleman ML, Hodson ME (2003) Fe-sulphate-rich evaporative mineral precipitates from the Rio Tinto, southwest Spain. Mineral. Mag. 67(2):263-278.

Camanho PP, Davila CG, De Moura M (2003) Numerical simulation of mixed-mode progressive delamination in composite materials. Journal of composite materials 37(16):1415-1438.

Celestin J, Fall M (2009) Thermal conductivity of cemented paste backfill material and factors affecting it. International Journal of Mining, Reclamation and Environment 23(4):274–290.

Cihangir F, Ercikdi B, Kesimal A, Deveci H (2012) Utilisation of alkali-activated blast furnace slag in paste backfill of sulphide mill tailings: Effect of binder type and dosage. Miner. Eng. 30:33-43.

Côté J, Konrad J-M (2005) A generalized thermal conductivity model for soils. Canadian Geotechnical Journal 42(2):443-458.

Cui L, Fall M (2015) A coupled thermo–hydro-mechanical–chemical model for underground cemented tailings backfill. Tunnelling and Underground Space Technology 50:396-414.

Cui L, Fall M (2017) Multiphysics modelling of arching effects in fill mass, Comput. Geotech. 83:114–131.

Deb D, Sreenivas T, Dey GK, Panchal S (2017) Paste Backfill Technology: Essential Characteristics and Assessment of its Application for Mill Rejects of Uranium Ores. Transactions of the Indian Institute of Metals, 70(2):487-495.

Deng XJ, Klein B, Tong LB, De Wit B (2018) Experimental study on the rheological behaviour of ultra-fine cemented backfill. Constr. Build. Mater. 158:985-994.

Dudeney AWL, Chan BKC, Bouzalakos S, Huisman JL (2013) Management of waste and wastewater from mineral industry processes, especially leaching of sulphide resources: state of the art. Int. J. Min. Reclam. Environ. 27:2-37.
Dugdale DS (1960) Yielding of steel sheets containing slits. Journal of the Mechanics and Physics of Solids 8:100–104.
El Mkadmi N, Aubertin M, Li L (2014). Effect of drainage and sequential filling on the behaviour of backfill in mine stopes. Canadian Geotechnical Journal 51:1–15.
Ercikdi B, Baki H, Izki M (2013) Effect of desliming of sulphide-rich mill tailings on the long-term strength of cemented paste backfill. J. Environ. Manage. 115:5-13.
Edraki M, Baumgartl T, Manlapig E, Bradshaw D, Franks DM, Moran CJ (2014) Designing mine tailings for better environmental, social and economic outcomes: a review of alternative approaches. J. Cleaner Prod. 84:411-420.
Fahey M, Helinski M, Fourie A (2009) Some aspects of the mechanics of arching in backfilled stopes. Can. Geotech. J. 46(11):1322–36.
Fall M, Benzaazoua M (2005) Modelling the effect of sulphate on strength development of paste backfill and binder mixture optimization. Cem. Concr. Res. 35(2):301-314.
Fall M, Benzaazoua M, Ouellet S (2005) Experimental characterization of the influence of tailings fineness and density on the quality of cemented paste backfill. Miner. Eng. 18(1):41-44.
Fall M, Belem T, Samb S, Benzaazoua M (2007) Experimental characterization of the stress-strain behaviour of cemented paste backfill in compression. J. Mater. Sci. 42(11):3914-3992
Fall M, Benzaazoua M, Saa EG (2008) Mix proportioning of underground cemented tailings backfill. Tunn. Undergr. Space. Technol. 28(1):80-90.
Fall M, Celestin JC, Pokharel M, Toure M (2010) A contribution to understanding the effects of curing temperature on the mechanical properties of mine cemented tailings backfill. Engineering Geology, 114(3-4):397-413.
Fall M, Nasir O (2010) Mechanical behaviour of the interface between cemented tailings backfill and retaining structures under shear loads. Geotech. Geol. Eng. 28(6):779-790.
Fall M, Pokharel M (2010) Coupled effect of sulphate and temperature on the strength development of cemented backfill tailings: Portland cement paste backfill. Cem. Concr. Compos. 32(10):819-828.
Fang K, Fall M (2020) Insight into the mode I and mode II fracture toughness of the cemented backfill-rock interface: Effect of time, temperature and sulphate. Construction and Building Materials 262: 120860
Fourie A (2009) Preventing catastrophic failures and mitigating environmental impacts of tailings storage facilities. Procedia Earth Planet. Sci. 1:1067-1071.
Geubelle PH, Baylor J (1998) Impact-induced delamination of laminated composites: a 2D simulation. Composites Part B Engineering, 29(5):589–602.
Ghirian A, Fall M (2013) Coupled thermo-hydro-mechanical–chemical behaviour of cemented paste backfill in column experiments. Part I: physical, hydraulic and thermal processes and characteristics. Eng. Geol. 164:195-207.
Ghirian A, Fall M (2014) Coupled thermo-hydro-mechanical-chemical behaviour of cemented paste backfill in column experiments. Engineering Geology 170:11-23.
Ghirian A, Fall M, (2016) Strength evolution and deformation behaviour of cemented paste backfill at early ages: effect of curing stress, filling strategy and drainage. International Journal of Mining Science and Technology 26(5):809-817.
Grice T (2001) Recent mine developments in Australia. Proceedings of the 7th International Symposium on Mining with Backfill (MINEFILL), 351-357.
Haruna S, Fall M (2020). Strength Development of Cemented Tailings Materials Containing Polycarboxylate ether-based Superplasticizer: Experimental Results on the Effect of Time and Temperature. Canadian Journal of Civil Engineering, https://doi.org/10.1139/cjce-2019-0809
Helinski M, Fahey M, Fourie A (2010) Behaviour of cemented paste backfill in two mine stopes: measurements and modelling. J. Geotech. Geoenviron. 137(2):171–82.
Hustrulid WA, Hustrulid WA, Bullock RL, Bullock RC (2001) Underground Mining Methods: Engineering Fundamentals and International Case Studies. Society for Mining, Metallurgy, and Exploration, Colorado, USA.
Huynh L, Beattie DA, Fornasiero D, Ralston J (2006) Effect of polyphosphate and naphthalene sulfonate formaldehyde condensate on the rheological properties of dewatered tailings and cemented paste backfill, Miner. Eng. 19(1):28-36.
Jiang HQ, Fall M, Cui L (2016) Yield stress of cemented paste backfill in sub-zero environments: experimental results. Miner. Eng. 92:141-150.

Jiang H, Fall M (2017). Yield stress and strength of saline cemented tailings materials in sub-zero environments: slag-paste backfill. Journal of Sustainable Cement-Based Materials 6 (5), 314-331.
Jiang H, Qi Z, Yilmaz E, Han J, Qiu J, Dong C (2019) Effectiveness of alkali-activated slag as alternative binder on workability and early age compressive strength of cemented paste backfills. Constr. Build. Mater. 218:689-700.
Johnson SB, Franks GV, Scales PJ, Boger DV, Healy TW (2000) Surface chemistry rheology relationships in concentrated mineral suspensions. Int. J. Miner. Process. 58:267-304.
Jones H, Boger DV (2012) Sustainability and waste management in the resource industries. Ind. Eng. Chem. Res. 51:10057-10065.
Ke X, Hou HB, Zhou M, Wang Y, Zhou X (2015) Effect of particle gradation on properties of fresh and hardened cemented paste backfill. Constr. Build. Mater. 96:378-382.
Kesimal A, Ercikdi B, Yilmaz E (2003) The effect of desliming by sedimentation on paste backfill performance. Miner. Eng. 16:1009-1011.
Kesimal A, Yilmaz E, Ercikdi B, Deveci H (2005) Effect of properties of tailings and binder on the short-and long-term strength and stability of cemented paste backfill. Mater. Lett. 59(28):3703-3709.
Kesimal A, Yilmaz E, Erikdi B (2004) Evaluation of paste backfill mixtures consisting of sulphide-rich mill tailings and varying cement contents. Cem. Concr. Res. 34(10):1817-1822.
Kjellsen KO, Detwiler RJ, Gjørv OE (1991) Development of microstructures in plain cement pastes hydrated at different temperatures. Cem. Concr. Res. 21(1):179–89.
Kolditz O, Nagel T, Shao H, Wang W, Bauer S (2018) Thermo-Hydro-Mechanical-Chemical Processes in Fractured Porous Media: Modelling and Benchmarking: From Benchmarking to Tutoring: Springer.
Koupouli NJF, Belem T, Rivard P, Effenguet H (2016) Direct shear tests on cemented paste backfill-rock wall and cemented paste backfill-backfill interfaces. J. Rock. Mech. Geotech. Eng. 8(4):472-479.
Landriault D (2001) Backfill in underground mining. In: Hustrulid, W.A. (Ed.), Underground Mining Methods: Engineering Fundamentals and International Case Studies. Society for Mining, Metallurgy, and Exploration, Colorado, USA, 601-614.
Le Roux KA, Bawden WF, Grabinsky MWF (2002) Comparison of the material properties of in situ and laboratory prepared cemented paste backfill. In: Annual conference, BC, Canada, 201-209.
Li L, Aubertin M (2008) An improved analytical solution to estimate the stress state in subvertical backfilled stopes. Canadian Geotechnical Journal 45(10):1487-1496.
Li Y, Zhang Y (2015) Quantitative estimation of joint roughness coefficient using statistical parameters. International Journal of Rock Mechanics and Mining Sciences (77):27-35.
Li W, Fall M (2016) Sulphate effect on the early age strength and self-desiccation of cemented paste backfill. Construct. Build. Mater. 106:295-304.
Lin F, Meyer C (2009) Hydration kinetics modeling of Portland cement considering the effects of curing temperature and applied pressure. Cem. Concr. Res. 39:255-265.
Lottermoser BG (2010) Mine Wastes. Springer-Verlag Berlin Heidelberg, New York.
Lu X, Wang H (2012) Microbial oxidation of sulphide tailings and the environmental consequences. Elements 8:119-124.
Marchon D, Kawashima S, Bessaies-Bey H, Mantellato S, Ng S (2018) Hydration and rheology control of concrete for digital fabrication: Potential admixtures and cement chemistry. Cem. Concr. Res. 112:96-110.
Marston A (1930) The theory of external loads on closed conduits in the light of latest experiments. Highway research board proceedings, Ames Iowa.
Mehdipour I, Khayat KH (2018) Understanding the role of particle packing characteristics in rheo-physical properties of cementitious suspensions: a literature review. Constr. Build. Mater. 161:340-353.
Monteiro P, Mehta PK (2014) Concrete: Microstructure, Properties, and Materials. McGraw-Hill Education.
Nasir O, Fall M (2008) Shear behaviour of cemented pastefill-rock interfaces. Eng. Geol. 101(3):146-153.
Needleman A (1987) A continuum model for void nucleation by inclusion debonding. Journal of Applied Mechanics 54:525-531.
Needleman A (1990) An analysis of tensile decohesion along an interface. Journal of the Mechanics and Physics of Solids 38:289-324.
Nguyen QD, Boger DV (1985) Direct yield stress measurement with the vane method. J. Rheol. 29(3):335-347.
Niroshan N, Sivakugan N, Veenstra RL (2018) Flow characteristics of cemented paste backfill. Geotech. Geol. Eng. 36:2261-2272.
Ogata S, Yasuhara H, Kinoshita N, Cheon DS, Kishida K (2018) Modelling of coupled thermal-hydraulic-mechanical-chemical processes for predicting the evolution in permeability and reactive transport behaviour within single rock fractures. International journal of rock mechanics and mining sciences 107, 271-281.

Ouattara D, Yahia A, Mbonimpa M, Belem T (2017) Effects of superplasticizer on rheological properties of cemented paste backfills. Int. J. Miner. Process. 161:28-40.
Ouellet S, Bussière B, Mbonimpa M, Benzazoua M, Aubertin M (2006) Reactivity and mineralogical evolution of an underground mine sulphidic cemented backfill. Miner. Eng. 19:407-419.
Park K, Ha K, Choi H, Lee C (2015) Prediction of interfacial fracture between concrete and fiber reinforced polymer (FRP) by using cohesive zone modelling. Cement and Concrete Composites 63:122-131.
Pierce ME (1997) Laboratory and numerical analysis of the strength and deformation behaviour of paste backfill, Master's thesis. Department of Mining Engineering, Queen's University, Kingston.
Porsani JL, Jesus FANd, Stangari MC (2019) GPR Survey on an Iron Mining Area after the Collapse of the Tailings Dam I at the Córrego do Feijão Mine in Brumadinho-MG, Brazil. Remote Sensing, 11(7), 860.
Qi C, Fourie A (2019). Cemented paste backfill for mineral tailings management: Review and future perspectives. Miner. Eng.144, 106025.
Rankine RM, Sivakugan N (2007) Geotechnical properties of cemented paste backfill from Cannington Mine, Australia. Geotech. Geol. Eng. 25:383-393.
Rusdinar Y, Edraki M, Baumgartl T, Mulligan D (2013) Long term performance of hydrogeochemical riverine mine tailings deposition at Freeport Indonesia. Mine Water Environ. 32 (1):56-70.
Haruna S, Fall M (2019) Time-and temperature-dependent rheological properties of cemented paste backfill that contains superplasticizer. Powder technology. 360, 731-740.
Haruna S, Fall M (2020) Strength Development of Cemented Tailings Materials Containing Polycarboxylate ether-based Superplasticizer: Experimental Results on the Effect of Time and Temperature. Canadian Journal of Civil Engineering(ja).
Skousen J, Zipper CE, Rose A, Ziemkiewicz PF, Nairn R, McDonald LM, Kleinmann RL (2017) Review of passive systems for acid mine drainage treatment. Mine Water and the Environment, 36(1):133-153.
Sun W, Wu AX, Hou KP, Yang Y, Liu L, Wen YM (2016) Experimental study on the microstructure evolution of mixed disposal paste in surface subsidence areas. Minerals, 6, 42.
The Mining Association of Canada (2019) Mining Facts. Available at http://mining.ca/resources/mining-facts
Tvergaard V, Hutchinson JW (1992) The relation between crack growth resistance and fracture process parameters in elastic-plastic solids. Journal of the Mechanics and Physics of Solids 40:1377–1397.
Veenstra RL (2013) A design procedure for determining the in situ stresses of early age cemented paste backfill. PhD thesis, University of Toronto, 275
Wang C, Harbottle D, Liu Q, Xu Z (2014) Current state of fine mineral tailings treatment: A critical review on theory and practice. Miner. Eng. 58:113-131.
Wang L, Ji B, Hu Y, Liu R, Sun W (2017) A review on in situ phytoremediation of mine tailings. Chemosphere, 184:594-600.
Westerholm M, Lagerblad B, Silfwerbrand J, Forssberg E (2008) Influence of fine aggregate characteristics on the rheological properties of mortars. Cem. Concr. Compos. 30:274-282.
WISE Uranium Project (2019) http://www.wise-uranium.org/mdaf.html
Wu D, Fall M, Cai SJ (2014) Numerical modelling of thermally and hydraulically coupled processes in hydrating cemented tailings backfill columns. Int. J. Min. Reclam. Environ. 28(3):173-199.
Xie D, Waas AM (2006) Discrete cohesive zone model for mixed-mode fracture using finite element analysis. Engineering Fracture Mechanics 73(13):1783-1796.
Yilmaz E, Belem T, Bussiere B, Mbonimpa M, Benzaazoua M (2015). Curing time effect on consolidation behaviour of cemented paste backfill containing different cement types and contents. Const. Build. Mater. 75:99–111.
Yilmaz E, Benzaazoua M, Belem T, Bussière B (2009) Effect of curing under pressure on compressive strength development of cemented paste backfill. Minerals Engineering 22(9):772-785.
Yilmaz E, Kesimal A, Ercidi B (2004) Strength development of paste backfill simples at Long term using different binders. Proceedings of 8th symposium MineFill04, China.
Yilmaz E, Fall M (2017) Paste tailings management: Springer.
Yilmaz E (2015) Environmental characterization of surface paste disposal. LAP LAMBERT Academic Publishing, ISBN: 978–3–659-36697-0, Saarbrucken, Deutschland/Germany
Yu Y.X, Ma LQ, Xu HX, Sun XF, Zhang ZJ, Ye GC (2018) DLVO theoretical analyses between montmorillonite and fine coal under different pH and divalent cations. Powder. Technol. 330:147-151.

Chapter 4 Testing of CPB-Rock Interface Shear Behaviour

4.1 Introduction

The interaction between CPB and surrounding rock mass is governed by complex multiphysics processes. Consequently, the shear performance of the CPB-rock interface varies under different thermal, hydraulic, mechanical, and chemical conditions. However, based on the literature review of previous research work (chapter 3), there are limited studies conducted on the shear behaviour of the CPB-rock interface, and none of them have addressed the effects of thermal (curing temperature), chemical (sulphate ions), hydraulic (drainage) and mechanical (curing stress) factors on the shear behaviour of the CPB-rock interface. Therefore, to design CPB structures economically as well as ensure the stability of CPB structures, series of laboratory experiments focusing on the shear behaviour of CPB-rock interface under different multiphysics (chemical, mechanical, hydraulic, and thermal) conditions are conducted in this chapter.

Section 4.2 illustrates the changes in the shear strength properties of the early-age CPB-rock interface due to the existence of different amounts of sulphate ions. It is found that sulphate ions can positively or negatively affect the evolution of the shear strength properties, depending on the initial sulphate contents and curing ages. Section 4.3 describes the effect of temperature on the speed and the degree of the cement hydration, and consequently, the shear behaviour of the interface samples subjected to different thermal conditions is investigated. A higher temperature usually speeds up the process of the cement hydration, and as a result, the shear strength of the interface increases with temperature. However, for samples cured at 35°C for 28 days, the shear strength is slightly lower than that of those cured at 20°C due to the crossover effect. Section 4.4 shows the shear behaviour of CPB-rock interface samples cured with different stresses and drainage conditions. The shear strength of the interface is found positively associated with the magnitude of the curing stress. Besides, a drained condition is beneficial to the strength development due to the stronger matric suction and the finer pore structure at the interface. The sulphate attack on the shear strength properties of the advanced-age interface is presented in section 4.5 while the effect of the rock type as well as the surface morphology on the shear behaviour of the CPB-rock interface is shown in section 4.6. For highly-sulphated samples, the shear strength experiences a slight reduction after been cured for 90 days because of the physical damage in the microstructure caused by the generation of excessive amount of expansive cement hydration products. However, the increasing shear strength of samples with sulphate contents lower than 5000 ppm is due to the higher degree of cement hydration with time. Moreover, the shear strength of the CPB-rock interface rises with surface roughness because of the larger contacting area between CPB and rock. The specific details and findings of these experiments are presented and discussed in section 4.2, 4.3, 4.4, 4.5 and 4.6.

4.2 Paper II: Chemically induced changes in the shear behaviour of interface between rock and tailings backfill undergoing cementation

Published in *Rock Mechanics and Rock Engineering*, 2019, 52(9): 3047-3062.

Kun Fang, Mamadou Fall

Abstract

Tailings are man-made soils generated by mining activities. When mixed with cement and water, they form a cemented soil called cemented paste backfill (CPB). CPB is commonly used to backfill underground cavities created by ore extraction. The shear behaviour and resistance of the CPB-rock interface are important parameters for the geotechnical design of underground CPB structures. However, CPB can contain a relatively high amount of sulphate, and no studies have been performed to investigate the effect of the initial sulphate content of CPB on the behaviour and resistance of the interface between rock and tailings backfill that is undergoing cementation. The main objective of this experimental investigation is to therefore examine the effects of the initial sulphate content (0 ppm, 5,000 ppm, 15,000 ppm, and 25,000 ppm) of CPB on the shear behaviour of the CPB-rock interface at the early ages of curing (1 day, and 3 and 7 days). The obtained results show that for samples at a very early age of 1 day, an increase in the sulphate content reduces the shear strength of the CPB-rock interface, whereas for those cured for a longer period of 7 days, the sulphate can either positively or negatively affect the shear strength of the interface depending on the sulphate content. The findings are important for barricade opening and scheduling the extraction of primary stopes, which contribute to improving mining productivity.

Keywords: Cemented paste backfill; tailings; rock; sulphate content; shear behaviour; interface

4.2.1 Introduction

Mining is an important activity that contributes to different economies worldwide. For example, mining contributed \$57.6 billion CAD to the gross domestic product (GDP) of Canada, and accounted for 19% of the value of Canadian goods export in 2016 (Mining Association of Canada, 2018). Mining is also an important part of the economy in China with an increase in metal production (including copper (Cu), lead (Pb), zinc (Zn), aluminum (Al), magnesium (Mg), gold (Au), silver (Ag) and platinum (Pt)) from 18.9 million tons in 2006 to 47.1 million tons in 2015 (Chinese Industry Information, 2016). On the other hand, the mining industry is also considered to be the largest solid waste producer (e.g., tailings, waste rock) worldwide. Among the different types of solid wastes, tailings have some of most detrimental effects on the ecosystem and society. Traditionally, tailings are disposed and stored in tailings storage facilities (TSFs, e.g., embankments and dams) above ground. However, these facilities have suffered from numerous geotechnical failures in the past. Therefore, they pose significant threats to the safety of the local community. Moreover, traditional surface tailings management methods can also be a major source of acid mine drainage (AMD), which can pollute the surface water, groundwater as well as the environment (Buckby et al., 2003). All of these issues have made it necessary to find alternative methods to manage tailings in a safer, more economical and environmentally friendly way.

Cemented paste backfilling is regarded as an innovative method and it was first introduced in the Bad Grund Mine (Germany) in the late 1970s. Cemented paste backfill (CPB) materials mainly consist of thickened tailings (with a solid percentage of 70%~85%), binder (commonly 3%~7%) and water. Cemented paste backfilling has been increasingly adopted in many underground mines worldwide (Brackebusch, 1994; Hassani and Archibald, 1998; Fall and Nasir, 2010). This method (a) ensures the stability of underground structures, (b) improves the recovery ratio (that is, increases mine productivity), and (c) provides a more environmentally friendly means of the underground disposal of tailings (Fall et al., 2005). The CPB is prepared in a backfill plant, usually located on the mine surface, and then transported through pipelines to fill the underground mine cavities (stopes).

One of the main design criteria of CPB structures is mechanical stability, which is critical to ensure the safety of the mine workers. Moreover, mechanical failure of CPB structures often has severe financial consequences for a mine. A key factor that can affect the mechanical stability of CPB structures is the shear strength and behaviour of the interface between the CPB and rock mass that is surrounding or adjacent to the CPB structure. The shear strength of CPB-rock interface plays a critical role in the arching effect. Therefore, an understanding and assessment of the shear behaviour or properties of the CPB-rock interface are critical for the evaluation and prediction of the arching effect in CPB. Backfill arching, which involves load transfer and stress redistribution, needs to be considered in the geotechnical design or stability assessment of CPB structures. The arching effect is induced by shear stress along the interface between the CPB and the surrounding or adjacent rockmass (Pirapakaran and Sivakugan, 2007) and when it occurs, the vertical stress in the backfilled body is significantly less than the in-situ stress due to self-weight (Marston, 1930). This means that considering the arching effect can effectively reduce the cost of CPB design, as in doing so, reduces the amount of cement used, which can be as much as 75% of the cost of CPB (Grice, 2001). A schematic diagram of the arching effect in CPB and vertical stress distribution is shown in Figure 4.1.

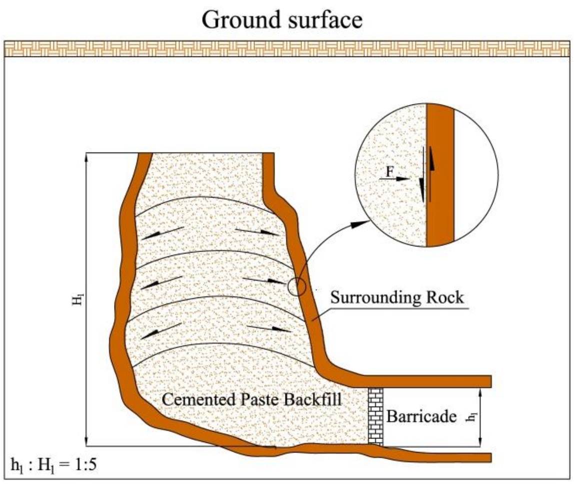

(a) Interaction between CPB and surrounding rock

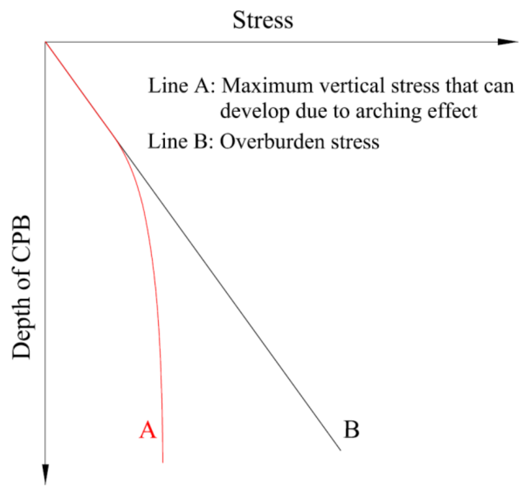

(b) Arching and maximum vertical stress distribution in CPB

Figure 4.1 Schematic diagram of arching effect and stress distribution in CPB

From the discussion above, it is evident that the assessment and an understanding of the shear behaviour and properties at the interface between the rock and CPB are essential for the safe and cost-effective design of CPB structures. However, to date, only a few studies have been conducted on the interface behaviour of CPB-rock (e.g., Aubertin et al., 2003; Nasir and Fall, 2008; Fall and Nasir, 2010; Koupouli et al., 2016). Despite the substantial improvement in understanding of the shear properties of CPB-rock interface, none of these studies have addressed the effect of sulphate on the interface properties and behaviour of CPB-rock. Since CPB often contains sulphate ions (Orejarena et al., 2010; Li and Fall, 2016), there is the need to address this knowledge gap. Sulphate ions in CPB systems mainly originate from the oxidation of sulphide minerals in the tailings, use of mine processed water as the mixing water, oxidization of cyanide with the use of sulphur dioxide, and the addition of gypsum (a sulphate material; $CaSO_4 \cdot 2H_2O$) or anhydrite (an anhydrous calcium sulfate; $CaSO_4$) to reduce the setting time of cement (Fall and Benzaazous, 2005; Ercikdi et al., 2009). Therefore, the main objective of this paper is to experimentally study and present the results of the effect of sulphate on the shear behaviour of the CPB-rock interface with CPB cured at the early ages of 1, 3, and 7 days.

4.2.2 Experimental Program

4.2.2.1 Materials

4.2.2.1.1 Tailings

Two types of tailings were used to prepare the CPB: natural and artificial tailings. Natural tailings (NT; Figure 4.2(b)) were obtained from a backfill plant of a polymetallic mine located in northern Canada. However, to eliminate or reduce the uncertainties in the results due to the use of NT (the chemical composition of NT can change during storage and/or the preparation of CPB and thus affect the results), artificial tailings (silica tailings (ST); Figure 4.2(a)) were also used in lieu of NT. The ST have a grain size similar to that of the NT (Figure 4.3). The mineralogical composition and grain size distribution of the tailings used are shown in Table 4.1 and Figure 4.3, respectively. The ST contain 99.8% silicon dioxide (SiO_2) and are essentially made of quartz, which is the dominant mineral found in hard rock mines in Canada. Besides, the ST also have a particle size distribution similar to the average particle size distribution of tailings found in nine Canadian mines (see Figure 4.3). The NT are rich in oxides such as pyrite which could oxidize during CPB preparation (Nasir and Fall, 2008).

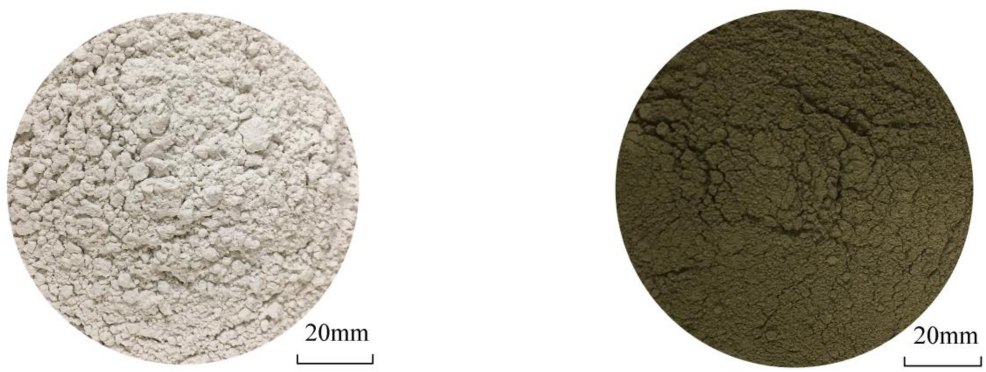

(a) Silica tailings (b) Natural tailings

Figure 4.2 Grain size of silica tailings vs. natural tailings (polymetallic tailings)

Table 4.1 Mineralogical composition of tailings used in this study

Tailings/ Mineral	Quartz (wt.%)	Talc (wt.%)	Dolo-mite (wt.%)	Magnesite (wt.%)	Chlo-rite (wt.%)	Magne-tite (wt.%)	Pyrite (wt.%)	Pyrrhotite (wt.%)	Other (wt.%)
NT	11.9	16.4	5.7	7.6	18.2	11.4	15.4	3.1	10.3
ST	99.8	/	/	/	/	/	/	/	

4.2.2.1.2 Binder

The binder used in this study for all the samples is 4.5 wt.% of portland cement Type I (PCI). Table 4.2 shows the chemical composition of the PCI.

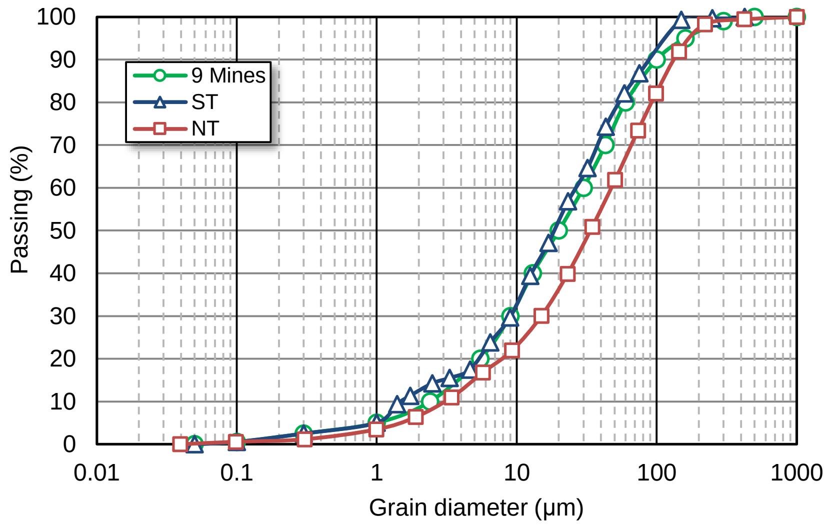

Figure 4.3 Grain size distribution of silica tailings (ST) and natural tailings (NT), and average grain size distribution of tailings from nine eastern Canadian mines

Table 4.2 Chemical composition of portland cement Type I

Component Unit	SO_3 (wt.%)	Fe_2O_3 (wt.%)	Al_2O_3 (wt.%)	SiO_2 (wt.%)	CaO (wt.%)	MgO (wt.%)
PCI	3.82	2.70	4.53	18.03	62.82	2.65

4.2.2.1.3 Rock samples

The rock used for the samples was granite with an average uniaxial compressive strength of 160 MPa. The granite was cut into samples with dimensions of 60×60×10 mm by using a special rock cutter. Then, the surface of the samples was polished. To study the effects of surface roughness on the properties of the CPB-rock interface, granite samples with two different levels of roughness was prepared (see Figure 4.4). The roughness was evaluated by determining the joint roughness coefficient (JRC) (Tse and Cruden, 1979; Maerz et al., 1990; Yang et al., 2001). To quantitatively determine the JRC of the samples, the coordinates along the profile centerline were also measured by using a highly precise linear variable differential transformer (LVDT). Then, the JRC of the granite samples with two different levels of roughness can be derived from the equation in Yu and Vayssade (1991):

$$Z_2 = \left[\frac{1}{L} \sum \frac{(y_{i+1} - y_i)^2}{(x_{i+1} - x_i)^2} \right]^{1/2} \tag{4-1}$$

$$JRC = 32.69 + 32.98 \log Z_2 \quad (4\text{-}2)$$

where Z_2 is a surface parameter that indicates the root mean square of the first derivative of the profile, L is the number of the discrete points along the centerline and (x_i, y_i) are the coordinates of a discrete point.

Figure 4.4 Granite samples with different levels of roughness

Barton and Choubey (1977) provided roughness profiles with JRC values that ranged from 0 to 20 for assessing the roughness of rock surfaces, in which 18-20 denotes very rough surfaces. The JRC values of the two granite profiles were determined accordingly as 0 and 1.76 respectively, as shown in Table 4.3.

Table 4.3 JRC values of granite samples

Granite	Width of grooves	Slope of grooves	JRC of profile
R0	/	/	0
R1	1.83	0.76	1.76

4.2.2.1.4 Mixing water

Distilled water was used as mixing water in the experiment. Specific amounts of ferrous sulphate heptahydrate ($FeSO_4 \cdot 7H_2O$) were mixed into the distilled water for sulphate contents of 0 ppm, 5,000 ppm, 15,000 ppm and 25,000 ppm.

4.2.2.2 Testing method and sample preparation

4.2.2.2.1 Testing apparatus

A direct shear device which is used to test the shear behaviour and resistance of the CPB-rock interface in this study is shown in Figure 4.5. The two LVDTs are used to measure the horizontal and vertical displacements respectively, while the load cell is used for load measurements. To ensure that the experimental data are relevant to the interface, the CPB and granite samples are placed between the two halves of the shear box. In other words, the lower half of the shear box contains the granite part of the sample while the upper half of the shear box holds the CPB part of the sample. In addition, several steel balls are also placed on the perimeter between the two halves of the shear box to ensure that the sliding plane is right at the interface of the CPB and rock. A constant normal stress was applied to the samples by a vertical arm above the shear box and when shearing, the lower half of the shear box was driven by a motor with a speed of 0.5 mm/min while the upper half of the shear box did not move.

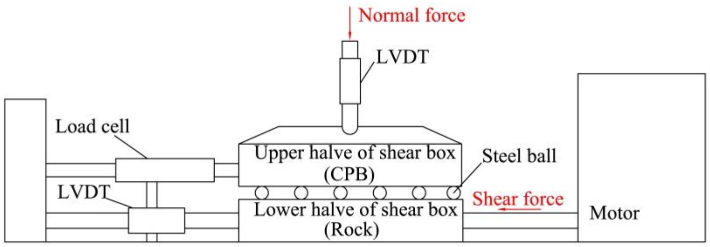

Figure 4.5 Schematic diagram of direct shear device

4.2.2.2.2 Sample preparation and curing

CPB was prepared with different sulphate contents (0 ppm, 5,000 ppm, 15,000 ppm and 25,000 ppm). The required amounts of tailings, PCI and water (with a water-to-cement ratio of 7.35) were mixed together by using a food mixer for 7 minutes until a homogeneous paste was obtained. Then, the prepared CPB was poured into a plastic square container which already contained the granite. The size of the plastic container is 60×60×30 mm. After removing the air bubbles that formed on the interface of the samples through manual vibration, the samples were wrapped with plastic film to prevent water evaporation and then cured at room temperature (~20°C) for 1 day, 3 days and 7 days. The interface of some of the samples with different initial sulphate contents and cured for one day is shown in Figure 4.6.

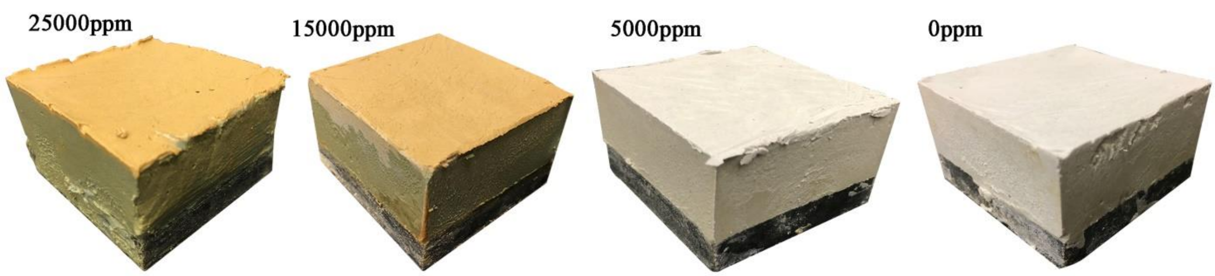

Figure 4.6 CPB samples (made with ST) with different sulphate contents (cured for one day)

4.2.2.2.3 Testing method

Over 140 samples were prepared to study the effect of sulphate on the shear behaviour of the CPB-rock interface (with a smooth surface). In addition, over 50 samples (with sulphate contents of 0 ppm and 5,000 ppm) were also prepared and cured for 1, 3 and 7 days to assess the combined effects of surface roughness and sulphate on the shear strength of the CPB-rock interface. After curing for the specified time, all of the samples were subjected to shear testing under three constant normal stresses (50 kPa, 100 kPa and 150 kPa). Each test was repeated at least three times for accuracy and to ensure the repeatability of the results. The results of the tests on shear stress, and horizontal and vertical displacements were collected with a software called LabVIEW.

4.2.2.3 Microstructural analyses and electrical conductivity monitoring

The microstructure of CPB was examined using electrical conductivity (EC) measurements, and thermo-gravimetric (TG) and differential thermo-gravimetric (DTG) analyses. The TG and DTG analyses can record the weight loss and thermal decomposition rate of the samples under different temperatures, respectively. The TG and DTG analyses were performed on the powdered cement paste (with an initial water-to-cement (w/c) ratio =2) of the CPB by using a Q5000IR thermo-gravimetric analyzer, which accommodates temperatures up to 1000°C. Prior to carrying out the microstructural testing, the samples were dried in an oven at 50°C until they reached mass stabilization.

EC monitoring, which is an effective way to assess the progression of cement hydration as well as track the structural changes that occur within hydrating cementitious materials (Hansson and Hansson, 1985; Courard et al., 2014; Li and Fall, 2016), was also carried on the CPB samples. EC monitoring was performed by inserting a 5TE sensor into the CPB sample and connecting the sensor to the EM50, a data logger for data recording. The result can show the rate of ion movement, which is closely associated with chemical reactions and the water content.

4.2.3 Results and discussion

4.2.3.1 Effect of sulphate on shear behaviour of CPB-rock interface

Figure 4.7 shows typical shear displacement-shear stress curves of the CPB-rock interface with different initial sulphate contents of the CPB (cured for 1 day), while Figure 4.8 provides the corresponding shear displacement-vertical displacement curves. It can be clearly observed in Figure 4.7 that regardless of the sulphate content and type of tailings (ST or NT), all of the curves are relatively similar, which show an increase up to the peak shear stress (upward slope), and then followed by a slight decrease (downward slope). This shows the strain hardening and softening characteristics of the CPB-rock interface. Meanwhile, it can also be noticed that an increase in sulphate somewhat reduces the strain-softening behaviour, and the CPB-rock interface has larger shear displacement prior to reaching the peak shear stress. Furthermore, an increase in the sulphate content significantly reduces the peak shear stress of the CPB-rock interface. These are all due to the presence of sulphate ions in the CPB (Fall and Benzaazoua, 2005). Specifically, the rapid reaction of sulphate ions and tricalcium aluminate (C_3A ($3CaO▪Al_2O_3$), a constituent of cement) produces ettringite (Eq.(4-3)), which thinly coats the unhydrated cemented particles (Yilmaz and Fall, 2017). Consequently, water cannot enter the unhydrated cemented particles. A higher sulphate content means that more ettringite will be produced and as a result, there is a greater likelihood that water cannot enter the unhydrated cement particles. This phenomenon is known as the inhibition effect of sulphate on cement hydration. This inhibition effect is experimentally supported by the EC monitoring results of the CPB samples with sulphate contents of 0 ppm, 5,000 ppm and 25,000 ppm as shown in Figure 4.9. It can be observed from the figure that regardless of the sulphate content, the EC values decrease after reaching the first peak. The initial increase in electrical conductivity as shown in the figure is mainly because of the increase of ionic concentration and mobility of ions (e.g., Ca^{2+}, OH^- and SO_4^{2-}). Besides, the transformation of partial ettringite into monosulfate hydrate also contributes to the increase in electrical conductivity. In contrast, the subsequent reduction in electrical conductivity is due to the consumption of ions by cement hydration, thereby results in the formation of cement hydration products (Morsy et al., 1997; Morsy, 1999). It can be seen from the figure that for the samples with no sulphate, the EC peaks at 5.23 mS/cm after only 3 hours, while that of samples with a sulphate content of 5000 ppm and 25,000 ppm peaks at 4.89 mS/cm and 2.77 mS/cm after 28 hours and 46 hours of curing, respectively. These results indicate that a longer time is required to reach the peak EC for samples that contain sulphate, which is attributed to the retardation of cement hydration. Besides, the lower reduction rate of electrical conductivity with sulphate content after peak value means slow consumption of ions by cement hydration, which also verifies the inhibition effect of sulphate on cement hydration. In addition, the main hydration product in the sample that does not contain sulphate is calcium silicate hydrate (C-S-H), which is considered to be a major binding phase in hardened cement (Gani, 1997; Fall et al., 2010). This also accounts for the higher peak shear stress at the CPB-rock interface with CPB that does not have any sulphate.

$$\left[AlO_4\right]^- + 3\left[SO_4\right]^{2-} + 6\left[Ca\right]^{2+} + aq \rightarrow C_6A\bar{S}_3H_{32} \tag{4-3}$$

The typical shear displacement-vertical displacement curves in Figure 4.8 show that for the samples that are cured for one day, there is contraction of the interface with the development of shear displacement. Besides, a higher sulphate content results in larger contraction. This phenomenon can be explained by the higher compressibility of the samples with sulphate which is due to the inhibition effect of sulphate on cement hydration. On the one hand, the weak cementation of tailings particles means that there are fewer hydration products, such as C-S-H, calcium hydroxide (CH), ettringite and gypsum. The presence of C-S-H and appropriate amounts of expansive minerals (e.g., ettringite, gypsum) contribute to the stability of a solid structure (Li and Fall, 2016). On the other hand, inhibition of cement hydration retains a large volume of evaporable free water in the samples, which significantly reduces the effective stress. Figure 4.10 shows the leaching of free water from a sample.

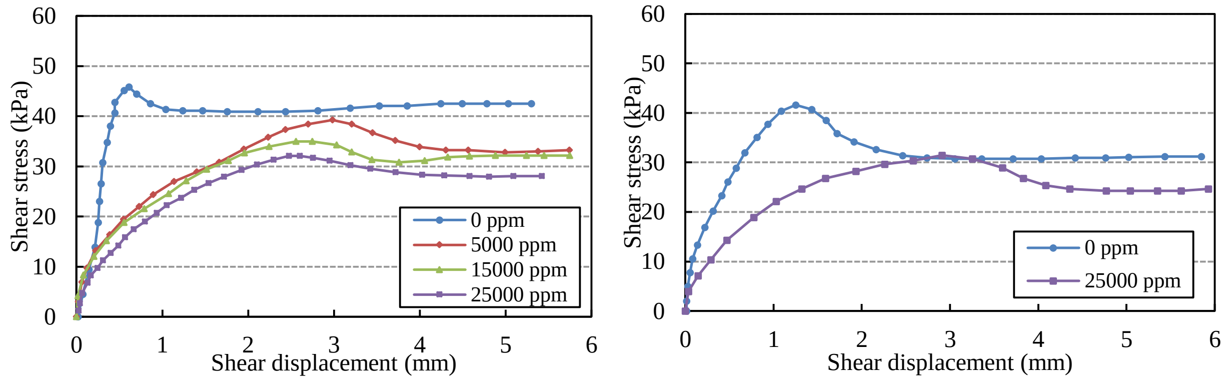

(a) CPB made with silica tailings (ST)

(b) CPB made with natural tailings (NT)

Figure 4.7 Plotted shear displacement-shear stress of CPB-rock interface (cured for 1 day; normal stress: 50 kPa)

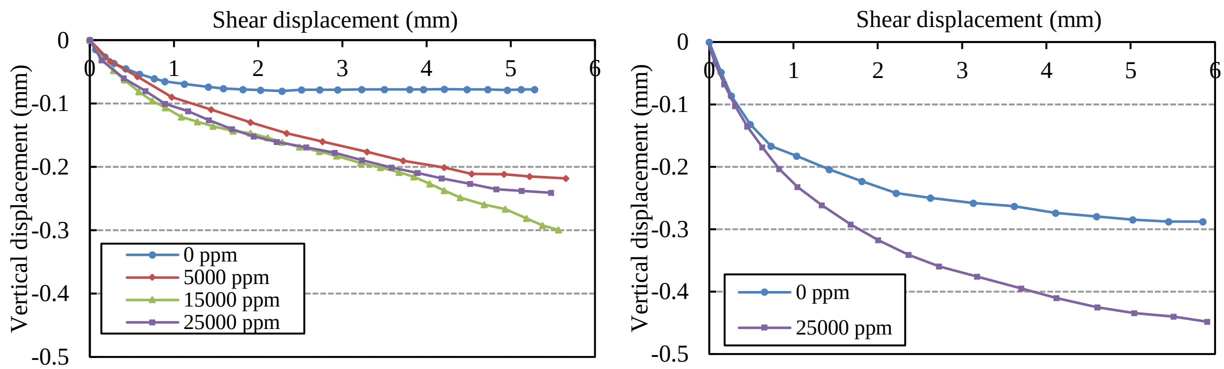

(a) CPB made with silica tailings (ST)

(b) CPB made with natural tailings (NT)

Figure 4.8 Plotted shear displacement-vertical displacement of CPB-rock interface (cured for 1 day; normal stress: 50 kPa)

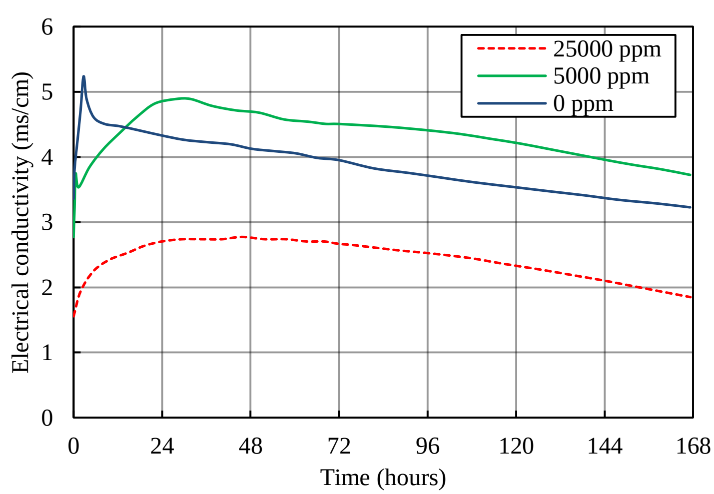

Figure 4.9 Results of electrical conductivity monitoring of CPB with different sulphate contents at early ages of curing

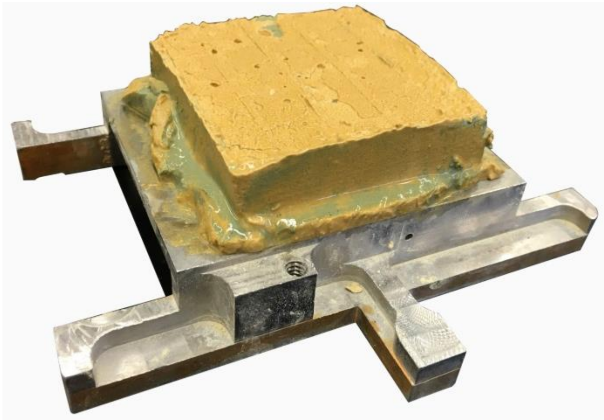

Figure 4.10 Sample with 25,000 ppm of sulphate cured for 1 day after direct shear test

Figure 4.11 shows the typical shear stress-shear displacement and vertical displacement-shear displacement curves of the CPB-rock interface with different sulphate contents (cured for 1 day) at normal stress of 150 kPa. A comparison of the results shown in Figures 4.7, 4.8 and 4.11 indicates that a higher normal stress is associated with higher interface shear strength and larger contraction of the interface samples regardless of the sulphate content. This increase in the interface shear strength with higher normal stress is because as normal stress is increased on the shear plane of the interface, there is increased contact between the surface of the granite and the tailings particles. This leads to more frictional resistance between the tailings grains and the surface of the granite, thus resulting in higher shear strength (Fall and Nasir, 2010). The larger contraction of the interface observed for the samples subjected to higher normal stresses is the result of a higher reduction of local voids and compressibility of the CPB that has been cured for 1 day, which are associated with a higher applied normal stress (Fall and Nasir, 2010).

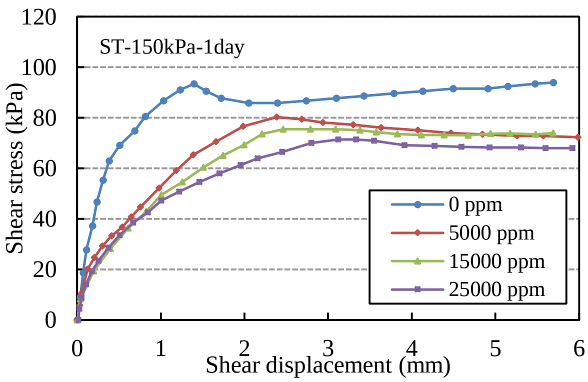

(a) Shear displacement-shear stress curves

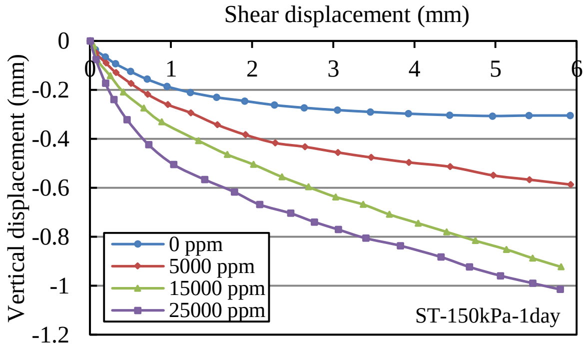

(b) Shear displacement-vertical displacement curves

Figure 4.11 Shear behaviour of CPB-rock interface with different sulphate contents under normal stress of 150 kPa

Figure 4.12 shows the peak shear stress at the CPB-rock interface with different sulphate contents and different types of tailings (NT and ST), and two typical shear strength envelopes of the interface of the samples with 0 ppm and 25,000 ppm of sulphate, which are obtained by fitting linear regression lines. For the samples with 0 ppm and 25,000 ppm of sulphate (with ST), the R^2 of the regression lines is approximately 0.998, while that for the samples with NT is 1. From the results, it is obvious that the shear failure envelope of the interface of the samples that are cured for one day follows the Mohr-Coulomb failure criterion (Eq.(4-4)) regardless of the type of tailings and sulphate content. Thus, both the friction angle and adhesion (cohesion) of the interface can be easily calculated based on Eq.(4-4).

$$\tau = c + \sigma_n \tan(\varphi) \tag{4-4}$$

where τ is the shear stress at the interface, σ_n is the normal stress, c is the adhesion of the interface and φ is the friction angle of the interface. For the samples that were cured for 1 day with ST, the friction angle of the interface is decreased from 25.2° to 21.1° when the sulphate content is increased from 0 ppm to 25,000 ppm, respectively, while the adhesion of the interface is reduced from 22 kPa to 13.9 kPa. In contrast, the adhesion of the samples with NT is decreased from 14.3 kPa to 5.7 kPa when the sulphate content is increased from 0 ppm to 25,000 ppm, respectively. These decreases are due to the sulphate induced inhibition of cement hydration as explained earlier.

4.2.3.2 Effect of curing time and sulphate on interface shear behaviour and strength of CPB-rock interface

Figure 4.13 shows typical effects of curing time of the CPB on the shear stress versus displacement relationships (Figure 4.13(a)) and shear displacement versus vertical displacement (Figure 4.13(b)) of CPB-rock interface with a sulphate content of 5000 ppm. Figure 4.13(a) shows that a longer curing time results in higher peak shear stress at the CPB-rock interface. Besides, the average deformation modulus of the CPB-rock interface is increased from 0.08 MPa on the first day of curing to 1.22 MPa on the seventh day of curing. Meanwhile, with time, the compressibility of the samples is gradually reduced (Figure 4.13(b)). This increase in peak stress and deformation modulus as well as decrease in compressibility with longer curing time are due to the formation of more cement hydration products (e.g., C-S-H), as a result of the increased cement hydration with curing time (Metha, 1986; Gani, 1997; Ercikdi et al., 2009, Fall and Nasir, 2010; Fall et al., 2010).

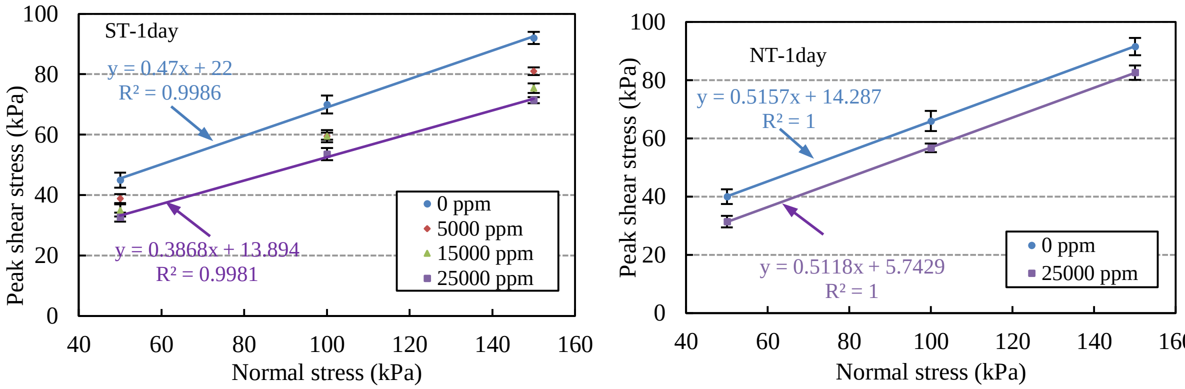

(a) CPB with silica tailings (ST)

(b) CPB with natural tailings (NT)

Figure 4.12 Peak shear stress vs normal stress at CPB-rock interface (cured for 1 day)

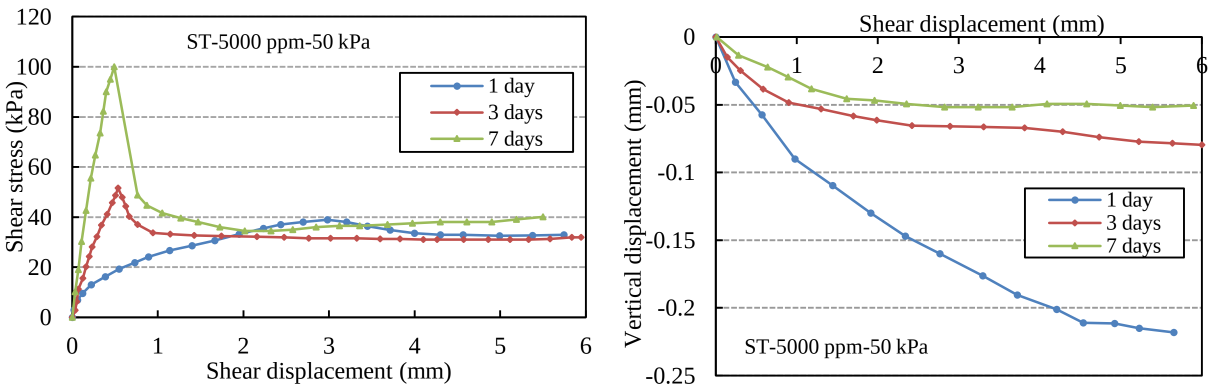

(a) Shear displacement-shear stress curves

(b) Shear displacement-vertical displacement curves

Figure 4.13 Development of shear stress versus horizontal displacement, and vertical displacement versus horizontal displacement of CPB-rock interface with curing time (sulphate content of 5000 ppm)

Figure 4.14 illustrates the typical results of the evolution of the shear strength of the CPB-rock interface with different initial sulphate contents. It can be observed that the peak shear stress increases with different sulphate contents at the CPB-rock interface, as the curing time is increased. This increase in peak shear stress is due to the formation of more cement hydration products (e.g., C-S-H, CH, which not only increase the binding force at the interface but also refine the pore structure of CPB) with longer curing time as explained previously.

However, Figure 4.14 also shows that the rate of shear strength increase and the shear strength values are strongly impacted by the initial sulphate content. For the first three days of aging, the samples with no sulphate have the highest shear strength and rate of shear strength increase. However, after curing for seven days, the samples with 5000 ppm of sulphate show the highest shear strength, followed by those with 0 ppm, 15,000 ppm and 25,000 ppm of sulphate. This higher interface shear strength and rate of shear strength increase observed for the CPB-rock interface with no sulphate in the first three days of curing is because the cement hydration of the samples with sulphate is inhibited by the sulphate ions as discussed previously. This argument is also experimentally supported by the results of the TG/DTG analyses on the samples cured for three days with 0 ppm and 25,000 ppm of sulphate. The results of the thermal analyses are presented in Figure 4.15. It is well known that the peak or weight loss between temperatures of 30°C-105°C results from the evaporation of free and bound water, and weight loss between 110°C-200°C is due to the dehydration of the hydration products, such as C-S-H, ettringite and gypsum (ettringite and gypsum are known as expansive hydrated minerals; gypsum is regarded as secondary hydrated product and formed by a reaction between the sulphate ions and CH), while significant weight loss between 400°C-450°C and 600°C-750°C is attributed to the decomposition of CH and calcite, respectively (Nonnet et al., 1999; Sha et al., 1999; Zhou and Glasser, 2001; Pane and Hansen, 2005; Fall et al., 2010). The results of the thermal analyses showed that the weight loss at 30°C-105°C for CPB with 25,000 ppm of sulphate is more than that of the samples with no sulphate. This means more water is consumed by cement hydration in the samples with no sulphate. Furthermore, the higher loss in weight of the samples with no sulphate at 400°C-450°C indicates more CH is formed in these samples, i.e. these samples have a higher degree of cement hydration. These experimental observations again verify that sulphate can inhibit the cement hydration of CPB at the early ages.

The higher shear strength values observed at the interface of the samples with 5000 ppm of sulphate (in comparison to sulphate-free sample) after curing for 7 days are due to the precipitation of appropriate (but not excessive) amounts of expansive minerals, such as gypsum and ettringite, in the empty capillary pores of the CPB caused by the reaction of the sulphate ions with CH and C_3A. This precipitation leads to the refinement of the pore structure of the CPB and thus increases the amount of contact between the CPB and surface of the granite, which in turn, results in increased interface shear strength. This argument is supported by the scanning electron microscopy results of CPB with sulphate content by Fall and Benzazoua (2005). Moreover, several other studies (Pokharel and Fall, 2013; Li and Fall, 2016) have demonstrated or concluded that the formation of moderate amounts of gypsum and ettringite in the capillary pores of CPB results in finer pore structure of the CPB, and thus higher strength. However, from Figure 4.14, it is also observed that the shear strength of samples with sulphate contents of 15000 ppm and 25000 ppm is lower than that of sample with 5000 ppm of sulphate content. The lower shear strength of highly sulphated samples is mainly because higher initial sulphate content results in stronger inhibition of cement hydration. Specifically, the thickness of the diffusion barrier around cement particles grows with sulphate content. As a result, it takes longer time for water to pass through the barrier and reacts with cement particles. The inhibited cement hydration degree with high sulphate content is shown in Figure 4.9 amd 4.15. This argument has also been demonstrated in numerous previous studies on sulphate-bearing CPB (Hassani and Archibald, 1998; Li and Fall, 2016) and concrete materials (Tzouvalas et al., 2004). In addition to the sulphate-induced inhibition of cement hydration, the adsorption of sulphate by C-S-H should be considered as an additional factor that contributes to the reduction in shear strength. It is well-documented that sulphate ions can be adsorbed by C-S-H and a higher sulphate content leads to a higher adsorption of sulphate by C-S-H (Jeleni et al., 1977; Barbarulo, 2002; Fall and Pokharel, 2010). This could lead to the formation of C-S-H gel, lower quality C-S-H with for instance, weaker binding ability to other hydration products, thereby resulting in strength reduction since the strength of portland cement-bound materials is mainly determined by C-S-H (Jeleni et al., 1977; Barbarulo, 2002; Divet and Randriambololona, 1998; Fall and Pokharel, 2010). The results presented above suggest that, for the studied interfaces, competing effects are found between the factors that lead to shear strength increase (refinement of the pore structure of CPB, precipitation of more hydration products, such as C-S-H,) and decrease (inhibition of cement hydration; sulphate absorption by C-S-H) as the initial sulphate content of the CPB increases. In other words, this means that the competing effects between the factors of shear strength decrease and increase play a significant role in determining the arching effect in a CPB structure.

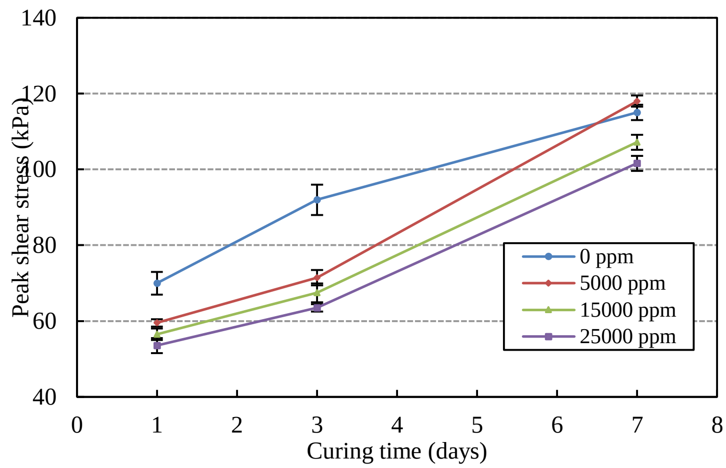

Figure 4.14 Development of shear strength of interface with curing time for different initial sulphate contents (normal stress: 100 kPa)

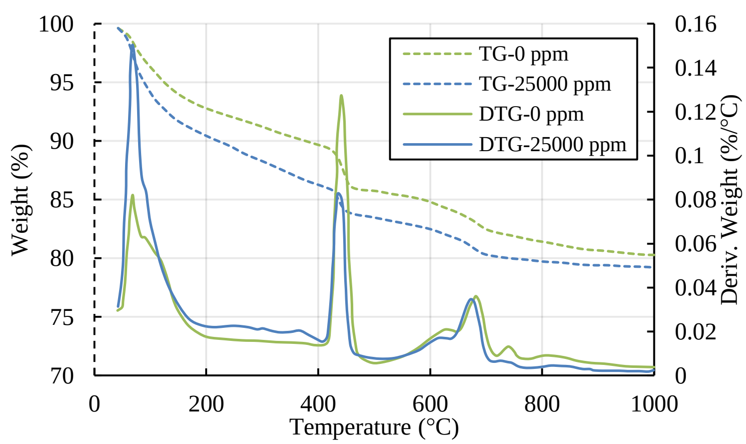

Figure 4.15 Results of TG/DTG analysis for CPB samples cured for three days

Figures 4.16 and 4.17 are plots of the typical effects of curing time of the CPB on the shear envelopes of the interface of the CPB-rock with 5000 ppm of sulphate as well as on the friction angle and adhesion of the interface of CPB-rock with different initial sulphate contents, respectively. Figure 4.16 shows that, regardless of the curing time, the shear envelope of the CPB-rock interface with 5000 ppm of sulphate can be also well described by the Mohr-Coulomb failure criterion. Furthermore, this figure shows that the friction angle values of the interface slightly increase (which range from 22.8° to 24.2°) as the age of the sample increases. This finding is in agreement with the results of previous experimental studies on the shear behaviour of CPB-rock interfaces (Koupouli et al., 2016; Fall and Nasir, 2010; Nasir and Fall, 2008) and cemented soils (Wissa and Ladd, 1965; Uddin et al., 1997; Muhunthan and Sariosseiri, 2008). This slight increase in the friction angle can be attributed to the fact that a longer curing time results in the formation of more hydration products and thus, stronger asperities on the CPB surface, thereby increasing the friction at the interface (Nasir and Fall, 2008). An additional factor is that the formation of more cement hydration products is associated with an increase in the interlocking of the larger effective particles cemented together from smaller particles, thus increasing the friction angle (Acar and EI-Tahir, 1986; Clough et al., 1989). Moreover, Figures 4.16 and 4.17 show that the adhesion of the interface increases as the curing time increases. This increase is due to the formation of more cement hydration products (e.g., C-S-H, CH) with longer curing time, which results in stronger binding force of the cement between the CPB and the rock (Koupouli et al., 2016; Fall and Nasir, 2010; Nasir and Fall, 2008).

However, Figure 4.17 also shows that the time-dependent change of the friction angle and adhesion at the interface is greatly affected by the initial sulphate content. It can be observed that as the sulphate content increases, the adhesion of the interface decreases (except for the interface of the 7 day sample with 5000 ppm of sulphate). This decrease is due to the inhibition of the cement hydration by the sulphate ions as discussed previously. The higher adhesion at the interface of the 7 day sample with 5000 ppm of sulphate is attributed to the precipitation of an appropriate amount of ettringite and gypsum in the empty pores of the CPB, which in turn, increases the contact between the CPB and the surface of the rock, as discussed previously. Consequently, due the cementing effect of gypsum (Haeri et al., 2005) there is increased adhesion at the interface. Moreover, Figure 4.17 shows that the interface of the samples that contain sulphate have a lower friction angle than that with no sulphate. This could be attributed to the sulphate induced inhibition of cement hydration which leads to the formation of weaker asperities on the surface of CPB, thereby reducing the friction angle at the interface.

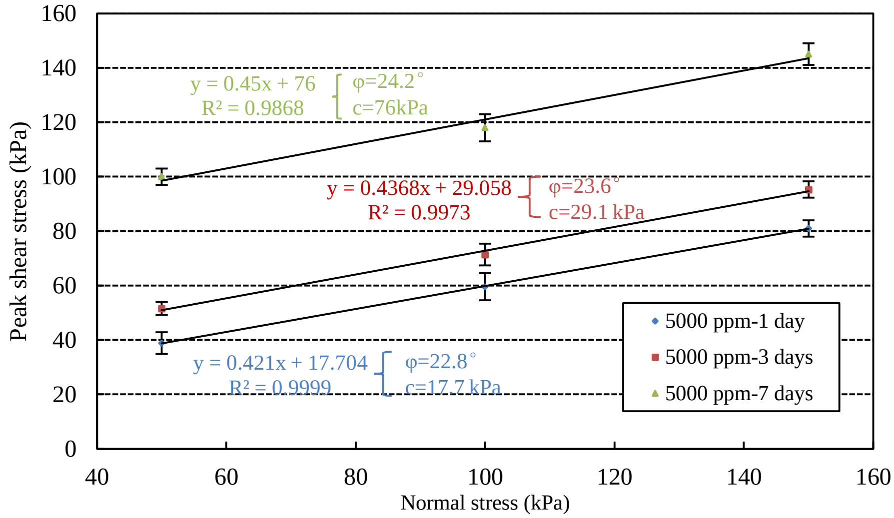

Figure 4.16 Shear envelopes of the CPB-rock interface vs. curing time (5000 ppm)

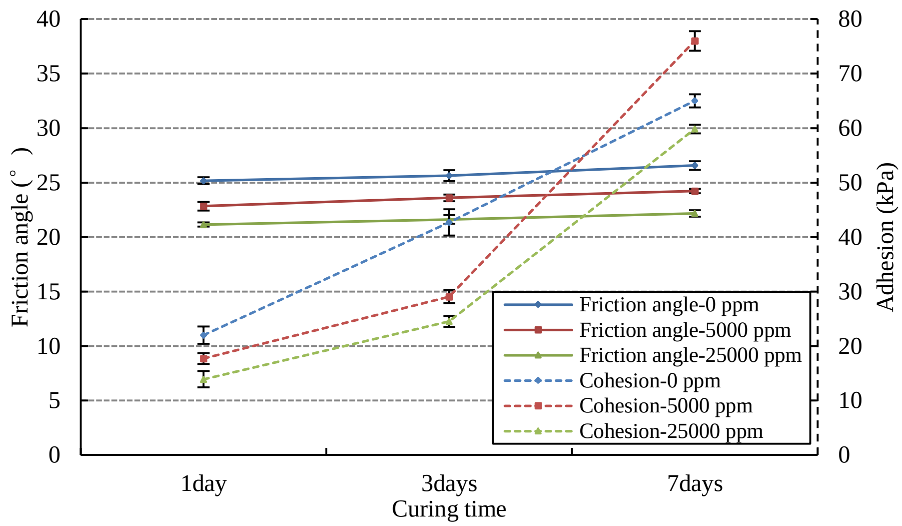

Figure 4.17 Effect of curing time of CPB on friction angle and adhesion of CPB-rock interface with different initial sulphate contents

The sulphate induced reduction in friction angle (as shown in Figure 4.17) affects the design of CPB structure significantly. The aforementioned introduction introduces that the presence of arching effect in the case of narrow backfilled stopes can reduce the effective vertical stress in CPB structure. The studies conducted by Aubertin et al. (2003) and Li and Aubertin (2008) show that the effective vertical stress is related to the friction angle between CPB and rock, and it can be expressed as:

$$\sigma_v' = \frac{\gamma B}{2k_a \tan\varphi}\left[1-\exp\left(\frac{-2k_a H \tan\varphi}{B}\right)\right] \tag{4-5}$$

where σ_v' is the effective vertical stress, k_a is the active ratio of the lateral stress to vertical stress, γ is the unit weight of the CPB, B and H are the width and height of CPB structure. We assume there is a stope with a dimension of 40×6 m (height × width); the unit weight of CPB is 27 kN/m^3 and the active ratio of the lateral stress to vertical stress is 0.4. From Eq.(4-5), it can be concluded that for samples with sulphate contents of 0 ppm and 25000 ppm (cured for 7 days), the reduction in friction angle from 26.6° to 22.1° leads to an increase in effective vertical stress from 376.3 kPa to 441.2 kPa. In other words, the sulphate induced reduction in friction angle reduces the arching effect in CPB structure. Hence, more cement are required to be used to maintain the stability of the structure, this in turn increase the cost of CPB design (Grice, 2001).

4.2.3.3 Effect of interface roughness on interface shear behaviour

Figure 4.18 presents typical shear displacement-shear stress curves of the CPB-rock interface with different roughness and sulphate contents (0 ppm, 5,000 ppm) at a normal stress of 50 kPa for different curing times (1 day, 7 days), while Figure 4.19 illustrates the corresponding shear displacement-vertical displacement curves of these samples. Figure 4.20 presents typical shear displacement-shear stress curves as well as shear displacement-vertical displacement curves of the interface of CPB-rock that has been cured for 7 days with different sulphate contents (0 ppm, 5,000 ppm) and rougher surface at a normal stress of150 kPa.

The results presented in Figure 4.18 show that regardless of the curing time and sulphate content, the roughness of the interface has a significant effect on its shear strength. A rougher surface is associated with higher interface shear strength as expected. However, the magnitude of this effect depends on the sulphate content; it is less pronounced for the interface of samples with sulphate. For example, the peak shear stress of a smooth interface (R0) cured for one day is 46 kPa, i.e. 27.6% lower than that of the rougher interface (R1), while that of R0 and R1 with sulphate is 43 kPa and 45.7 kPa, respectively. This increase in the interface shear strength with a rougher surface can be attributed to the increase in the interlocking between the asperities on the CPB and rock surface as the roughness of the rock surface increases. Similar observations have been made in previous studies (Chen et al., 2015; Taha and Fall, 2013). The observed reduced effect of surface roughness on the interface shear strength of samples with sulphate is due to the sulphate induced inhibition of cement hydration (see Figures 4.9 and 4.15), which results in the formation of weaker asperities on the surface of the CPB.

From Figure 4.18, it can also be observed that the effect of the interface roughness on the shear strength of the interface of the studied samples is more significant as the curing time is increased from 1 day to 7 days. The reason is the increase in the degree of hydration with time. Indeed, when the curing time of the CPB is increased, CPB tends to harden due to the progression of binder hydration. This hardening will result in stronger binding force of the cement between the surface of the CPB and the rock as well as stronger asperities on the surface of the CPB, thereby increasing the critical stress value needed to break the binding forces and asperities (Nasir and Fall, 2008). A comparison of the shear displacement-shear stress curves with a normal stress of 50 kPa (Figure 4.18) and those with 150 kPa (Figure 4.20(a)) shows a higher interface shear strength as the normal stress is increased. The process responsible for this increase is already explained above.

The stronger binding forces of the cement at a more advanced curing time (7 days) are also the reason for the initial peak shear stress observed on the interface of the 7 day samples (see Figure 4.18 and 4.20(a)), regardless of sulphate and roughness. Indeed, this first peak is attributed to the failure of the binding forces of the cement between the CPB and the rock surface (bond failure of the cohesive interface). Similar observations have also been made in previous studies on the shear behaviour of cemented concrete-rock joints (Saiang et al., 2005; Tian et al., 2015). This first peak is not observed for the interface of the 1 day samples due to the weak binding force of the cement. This is because at the very early ages (1 day), cementation is still weak, and inhibition of cement hydration by the sulphate ions also results in weak cementation. Figures 4.18(b) and 4.20(b) also show that after the first peak, the shear stress of the interface of the 7 day samples with a rougher surface is reduced as the shear displacement increases. Thereafter, the shear stress increases again until a new peak stress (second peak in shear stress) emerges. After the second peak, the shear stress is reduced as the shear displacement increases until reaching a residual value. This second peak in shear stress represents the maximum shear stress derived from friction of the non-cemented CPB–rock interface. The shear stress increases up to the second peak and then decreases because the increase causes the interface to dilate (will be discussed in more detail below and shown in Figures 4.19 and 4.20(b)). During this time, the asperities contact area or the contact area between the CPB and the rock surface is gradually reduced with increasing shear displacement. This reduced contact area leads to an increase in the contact normal stress. The interface continues to slide until critical displacement in which the local stress (critical stresses) of the asperities exceeds the strength of the asperities on the CPB surface. At this critical local stress, the major asperities on the CPB surface can no longer sustain the loading, and failure of the interface takes place (Nasir and Fall, 2008). It should be anticipated that the asperities on the CPB surface will be the most affected or changed due to the relatively low strength of the CPB in comparison to that of the rock. This argument is supported by the post-shear picture of the interface of a 7 day-CPB-rock presented in Figure 4.21. It can be clearly observed that the asperities on the CPB are damaged or fractured. From the results presented above, it can be concluded that the roughness not only increases the peak shear stress, but also leads to a second peak in shear stress.

The vertical displacement-shear displacement curves of the smooth and rough interfaces of the CPB-rock at a low normal stress (50 kPa) and for various curing times (1 and 7 days; see Figure 4.19) show that the samples cured for 1 day (Figure 4.19(a)) mainly show contraction regardless of the surface roughness and sulphate content. The reason for this contraction is that at a very early age (one day of curing), the cementation of the tailings particles is weak, which leads to high compressibility of the CPB and weak asperities on the surface of the CPB. Moreover, the sulphate induced inhibition of cement hydration increases the compressibility and weak asperities on the interface of the samples that have sulphate, thereby resulting in more contraction in the 1 day samples with sulphate. A comparison of the vertical displacement-shear displacement curves of the interface of the 1 and 7 day samples shows that the former show more contraction than the latter because there is an increase in the degree of cement hydration with time, which in turn, reduces the compressibility of the CPB as explained in previous studies (Fall and Nasir, 2010; Xia and Lee, 2008; Gani, 1997; Metha, 1986). However, Figure 4.19(b) shows that while the smooth interface of the 7 day sample shows only contraction, the samples with a rougher interface, first show contraction, followed by dilation, and subsequently contraction, regardless of the sulphate content. However, the magnitude of the dilation is reduced as the normal stress is increased (Figure 4.20(b)). The observed dilation of the rougher interface is the result of the relative asperity movement. Another interesting point pertains to the deformation behaviour of the interface of the 7 day samples, which is shown in Figure 4.19(b). It can be observed that the interface of the 7 day samples with sulphate shows less contraction than the samples without sulphate, regardless of the surface roughness. This lower contraction is the result of the formation of adequate (not excessive) quantities of expansive minerals (ettringite, gypsum) in the capillary pores of the CPB due to the reaction of the sulphate ions with C_3A and CH as discussed previously. The formation of these minerals causes a reduction in the porosity or void ratio of the CPB with sulphate, thereby reducing its compressibility. Moreover, it can be concluded from the comparison of the results in Figures 4.19(b) and 4.20(b) that a higher normal stress reduces the magnitude of the aforementioned dilation. This is because a higher normal stress would lead to greater asperity deterioration on the CPB surface.

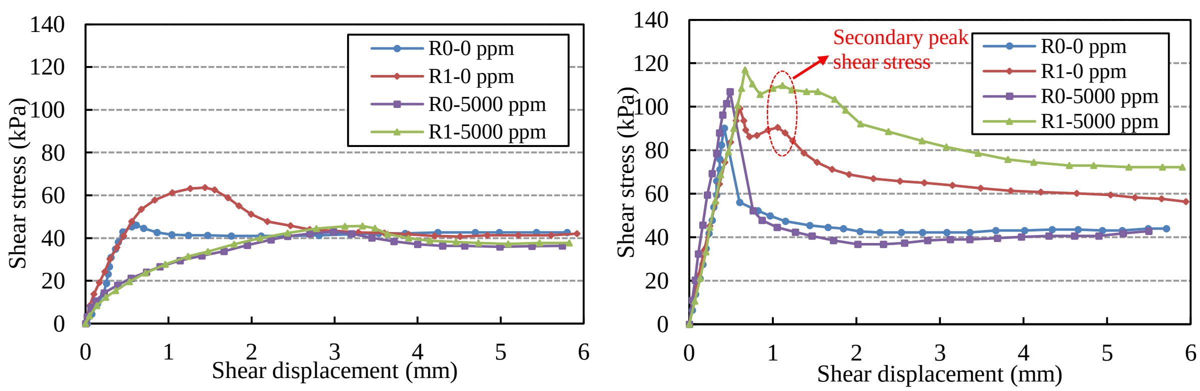

(a) 1 day of curing

(b) 7 days of curing

Figure 4.18 Shear displacement-shear stress curve of CPB-rock interface (CPB made with ST; normal stress: 50 kPa)

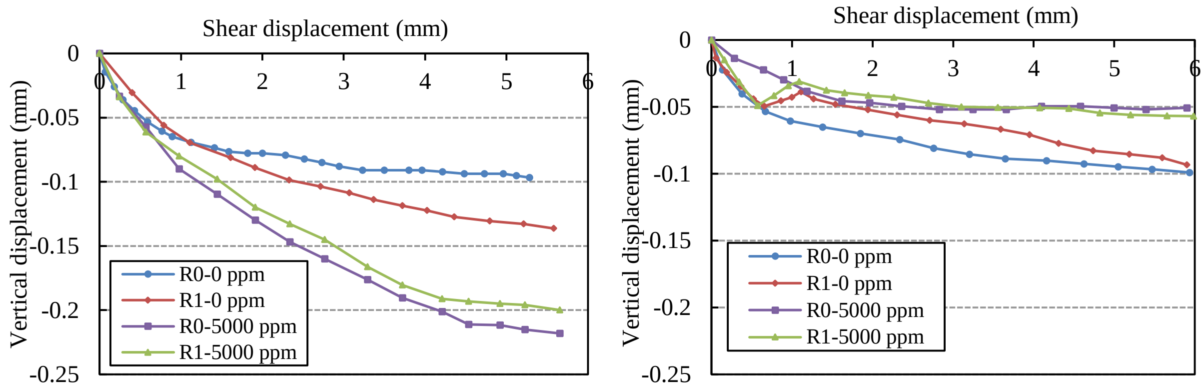

(a) 1 day of curing

(b) 7 days of curing

Figure 4.19 Shear displacement-vertical displacement curve of CPB-rock interface (CPB made with ST; normal stress: 50 kPa)

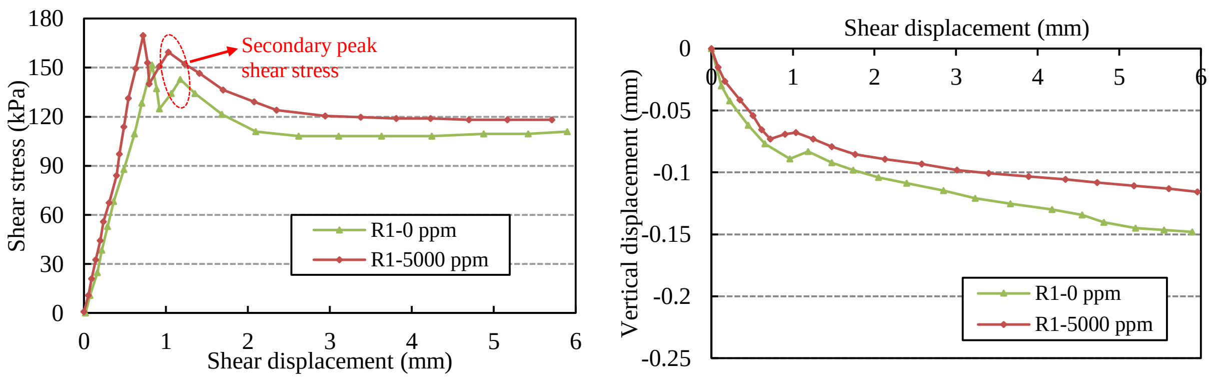

(a) Shear displacement-shear stress curves

(b) Shear displacement-vertical displacement curves

Figure 4.20 Shear behaviour of CPB-rock with rougher interface under normal stress of 150 kPa (seven days of curing; 150 kPa; surface roughness: R1)

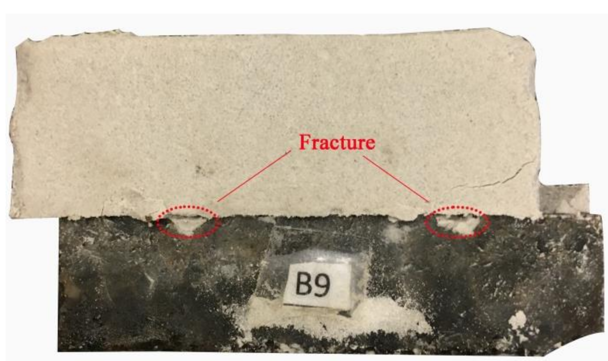

Figure 4.21 Post-shear picture of interface of 7 day CPB-rock sample with no sulphate

4.2.4 Summary and conclusions

In this paper, the results of an experimental study on the effect of initial sulphate content in CPB on the shear strength behaviour of the interface between rock and paste backfill undergoing cementation are presented and discussed. The following conclusions are thus made:

- Sulphate has a significant impact on the shear behaviour and strength of the interface between rock and CPB. This effect can be positive (increase in interface shear strength) or negative (decrease in shear strength). The obtained results show that the initial sulphate content and curing time determine whether sulphate has a positive or negative effect on the interface shear strength.

- Sulphate has a negative effect on the shear strength of the interface of the CPB-rock samples at a very early age (1 day) due to the inhibition of cement hydration by sulphate ions.

- Sulphate can have has two opposite effects on the shear strength of the interface of CPB-rock after 7 days of curing. A relatively low amount of sulphate (5,000 ppm) leads to an increase in the interface shear strength of the studied samples (due to the precipitation of an appropriate amount of expansive minerals in the pores of CPB), while higher sulphate contents (15,000 ppm or 25,000 ppm) result in reduced shear strength. This decrease in shear strength is mainly attributed to the combined effects of the following factors: (i) stronger inhibition of cement hydration, and (ii) adsorption of sulphate by C–S–H.

- There are competing effects between the factors of shear strength increase (refinement of the pore structure of CPB, precipitation of more hydration products) and decrease (inhibition of cement hydration; sulphate absorption by C-S-H) as the initial sulphate content of the CPB is increased.

- The shear failure envelope of the interface of the CPB-rock samples in this study follows the Mohr-Coulomb failure criterion regardless of the sulphate content, curing time, type of tailings and rock surface roughness.

- A rougher surface results in higher interface shear strength and the effect of the roughness of the interface on shear strength is more significant as the curing time is increased. However, the magnitude of this effect depends on the sulphate content; it is less pronounced for the interface of samples with sulphate.

The results presented in this paper will contribute to a better understanding of the shear behaviour of the CPB-rock interface which is crucially important in assessing the arching effect in CPB mass as well as in stability analyses of underground CPB structures.

4.2.5 References

Acar YB, EI-Tahir AE (1986) Low strain dynamic properties of artificially cemented sand. Journal of Geotechnical Engineering 121(11):1001-1015.

Aubertin M, Li L, Arnoldi S, Belem T, Bussière B, Benzaazoua M, Simon R (2003) Interaction between backfill and rock mass in narrow stopes. Soil and rock America 1:1157-1164.

Barbarulo R (2002) Comportement des matériaux cimentaires: actions des sulfates et de la temperature. Dissertation, École Normale Supérieure de Cachan, France – Université Laval, Canada; [in French]

Brackebusch FW (1994) Basic of paste backfill system. Miner. Eng. 46:1175-1178.

Barton N, Choubey V (1977) The shear strength of rock joints in theory and practice. Rock mechanics 10(1):1-54.

Buckby T, Black S, Coleman ML, Hodson ME (2003) Fe-sulphate-rich evaporative mineral precipitates from the Rio Tinto, southwest Spain. Mineral. Mag .67(2):263-278.

Chen X, Zhang J, Xiao Y, Li J (2015) Effect of roughness on shear behaviour of red clay - concrete interface in large-scale direct shear tests. Canadian Geotechnical Journal 52:1122–1135.

Chinese Industry Information (2016). Analysis on Production and Reserves of Non-ferrous Metal Ore in China in 2016. Available at: http://www.chyxx.com/industry/201611/470424.html In Chinese.

Clough GW, Iwabuchi J, Rad NS, Kuppusamy T (1989) Influence of cementation on liquefaction of sands. Journal of Geotechnical Engineering 115(8):1102-1117.

Courard L, Michel F, Perkowicz S, Garbacz A (2014) Effects of limestone fillers on surface free energy and electrical conductivity of the interstitial solution of cement mixes. Cem. Concr. Compos. 45:111-116.

Divet L, Randriambololona R (1998) Delayed ettringite formation: the effect of temperature and basicity on the interaction of sulphate and CSH phase, Cem. Concr. Res. 28(3):357-363.

Ercikdi B, Kesimal A, Cihangir F, Deveci H, Alp, İ (2009) Cemented paste backfill of sulphide-rich tailings: Importance of binder type and dosage. Cem. Concr. Compos. 31(4):268-274.

Fall M, Benzaazoua M (2005) Modelling the effect of sulphate on strength development of paste backfill and binder mixture optimization. Cem. Concr. Res. 35:301-314.

Fall M, Benzaazoua M., Ouellet S (2005). Experimental characterisation of the influence of mill tailings fineness and density on the quality of cemented paste backfill. Miner. Eng. 18 (1): 41-44

Fall M, Celestin J, Pokharel M, Touré M (2010) A contribution to understanding the effects of curing temperature on the mechanical properties of mine cemented tailings backfill. Eng. Geol. 114(3-4):397-413.

Fall M, Nasir O (2010) Mechanical behaviour of the interface between cemented tailings backfill and retaining structures under shear loads. Geotech. Geol. Eng. 28(6):779-790.

Fall M, Pokharel M (2010) Coupled effects of sulphate and temperature on the strength development of cemented tailings backfills: Portland cement-paste backfill. Cem. Concr. Compos. 32(10):819-828.

Gani MSJ (1997) Cement and Concrete, Chapman & Hall, London, UK.

Grice T (2001) Recent mine developments in Australia. Proceedings of the 7th International Symposium on Mining with Backfill (MINEFILL) 351-357.

Haeri S. M, Hamidi A, Tabatabaee N (2005)The Effect of Gypsum Cementation on the Mechanical Behaviour of Gravely Sands. Geotech. Test. J. 28(4):380-390.

Hansson LH, Hansson CM (1985) Ion conduction in cement based materials. Cem. Concr. Res. 15(2):201-212.

Hassani F, Archibald J (1998) Mine backfill. Canadian Institute of mine, Metallury and Petroleum, Canada.

Husem M, Gozutok S (2005) The effects of low temperature curing on the compressive strength of ordinary and high performance concrete. Constr. Build. Mater. 19(1):49-53.

Jelenic´ I, Panovic´ A, Halle R, Gac´eša T (1977) Effect of gypsum on the hydration and strength development of commercial Portland cements containing alkali sulphates. Cem. Concr. Res. 7(3):239-245.

Koupouli NJF, Belem T, Rivardb P, Effenguet H (2016) Direct shear tests on cemented paste backfill-rock wall and cemented paste backfill-backfill interfaces. J. Rock. Mech. Geotech. Eng. 8(4):472-479.

Lade PV, Overton DD (1989) Cementation effects in friction materials. Journal of Geotechnical Engineering 115(10):1373-1387.

Li L, Aubertin M (2008) An improved analytical solution to estimate the stress state in subvertical backfilled stopes. Canadian Geotechnical Journal 45(10):1487-1496.

Li WC, Fall M (2016) Sulphate effect on the early age strength and self-desiccation of cemented paste backfill. Constr. Build. Mater. 106:296-604.

Maerz NH, Franklin JA, Bennett CP (1990) Joint roughness measurement using shadow profilometry. International Journal of Rock Mechanics and Mining Sciences & Geomechanics Abstracts 27(5):329-343.

Marston A (1930) The theory of external loads on closed conduits in the light of latest experiments. Highway research board proceedings, Ames Iowa.

Metha PK (1986) Concrete: Structure, Properties and Materials. Prentice-Hall Inc, Englewood Cliffs, N.J.

Morsy MS, El-Enein SA, Hanna G (1997) Microstructure and hydration characteristics of artificial pozzolana-cement pastes containing burnt kaolinite clay. Cem. Concr. Res. 27(9):1307-1312.

Morsy MS (1999) Effect of temperature on electrical conductivity of blended cement pastes1. Cem. Concr. Res. 29(4):603-606.
Muhunthan B, Sariosseiri F (2008) Interpretation of geotechnical properties of cement treated soils.
Nasir O, Fall M (2008) Shear behaviour of cemented pastefill-rock interfaces. Eng. Geol. 101(3):146-153.
Nonnet E, Lequeux N, Boch P (1999) Elastic properties of high alumina cement castables from room temperature to 1600°C. J. Eur. Ceram. Soc. 19(8):1575-1583.
Orejarena L, Fall M (2010) The use of artificial neural networks to predict the effect of sulphate attack on the strength of cemented paste backfill. Bull. Eng. Geol. Environ. 69(4):659-670.
Pane I, Hansen W (2005) Investigation of blended cement hydration by isothermal calorimetry and thermal analysis. Cem. Concr. Res. 35(6):1155-1164.
Pirapakaran K, Sivakugan N (2007) A laboratory model to study arching within a hydraulic fill stope. Geotech. Test. J. 30(6):1-8.
Pokharel M, Fall M (2013) Combined influence of sulphate and temperature on the saturated hydraulic conductivity of hardened cemented paste backfill. Cem. Concr. Compos. 38:21-28.
Saiang D., Malmgren L., Nordlund E. (2005) Laboratory Tests on Shotcrete-Rock Joints in Direct Shear, Tension and Compression. Rock Mechanics and Rock Engineering 38(4):275-297
Sha W, O'Neill E, Guo Z (1999) Differential scanning calorimetry study of ordinary Portland cement. Cem. Concr. Res. 29(9):1487-1489.
Taha A, Fall M (2013) Shear behaviour of sensitive marine clay-concrete interfaces. J Geotech. Geoenviron. Eng. 19(4):644-650.
The Mining Association of Canada (2018) Mining Facts. Available at http://mining.ca/resources/mining-facts
Tian HM, Chen WZ, Yang DS, Tang JP (2015) Experimental and numerical analysis of the shear behaviour of cemented concrete-rock joints. Rock. Mech. Rock. Eng. 48:213-222.
Tse R, Cruden DM (1979) Estimating Joint Roughness Coefficients. Int. J. Rock. Mech. Min. Sci. 16(5):303-307.
Tzouvalas G, Dermatas N, Tsimas S (2004) Alternative calcium sulfate-bearing materials as cement retarders: Part I. Anhydrite, Cem. Concr. Res. 34:2113-2118.
Uddin K, Balasubramaniam AS, Bergardo DT (1997) Engineering behaviours of cement-treated Bangkok soft clay. Geotechnical Engineering Journal 28(1):89-119.
Wissa AE, Ladd CC (1965) Shear strength generation in stabilized soils (No. RR-R65-17). Massachusetts Inst of Tech Cambridge Soil Mechanics Div.
Xia HW, Lee FH (2008) Curing time effect on behaviour of cement treated marine clay. International Journal of Marine and Environmental Sciences 2(7):144-151.
Yang ZY, Lo SC, Di CC (2001) Reassessing the joint roughness coefficient (JRC) estimation using Z2. Rock. Mech. Rock. Eng. 34(3):243-251.
Yilmaz E, Fall M (2017) Paste tailings management. Springer International Publishing.
Yu XB, Vayssade B (1991) Joint profiles and their roughness parameters. International Journal of Rock Mechanics and Mining Sciences & Geomechanics Abstracts 28:333-6.
Zhou Q, Glasser F (2001) Thermal stability and decomposition mechanisms of ettringite at < 120°C. Cem. Concr. Res. 31(9):1333-1339.

4.3 Paper III: Effects of curing temperature on shear behaviour of cemented paste backfill-rock interface

Published in *International Journal of Rock Mechanics and Mining Sciences*, 2018, 112: 184-192.

Kun Fang, Mamadou Fall

Abstract

Understanding the shear behaviour of the interface between rock and cemented paste backfill (CPB) is critical for the cost-effective geotechnical design of underground CPB structures. Curing temperature is one of the key factors that can affect the shear behaviour and resistance of the CPB-rock interface. However, no studies have been performed to investigate its effects on the shear behaviour of the interface between rock and tailings backfill that is undergoing cementation. The main objective of this study is to therefore experimentally study the effects of three different curing temperatures (2°C, 20°C, and 35°C) on the shear behaviour and strength of the CPB-rock interface. The obtained results show that higher curing temperatures (up to 35°C in this study) can increase the rate of cement hydration and self-desiccation, thus increasing the peak shear stress at the interface between early age CPB and rock. However, the sample cured for a longer time of 28 days at a higher temperature of 35°C has a lower shear strength than that cured at a lower temperature of 20°C. This lower shear strength is due to the crossover effect. The findings presented in this paper will contribute to a better assessment of the stability of backfill structures and a better design for them.

Keywords Cemented paste backfill; tailings; rock; temperature; shear behaviour; interface

4.3.1 Introduction

After cement paste backfilling was first introduced in the Bad Grund Mine (Germany) in the late 1970s, the method has since been widely used in many underground mines worldwide as a tailings management method due to its economic and environmental benefits, such as higher ore recovery ratio, safer work conditions as well as environmental friendliness (Hassani and Archibal, 1998; Yilmaz et al., 2004; Benzaazoua et al., 2004). Cemented paste backfill (CPB), which mainly consists of thickened tailings (with a solid percentage of 70%-85%), binder (typically 3-7 wt%) and water, is prepared in a backfill plant usually located on the mine surface. Then, the homogeneous paste is transported to underground mine cavities through pipes by pumping or gravity, mainly to ensure the stability of the surrounding structures (e.g., rock, CPB, orebody), and thus contributes to a safe work place for miners. Hence, mechanical stability is one of the key design criteria of CPB structures. The mechanical failure of CPB structures not only jeopardizes mining productivity, but also greatly threatens the safety of workers underground as well as has substantial financial ramifications for the mine.

With geographically widespread applications around the world (Australia, Canada, China, South Africa, etc.) and at various mine depths, the CPB structure is inevitably exposed to different environments at various temperatures as discussed below. Hence, studying the properties of CPB as well as the stability of CPB structures at different temperatures is vitally important for designing safer and more economical CPB structures. Indeed, many previous studies on concrete have concluded that the temperature has considerable effects on cement binder hydration (Schneider, 1988; Kim et al., 1998), and thus on the properties of concrete, such as strength and deformation behaviour. Besides, some academics have also noted that temperature significantly affects the changes in the strength and pore structure development of CPB (Fall et al., 2010; Fall and Samb, 2008).

The results of such studies suggest that the curing temperature of backfill could potentially affect the shear strength and behaviour of the interface between the CPB and nearby rockmass (Figure 4.22), and thus influence the stability and design of CPB structures. Moreover, many previous investigations have confirmed that the vertical stress in the backfilled body is significantly less than the overburden stress due to the arching effect (Thompson et al., 2009; Li et al., 2014; Cui and Fall, 2017). The arching effect is primarily the result of CPB consolidation as well as changes in the properties of the CPB-rock interface. This means taking into consideration the arching effect can reduce the amount of cement consumed, which can be up 75% of the cost of CPB (Grice, 2001). Hence, a better understanding of the effect of curing temperature on the properties of the CPB-rock interface not only can ensure better stability assessments of CPB structures, but also enable the more cost-effective design of CPB structures. Besides, it can also reduce the mining cycle time and speed up the mining process, thus improve mining efficiency. However, to date, there are no published studies on the influence of curing temperature on the shear properties/behaviour of the CPB-rock interface. It is therefore necessary and urgent to address this knowledge gap because CPB and the CPB-rock interface can be exposed to different temperatures in underground mine operations as briefly discussed below.

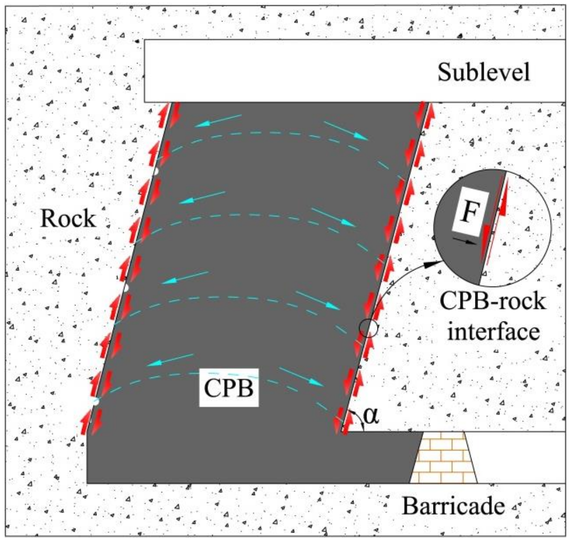

Figure 4.22 Underground CPB structure and surrounding rock

First, the temperature in shallow orebodies is closely related to the geographical location of the mine and seasonal variations of the climate. For example, in the northern part of Canada, permanently frozen ground can reach a depth of up to 1000 m (Udd, 2006), which means that the temperature in orebodies is mostly less than 0°C. Aside from the geographical factor, cement-binder hydration, which is an exothermic reaction, and geothermal gradients (with depth of the mine) also contribute to the variations of the environmental and backfill temperatures. Indeed, the exothermic process of cement-binder hydration is considered to be the most significant heat source for CPB (Fall et al., 2010). Some of the field studies have found that the temperature of the CPB can increase up to 50°C after curing for 4 days due to the heat released by binder hydration (Williams et al., 2001). Moreover, with increasing depth of mining activity, the heat induced by geothermal gradients increasingly affects the CPB temperature. For example, an observation made by Rawlings and Phillips of the South Deep mine in South Africa, which is one of the largest gold mines, shows that the rock temperature increases from 50°C at a depth of 4000 m to 70°C at 5000 m; while another example is the Kunlun Mts. areas in China, which has an average geothermal gradient of 5.6°C/100 m (Rawlings and Phillips, 2001; Wu et al., 2010). To sum up, there are many sources of heat, and the temperature in each specific mine is also unique. Hence, studying the influence of temperature on the shear properties and behaviour of the CPB-rock interface has great practical importance for CPB design, barricade opening and scheduling the extraction of primary stopes.

Therefore, the main objective of this paper is to experimentally study the effect of different curing temperatures (2°C, 20°C, and 35°C) and curing times (1, 3, 7 and 28 days) on the shear properties and behaviour of the CPB-rock interface.

4.3.2 Materials and experimental program

4.3.2.1 Materials used

4.3.2.1.1 Tailings

Natural tailings (NT) and artificial tailings are used in this study. NT contain some reactive components (for e.g. pyrite) that can oxidize during storage and/or the preparation of CPB, and thus bring some uncertainties in the results. Hence, to reduce ambiguity in the results due to the use of NT, artificial tailings (silica tailings (ST)) are also used to produce the CPB-rock samples in this study. The ST consist of 99.8% silicon dioxide (SiO_2) and have a similar particle size distribution as NT and the average grain size distribution of tailings found in nine mines in Eastern Canada (Figure 4.23). The mineralogical composition of NT and ST is provided in Table 4.4.

Table 4.4 Mineralogical composition of tailings used in this study

Tailings/Mineral	Quartz (wt.%)	Talc (wt.%)	Dolomite (wt.%)	Magnetite (wt.%)	Chlorite (wt.%)	Magnetite (wt.%)	Pyrite (wt.%)	Pyrrhotite (wt.%)	Other (wt.%)
NT	11.9	16.4	5.7	7.6	18.2	11.4	15.4	3.1	10.3
ST	99.8	/	/	/	/	/	/	/	

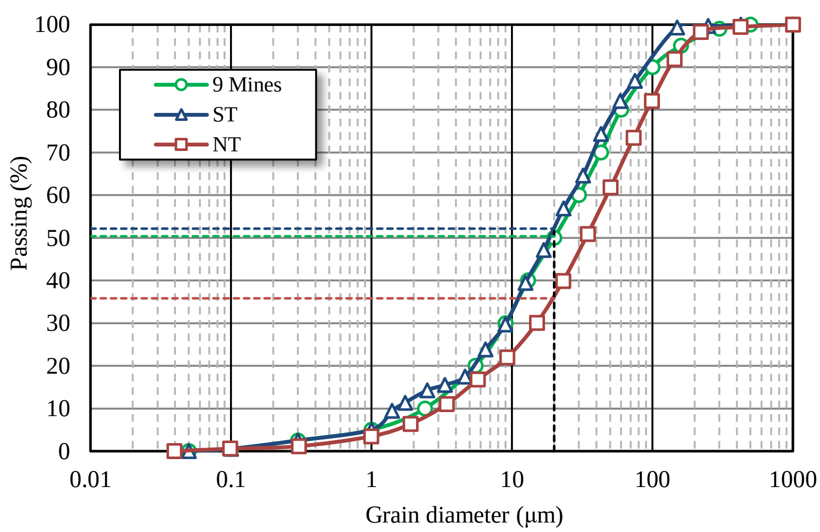

Figure 4.23 Grain size distribution of silica tailings (ST) and natural tailings (NT), and average grain size distribution of tailings from nine mines in Eastern Canada

4.3.2.1.2 Binder

The properties of CPB are closely related to the type and amount of binder used (Fall et al., 2010). In this study, Portland cement Type I (PCI) with a weight proportion of 4.5% is used to prepare the CPB-rock samples. PCI is the most common type of binder used for preparing CPB in practice. The chemical composition of PCI is shown in Table 4.5.

4.3.2.1.3 Rock samples

A special rock cutter was used to cut the bars of granite into smaller sized samples with dimensions of 60×60×10 mm. The average uniaxial compressive strength (UCS) of the granite is 160 MPa. In order to eliminate the influence of the roughness of rock on the shear behaviour of the CPB-rock interface, the rock was polished until the joint roughness coefficient (JRC) was determined to be equal to zero in accordance with the typical roughness profiles proposed by Tse and Cruden (Tse and Cruden, 1979).

Table 4.5 Chemical composition of Portland cement Type I

Component Unit	SO_3 (wt.%)	Fe_2O_3 (wt.%)	Al_2O_3 (wt.%)	SiO_2 (wt.%)	CaO (wt.%)	MgO (wt.%)
PCI	3.82	2.70	4.53	18.03	62.82	2.65

4.3.2.1.4 Tap water

Tap water was used to mix the binder and tailings (with a water-cement ratio (w/c) of 7.35). The chemical composition of the water is given in Table 4.6.

Table 4.6 Chemical composition of tap water

Element	SO_4^{2-} (ppm)	Ca (ppm)	Na (ppm)	Mg (ppm)	Si (ppm)	Al (ppm)	Fe (ppm)
	88	46.6	5.3	2.6	0.64	0.13	0.03

4.3.2.2 Testing apparatus and sample preparation

4.3.2.2.1 Testing apparatus

A direct shear device is used in this study to examine the shear behaviour and resistance of the CPB-rock interface as shown in Figure 4.24. The load cell is fixed at the end of the device and used for load measurements, while the two linear variable differential transformers (LVDTs) are used to measure the horizontal and vertical displacements respectively. The CPB and granite samples are placed between the two halves of the shear box to ensure that the data collected by the computer software (Labview) are relevant to the CPB-rock interface. That is, the granite part of the sample is in the lower half of the shear box while the CPB part of the sample is in the upper half of the shear box. Also, several steel balls are placed on the perimeter between the two halves of the shear box to ensure that the sliding plane is right at the interface of the CPB and rock. The samples were subjected to a constant normal stress which was applied by a vertical arm above the shear box. When shearing, the upper half of the shear box did not move, while the lower half was driven by a motor that was operated at a speed of 0.5 mm/min.

4.3.2.2.2 Sample preparation and testing procedure

CPB was prepared by mixing the required amounts of tailings, PCI and water in a food mixer, and then stirred for about seven minutes until a homogeneous paste was obtained. After placing the granite into a plastic square container with dimensions of 60×60×30 mm, the prepared CPB was poured on top of the granite. Thereafter, the plastic container underwent manual vibration to remove air bubbles that formed on the CPB-rock interface. The container was then covered with a plastic film to prevent water from evaporating. Lastly, the sealed container was cured in a temperature-controlled chamber at three different temperatures of 2°C, 20°C and 35°C for 1, 3, 7 and 28 days. The interface of some of the CPB-rock samples cured for one day at the three different curing temperatures is shown in Figure 4.25.

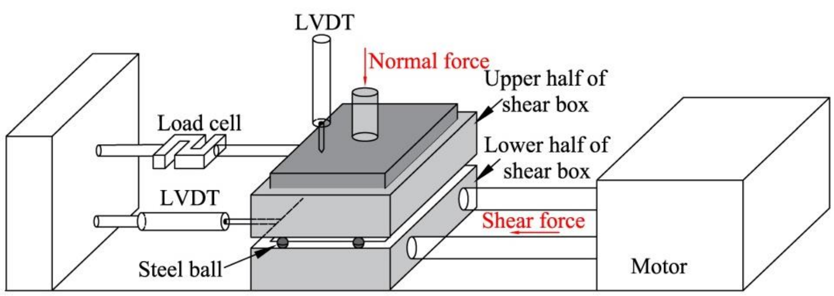

Figure 4.24 Schematic diagram of the direct shear device

Figure 4.25 CPB-rock samples (made with ST) cured at three different temperatures for one day

4.3.2.3 Testing methods

4.3.2.3.1 Shear test of CPB-rock interface

All of the samples were subjected to direct shear testing after being cured for 1, 3, 7 and 28 days. To determine the shear strength envelope of the CPB-rock interface, three constant normal stresses (50 kPa, 100 kPa and 150 kPa) were applied onto the samples during testing. In addition, each test was repeated least three times to ensure the repeatability of the results. Therefore, over 135 tests have been conducted in this study. The experiment details are provided in Table 4.7.

4.3.2.3.2 Microstructural analyses

The microstructure of the samples was studied by applying a number of techniques, including thermal gravity (TG), differential thermal gravimetric (DTG) and mercury intrusion porosimetry (MIP), which were carried out to assess the effect of curing temperature on the microstructural development of the CPB. By using a Q5000IR thermo gravimetric analyzer which can observe temperatures up to 1000°C, TG and DTG analyses were carried out on dried and powdered cement paste (with an initial w/c = 2 which represents the high volume of water in CPB), and the weight loss and thermal decomposition rate of the samples were recorded at different temperatures. MIP was used to study the influence of cement hydration products on the pore structure or pore size distribution of CPB. The analysis was performed on CPB samples (dried at 45°C for 4 days earlier) by using a Micromeritics AutoPore III 9420 mercury porosimeter, which measures the volume distribution of pores by mercury intrusion or extrusion.

Table 4.7 Experiment details

Tailings type	Binder content (%)	w/c ratio	Curing time	Normal stress/kPa	Curing temperature/°C
NT	4.5	7.35	1 day	50	2, 20, 35
NT	4.5	7.35	1 day	100	2, 20, 35
NT	4.5	7.35	1 day	150	2, 20, 35
ST	4.5	7.35	1 day	50	2, 20, 35
ST	4.5	7.35	1 day	100	2, 20, 35
ST	4.5	7.35	1 day	150	2, 20, 35
ST	4.5	7.35	3 days	50	2, 20, 35
ST	4.5	7.35	3 days	100	2, 20, 35
ST	4.5	7.35	3 days	150	2, 20, 35
ST	4.5	7.35	7 days	50	2, 20, 35
ST	4.5	7.35	7 days	100	2, 20, 35
ST	4.5	7.35	7 days	150	2, 20, 35
ST	4.5	7.35	28 days	50	2, 20, 35
ST	4.5	7.35	28 days	100	2, 20, 35
ST	4.5	7.35	28 days	150	2, 20, 35

4.3.2.3.3 Monitoring suction and volumetric water content

To study the effect of curing temperature and curing time on the changes in the self-desiccation of CPB, i.e. the consumption of capillary water by cement hydration, the pore water pressure or suction of the samples as well as their volumetric water content (VWC) were monitored. The suction was recorded by using an MPS-6 matrix water potential sensor ((Decagon Devices, Inc.), whereas a 5TE sensor was used to monitor the VWC. The MPS-6 matrix water potential sensor and 5TE sensor were installed at the interface between the CPB and rock. The rock was placed inside a plastic cylinder (with a diameter of 10 cm and height of 20 cm), which was then filled with cement paste. The MPS-6 sensor can take measurements of suction from -9 kPa to -100,000 kPa. The six calibration points of MPS-6 result in an accuracy of ± (10% of reading + 2 kPa) over the range of −9 kPa to −100 kPa. Moreover, this matrix water potential sensor can operate well at temperatures from -40°C to 60°C. The 5TE sensor measures the VWC at a range of 0-80% with an accuracy of ±0.01 from 1-40% and an accuracy of ±0.15 from 40-80%. The suction and VWC data were recorded by connecting the sensors, MPS-6 and 5TE, to an EM50 data logger.

4.3.2.3.4 Electrical conductivity monitoring

Electrical conductivity (EC) monitoring was also carried on the CPB-rock samples, which was performed by inserting a 5TE sensor into the interface between the rock and CPB. Then, the sensor was connected to the EM50 data logger for data recording. The 5TE sensor has an EC measurement range from 0 dS/m to 23 dS/m, with an accuracy of ±10% from 0 to 7 dS/m. The EC results can show the rate of ion movement, which is closely related to chemical reactions and water content. Hence, EC monitoring is an effective way to assess the progression of cement hydration as well as track the structural changes that occur within hydrating cementitious materials (Hansson and Hansson, 1985; Courard et al., 2014).

4.3.3 Results and discussion

4.3.3.1 Effects of curing temperature on shear behaviour of CPB-rock interface

Figures 4.26 and 4.27 show the typical shear behaviour of the CPB-rock interface cured at three different temperatures for 7 days (with a normal stress of 50 kPa). The shear displacement-shear stress curves presented in Figures 4.26(a) and 4.27(a) show that for any type of tailings and given curing temperature, all of the shear stress curves of the CPB-rock interfaces show similar trends, with an increase up to the peak shear stress, followed by a decrease to residual shear stress. It can also be observed that the highest curing temperature of 35°C in this study corresponds to the highest peak shear stress. The shear strength and elastic shear modulus of the CPB-rock interface also increase at a higher curing temperature. Furthermore, Figures 4.26(a) and 4.27(a) show that the shear stress of the 7 day CPB-rock samples cured at 20°C and 35°C, i.e. at higher curing temperatures, experience sudden bond failure of the cohesive surface which was also observed on cemented shotcrete-rock joints by other academics, including Swedenborg (2001), Saiang et al. (2005) and Tian et al. (2015). However, the shear strength of the CPB-rock interface in which the CPB is made with ST is generally higher than that of the CPB-rock interface in which the CPB is made with NT, regardless of the curing temperature. This is attributed to the presence of chemical components (sulphate) in NT, which has an inhibition effect on cement hydration.

The corresponding vertical displacement-shear displacement curves of the CPB-rock interface Figures 4.26(a) and 4.27(a) show that regardless of the curing temperature and type of tailings, the interface of all of the CPB-rock samples shows significant contraction at the beginning of the direct shear test because as soon as normal stress is applied, the surface of both the CPB and rock move closer together (Fall and Nasir, 2010). However, with increasing shear displacement up to peak shear displacement, the samples cured at higher temperatures of 20°C and 35°C show dilating behaviour, while the sample cured at a lower temperature of 2°C continues to contract. For subsequent shear deformation beyond the peak shear displacement, all of the samples show in general, contraction at the interface. Moreover, it can be also observed in Figures 4.26(a) and 4.27(a) that the vertical contraction (deformation) at the interface is greater at lower curing temperatures.

Figure 4.28 presents the peak shear stresses at the CBP-rock interface of the 7-day samples cured at different temperatures and the corresponding shear strength envelopes. These shear envelopes are obtained by fitting linear regression lines through each set of data on the peak shear stress vs. normal stress at the interface. From the results, it is obvious that the shear failure envelopes of the interface of the CPB-rock samples follow the Mohr-Coulomb failure criterion (Eq.(4-6)), regardless of the curing temperature. Consequently, the following Mohr–Coulomb type equation is used to find the values of the friction angle (φ) at the interface and adhesion or cohesion (c) for the range of normal stresses:

$$\tau = c + \sigma_n \tan(\varphi) \tag{4-6}$$

where τ is the shear stress of the CPB-rock interface, σ_n is the normal stress, c and φ are the adhesion and friction angle of the interface, respectively. The figure shows that the R^2 of the two regression lines of the interface of the samples cured at 20°C and 35°C is approximately 1, while for samples cured at a low temperature of 2°C, the R^2 is 0.96. Besides, for the 7 day samples, the adhesion of the interface increases from 31.8 kPa to 72.8 kPa when the curing temperature is increased from 2°C to 35°C. Meanwhile, the friction angle also experiences a slight increase from 25.7° at 2°C to 30.3° at 35°C.

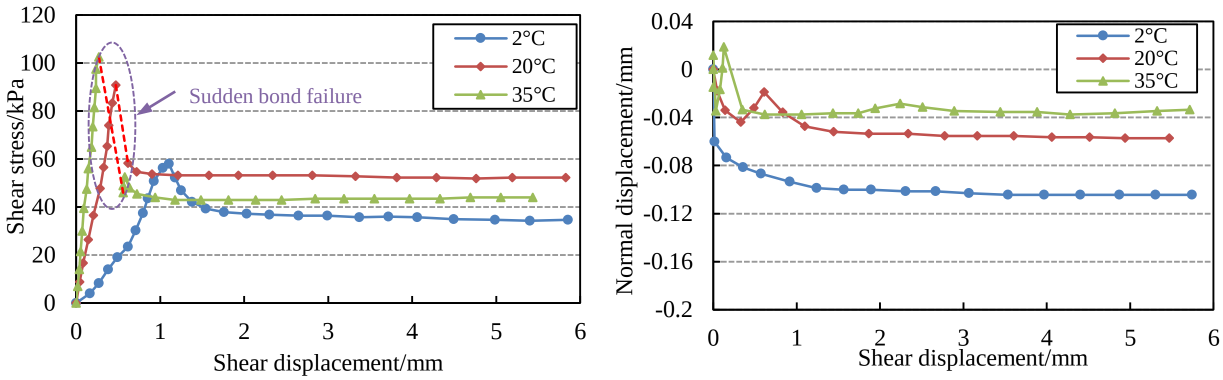

(a) Shear displacement-shear stress curve (b) Shear displacement-vertical displacement curve

Figure 4.26 Effect of curing temperature on shear behaviour of CPB–rock interface (made with ST; cured for 7 days; normal stress = 50 kPa)

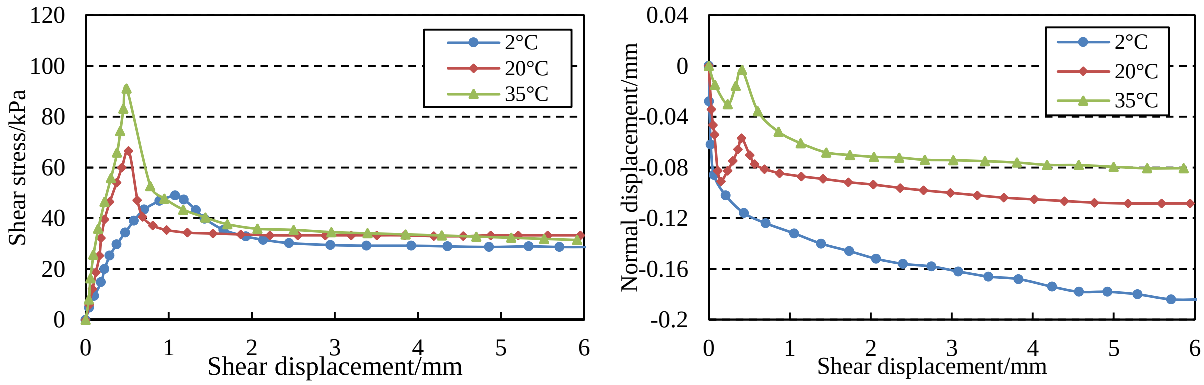

(a) Shear displacement-shear stress curve (b) Shear displacement-vertical displacement curve

Figure 4.27 Effect of curing temperature on shear behaviour of CPB–rock interface (made with NT; cured for 7 days; normal stress = 50 kPa)

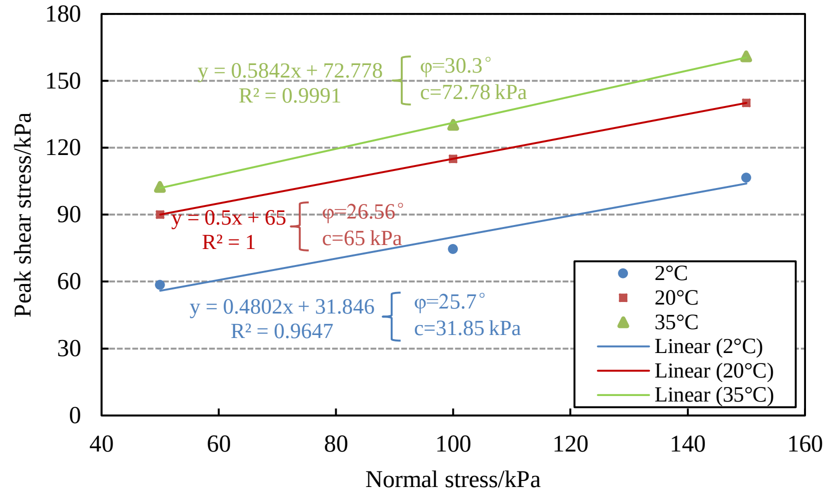

Figure 4.28 Peak shear stress vs normal stress of CPB–rock interface (cured for 7 days)

The increase in shear strength and interface shear parameters (adhesion, friction angle), smaller contraction of the interface as well as larger shear dilation of the interface with higher curing temperatures can be mainly attributed to the combined effects of two factors: (i) temperature induced increase in the rate of cement hydration; and (ii) temperature induced increase in self-desiccation, which are both discussed below.

4.3.3.1.1 Temperature induced increase in rate of cement hydration

It is well known that higher temperatures increase the rate of cement hydration. As a result, more cement hydration products are generated (Taylor, 1961; Lothenbach, 2007) in the samples cured at higher temperatures. The main product of cement hydration is calcium silicate hydrate (C-S-H), which is known as the major binding phase in hardened cement (Gani, 1997; Fall and Pokharel, 2010; Pokharel and Fall, 2013). Consequently, the larger volume of C-S-H results in a stronger binding force between the CPB and rock as the curing temperatures is increased, thereby increasing the peak shear stress as well as leading to more marked bonding failure of the cohesive interface. Moreover, the precipitation of other types of cement hydration products (e.g., ettringite, gypsum) into the empty capillary pores of the CPB increases the area of contact between CPB and the rock, which in turn leads to a stronger interlocking interface structure of the samples cured at higher temperatures. This also contributes to the increase in shear strength of the CPB-rock interface.

The increasing amount of cement hydration products (C-S-H, ettringite, calcium hydroxide (CH) and gypsum) at higher temperatures is demonstrated by the experimental evidence presented in Figure 4.29. This figure presents the results of TG and DTG analyses on the powdered cement paste of the CPB samples cured at 20°C and 35°C. It is well known that the peak or weight loss situated between 30°C-105°C results from the evaporation of bound water, and the weight loss between 110°C-200°C is due to the dehydration of hydration products, such as ettringite, gypsum and C-S-H, while the significant weight loss at 400°C-450°C and 600°C-750°C is attributed to the decomposition of CH and calcite, respectively (Nonnet, 1999; Sha et al., 1999; Zhou and Glasser, 2001; Pane and Hansen, 2005; Li and Fall, 2018). A comparison of the plotted TG and DTG of the cement paste of the CPB samples cured at 20°C and 35°C indicates that their weight loss due to water evaporation is similar, while that caused by the dehydration reaction of the cement hydration products (at temperatures between 110°C to 200°C) of the sample cured at 35°C is greater than the sample cured at 20°C. This means that more cement hydration products are generated in the CPB sample cured at 35°C. The rapid increase in the rate of cement hydration due to a higher curing temperature is also found in the EC of the CPB-rock samples cured at different temperatures (2°C, 20°C and 35°C) as presented in Figure 4.30. It can be clearly observed in the figure that samples cured at higher temperatures require less time before the EC reaches the maximum value, which indicates the acceleration of the cement hydration process at higher temperatures. Indeed, the EC values peak after curing for 9.5 hours, 4.8 hours and 1.25 hours at a curing temperature of 2°C, 20°C and 35°C, respectively. These results again confirm that the cement hydration rate increases at a higher curing temperature.

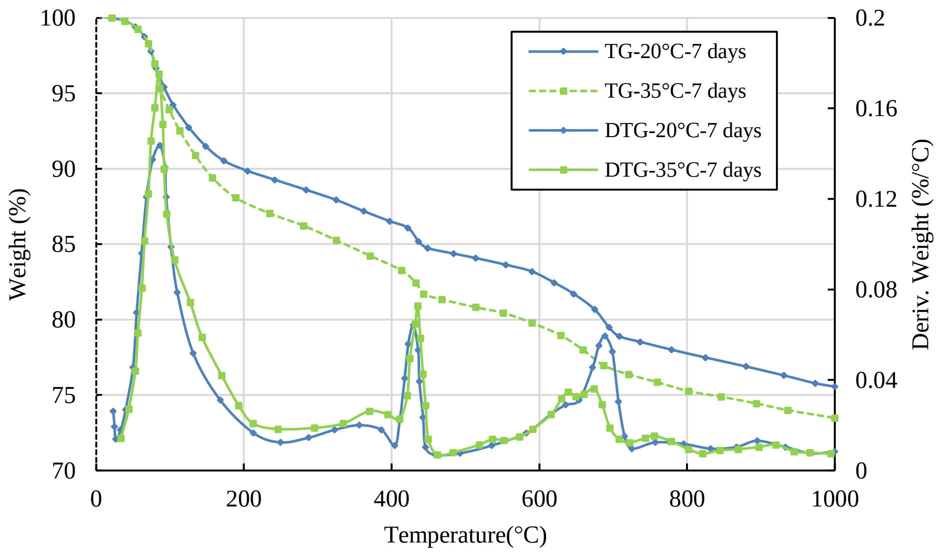

Figure 4.29 Plotted TG and DTG of cement paste of CPB-rock samples cured at 20°C and 35°C (cured for seven days)

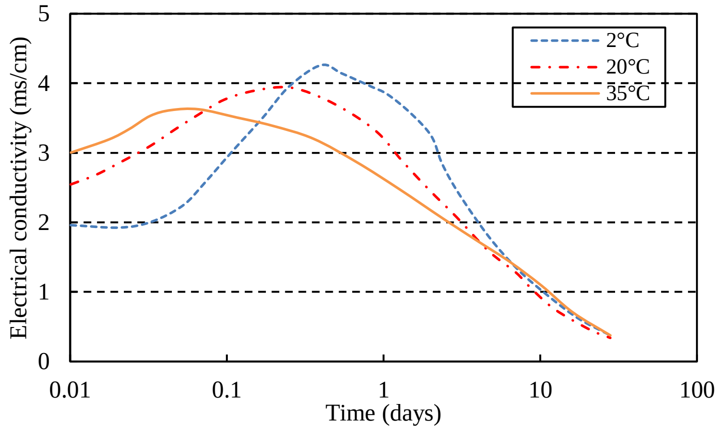

Figure 4.30 Changes in electrical conductivity of samples cured at different temperatures

The observed contraction at the interface is larger with reduced curing temperature because of the weaker cementation or less cement hydration at lower temperatures, which in turn, results in higher compressibility of the CPB-rock samples. Increased compressibility of cemented materials with less cement hydration has been reported or demonstrated in many previous studies (Xia and Lee, 2008; Uddin et al., 1997; Lorenzo and Bergado, 2004; Monteiro and Metha, 1993). The observed dilation of the interface of the samples cured at higher temperatures is the result of the relative movement of the asperity, which is stronger on the surface of the CPB sample cured at higher temperatures. A higher curing temperature results in higher binder hydration, and thus the formation of more cement hydration products as discussed previously (Figure 4.29). In other words, the CPB increases in hardness as the curing temperature increases, which will result in stronger asperities on the surface of the CPB.

4.3.3.1.2 Temperature-induced increase of self-desiccation

Cement hydration causes a net reduction of the total volume of water and solids, thereby decreasing the pore water pressure or moisture content in cementitious materials or CPB (Helinski et al., 2007). This phenomenon, called self-desiccation, is significantly influenced by temperature (Wang et al., 2016). Higher temperature leads to more intense self-desiccation because the process increases the rate of cement hydration, thereby resulting in more and faster consumption of the water in the capillary pores of the cemented material (Wang et al., 2016; Sant, 2012). In other words, the temperature induced increase of self-desiccation can lead to the generation of higher suction or capillary pressure at the CPB-rock interface. Higher suction or capillary pressure contributes to increases in the shear strength of the interface and modulus of elasticity. Numerous previous studies have demonstrated that higher suction can result in higher shear strength and modulus of elasticity of porous media (Fredlund et al., 1978; Vanapalli et al., 1996; Khalili et al., 2004) and soil-structure interface (Borana et al., 2016; Hossain and Yin, 2013). This increase of self-desiccation as the curing temperature is increased is experimentally shown by using the monitoring results; see Figures 4.31 and 4.32. Figure 4.31 illustrates the time-dependent change of the

VWC of the CPB-rock interface with various curing temperatures, while Figure 4.32 shows the changes in the matrix suction of the CPB-rock interface with various curing temperatures. The two figures clearly show that the VWC and matrix suction of the CPB-rock samples and their changes with time are strongly dependent on the curing temperature of the backfill. Higher curing temperatures lead to lower VWC values but higher matrix suction values, particularly at the early ages. In other words, a higher curing temperature results in more intense self-desiccation. For example, the measured VWC and recorded suction values for the 7 day samples is 0.44, 0.41 and 0.39, and 179, 250 and 284 kPa at curing temperatures of 2°C, 20°C and 35°C, respectively.

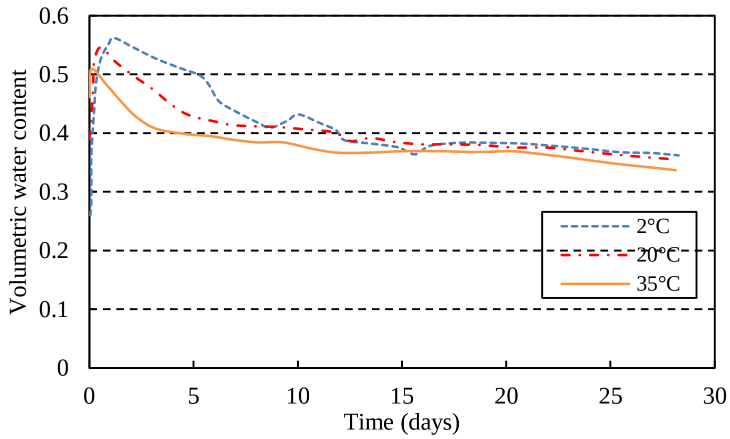

Figure 4.31 Effect of curing temperature on changes in volumetric water content

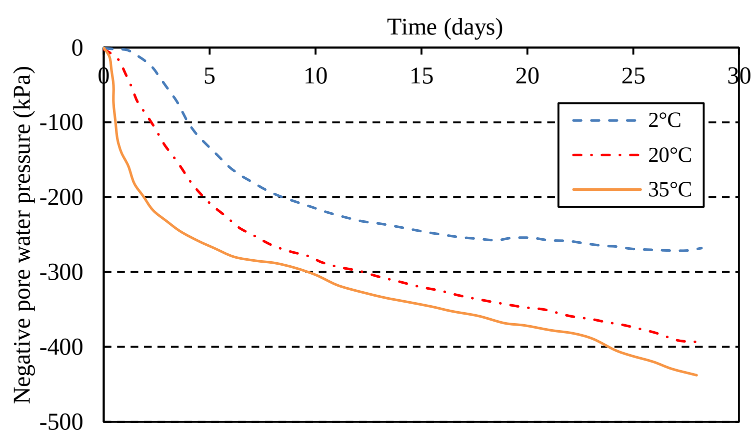

Figure 4.32 Effect of curing temperature on changes in matrix suction

4.3.3.2 Effect of curing temperature and curing time on shear behaviour of CPB-rock interface

4.3.3.2.1 Combined effect of curing temperature and curing time on shear behaviour and peak shear stress of CPB-rock interface

Figure 4.33 shows the typical effects of curing time on the relationship between the shear stress and displacement (Figure 4.33(a)) and vertical displacement and displacement (Figure 4.33(b)) of CPB-rock samples cured at 20°C (normal stress of 100 kPa). It can be clearly observed in Figure 4.33(a) that the shear strength increases with a longer curing time. The peak shear stress at the CPB-rock interface increases from 70 kPa on the first day to 142 kPa on the twenty-eighth day. Besides, for samples cured at 20°C, the sudden bond failure mentioned above only occurs after 7 days of curing. It can also be observed that the average deformation modulus of the CPB-rock interface cured for 1, 3, 7 and 28 days is 0.34 MPa, 1.4 MPa, 1.8 MPa and 3.4 MPa, respectively. Meanwhile, the compressibility of the samples is considerably reduced with curing time, and the CPB-rock interface of the samples cured for 28 days even experiences dilation. The increase in the shear strength and decrease in compressibility with curing time are due to the increased cement hydration. This argument is supported by the thermal analyses shown in Figure 4.34, in which the weight loss at temperatures of 110°C-200°C and 400°C-450°C for the 28 day samples are higher than those that are only cured for 7 days. This means that more ettringite, C-S-H and CH are generated in the former. The C-S-H can increase the binding force between particles, while the precipitation of more hydration products (e.g. ettringite, CH) results in the refinement of the pore structure within the CPB, and thus increase the shear strength of the CPB-rock interface as explained previously. The observed dilating behaviour at the interface in the advanced ages (28 days) is due to the stronger asperity on the surface of the CPB, as a result of increased cement hydration.

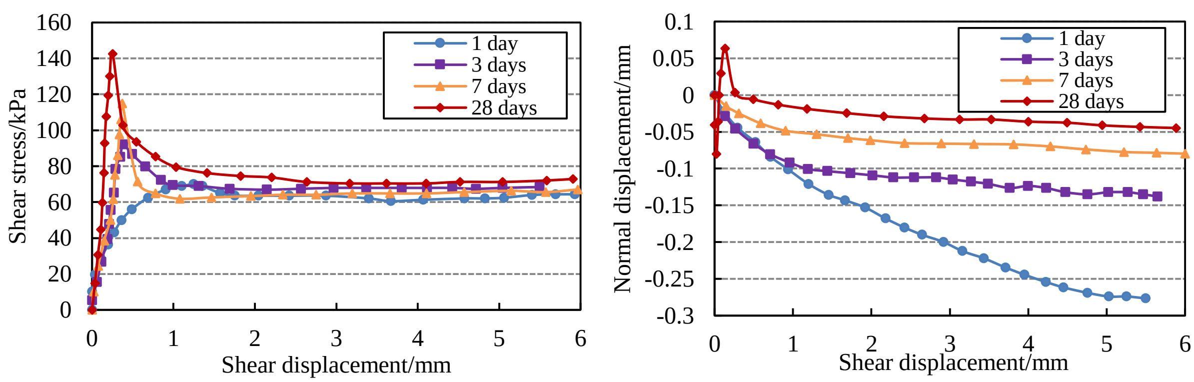

(a) Shear displacement-shear stress curve

(b) Shear displacement-vertical displacement curve

Figure 4.33 Effect of curing time on shear behaviour of CPB–rock interface for sample cured at 20°C (normal stress = 100 kPa; CPB made with ST)

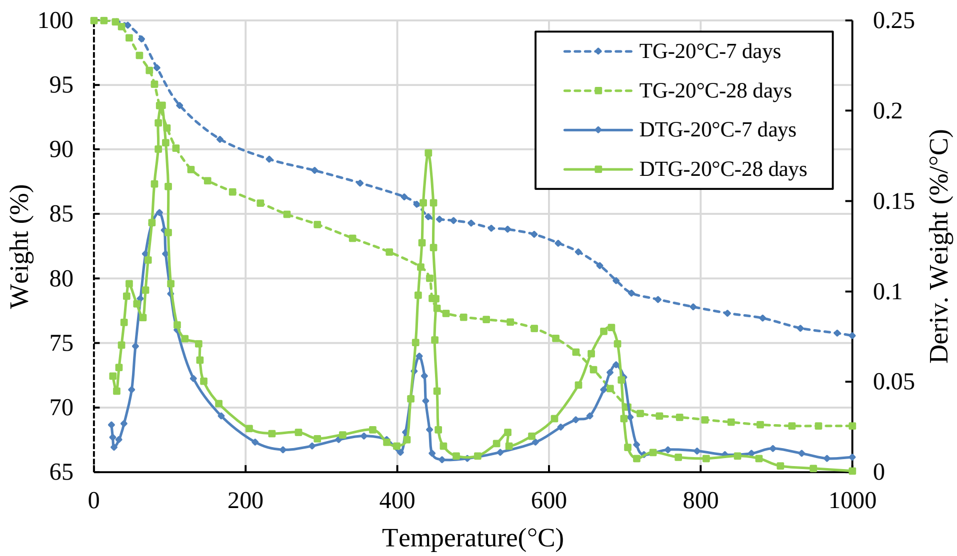

Figure 4.34 TG/DTG analyses on cement paste of CPB-rock samples cured for 7 and 28 days (20°C)

However, the time-dependent changes of the shear strength of the CPB-rock interface are also significantly influenced by the curing temperature as illustrated by the results presented in Figure 4.35. The combined effects of curing temperature and curing time on peak shear stress changes are presented in Figure 4.35 (normal stress: 50 kPa). It can be observed that the CPB-rock samples cured at higher temperatures show higher shear strength of the interface (except for samples cured at 35°C for 28 days; this will be discussed later). Moreover, the rate of increase of the shear strength of the CPB-rock interface is significantly influenced by the curing temperature. The shear strength of samples cured at 2°C increases from 30 kPa after 1 day of curing to 71 kPa after 28 days of curing. In contrast, the peak shear stress of samples cured at 20°C and 35°C increases from 45 kPa and 56 kPa after one day of curing to 126 kPa and 121 kPa after 28 days of curing, respectively.

The higher shear strength and rate of increase in shear strength of the interface observed for samples cured at higher temperatures are due to the temperature-induced acceleration of cement hydration and self-desiccation. As a result, more hydration products are generated (e.g., ettringite, C-S-H) in the samples, and the samples also develop higher suction when cured at higher temperatures, which in turn, lead to higher shear strength and rate of increase in shear strength of the interface. This increase in cement hydration and self-desiccation due to temperature has been already demonstrated and discussed previously. The advantages of the refinement of the pore structure of CPB due to the precipitation of more hydration products are supported by the results of the MIP test which are presented in Figure 4.36(a). The figure shows the pore size distribution of CPB cured at two different temperatures of 20°C and 35°C for 7 days. It can be clearly observed that the CPB sample cured at 35°C has a finer pore structure than that cured at 20°C. The finer pore structure is indicative of the precipitation of more hydration products in the capillary pores of CPB as the higher temperature significantly reduces the coarseness of the pore structure, thereby increasing the contact area between the CPB and the rock surface, which in turn contributes to the increase of the shear strength of the interface as discussed earlier. The pore size distribution of CPB cured for 7 and 28 days, as shown in Figure 4.36(b), shows that aside from higher curing temperatures, a longer curing time also leads to refinement of the pore structure. It can be seen that the 28-day CPB has a denser microstructure than the 7-day sample. This suggests that a more refined pore structure with longer curing time is also another factor that contributes to the increase in the shear strength of the CPB-rock interface.

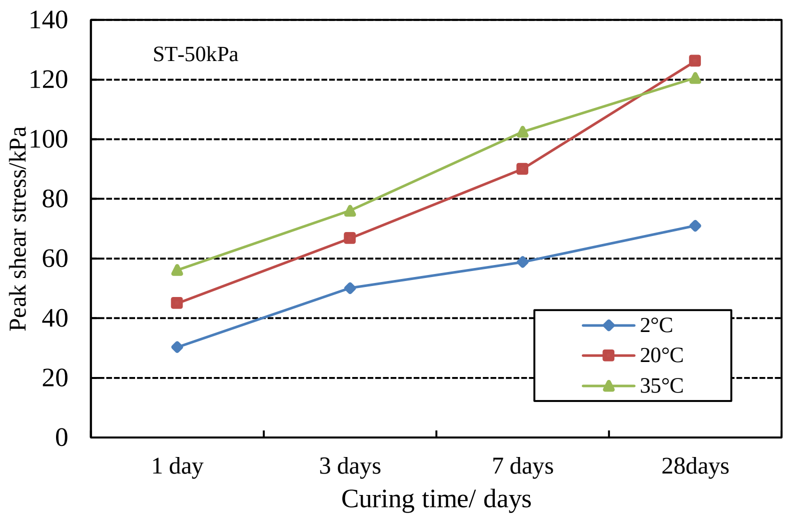

Figure 4.35 Peak shear stress development at CPB-rock interface

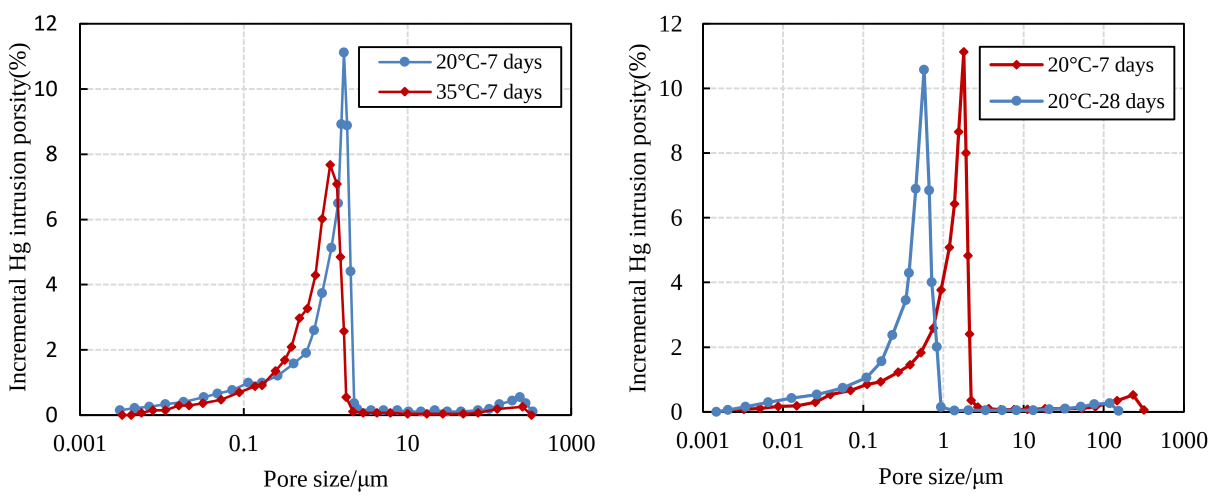

(a) Effect of curing temperature on pore size distribution (after 7 days)

(b) Effect of curing time on pore size distribution (20°C)

Figure 4.36 MIP pore size distribution of CPB

The lower shear strength of the interface of the CPB-rock sample cured at 35°C for 28 days (in comparison to that cured at 20°C) is due to the crossover effect, which mainly happens in cementitious materials cured at higher temperatures at the advanced ages (Kjellsen et al., 1991; Escalante-Garcia and Sharp, 2001). This phenomenon of reduced mechanical strength due to temperature is also observed in conventional concrete (Alexander and Taplin, 1962). The presence of the crossover effect is commonly caused by the: (i) formation of microcracks (Carino, 1981). With increased temperatures, the initial water pressure and voids in the samples increase. When the stress surpasses the tensile strength, microcracks form in the CPB. Then, the physical damage reduces the adhesion and peak shear stress; (ii) non-uniform distribution of cement hydration products (Kjellsen et al., 1990). A higher temperature generally causes rapid hydration which produces large amounts of cement hydration products. Due to their low solubility and diffusivity, cement hydration products cannot diffuse to a significant distance. Meanwhile, the dense hydration products around the cement grains serve as diffusion barriers, which further prevent the hydration products from migrating. Thus, a higher curing temperature results in a coarser pore structure at the advanced ages; and (iii) destabilization of ettringite (Pokharel and Fall, 2013). The solubility of ettringite increases with increasing temperatures, which also causes the coarsening of the pore structure.

4.3.3.2.2 Combined effects of curing temperature and curing time on adhesion and friction angle of CPB-rock interface

Figure 4.37 illustrates the development of the adhesion and friction angle of the CPB-rock interface for the samples cured at three different temperatures with curing time. It can be seen that the time-dependent change of the friction angle and adhesion of the interface are significantly influenced by the curing temperature. For example, the friction angle increases from 24.1° on the third day of curing to 29.9° on the twenty-eighth day of curing at a temperature of 2°C. In contrast, the friction angle of the interface of the samples cured at 20°C and 35°C increases from 25.2° and 26.5° on the first day of curing to 32.2° and 30.7° on the twenty-eighth day of curing, respectively. Moreover, a higher curing temperature corresponds to a higher rate of increase of the friction angle and in the adhesion. The larger friction angle and higher rate of increase of the friction angle with curing temperature are attributed to increased cement hydration with higher temperatures (Figure 4.29), which results in stronger asperities on the CPB and rock, thereby increasing the friction at the interface (Acar and EI-Tahir, 1986; Clough et al., 1989; Nasir and Fall, 2008; Lade and Overton, 1989). The greater cement hydration also produces more cement hydration products (C-S-H, CH, ettringite), and thus results in a stronger binding force or adhesion between the CPB and the interface. The lower friction angle and interface adhesion of the sample cured at 35°C for 28 days (in comparison to that cured at 20°C) are resultant of the crossover effect, which causes physical damage and a coarse pore structure in the CPB (thus reducing the contact area between the CPB and the rock surface).

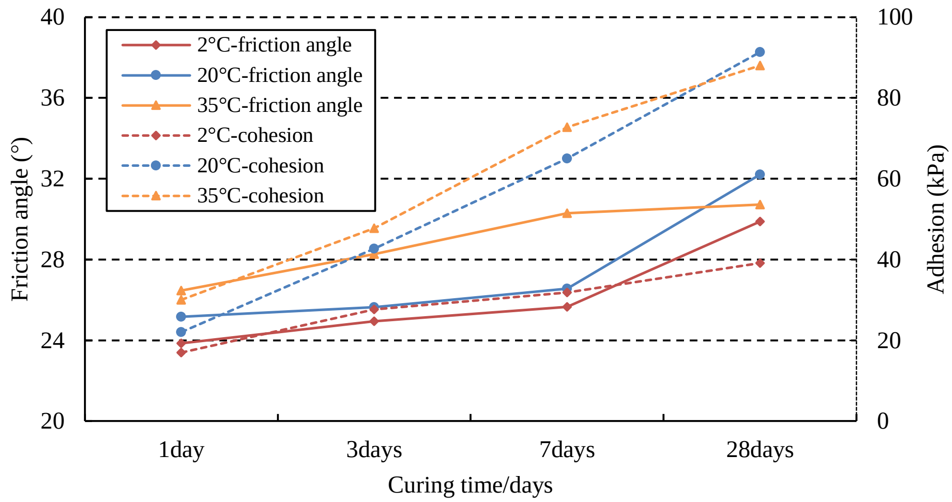

Figure 4.37 Development of adhesion and friction angle of CPB-rock interface

4.3.4 Summary and conclusions

The experimental results in this paper show the effect of curing temperature on the shear behaviour of the interface between rock and tailings backfill that is undergoing cementation. The main conclusions derived from this study are summarized as follows:

- Temperature has a significant impact on the shear behaviour and strength of the interface between CPB and rock. The obtained results show that the curing temperature and curing time both determine the changes in shear strength and properties of the CPB-rock interface.

- Higher curing temperatures (up to 35°C in this study) improve the rate of cement hydration and self-desiccation. As a result, the shear strength of the CPB-rock interface is significantly increased. In contrast, the compressibility of CPB is reduced with curing temperature and the interface of the CPB-rock sample cured at a higher temperature experience higher shear dilation.

- The shear failure envelope of the interface of the CPB-rock samples follows the Mohr-Coulomb failure criterion, and both the friction angle and adhesion of the interface increase with temperature. However, the interface of the samples that are cured for a long time (28 days in this study) has less adhesion and smaller friction angle when cured at 35°C (in comparison to 20°C) due to the crossover effect which is resultant of high temperatures.

The results presented in this paper will contribute to a better understanding of the shear behaviour of the CPB-rock interface at various temperatures, which is critical for the assessment of the arching effect in CPB mass, and the cost-effective design of CPB structures.

Acknowledgements

The authors would like to thank the Natural Sciences and Engineering Research Council of Canada (NSERC) and the University of Ottawa.

4.3.5 References

Acar YB, EI-Tahir AE (1986) Low strain dynamic properties of artificially cemented sand. Journal of Geotechnical Engineering 121(11):1001-1015.

Alexander K, Taplin J (1962) Concrete strength, paste strength, cement hydration, and the maturity rule. Australian Journal of Applied Science, 13(4):277-284.

Benzaazoua M, Fall M, Belem T (2004) A contribution to understanding the hardening process of cemented pastefill. Miner. Eng. 17(2):141-152.

Borana L, Yin JH, Singh DN, Shukla SK (2016) Interface Behaviour from Suction-Controlled Direct Shear Test on Completely Decomposed Granitic Soil and Steel Surfaces. Int. J. Geomech. 16(6):D4016008

Carino NJ (1981) Temperature Effects on the Strength–Maturity Relation of Mortar, Report No. NBSIR 81-2244. National Bureau of Standards, Washington, D.C. 90.

Clough GW, Iwabuchi J, Rad NS, Kuppusamy T (1989) Influence of cementation on liquefaction of sands. Journal of Geotechnical Engineering 115(8):1102-1117.

Courard L, Michel F, Perkowicz S, Garbacz A (2004) Effects of limestone fillers on surface free energy and electrical conductivity of the interstitial solution of cement mixes. Cem. Concr. Compos. 45:111-116.

Cui, L, Fall M (2017) Multiphysics modelling of arching effects in fill mass. Comput. Geotech. 83:114-131.

Escalante-Garcia JI, Sharp JH (2001) The microstructure and mechanical properties of blended cements hydrated at various temperatures. Cem. Concr. Res. 31(5):695–702.

Fall M, Célestin JC, Pokharel M, Touré M (2010) A contribution to understanding the effects of curing temperature on the mechanical properties of mine cemented tailings backfill. Eng. Geol. 114(3):397-413.

Fall, M., Nasir, O (2010) Mechanical behaviour of the interface between cemented tailings backfill and retaining structures under shear loads. Journal of Geotechnical and Geological Engineering 26(6): 779-790.

Fall M, Pokharel M (2010) Coupled effects of sulphate and temperature on the strength development of cemented tailings backfills: Portland cement-paste backfill. Cem. Concr. Compos. 32:819–828.

Fall M, Samb S (2008) Pore structure of cemented tailings materials under natural or accidental thermal loads. Mater. Charact. 59(5):598-605.

Fredlund DG, Morgenstern NR, Widger RA (1978) The shear strength of unsaturated soils. Canadian Geotechnical Journal 15(3):313-321.

Gani MSJ (1997) Cement and Concrete, Chapman & Hall, London, UK.

Grice T (2001) Recent mine developments in Australia. Proceedings of the 7th International Symposium on Mining with Backfill (MINEFILL) 351-357.

Hansson LH, Hansson CM (1985) Ion conduction in cement based materials. Cem. Concr. Res. 15(2):201-212.

Hassani F, Archibal J (1998) Mine backfill. Canadian Institute of Mine, Metallury and Petroleum, Canada.

Helinski M, Fourie A, Fahey M, Ismail M (2007) Assessment of the self-desiccation process in cemented mine backfills. Canadian Geotechnical Journal 44(10):1148-1156.

Hossain MA, Yin JH (2013) Unsaturated soil-cement interface behaviour in direct shear tests. Aust. Geomech. J. 48(3):141-153.

Khalili N, Geiser F, Blight GE (2004) Effective stress in unsaturated soils: review with new evidence. Int. J. Geomech. 4(2): 115-126.

Kim JK, Moon YH, Eo SH (1998) Compressive strength development of concrete with different curing time and temperature. Cem. Concr. Res. 12:1761–1773.

Kjellsen KO, Detwiler RJ, Gjorv OE (1991) Development of microstructures in plain cement pastes hydrated at different temperatures. Cem. Concr. Res. 21(1):179–189.

Kjellsen KO, Detwiler RJ, Gjorv OE (1990) Pore structure of plain cement pastes hydrated at different temperatures. Cem. Concr. Res. 20(6):927–933.

Lade PV, Overton DD (1989) Cementation effects in friction materials. Journal of Geotechnical Engineering 115(10):1373-1387.

Li L, Aubertin JD, Dubé JS (2014) Stress distribution in a cohesionless backfill poured in a silo. The Open Civil Engineering Journal 8(1):1-8.

Li, W., Fall, M (2018) Strength and self-desiccation of Slag-Cemented paste backfill: Link to initial sulphate concentration. Cem. Concr. Compos. 89:160-168.

Lorenzo GA, Bergado. DT (2004) Fundamental parameters of cement-admixed clay – new approach. J. Geotech. Geoenviron. Eng. ASCE. 130(10):1042-1050.
Lothenbach B, Winnefeld F, Alder C, Wieland E, Lunk P (2007) Effect of temperature on the pore solution, microstructure and hydration products of Portland cement pastes. Cem. Concr. Res. 37(4):483-491.
Monteiro PJM, Metha PK (1993) Concrete: Structure, Properties and Materials. Prentice-Hall Inc, Englewood Cliffs.
Nasir O, Fall M (2008) Shear behaviour of cemented pastefill-rock interfaces. Eng. Geol. 101(3):146-153.
Nonnet E, Lequeux N, Boch P (1999) Elastic properties of high alumina cement castables from room temperature to 1600°C. J. Eur. Ceram. Soc. 19(8):1575–1583.
Pane I, Hansen W (2005) Investigation of blended cement hydration by isothermal calorimetry and thermal analysis. Cem. Concr. Res. 35(6):1155–1164.
Pokharel M, Fall M (2013) Combined influence of sulphate and temperature on the saturated hydraulic conductivity of hardened cemented paste backfill. Cem. Concr. Compos. 8:21-28.
Rawlings CA, Phillips HR (2001) Reduction of mine heat loads. Proceedings of the 7th International Mine Ventilation Congress, 381–389.
Saiang D, Malmgren L, Nordlund E (2005) Laboratory tests on shotcrete-rock joints in direct shear, tension and compression. Rock Mech. Rock Eng. 38(4):275-297.
Sant G (2012) The influence of temperature on autogenous volume changes in cementitious materials containing shrinkage reducing admixtures. Cem. Concr. Compos. 34(7):855-865.
Schneider U (1988) Concrete at high temperatures-a general review. Fire Saf. J. 13(1):55-68.
Sha W, O'Neill E, Guo Z (1999) Differential scanning calorimetry study of ordinary Portland cement. Cem. Concr. Res. 29(9):1487–1489.
Swedenborg S (2001) Rock mechanical effects of cement grouting in hard rock. PhD Dissertation, Chalmers University of Technology.
Taylor HFW (1964) The chemistry of cements, vol. 1, 1st ed. London: Academic Press.
Thompson BD, Grabinsky M, Bawden W, Counter D (2009) In-situ measurements of cemented paste backfill in long-hole stopes. In: Proceedings of 3rd CANUS rock mechanics symposium, Toronto.
Tian HM, Chen WZ, Yang DS, Yang JP (2015) Experimental and numerical analysis of the shear behaviour of cemented concrete–rock joints. Rock Mech. Rock Eng. 48(1):213-222.
Tse R, Cruden DM (1979) Estimating Joint Roughness Coefficients. Int. J. Rock Mech. Min. Sci. 16(5):303–307.
Uddin K, Balasubramaniam AS, Bergado DT (1997) Engineering Behaviour of Cement-Treated Bangkok Soft Clay. Geotech. Eng. 28(1):89-121.
Udd J (2006) A bibliography on deep mining. Proceedings of the core project on deep mining.
Vanapalli SK, Fredlund DG, Pufahl DE, Clifton AW (1996) Model for the prediction of shear strength with respect to soil suction. Canadian Geotechnical Journal 33(3): 379-392.
Wang Y, Fall M, Wu A (2016) Initial temperature-dependence of strength development and self-desiccation in cemented paste backfill that contains sodium silicate. Cem. Concr. Compos. 67:101-110.
Williams TJ, Denton DK, Larson MK, Rains, R.L, Seymour JB, Tesarik DR (2001) Geomechanics of Reinforced cemented backfill in an underground stope at the Lucky Friday Mine. Mullan, Idaho, 1-18.
Wu Q, Zhang T, Liu Y (2010) Permafrost temperatures and thickness on the Qinghai-Tibet Plateau. Global Planet. Change. 72(1-2):32-38.
Xia HW, Lee FH (2008) Curing time effect on behaviour of cement treated marine clay. International Journal of Marine and Environmental Sciences 2(7):144-151.
Yilmaz E, Kesimal A, Ercidi B (2004) Strength development of paste backfill simples at Long term using different binders. Proceedings of 8th symposium MineFill04, China.
Zhou Q, Glasser F (2001) Thermal stability and decomposition mechanisms of ettringite at <120 C. Cem. Concr. Res. 31(9):1333–1339.

4.4 Paper IV: Shear Behaviour of the Interface between Rock and Cemented Backfill: Effect of Curing Stress, Drainage Condition and Backfilling Rate

Published in *Rock Mechanics and Rock Engineering*, 2020, 53(1):325-336

Kun Fang, Mamadou Fall

Abstract

In-situ field, many factors, for example curing stress, drainage conditions as well as backfilling rate, have huge effects on the geotechnical properties and stability of cemented paste backfill (CPB) structures, which is an evolutive cemented soil mainly used for underground mine support. Having a comprehensive knowledge of the shear characteristics of the interface between CPB and rock, especially the shear resistance, is beneficial to a safer and more economical design of underground CPB structures. Unfortunately, no studies to date have investigated the effects of curing stress, drainage condition and backfilling rates on the interaction between CPB and surrounding rock mass. Hence, an experimental investigation is performed in this research to study the potential influences of curing stress (0 kPa, 50 kPa, and 150 kPa), drainage conditions (drained and undrained) and backfilling rate (20 kPa/3 hours, 30 kPa/3 hours, and 40 kPa/3 hours) of CPB on the shear performance of the interface. Finally, it was found out that higher curing stress and higher backfilling rate contribute to the shear strength development of the studied interface, as a result of increased effective stress and matrix suction at the interface. Moreover, in comparison to undrained condition, the drained condition benefits to the shear strength acquisition at the interface. The findings are practically important for opening barricades and designing filling sequences.

Keywords: interface, cemented paste backfill, curing stress, drainage condition, backfilling rate

4.4.1 Introduction

Tailings are the inevitable byproducts of mining activities worldwide. They are often rich in sulfuric acid and other toxic metals. Consequently, they can cause acid mine drainage (AMD). Large volumes of tailings that accumulate on the ground surface or the inappropriate disposal of tailings can therefore severely pollute the surface water and land (Aubertin et al., 2002; Buckby et al., 2003). Moreover, the potential failure of man-made facilities for storing tailings, such as dams, embankments, also poses a huge threat to the safety of communities and human health. For example, the tailings dam failure, which was happened in China in 2008, resulted in the death of about 277 individuals. In addition, more than 26 million cubic meters of tailings were released (Sun et al., 2012). Therefore, finding an environmentally-friendly tailing management method will not only benefit the ecology, ecosystem and people, but also increase the profits of mines.

During the last four decades, cement paste backfilling has been used in lieu of other backfilling methods due to its prominent advantages in managing tailings (Hassani and Archibald, 1998; Benzaazoua et al., 2004). Cement paste backfilling is an innovative mining method that replaces the ore bodies with a heterogeneous material that made of a mixture of thickened mill tailings, hydraulic binder and water. The proportions of the tailings and binder are 75%-85% and 3%~7%, respectively (Yilmaz et al., 2009; Fang and Fall, 2019). The cement paste backfill (CPB) material is usually produced at ground surface and then transported to underground mined-out voids by pumping or gravity. With the support of these CPB structures, the adjacent orebody can also be safely mined. Hence, in addition to environmental benefits, CPB is also an effective way to increase the recovery ratio of the extraction activity, ensure the stability of underground mining structures.

The mechanical properties (e.g., unconfined compressive strength (UCS), peak shear stress) of CPB are the most important characters when it comes to the design or stability assessment of CPB structures. There has been significant progress in the literature in determining the effects of factors that impact the development of the UCS of CPB, such as the water content, tailing fineness, and curing temperature (Belem et al., 2000; Fall and Benzaazoua, 2005; Fall et al., 2010). The typical interaction between rock mass and backfilling body (e.g., CPB), shown in Figure 4.38, shows that the peak shear stress of the studied interface is an important mechanical property in assessing the stability of underground structures. For example, Nasir and Fall (2008) found the interface strength and properties, including friction angle and adhesion, differ from those of CPB material, and therefore the stability of CPB structures should not be evaluated by only referring to the strength of CPB body alone. Furthermore, the arching effect, which plays a critical role in controlling the stability of geotechnical structures, is also found to be associated with the mechanical behaviour of the CPB-rock interface. When the arching effect takes place, most of the self-weight load was transferred to surrounding rock mass, and as a result, the effective vertical stress below the arching structure is considerably decreased. This phenomenon is also confirmed by the field measurements conducted by Helinski et al. (2011). Hence, the strength of CPB structures that are designed without taking the arching effect into consideration is higher than the required bearing capacity of CPB. The design of such CPB structures means consumption of more cement, the cost of which represents up to the majority (75%) of the investment of CPB (Fall and Benzaazoua, 2005)**.** Therefore, an in-depth knowledge of the arching effect and the shear performance of the interface not only can guarantee superior evaluation of the geotechnical of CPB structures, but also result in more economical CPB designs.

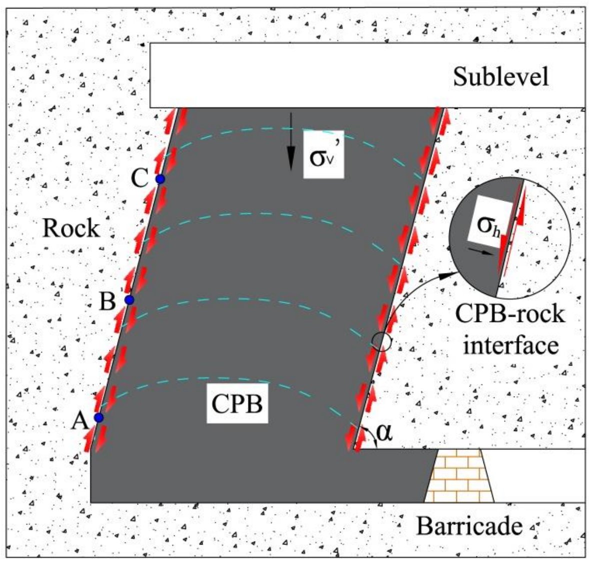

Figure 4.38 Interaction between CPB structure and surrounding rock mass (σ_v' : effective vertical stress; σ_h : horizontal pressure)

Even though many studies on the development of mechanical characteristics of CPB have been conducted (Kesimal et al., 2005; Simms and Grabinsky, 2009; Ercikdi et al., 2014), the fundamental knowledge of the shear properties of the CPB-rock interface is far from sufficient. To date, despite the limited researches on the interface shear behaviours (Nasir and Fall, 2008; Koupouli et al., 2016; Fang and Fall, 2018), the data are all collected from laboratory tests, and no studies have been conducted with the consideration of in-situ situations, such as curing stress, drainage and filling rate of the stopes. For example, the samples prepared in previous studies are cured without pressure. However, CPB structures in the field are usually exposed to substantial vertical and horizontal pressures (Ghirian and Fall, 2015). Moreover, the effects of drainage conditions and backfilling rates on the evolution of matrix suction in CPB also affect the effective stress (Helinski et al., 2006; Ghirian and Fall, 2016), which determine the magnitude of lateral pressure as shown in Eq.(4-7) (without considering the arching effect):

$$\sigma_h = k_a \sigma_v' \sin\alpha \tag{4-7}$$

where σ_h denotes the horizontal pressure (similar to the curing stress in the lab) at the interface, α refers to the inclined angle of the backfilling body, k_a is the active earth pressure coefficient, which can be expressed as an equation of friction angle of CPB, ϕ, ($k_a = (1-\sin\phi)/(1+\sin\phi)$), and $\sigma_v^{'}$ means the effective vertical stress, which equals to (Aubertin et al., 2003):

$$\sigma_v^{'} = \gamma B \left[\frac{1-\exp(-2k_a H \tan\phi^{'}/B)}{2k_a \tan\phi^{'}} \right] \tag{4-8}$$

where γ refers to the CPB's unit weight, B and H denote the width and depth of the studied backfilling structure, while $\phi^{'}$ means the interface friction angle.

According to Eqs.(4-7) and (4-8), the horizontal pressure at three points shown in Figure 4.38 varies significantly because they are at different depths. The difference in the horizontal pressure leads to variation in the interface shear strength. However, to date, the effects of horizontal pressure, drainage conditions as well as the backfilling rates on the shear bearing capability of CPB-rock interface have not been investigated. Therefore, given the research gap and the shortcomings in simulating field conditions, the authors of this paper apply an apparatus called the uOttawa Backfill Curing System (Ghirian and Fall, 2013, 2015; Cui and Fall, 2016) to analyze the effects of the aforementioned factors on the shear performance and properties of the interface.

4.4.2 Experimental program and microstructural analyses

4.4.2.1 Experimental materials

Synthetic tailings (silica tailings (ST)), binder (Portland cement type I, PCI) and water are three main materials used in this study for producing the CPB part of the interface samples. The ST share similar physical property (e.g., particle size distribution) with respect to nature tailing (NT) (Aldhafeeri and Fall, 2017). However, the use of ST can eliminate uncertainties that are otherwise found with the use of NT (which contains reactive minerals that can interfere with cement hydration process). The ST and PCI (weight proportion of 4.5%) were mixed with tap water, and the water-cement (w/c) ratio is controlled as 7.35.

Granite, which has an average UCS of 160 MPa, was used as the rock component of the sample. Before preparing the sample, the granite was shaped into small pieces with a size of 60×60×10 mm, which is exactly the same as the inside size of the shear box. Furthermore, the surface of the granite was carefully polished, and the roughness was determined to be zero (Tse and Cruden, 1979).

4.4.2.2 Experimental program

4.2.2.1 Apparatus used

Two key apparatuses are used in this study. The first one is a direct shear device, with a schematic diagram provided in Nasir and Fall (2008). The results of the direct shear test (which was conducted according to ASTM D3080-04) include the information of the shear strengths with respect to different normal stress, based on which the shear strength properties (including friction angle as well as adhesion) of the interface can be easily deduced.

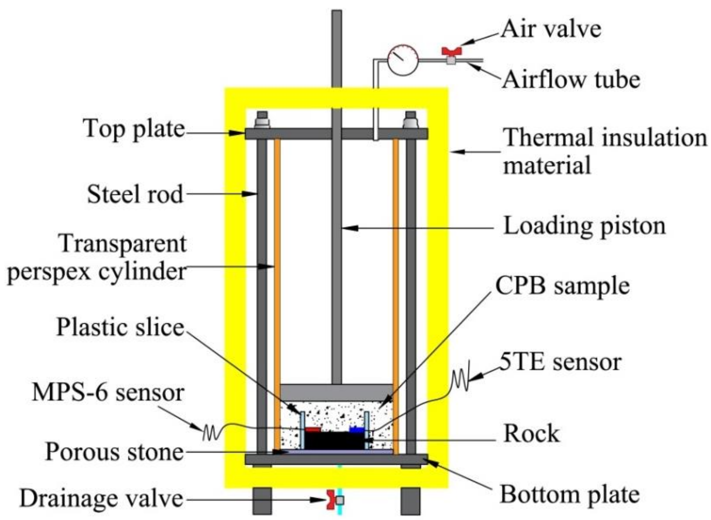

Figure 4.39 Schematic diagram of uOttawa Backfill Curing System (Ghirian and Fall, 2013; Cui and Fall, 2016)

The other apparatus is the uOttawa Backfill Curing System, which cures CPB samples under various thermal, hydraulic, stress and chemical conditions. A schematic diagram of the backfill curing system is illustrated in Figure 4.39. As can be seen from the figure, the sample was circled by a transparent Perspex cylinder, the diameter and height of which are 100 mm and 300 mm, respectively. On the top of the sample is a loading piston, which can move downwards vertically under the action of air pressure. The air valve can provide a pressure up to 600 kPa (Ghirian and Fall, 2013, 2015, 2016), and according to the average density of CPB, this air pressure allows a simulation of 35 m-high CPB structure (if the arching effect is neglected). Meanwhile, the controlling of different drainage conditions of samples in this test is achieved by closing or opening the drainage valve, which is connected to the bottom plate. The two plates (top and bottom plates) and cylinder are hold and tighten together by using three steel rods. In addition, to block the heat produced by cement hydration from dissipating to the surrounding environment, a thermal insulation material (e.g., glass wool blanker) is also used to insulate the system. In total, four backfill curing systems are adopted in the experiments, including one for monitoring purposes and three for different curing conditions. In the cylinder where the monitoring take place, two sensors, namely MPS-6 and 5TE (see Section 2.3.2), are set at the interface, which is shown in Figure 4.39. Furthermore, the rock sample is surrounded by four sheets of plastic, which allow the sample to fit into the shear box after curing. Otherwise, further trimming of the samples will inevitably impact the shear characteristics of the interface sample.

4.2.2.2 Testing procedure

The paste material was produced by mixing and stirring certain amount of ST, binder and water with a B20F mixer for 7 minutes. The obtained paste was then cast to the surface of the rock which was surrounded by four sheets of plastic slice (with a height of 30 mm). Thereafter, the sample within the four sheets of plastic slice was placed into the backfill curing system (on top of the porous stone). The adjacent void space was filled with the remaining CPB until the container was fully covered, as shown in Figure 4.39. With the application of air pressure onto the piston, two scenarios were simulated to investigate the influence of curing pressure, drainage condition and backfilling rate on the mechanical properties of the CPB-rock interface. As can be seen from Figure 4.40 and Table 4.8, the two scenarios include: (1) Scenario A: three constant normal stresses: 0, 50, and 150 kPa (Sub-scenarios A-1, A-2 and A-3, respectively) are applied on the samples during curing time (1, 3, and 7 days), and (2) Scenario B: three different backfilling rates were applied to the interface of the samples: 20 kPa/3 hours, 30 kPa/3 hours, and 40 kPa/3 hours (Sub-scenarios B-1, B-2 and B-3, respectively) until reaching a stress of 150 kPa. The samples for the two scenarios above are all cured in drained or undrained conditions.

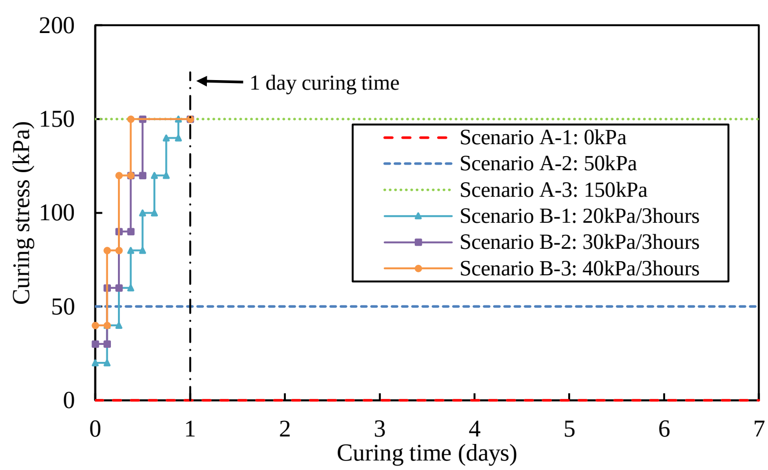

Figure 4.40 Curing stress vs. curing time with normal constant stress and backfilling rate

Table 4.8 Specific curing condition of two scenarios

Scenario	PCI content (%)	water-cement ratio	Curing time (days)	Curing stress (kPa)	Drainage condition	Normal stress (kPa)
A	4.5	7.35	1	0, 50, 150	Drained	50, 100, 150
A	4.5	7.35	3	0, 50, 150	Drained	50, 100, 150
A	4.5	7.35	7	0, 50, 150	Drained	50, 100, 150

A	4.5	7.35	1	0, 50, 150	Undrained	50, 100, 150
A	4.5	7.35	3	0, 50, 150	Undrained	50, 100, 150
A	4.5	7.35	7	0, 50, 150	Undrained	50, 100, 150
Scenario	PCI content (%)	water-cement ratio	Curing time (days)	Backfilling rate (kPa/3 hours)	Drainage condition	Normal stress (kPa)
B	4.5	7.35	1	20, 30, 40	Drained	50, 100, 150
B	4.5	7.35	1	20, 30, 40	Undrained	50, 100, 150

4.4.2.3 Microstructural analyses and monitoring program

4.4.2.3.1 Microstructural analyses

Thermal analyses (e.g., thermogravimetric and differential thermogravimetric analyses) and mercury intrusion porosimetry (MIP) test are two main microstructural analyses used in this paper to probe into the changes in the binder hydration degree as well as in the porosity of CPB. The thermal analyses are performed on cement paste, a mixture of PCI and water (with w/c=1), by using a Q5000IR thermogravimetric analyzer. This thermogravimetric analyzer allows the temperature to increase to 1000°C at different rates (herein 10°C per minute is used). Prior to the test, the cement paste sample is subjected to a pre-dried at 45°C for 4 days. The collected data of thermal analyses are used to analyze the degree and rate of the cement hydration. In contrast, the sample for MIP test is the dried (45°C for 4 days as well) CPB part of the interface sample, which is a mixture of ST, PCI and water. The MIP test was conducted with the Micromeritics AutoPore III mercury porosimeter. In addition to the porosity, the MIP results provide information about the pore size distribution of the tested CPB, which allow us to analyze the pore structure of the samples subjected to different curing conditions.

4.4.2.3.2 Temperature and matrix suction monitoring

The evolution of matrix suction and temperature in CPB (subjected to different curing stresses and drainage condition) is monitored by using a dielectric water potential sensor, MPS-6, which has the capacity to measure the matrix suction range from -9 kPa to -100,000 kPa. Besides, it can also record temperature changes from -40°C to 60°C. The changes in the matrix suction are indicative of the progression of self-desiccation (Li and Fall, 2016), while the changes in temperature reflect the degree of the cement hydration.

4.4.2.3.3 Volumetric water content monitoring

Similarly, another sensor 5TE is placed at the interface (as shown in Figure 4.39) to monitor the evolution of volumetric water content (VWC) with time. The specific measurement range and accuracy of 5TE sensor is introduced in (Fang and Fall, 2018). The monitoring results of VWC provide information on the amount of water drainage and consumed capillary water through cement hydration. Meanwhile, the 5TE sensor can record the changes in temperature in the CPB as well. The data collected by sensors MPS-6 and 5TE are both recorded by using the EM50 data logger.

4.4.3 Experimental results and interpretation

4.4.3.1 Influence of drainage condition on the interface shear behaviour

In most field cases, CPB structures are not fully drained. However, the amount of water drainage is based on the combined effects of the stope geometry, permeability of adjacent rock, overlying load and temperature (Helinski et al., 2011; EI Mkadmi et al., 2013). Different drainage conditions correspond to different mechanical performances and UCS of CPB (El Mkadmi et al., 2013; Cui and Fall, 2016). Therefore, it is critical to study the mechanical response of interface under different drainage conditions. Some typical direct shear test results (with a normal stress of 50 kPa) of samples (with a curing stress of 150 kPa) cured in both drained and undrained conditions are shown in Figure 4.41(a) and Figure 4.41(b)**,** respectively. From the figure, it is observed that the shear stress of the CPB-rock interface peaks quickly and then experiences a sharp decrease to residual shear stress, regardless of the drainage condition. This shear behaviour varies from those of the interface samples cured without curing stress, as introduced by Nasir and Fall (2008). Moreover, the interface samples cured in drained conditions generally show higher shear strengths compared to the CPB-rock interface in undrained conditions. This observation coincides with the effects of drainage conditions on the development of UCS of CPB material (Helinski et al., 2007; Ghirian and Fall, 2016). The processes responsible for the observed difference in peak shear stress of the interface samples cured in drained and undrained conditions will be discussed later.

The corresponding shear displacement–normal displacement curves of previous interface samples, as shown in Figure 4.42, show that irrespective of drainage conditions, the samples cured under 150 kPa normal stress all depict a dilation after the initial contraction, then followed by a continuous contraction. The initial contraction is due to the inherent compressibility of early ages CPB, and similar contraction behaviour was also observed in Fang and Fall (2018). The comparison of the magnitude of the initial contraction shown in Figures. 4.42(a) and 4.42(b) indicates that the undrained samples undergo larger contractions. In addition, the magnitude of the initial contraction is also reduced with curing time, regardless of the drainage condition. The smaller contraction of the drained samples (in comparison to the undrained samples) and the reduction in magnitude of contraction with curing time are both owing to the combined effects of following two processes: (i) the higher effective stress in the drained samples, and (ii) the refinement of the capillary pores in the CPB, which is because of the raised degree of binder hydration with time. Specifically, the drained condition corresponds to water drainage, and this decreases the pore water pressure in CPB, thereby increasing the effective stress. In addition, larger amount of water is reacted in cement hydration, the degree of which increases with time. Consequently, the effective stress increases with time as well (Ghirian and Fall 2013). The increased effective stress in drained samples with time is consistent with the results of the monitored changes in the VWC, as shown in Figure 4.43. As discussed later in more details, this figure shows that drained CPB has a lower VWC and the VWC decreases with time. As for the refinement of the capillary pores in the CPB, it is a result of precipitation of cement hydration products, such as calcium hydroxide (CH), gypsum, and ettringite. Besides, longer curing time corresponds to larger amount of products, and contraction therefore decreases with time (Metha, 1986; Ercikdi et al., 2009).

In contrast, the observed dilation is due to the relative movement of the asperities at the interface (Fall and Nasir, 2010). The dilation value, as shown in Figure 4.42, increases as the time is extended. In addition, the drained interface samples generally show higher dilation (in comparison to the undrained samples). The dilation increase with curing time is because of the increased degree of cement hydration. As known to all, calcium silicate hydrate (C-S-H) is majorly produced by binder hydration (Gani, 1997), and it is also regarded as the binding product in cementitious material. Consequently, the asperities at the interface increase in strength with more C-S-H. This in turn requires higher stress to break the asperities, which is phenomenologically presented as higher shear dilation. The higher dilation at the interface of the drained samples (compared to the undrained samples) can also be explained from the perspective of the increased strength of the asperities at the interface.

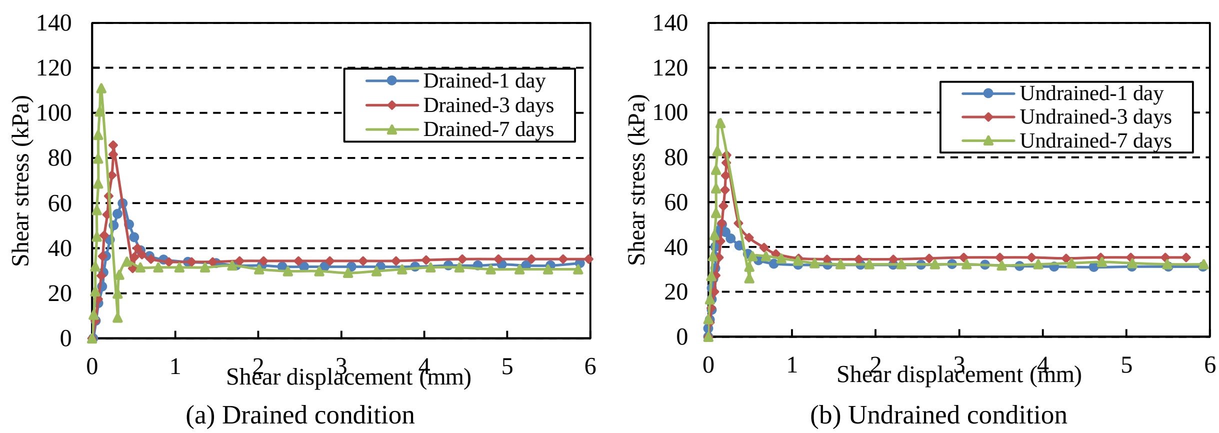

Figure 4.41 Plotted shear displacement–shear stress of interface samples (with a curing stress and normal stress of 150 kPa and 50 kPa, respectively)

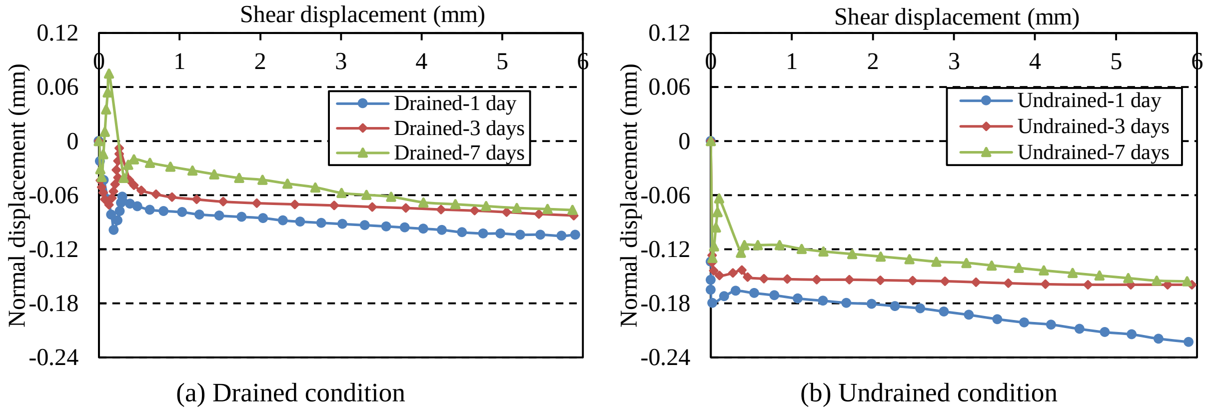

Figure 4.42 Corresponding normal displacement of interface with shear displacement

The observed raise in the peak shear stress of the undrained interface samples with time is because of the increased degree of cement hydration, and this is also noted in numerous previous studies (Nasir and Fall, 2008; Fang and Fall, 2018). However, the higher shear dilation and strength of the drained interface samples, is owing to the following three processes: (i) increased effective stress, as introduced previously; (ii) increased matrix suction at the interface, and (iii) higher temperature in the CPB. First, water drainage leads to a reduced volumetric water content within CPB. This in turn decreases the pore water pressure significantly. As a result, the effective stress and the shear strength at the interface are increased. A number of previous studies have concluded that a higher effective stress is beneficial to the development of mechanical strength of porous media (Ahnberg, 2007; Fahey et al., 2011). This reduction in water content due to the drainage condition is experimentally supported by the monitoring results of the evolution of VWC, the result of which is presented in Figure 4.43. From the figure, the VWC of the drained CPB is found to be significantly lower than that of the undrained CPB. This phenomenon is particularly obvious after one day of curing. Take the samples cured for 7 days as examples, the measured VWC of drained CPB is 0.033, whereas for the undrained CPB, the recorded VWC is 0.342. Secondly, the increase in matrix suction also contributes to the shear strength acquisition, as concluded by previous studies conducted by Fredlund et al. (1978) and Khalili et al. (2004). Similarly, the monitoring results of the matrix suction shown in Figure 4.43 also attest the positive effect of drained condition on the development of matrix suction. For undrained CPB, the matrix suction increases gradually to 129 kPa on the seventh day, while the matrix suction in the drained sample shows a sharp increase to 1000 kPa after more than four days of curing. The increase in the matrix suction of the undrained sample is mainly because of self-desiccation (Li and Fall, 2016), which is a result of water consumption by cement hydration. Whereas the higher matrix suction observed in the drained sample is ascribed to the effects of self-desiccation and water drainage. Hence, water drainage greatly contributes to the increase in matrix suction, thereby leading to a stronger peak shear stress at the drained interface samples. Thirdly, at the interface of the drained samples, the moisture in the CPB is partially replaced by air. As is well known, the thermal conductivity of air is 4% of that of water (Abdul-Hussain and Fall, 2012). Hence, the increasing amount of air within the CPB reduces the dissipation rate of heat, and the majority of the heat released by cement hydration is then reserved in CPB. As a result, the higher temperature in drained CPB speeds up the rate of cement hydration, and consequently, the shear strength is obviously increased. It has been well-established in the literature that higher temperatures speed up the cement hydration of cementitious material as well as increase its strength at the early ages (e.g., Metha, 1986; Fall et al., 2010). The monitoring results of temperature, as presented in Figure 4.44**,** show that after being cured for three days, the temperature in the drained sample is generally higher than that in the undrained CPB, which concurs with the argument that the drained condition corresponds to a lower thermal conductivity of the CPB, and less heat loss from the drained samples. The lower temperature in the drained samples during the first two days (in comparison to the undrained samples as shown in Figure 4.44) is because large amounts of the heat generated by cement hydration has dissipated with water drainage (advective transport of heat).

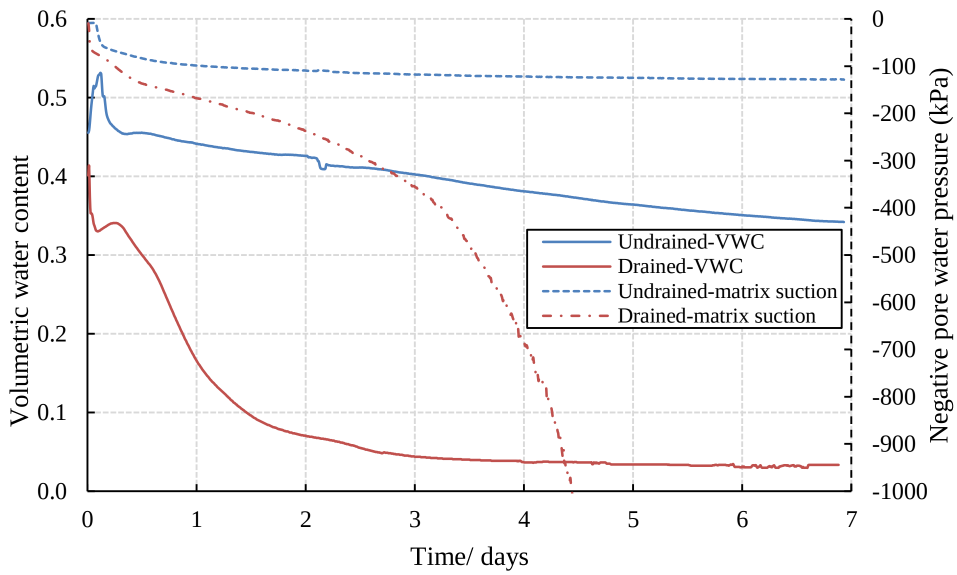

Figure 4.43 Changes in volumetric water content and matrix suction of drained and undrained CPB (curing stress: 150 kPa)

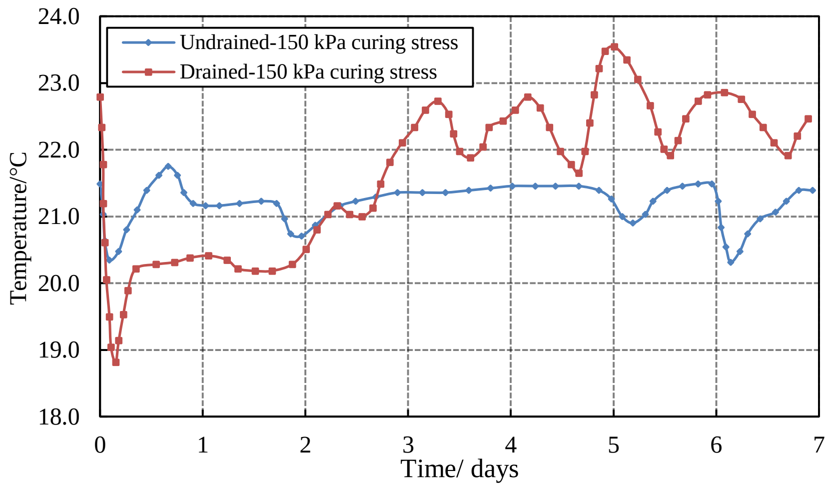

Figure 4.44 Changes in temperature in drained and undrained CPB (curing stress: 150 kPa)

4.4.3.2 Influences of constant curing stress on interface shear behaviour

Figure 4.45 illustrates some shear behaviour of the drained interface samples which are subjected to different curing stress, while Figure 4.46 presents the coupled influenced of time and curing stress on the development of peak shear stress of interface samples in both drained and undrained conditions. The shear strength of drained interface sample is found to increases with curing stress, as clearly shown in Figure 4.45(a). In addition, Figure 4.45(b) presents that the higher curing stress generally results in smaller contractions. Figure 4.46 shows that a higher curing stress is beneficial to the shear strength acquisition at the interface, regardless of curing time and drainage condition. However, for different drainage conditions, this stress-induced increase in shear strength is due to different processes which are discussed below.

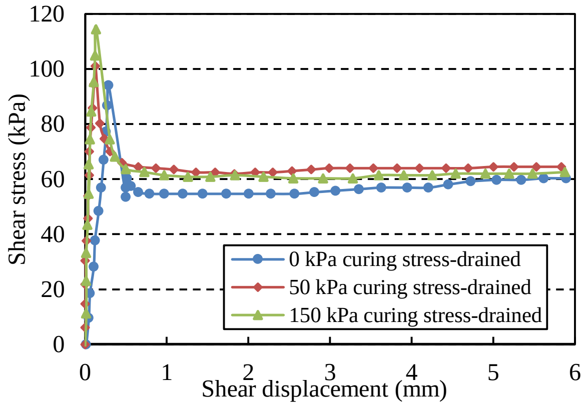

(a) Shear displacement-shear stress curve

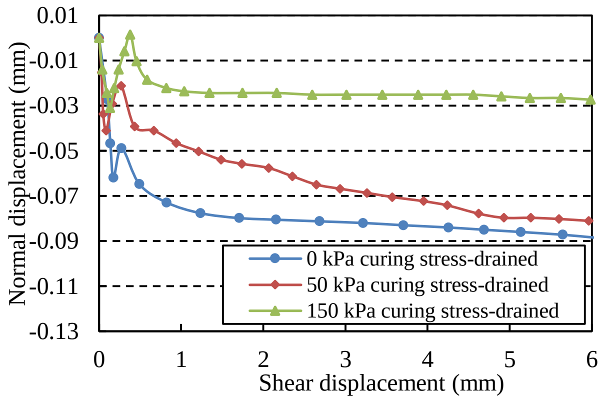

(b) Corresponding normal displacement of interface with shear displacement

Figure 4.45 Plotted shear performance of interface samples cured in drained conditions (curing time: 3 days; normal stress: 100 kPa)

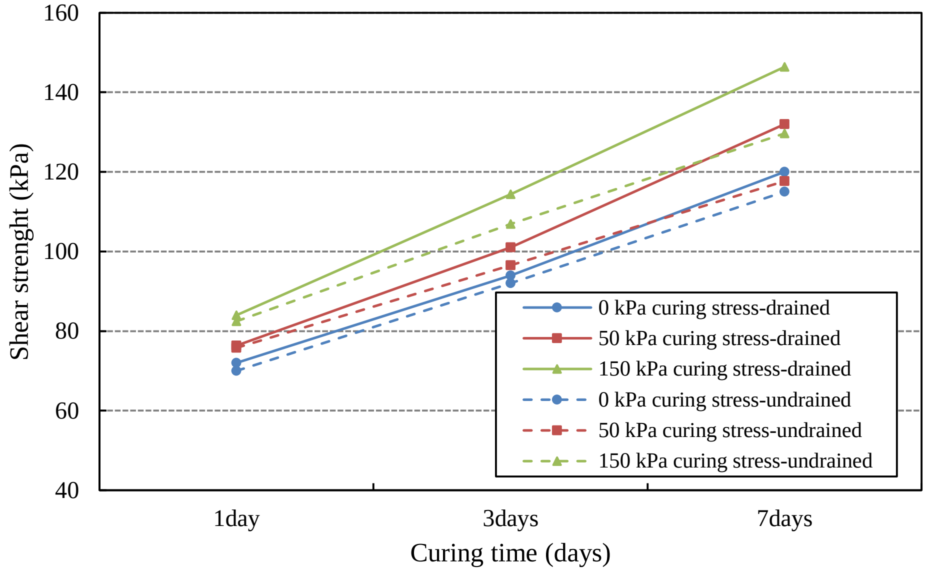

Figure 4.46 Development of peak shear stress of interface samples cured in drained and undrained conditions (normal stress: 100 kPa)

The higher shear strength of the drained interface sample with curing stress is due to the combined effects of reduced VWC and increased degree of cement hydration in the CPB. A higher curing stress increases the rate of water drainage, and consequently, the VWC is rapidly reduced. The monitoring results of the evolution of VWC with time, as shown in Figure 4.47, can be used to attest this argument. For example, the VWC in CPB with a curing stress of 0 kPa, 50 kPa and 150 kPa is reduced to 0.269, 0.062 and 0.033 after being cured for 7 days, respectively. With a reduced VWC, both the effective stress and the matrix suction obviously increase (Vanapalli et al., 1996). This then contributes to a stronger peak shear stress at the interface. Besides, the higher degree of binder hydration also accounts for the increasing shear strength of drained interface samples. As mentioned previously, water drainage leads to the replacement of water with air in CPB, and higher curing stress means a higher rate of water drainage (see plotted slope in Figure 4.47). Hence, a higher curing stress corresponds to a higher air content in the CPB. Given the difference in the thermal conductivity of water and air (Abdul-Hussain and Fall, 2012), the samples cured under a higher curing stress then has lower thermal conductivity. As a result, less heat generated by cement hydration can dissipate, and this leads to a higher temperature, which in turn is beneficial to the occurance of cement hydration (Kim et al., 1998; Wang et al., 2016)**.** Consequencely, more hydration products lead to a greater resistance at the interface (Fang and Fall, 2019). Interestingly, the stress-induced acceleration of cement hydration also contributes to the shear stress increase of the undrained interface samples (Zhou and Beaudoin, 2003; Ghirian and Fall, 2016). The results of thermal analyses on undrained CPB cured under different stresses, shown in Figure 4.48, prove the positive influence of higher curing stress on the increasing rate of binder hydration. It is well known that the change in weight at a temperature of 30°C-200°C in the thermal analysis is because of the dehydration of ettringite, gypsum and C-S-H, which are the main products of binder hydration (Sha et al., 1999). In contrast, the weight change at a temperature between 400°C-450°C is attributed to the disintegration of calcium hydroxide (CH) (Nonnet et al., 1999; Jiang et al., 2016; Fang and Fall, 2018). The difference in TG and DTG values of undrained cement sample cured with two different pressures, as shown in Figure 4.48, indicates the cement paste cured with 150 kPa curing stress suffers from a slightly higher weight loss at a temperature of 400°C-450°C. This means that larger volume of CH is generated by binder hydration. Besides, the higher curing stress also leads to the rearrangement of the particles and results in a denser pore structure of the CPB. The stress-induced refinement of the pore structure forms a stronger interlocking structure at the interface, thereby increasing the shear strength (Fang and Fall, 2018). The denser pore structure with larger curing stress is experimentally attested by the results of MIP test on the samples cured under different pressures for three days. The MIP test results shown in Figure 4.49 show the pore size distribution and cumulative pore volume with pressure of the undrained samples cured at 0 kPa and 150 kPa respectively. It can be noticed from the figure that as the curing stress is increased, the samples show lower cumulative pore volume and the threshold pore diameter decreases. For example, for the sample cured with a stress of 150 kPa, the threshold pore diameter, which is associated with the highest rate of mercury intrusion (Fall et al., 2009; Aldhafeeri et al., 2016), is equal to 1.55 μm, while that of the sampe cured without pressure is 2.08 μm. This suggests that higher curing stress can rearrange the particles of CPB, and therefore refine its capillary pores and decrease its porosity.

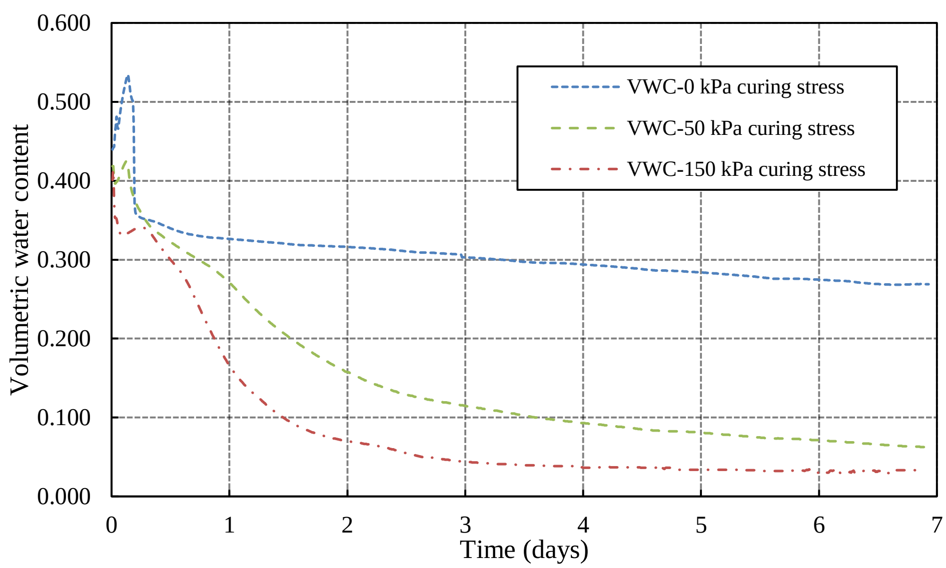

Figure 4.47 Changes in volumetric water content of drained CPB with curing stress

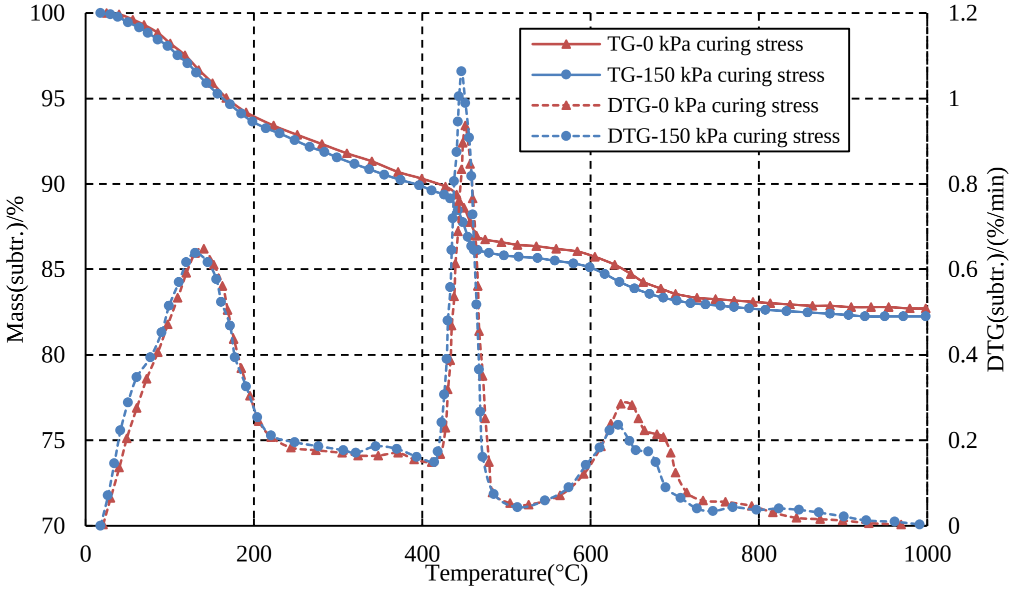

Figure 4.48 TG/DTG analysis on undrained cement paste samples cured with different stresses (curing time: 7 days)

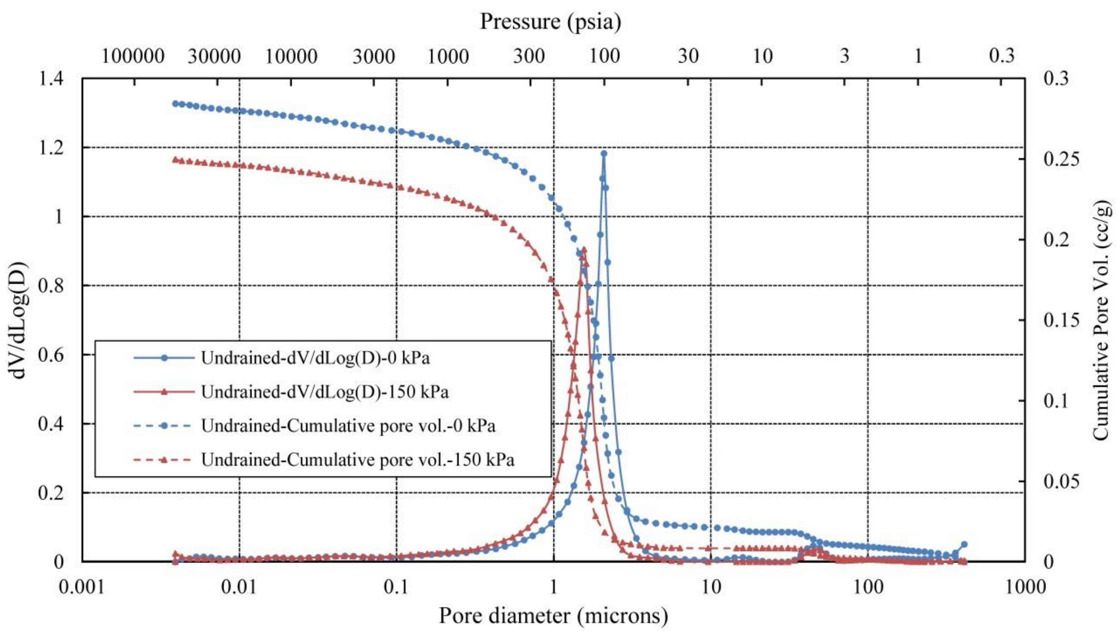

Figure 4.49 Results of MIP test of undrained CPB samples (cured for 3 days) cured at different stresses (dV/dlogD, where V is the pore volume and D is the corresponding pore diameter)

The smaller contraction of the drained interface samples cured at a higher curing stress (as shown in Figure 4.45(b)) is due to the considerable decrease in the volume of local voids. Besides, the precipitation of hydration products produced by the stress-induced acceleration of cement hydration also contributes to the decrease in porosity of CPB. These two factors contribute to less contractions of the CPB with higher curing stress. Moreover, the higher shear dilation with curing stress is a result of stronger asperities at the CPB-rock interface as explained in Section 3.1.

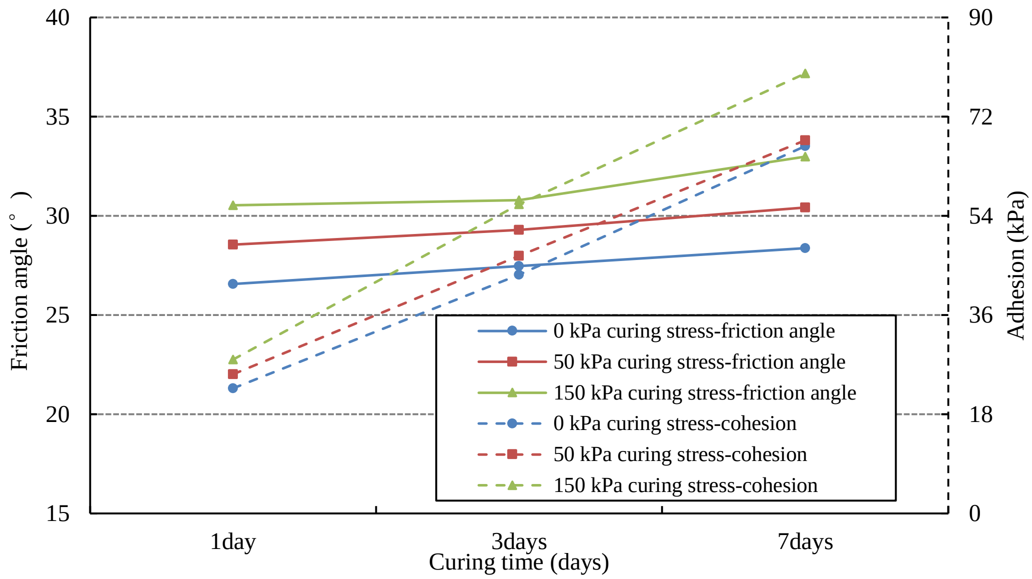

(a) Drained condition

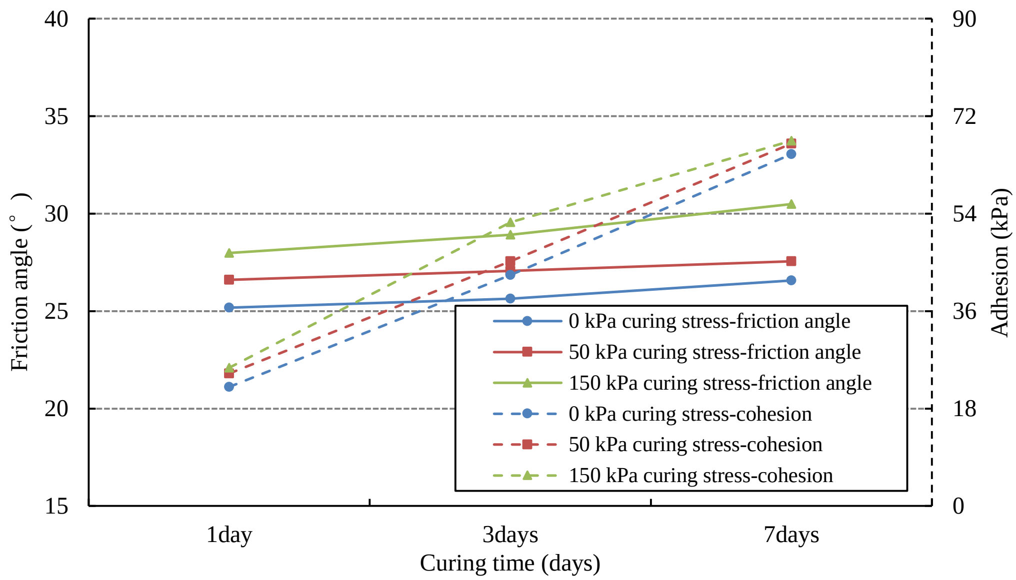

(b) Undrained condition

Figure 4.50 Changes in adhesion and friction angle of CPB-rock interface in different drainage condition

Many different failure criterions (e.g., generalized Tresca and Mises, Drucker-Prager, Hoek-Brown, etc.) can be adopted to deduce the shear parameters of geomaterials. In this paper, the Mohr-Coulomb failure criterion is adopted to calculate the mechanical parameters of the interface, and the evolution of time-dependent parameters (adhesion, friction angle) of the interface (cured under different drainage condition and curing stress) is illustrated in Figure 4.50. The increase in the friction angle and adhesion with time is ascribed to higher degree of binder hydration. This result is consistent with the conclusion made in earlier studies on the shear characteristics of the CPB-rock interface (Nasir and Fall, 2008; Koupouli et al., 2016) and cemented soil (Muhunthan and Sariosseiri, 2008). However, the greater mechanical parameters of the interface sample with curing stress, regardless of the drainage condition, are the results of enhanced degree of cement hydration and denser microstructure of the CPB. Specifically, the larger amount of C-S-H can increase the binding force (adhesion) as well as the strength of the asperities at the interface. Moreover, the denser pore structure increases the contacting area between the tailings particles and surface of the rock, which is beneficial to an increase in frictional resistance. It can be observed in Figure 4.50 that the drained interface sample has stronger mechanical parameters (adhesion and friction angle) when compared to those of undrained samples, and this is because of the increased effective stress, matrix suction and degree of cement hydration in the drained CPB as explained previously.

4.4.3.3 Effect of rate of increase in curing stress (backfilling rate) on shear strength and behaviour of interface samples

With the purpose of exploring the effects of the backfilling rate on the shear performance of the interface, some interface samples are prepared and cured with variable curing stress for 1 day (cured in undrained condition). The shear strengths of the interface samples cured with variable curing stress (with different increasing rates, namely, 20 kPa/3 hours, 30 kPa/3 hours, and 40 kPa/3 hours) are plotted in Figure 4.51 By linear regression fitting of each set of shear strength parameters and the corresponding normal stress, the strength envelopes of the interfaces can be obtained. Because the R^2 of the three fitted linear regression lines are approximately 1, the Mohr-Coulomb criterion is then perfectly used to describe the shear failure envelopes of interface samples. Besides, based on the fitted linear regression lines, the friction angle and adhesion of interface samples cured with variable curing stress can be easily deduced, which are also noted in Figure 4.51 From the figure, it is found that in general, a higher backfilling rate slightly improves the peak shear stress, friction angle, and adhesion of the interface. The higher shear strength with backfilling rate is because of the finer pore structure, which is along the same lines as the influence of curing pressure on the pore structure refinement (Ghirian and Fall, 2016). In contrast, the increasing frictional angle and adhesion with backfilling rate is similar to the aforementioned contributions of curing stress to the rate of cement hydration (see Figure 4.48).

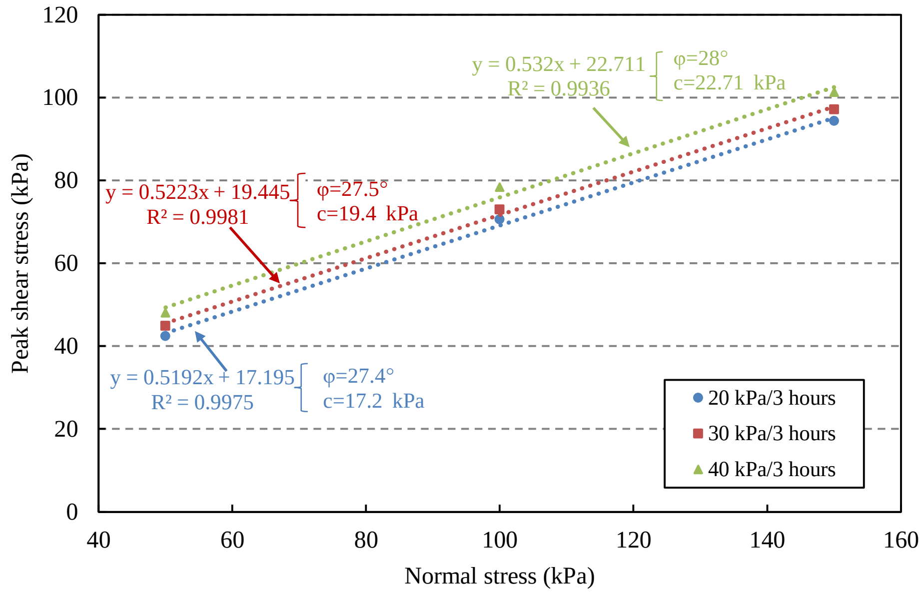

Figure 4.51 Effect of backfilling rate on mechanical properties of CPB-rock interface in undrained conditions (cured for 1 day)

4.4.4 Summary and conclusions

The influence of curing stress, drainage condition and backfilling rate on the shear performance and mechanical properties of CPB-rock interface have been investigated in this study, and based on the experimental results, the main conclusions of the study are summarized below:

- Curing stress contributes a lot to the increase in interface properties (e.g., shear strength, friction angle, and adhesion). A higher curing stress leads to a stronger matrix suction as well as lower thermal conductivity at the CPB-rock interface in drained condition, while for interface samples cured in undrained condition, a higher curing stress not only reduces the thermal conductivity but also leads to a denser pore structure. These processes benefit to the shear strength acquisition and changes in the adhesion and friction angle at the interface, regardless of the drainage condition.
- Drained conditions can increase the effective stress and matrix suction as well as reduce the thermal conductivity of CPB. Consequently, drained conditions contribute to increases in shear strength (compared to undrained conditions).
- A higher backfilling rate of CPB can also increase the shear strength, friction angle and adhesion at the interface. Besides, the regression results indicate the shear failure envelop of the interface can be described by the Mohr-Coulomb criterion, regardless of backfilling rate.
- A higher curing stress and drained condition contribute to a decrease in the compressibility of the CPB. As a result of lower PWP and stronger asperities at the interface, the samples cured at a

higher curing stress and/or in drained conditions have higher shear dilation during direct shear testing.

The results of this investigation help to better understand the shear performance of the CPB-rock interface under different curing stresses, drainage conditions, and backfilling rates. This is crucially important for assessing the arching effect and the stability of CPB structures.

Acknowledgements

The China Scholarship Council (CSC), University of Ottawa, and the Natural Sciences and Engineering Research Council of Canada (NSERC) are gratefully acknowledged by the authors for their supporting and funding. Besides, great appreciation also goes to Dr. Liang Cui and Dr. Saifen Zheng for their kind help.

4.4.5 References

Abdul-Hussain N, Fall M (2012) Thermo-hydro-mechanical behaviour of sodium silicate-cemented paste tailings in column experiments. Tunnelling and Underground Space Technology 29:85-93.

Ahnberg H (2007) On yield stresses and the influence of curing stresses on stress paths and strength measured in triaxial testing of stabilized soils. Canadian Geotechnical Journal 44(1):54-66.

Aldhafeeri Z, Fall M, Pokharel M, Pouramini Z (2016) Temperature dependence of the reactivity of cemented paste backfill. Applied Geochemistry 72:10-19.

Aldhafeeri Z, Fall M (2017) Sulphate induced changes in the reactivity of cemented tailings backfill. International Journal of Mineral Processing 166:12-23.

Aubertin M, Bussière B, Bernier L (2002) Environnement et gestion des résidus miniers. Presses Internationales Polytechnique, CD-ROM, Montréal, Québec, Canada.

Aubertin M, Li L, Arnoldi S, Belem T, Bussière B, Benzaazoua M, Simon R (2003) Interaction between backfill and rock mass in narrow stopes. Soil and rock America 1:1157-1164.

Belem T, Benzaazoua M, Bussiere B (2000) Mechanical behaviour of cemented paste backfill. In: Proc. of 53rd Candadian Geotechnical Conference, Montreal, Octobre, p. 373–380.

Benzaazoua M, Fall M, Belem T (2004) A contribution to understanding the hardening process of cemented pastefill. Minerals Engineering 17(2):141-152.

Buckby T, Black S, Coleman ML, Hodson ME (2003) Fe-sulphate-rich evaporative mineral precipitates from the Rio Tinto, southwest Spain. Mineralogical Magazine 67(2):263-278.

Cui L, Fall M (2016) Mechanical and thermal properties of cemented tailings materials at early ages: Influence of initial temperature, curing stress and drainage conditions. Construction and Building Materials 125:553-563.

El Mkadmi N, Aubertin M, Li L (2013) Effect of drainage and sequential filling on the behaviour of backfill in mine stopes. Canadian Geotechnical Journal 51(1):1-15.

Ercikdi B, Kesimal A, Cihangir F, Deveci H, Alp İ (2009) Cemented paste backfill of sulphide-rich tailings: Importance of binder type and dosage. Cement and Concrete Composites 31(4):268-274.

Ercikdi B, Yilmaz T, Kulekci G (2014) Strength and ultrasonic properties of cemented paste backfill. Ultrasonics 54(1):195-204.

Fahey M, Helinski M, Fourie A (2011) Development of specimen curing procedures that account for the influence of effective stress during curing on the strength of cemented mine backfill. Geotechnical and Geological Engineering 29(5):709-723.

Fall M, Adrien D, Celestin JC, Pokharel M, Toure M (2009) Saturated hydraulic conductivity of cemented paste backfill. Minerals Engineering 22(15):1307-1317.

Fall M, Benzaazoua M (2005) Modelling the effect of sulphate on strength development of paste backfill and binder mixture optimization. Cement and Concrete Research 35(2):301-314.

Fall M, Celestin JC, Pokharel M, Toure M (2010) A contribution to understanding the effects of curing temperature on the mechanical properties of mine cemented tailings backfill. Engineering Geology 114(3-4):397-413.

Fall M, Nasir O (2010) Mechanical behaviour of the interface between cemented tailings backfill and retaining structures under shear loads. Geotechnical and Geological Engineering 28(6):779-790.
Fang K, Fall M (2018) Effects of curing temperature on the shear behaviour of cemented paste backfill-rock interface. International Journal of Rock Mechanics and Mining Science 112:184-192.
Fang K, Fall M (2019) Chemically induced changes in the shear behaviour of the interface between rock and tailings backfill undergoing cementation. Rock Mechanics and Rock Engineering doi.org/10.1007/s00603-019-01757-0
Fredlund DG, Morgenstern NR, Widger RA (1978) The shear strength of unsaturated soils. Canadian Geotechnical Journal 15(3):313-321.
Gani MSJ (1997) Cement and Concrete, Chapman & Hall, London, UK.
Ghirian A, Fall M (2013) Experimental Investigations of the Thermo-Hydro-Mechanical-Chemical Behaviour of Cemented Paste Backfill, in: 23rd World Mining Congr., Canadian Institute of Mining, Metallurgy and Petroleum (CIM), Montreal, Canada.
Ghirian A, Fall M (2015) Coupled behaviour of cemented paste backfill at early ages in load cell experiments. Geotechnical and Geological Engineering 33(5):1141-1166.
Ghirian A, Fall M (2016) Strength evolution and deformation behaviour of cemented paste backfill at early ages: effect of curing stress, filling strategy and drainage. International Journal of Mining Science and Technology 26(5):809-817.
Hassani F, Archibal J (1998) Mine backfill. Canadian Institute of mine, Metallury and Petroleum, Canada.
Helinski M, Fahey M, Fourie A (2011) Behaviour of cemented paste backfill in two mine stopes. Journal of Geotechnical and Geoenvironmental Engineering 137(2):171–182.
Helinski M, Fourie AB, Fahey M (2006) Mechanics of early age cemented paste backfill. In: Jewell, R., Lawson, S., Newman, P. (Eds.), Proceedings of the 9th International Seminar on Paste and Thickened Tailings, Limerick, Ireland. Australian Centre for Geomechanics pp. 313–322 (April 3–7).
Helinski M, Fourie AB, Fahey F, Ismail M (2007) Assessment of the self-desiccation process in cemented mine backfills. Canadian Geotechnical Journal 44(10):1148–1156.
Jiang HQ, Fall M, Cui L (2016) Yield stress of cemented paste backfill in sub-zero environments: experimental results. Minerals Engineering 92:141-150.
Kesimal A, Yilmaz E, Ercikdi B, Alp I, Deveci H (2005) Effect of properties of tailings and binder on the short-and long-term strength and stability of cemented paste backfill. Materials Letters 59(28):3703-3709.
Khalili N, Geiser F, Blight GE (2004) Effective stress in unsaturated soils: review with new evidence. International Journal of Geomechanics 4(2):115-126.
Kim JK, Moon YH, Eo SH (1998) Compressive strength development of concrete with different curing time and temperature. Cement and Concrete Research 28(12):1761-1773.
Koupouli NJF, Belem T, Rivardb P, Effenguet H (2016) Direct shear tests on cemented paste backfill–rock wall and cemented paste backfill–backfill interfaces. Journal of Rock Mechanics and Geotechnical Engineering 8(4):472-479.
Li W, Fall M (2016) Sulphate effect on the early age strength and self-desiccation of cemented paste backfill. Construction and Building Materials 106:296-304.
Metha PK (1986) Concrete: Structure, Properties and Materials. Prentice-Hall Inc, Englewood Cliffs, N.J.
Muhunthan B, Sariosseiri F (2008) Interpretation of geotechnical properties of cement treated soils.
Nasir O, Fall M (2008) Shear behaviour of cemented pastefill-rock interfaces. Engineering Geology 101(3):146-153.
Nonnet E, Lequeux N, Boch P (1999) Elastic properties of high alumina cement castables from room temperature to 1600°C. Journal of the European Ceramic Society 19(8):1575–1583.
Sha W, O'Neill E, Guo Z (1999) Differential scanning calorimetry study of ordinary Portland cement. Cement and Concrete Research 29(9):1487–1489.
Simms P, Grabinsky M (2009) Direct measurement of matrix suction in triaxial tests on early-age cemented paste backfill, Canadian Geotechnical Journal 46(1):93-101.
Sun EJ, Zhang XK, Li ZX (2012). The internet of things (IOT) and cloud computing (CC) based tailings dam monitoring and pre-alarm system in mines. Safety Science 50(4):811-815.
Tse R, Cruden DM (1979) Estimating Joint Roughness Coefficients. International Journal of Rock Mechanics and Mining Sciences 16(5):303–307.
Vanapalli S, Fredlund D, Pufahl D, Clifton A (1996) Model for the prediction of shear strength with respect to soil suction. Canadian Geotechnical Journal 33(3):379-392.
Wang Y, Fall M, Wu AX (2016) Initial temperature-dependence of strength development and self-desiccation in cemented paste backfill that contains sodium silicate. Cement and Concrete Composites 67:101-110.

Yilmaz E, Benzaazoua M, Belem T, Bussière B (2009) Effect of curing under pressure on compressive strength development of cemented paste backfill. Minerals Engineering 22(9-10):772-785.

Zhou Q, Beaudoin JJ (2003) Effect of applied hydrostatic stress on the hydration of Portland cement and C3S. Advances in Cement Research 15(1):9-16.

4.5 Paper V: Shear behaviour of the interface between rock and cemented backfill exposed to internal sulphate attack

(Submitted)

Kun Fang, Mamadou Fall

Abstract

A clear understanding and accurate assessment of the mechanical properties or behaviour of the interface between cemented paste backfill (CPB) and rock is important for the safe and economical design of underground CPB structures, which are geotechnical structures intensively used in underground mining operations for ground support. However, no studies have been conducted to study the effect of sulphate on the long-term shear properties and behaviour of CPB-rock interface although CPB often contains a relatively high amount of sulphate ions. The main objective of this experimental investigation is to study the effects of the initial sulphate content (0 ppm, 5,000 ppm, 15,000 ppm, and 25,000 ppm) of CPB on the shear behaviour and properties of the interface between rock and CPB cured at advanced times (28, 90 and 150 days). The obtained results show that the sulphate has a significant effect on the long-term shear strength and behaviour of rock-CPB interface. It can either negatively or positively influence the shear properties of CPB-rock interface at advanced ages depending on the curing time and initial sulphate content. There is competition between the strength-decreasing and increasing factors. The dominant influencing factors depend on the curing time and initial sulfate content. The findings presented in this paper could provide critical information for the stability assessment of underground CPB structures, the design of optimized and safe CPB structures, and thus for the improvement of mining safety and productivity.

4.5.1 Introduction

Cemented hydraulic, rock and paste backfills are three main types of mine cemented backfill for underground mining operations. Cemented hydraulic backfill (CHB) is a mixture of mill tailings and cement (with a solid percentage of 60%~75%), while cemented rock backfill (CRB) is usually a mixture of waste rock, tailings and a small percentage of cement (Amaratunga and Yaschyshyn, 1997). However, due to the potential high geotechnical hazards posed by CHB (e.g., failure of backfill barricade) and its higher cost, the use of CHB has been increasingly restricted. In contrast, cemented paste backfill (CPB) has become more and more popular in underground mining operations during the last three decades (Brackebusch, 1994; Hassani and Archibal, 1998). CPB is a cementitious material produced by mixing thickened tailings (with a solid percentage of 70%-85%), binder (3%-7%, often) and water in paste backfill plant commonly located on the surface of the mine. Thereafter, the obtained CPB mixture is transported to underground through pipes by pumping or gravity to fill the voids created by ore extraction. The underground management of tailings can not only reduce the cost of constructing tailings storage facilities (TSFs, e.g., embankments and dams), but also solve or limit the environmental and/geotechnical issues caused by surface disposal of tailings (acid mine drainage (AMD), water and land pollution, potential threats of dam failure) (Buckby et al., 2003). In addition to its economic and environmental benefits, CPB maintains the stability of underground structures. The ore recovery ratio is then effectively improved as a result of supporting function by CPB structures. Moreover, some CPB structures, especially at mature ages, can also carry heavy equipment when exploiting the adjacent stopes (Yilmaz et al., 2004; Benzaazoua et al., 2004). Hence, the mechanical stability is one of the key design criteria of CPB structures.

The uniaxial compressive strength (UCS) of the CPB material is one of the key parameters that are commonly used to assess the mechanical stability of CPB structures. Many studies have been performed to investigate the UCS evolution of CPB under different thermal, hydraulic, mechanical and chemical conditions (Fall and Benzaazoua, 2005; Kesimal et al., 2005; Fall and Samb, 2009; Yilmaz et al., 2009; Simms and Grabinsky, 2009; Fall et al., 2010). However, another key factor that affects the mechanical stability of CPB structure is the shear strength and behaviour at the interface between the CPB and the surrounding or adjacent rock mass. The shear strength and behaviour of the CPB-rock interface is essential for arching effect (as shown in Figure 4.52), which can significantly reduce the vertical stress in backfilling body (in comparison to the in-situ stress due to self-weight) (Marston, 1930; Pirapakaran and Sivakugan, 2007). This means a better understanding of the shear properties of the CPB-rock interface will lead to a better evaluation of the loads transmitted from CPB to the surrounding structures. As a result, it can allow designing CPB structures with less consumption of cement, which represents up to 75% of the cost of CPB, thereby resulting in a more cost-effective design of CPB and barricades (Grice, 2001). On the other hand, the long-term CPB-rock interface shear behaviour or strength is also critical for the practicability and safety of mining operations in which the mining method of underhand cut-and-fill with CPB is used (Figure 4.52). In this method, the stability of the CPB structure above the mining work areas, in other words, the safety of the mine workers is influencing by the shear strength and behaviour of the CPB-rock interface. Moreover, mining excavations progress under the sillmats (structural elements used in cut-and-fill mining of low to moderate width, steeply dipping ore zones to enable that ore sill pillars may be mined out) must remain stable when exposed and subjected to mine induced stresses. The sillmat is often made of CPB with high cement content. The shear strength or shear strength parameters of the interface sillmat-rock are essential inputs in the assessment of the stability of the sillmat (De Souza and Dirige, 2001, 2002). Thus, The underestimation of the long-term shear strength of CPB-rock interface and improper design of sillmat would result in failure of the fill mass, which can have significant human (e.g., injuries, fatalities), social and financial consequences for the mines (De Souza and Dirige, 2001, 2002; Pakalnis et al., 2005). However, to date, only a few studies have been conducted on the shear properties or behaviour of the CPB-rock interface (Aubertin et al., 2003; Nasir and Fall, 2008; Fall and Nasir, 2010; Koupouli et al., 2016; Fang and Fall, 2018a). Despite the progress made in understanding the shear behaviour of the CPB-rock interface by these studies, none have focused on the effect of sulphate on the long-term shear properties and behaviour of rock-CPB interface. There is a need to address this research gap for the reasons mentioned above.

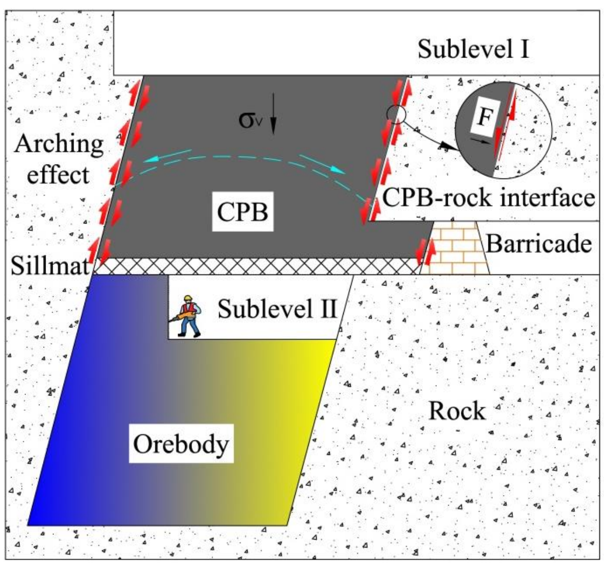

Figure 4.52 Underground advanced ages CPB structures and its supporting effect

There are many sources of sulphate ions in CPB systems (Fall and Benzaazoua, 2005), including the oxidation of sulphide minerals (e.g., pyrite) present in the tailings (primary sources of sulphate in CPB, the destruction of cyanides, present particularly in some gold mill tailings and/or mine process waters, using the method SO_2^-air, the addition of gypsum ($CaSO_4 \cdot 2H_2O$) or anhydrite ($CaSO_4$) to control the flash setting of the cement.

Therefore, the main objective of this paper is to experimentally study the influence of the initial sulphate content of CPB on the shear behaviour of the interface between rock and CPB cured at advanced times (28, 90 and 150 days).

4.5.2 Experimental Program

4.5.2.1 Materials used

4.5.2.1.1 Tailings

Artificial tailings (silicate tailings, ST), which contain 99.8% S_iO_2, are used in this study. ST is essentially made of quartz, a dominant mineral found in Canadian hard rock mines. Using ST helps to reduce the uncertainties in the results that can be caused by the use of natural tailings. Indeed, NT can contain various reactive minerals which can oxidize during the storage of the tailings and/or the preparation of the CPB samples as well as interact with the cement hydration process, and thus affect the accuracy and interpretation of the results (Wang and Fall, 2016). The ST have a particle size distribution similar to the average of nine Canadian mine tailings, as shown in Figure 4.53.

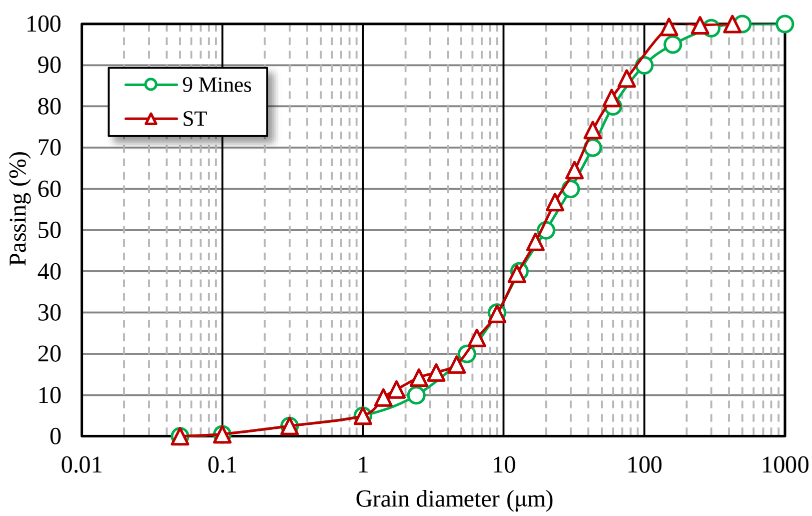

Figure 4.53 Grain size distribution of silica tailing (ST) and the average grain size distribution of tailings from 9 eastern Canadian mines

4.5.2.1.2 Binder

Portland cement type I (PCI) with a weight proportion of 4.5% is used to produce the CPB part of the sample. PCI is the most common type of cement used in CPB operations.

4.5.2.1.3 Mixing water

Distilled water (with a water-to-cement ratio (w/c) of 7.35) is used to prepare the mixing waters with various initial sulphate contents. To produce mixing waters with different sulphate contents (0 ppm, 5,000 ppm, 15,000 ppm and 25,000 ppm), specific amounts of ferrous sulphate ($FeSO_4 \cdot 7H_2O$) were added to the distilled water.

4.5.2.1.4 Rock samples

The rock used for the base part of the sample is granite and its average UCS is 160 MPa. After been cut into small cuboid pieces with dimensions of 60×60×10 mm, the surface of granite is then polished. According to the joint roughness coefficient (JRC) of typical roughness profiles proposed by Tse and Cruden (Tse and Cruden, 1979), the surface roughness of the rock was determined as zero.

4.5.2.2 Sample preparation and test plans

4.5.2.2.1 Samples preparation

A food mixer is used to produce the CPB mixture. After mixing and stirring the specific amounts of ST, PCI, water with various ferrous sulphate contents for 7 minutes, the obtained homogeneous paste is then poured into a plastic square container where the rock has been set inside. The plastic square container has a dimension of 60×60×30 mm, which is exactly the same as the size of the direct shear box. Thereafter, the whole sample is subjected to manual vibration. This is to ensure that there is no extra air or oxygen in the CPB. After removing the air, the containers are then covered with a plastic film (to avoid evaporation) and cured at a temperature of 20°C for different times. Examples of interface samples (cured for 150 days) with different initial sulphate contents are shown in Figure 4.54.

Figure 4.54 Interface samples with different initial sulphate contents (150 days curing time)

4.5.2.2.2 Testing plan

After being cured for certain days (28, 90 and 150 days), all the samples with various initial sulphate contents (0 ppm, 5,000 ppm, 15,000 ppm and 25,000 ppm) were subjected to direct shear tests under three constant normal stresses (50 kPa, 100 kPa and 150 kPa). The experimental scheme is shown in Figure 4.55. As shown in the figure, each node refers to an experimental condition; for example, the red node corresponds to the following condition: a normal stress of 100 kPa is applied on the sample with 5,000 ppm of initial sulphate content, which has been cured for 90 days. The nodes at the indigo plane mean all the samples are cured for 150 days. For the sake of accuracy, each test is repeated for at least three times. Therefore, more than 108 sets of direct shear tests are conducted in this study.

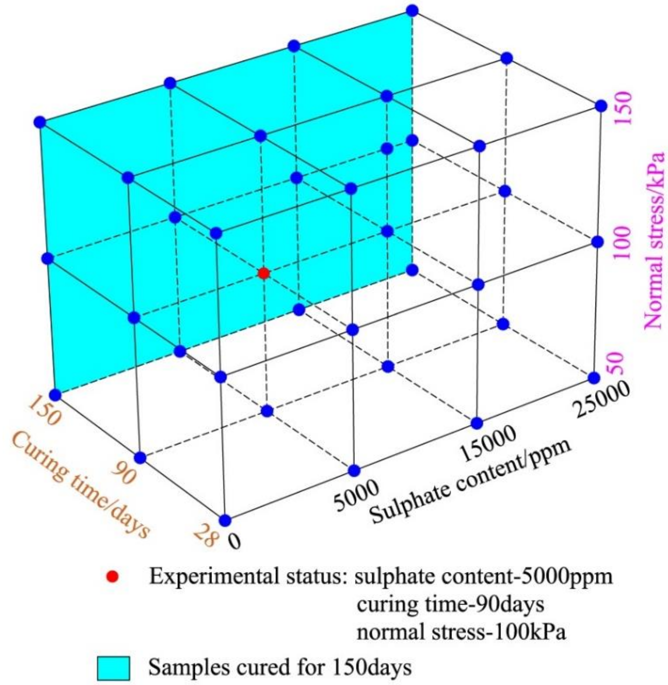

Figure 4.55 Experimental scheme

4.5.2.3 Mechanical tests and microstructural analyses

4.5.2.3.1 Direct shear test

Direct shear tests on the CPB-rock specimens were carried out by following the ASTM D3080-04. The tests were conducted at a speed of 0.5 mm/min. The results regarding shear stress, horizontal and normal displacement were collected by the computer software, Labview.

4.5.2.3.2 Microstructural analyses

Many microstructural techniques were used to assess the effect of sulphate on the microstructural characteristics of the CPB. The techniques include thermo-gravimetric (TG) analysis, differential thermogravimetric (DTG) analysis, X-ray diffraction (XRD) and mercury intrusion porosimetry (MIP) test. The TG and DTG analyses were conducted on dried and powdered cement paste (with an initial w/c =2 to simulate the high water content of CPB) by using a Q5,000IR thermogravimetric analyzer (which allows temperature rising up to 1000°C at a rate of 10°C per minute); the TG and DTG results are used to determine the degree and rate of hydration of cement pastes with different sulphate content. MIP test was performed on dried CPB samples (dried in an oven with a temperature 40°C~45°C for 4 days) by using a micromeritics AutoPore III 9420 mercury porosimeter. The results of MIP test are needed to analyze the pore size distribution of CPB with different sulphate contents. The XRD test was carried out on cement pastes of CPB by using a Scintag XDS-2000 diffractometer, which is a multi-purpose power diffractometer with a KEVEX Peltier cooled silicon detector. With the results of XRD analysis, the mineralogical compositions of the samples at different curing time and sulphate content were determined.

4.5.3 Results and discussions

Typical shear test results of CPB-rock interfaces with different initial sulphate contents are given and discussed in this section.

4.5.3.1 Effect of sulphate on the shear deformation behaviour of CPB-rock interface at advanced ages

Figure 4.56 shows typical shear displacement-shear stress curves of the CPB-rock interface with various initial sulphate contents (0, 5,000, 15,000 and 25,000 ppm) and cured for 28, 90 and 150 days (with a normal stress of 50 kPa). It can be observed that the shear stress curves of CPB-rock interfaces show a similar trend and shape, with an increase up to shear strength and then followed by a sudden bond failure, regardless of the sulphate content and curing time. The sudden bond failure is due to the failure of the binding forces of the cement between the CPB and the rock surface (bond failure of the cohesive interface) at low normal stress (Swedenborg, 2001; Saiang et al., 2005; Tian et al., 2015). It can also be seen that the peak shear stress (shear strength) of the interface specimens is not only a function of the curing time, but also of the initial sulphate contents as discussed below.

Figure 4.57 illustrates typical shear displacement-normal displacement curves of the aforementioned interface specimens with different sulphate contents and curing times. It can be seen from the figure that for all interface samples, there exist slight contractions at the beginning of the direct shear tests. These initial slight contractions are due to the inherent compressibility of CPB samples; similar contraction behaviour was also observed by Nasir and Fall (2008). Thereafter, all the CPB-rock interface samples experience obvious dilation until the bonding failure at the interface. For subsequent shear displacement beyond this point with highest shear dilation, the samples then generally suffer from continuous contracting behaviour.

The results presented in Figure 4.57 indicate that the initial sulphate content does not significantly affect the contraction behaviour of the studied interface specimens. However, the magnitude of the shear dilation is a function of the curing time and initial sulphate content, as also shown in Figure 4.58. This figure presents the magnitudes of shear dilation of differently sulphated CPB-rock interface samples with curing time. It can be seen from Figure 4.57 and Figure 4.58 that the value of maximum shear dilation increases gradually with curing time (with an exception of 150 day old samples with a sulphate content of 25,000 ppm; will be discussed below). This increase in shear dilation with curing time is attributed to the increase of the degree of cement hydration with time (Husem and Gozutok, 2005; Fall et al., 2010), which leads to the formation of stronger asperities at the surface of the CPB (Nasir and Fall, 2008; Fall and

Nasir, 2010; Koupouli et al., 2016). Stronger asperities are more resistant to damage during shearing or sliding between interfaces surfaces. Consequently, these interface samples with longer curing times show more net dilation. However, Figure 4.57 and 4.58 indicate that, although there is no significant differences (considering experimental errors associated with these tests) in the maximum shear dilation values of interface specimens with sulphate and without sulphate up to 90 days of curing time, the maximum shear dilation values of the 25,000 ppm samples are significantly lower than that of the sulphate-free interface samples or samples with lower sulphate contents (5,000 ppm, 15,000 ppm) when curing time rises to 150 days. This lower dilation of the 25,000 ppm samples can be attributed to the fact that the high sulphate content decreases the strength of CPB, and thus weakens the asperities at the surface on the CPB. Thus, weaker asperities will suffer more damage during shearing, thereby leading to lower shear dilation of the interface. This negative effect of high sulphate content on the strength of CPB is due to the combined effects of the following factors (will be discussed below): (i) the inhibition of cement hydration by sulphate; (ii) formation of expansive minerals (in particular, ettringite); (iii) coarsening of the pore structure of the CPB; and (iv) sulphate absorption by calcium silicate hydrate (C-S-H).

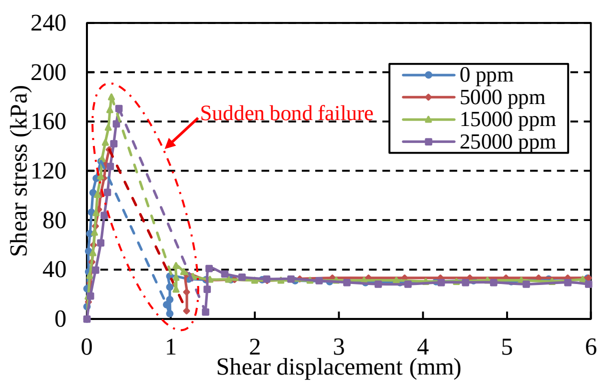

(a) 28 days of curing time

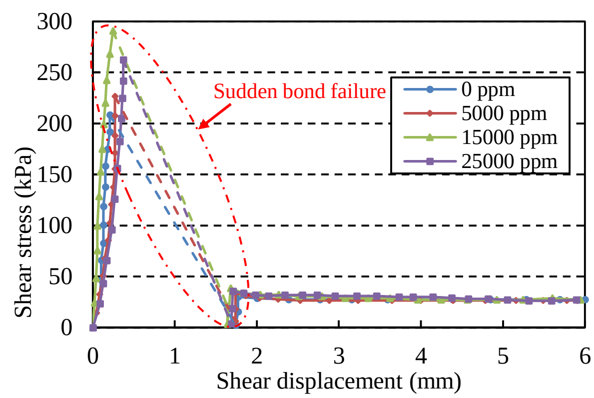

(b) 90 days of curing time

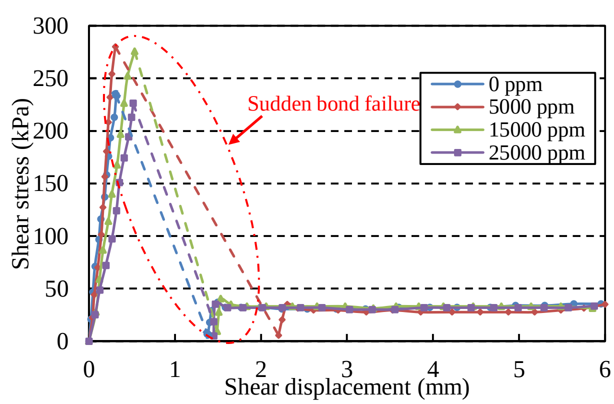

(c) 150 days of curing time

Figure 4.56 Plots of shear displacement-shear stress of CPB-rock interface (normal stress: 50 kPa)

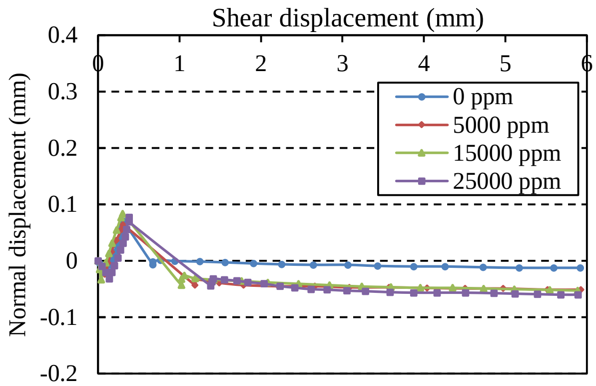

(a) 28 days of curing time

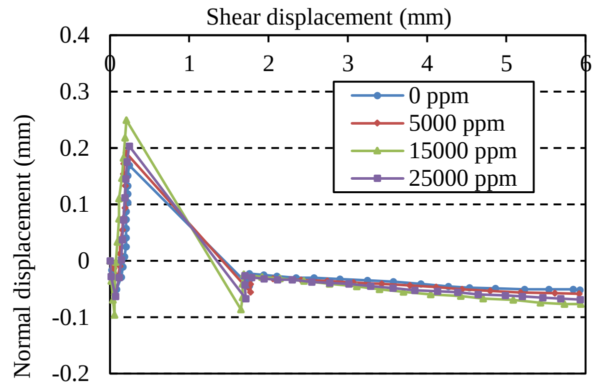

(b) 90 days of curing time

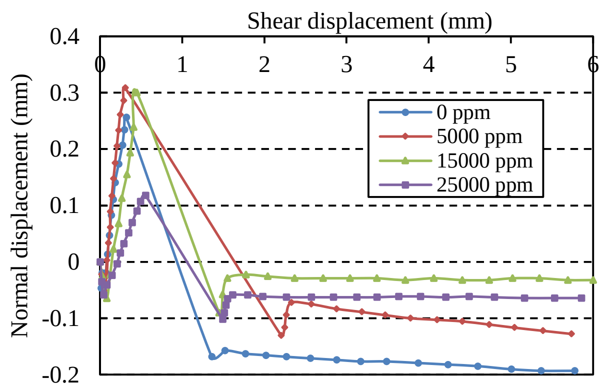

(c) 150 days of curing time

Figure 4.57 Plotted shear displacement-vertical displacement of CPB-rock interface (normal stress: 50 kPa)

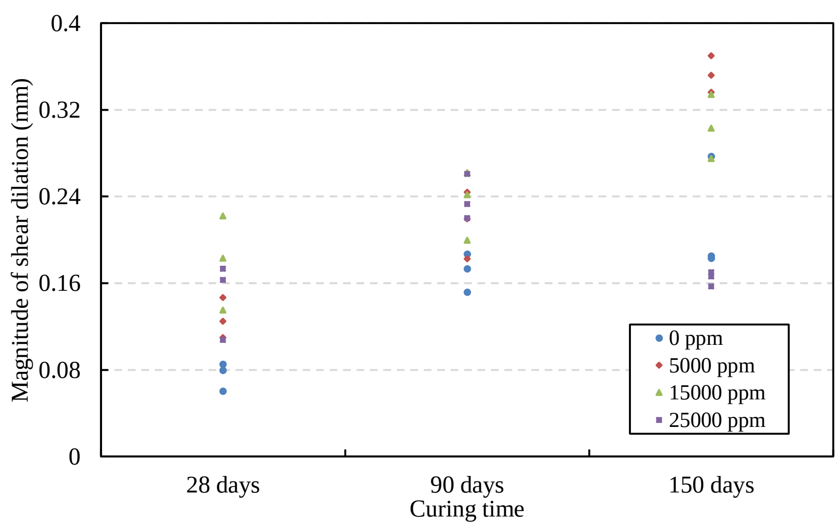

Figure 4.58 Evolution of shear dilation value at CPB-rock interface (normal stress: 50 kPa)

4.5.3.2 Effect of sulphate on the evolution of shear strength of CPB-rock interface

Figure 4.59 illustrates the time- and sulphate-dependent evolution of the shear strength of the CPB-rock interfaces. It can be clearly observed that the sulphate has a significant effect on the shear strength of the

CPB-rock interface. Furthermore, it can be noticed that, the nature and magnitude of the effects of the initial sulphate content on the shear strength evolution are function of the ages of CPB or curing time as discussed below.

Prior to the further discussion of the observed shear strength evolution of the CPB-rock samples with different sulphate content, it is necessary to recall the following key factors that can affect the mechanical strength of CPB or any cementitious material: (i) the amounts of calcium silicate hydrate (C-S-H) formed within the CPB system. C-S-H, a product of cement hydration, is considered to be the major binding phase in hardened cement system (Fall et al., 2010; Gani, 1997); and higher degree of cement hydration corresponds to higher amounts of C-S-H (Yilmaz et al., 2004; Pokharel and Fall, 2013). However, the sulphate adsorption by C-S-H leads to the formation of C-S-H gel of lower quality (e.g., lower intrinsic mechanical strength), thereby resulting in a reduction in strength of Portland cement based cementitious materials (e.g., CPB) (Bentur, 1976; Jelenić et al., 1977; Pelisser et al., 2012). It is also well known that the adsorption of sulphate by C-S-H also depends upon the concentration of sulphate as demonstrated by several studies. High sulphate content leads to higher adsorption (Fu et al., 1997; Ramlochan et al., 2003). (ii) the amounts of expansive minerals (e.g., ettringite, gypsum) formed within the CPB system due to the presence of sulphate ions. Gypsum is a product of a reaction between sulphate ions and calcium hydroxide (CH), while ettringite is generated by the reaction between sulphate ions and tricalcium aluminate (C_3A ($3CaO{\cdot}Al_2O_3$), a constituent of cement) (Li and Fall, 2016; Husem and Gozutok, 2005). The presence of expansive minerals can either positively or negatively influence the mechanical strength of CPB depending on the amounts of expansive minerals present within the pores of CPB and the volume of the CPB capillary pores (Fall and Pokharel, 2010; Li and Fall, 2018). On the one hand, the precipitation of sufficient (but not excessive) amounts of expansive minerals within the capillary pores of CPB leads to the refinement of the pore structure, thus contributing to an increase in mechanical strength of CPB (Pokharel and Fall, 2013). On the other hand, the formation of excessive amounts of expansive minerals causes physical damage and coarsens the pore structure within CPB, thereby decreasing the mechanical strength of CPB (Fall and Pokharel, 2010).

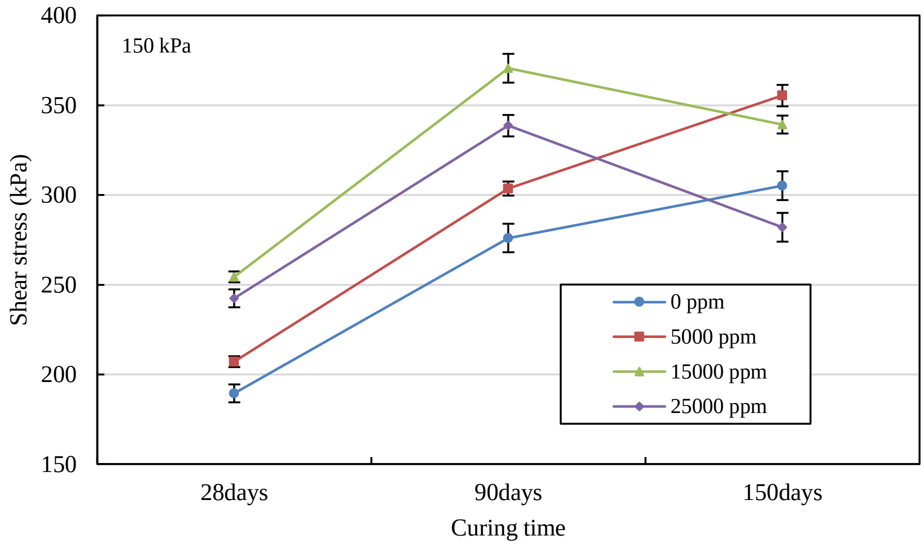

Figure 4.59 Evolution of peak shear strength of CPB-rock interface with different sulphate content (normal stress: 150 kPa)

4.5.3.2.1 28 days curing time

From Figure 4.56 and Figure 4.59, it can be observed that for samples cured for 28 days, the shear strength of the samples with sulphate is higher than that of sulphate-free samples. Moreover, the shear strength increases as the sulphate content increases, except for samples with the initial sulphate content of 25,000 ppm. The shear strength of the 25,000 ppm interface sample is lower than that of the 15,000 ppm specimen, but higher than that of the 5,000 and 0 ppm samples.

This higher shear strength of the sulphated interface specimens and the increase of shear strength as the sulphate content increases up to 15,000 ppm are due to the refinement of the pore structure of the CPB due to the precipitation of gypsum and ettringite as described previously. This refinement of the CPB pores increases the contact area between CPB and the rock, which in turn results in a stronger interlocking interface structure of these sulfate-bearing interface samples (Fang and Fall, 2018b). This leads to the increase in shear strength of the CPB-rock interface. This argument of pore refinement due to the precipitation of higher amount of gypsum and ettringite within the pores of sulphated CPB is supported by results of scanning electron microscope (SEM) analyses conducted on sulfated CPB sample (Fall and Benzaazous, 2005) as well as by the results of MIP analyses performed on samples with 0 ppm and 5,000 ppm of sulphate, respectively, as shown in Figure 4.60. The SEM observations of a paste backfill sample after 28 days curing presented in (Fall and Benzaazous, 2005), show that the pores within the sulphated paste backfill are filled with secondary gypsum. From Figure 4.60, it can be clearly observed that the pore structure of the sample with 5,000 ppm is significantly finer than that of a sulphate-free sample. Moreover, the larger amounts of expansive minerals within 5,000 ppm sample (in comparison to sample without sulphate) are illustrated by the results of thermal analyses presented in Figure 4.61. It is well known that the peak or weight loss situated between 30°C-105°C is a result of sulphate decomposition (Tagawa, 1984), while weight loss between 110°C-170°C is attributed to the dehydration of hydration products, such as C-S-H, ettringite and gypsum (Nonnet et al., 1999; Zhou and Glasser, 2001; Li and Fall, 2018). The higher weight loss of the 5,000 ppm sample at a temperature range of 110°C-170°C (compared with the sample without sulphate) suggests that there are more expansive minerals in the 5,000 ppm sample. The aforementioned lower strength of the 25,000 ppm samples (in comparison to the strength of samples with 15,000 ppm of sulphate content) is the results of the combined effects of two mechanisms: (i) the inhibition of the cement hydration by high sulphate content (Tzouvalas et al., 2004; Fall and Pokharel, 2010), which leads to a formation of lower amount of C-S-H in the 25,000 ppm specimen; (ii) the higher adsorption of sulphate by C-S-H as the sulphate content increases which leads to the formation of weaker C-S-H (Jelenić et al., 1977; Divet and Randriambolona, 1998; Bing and Cohen, 2000). Consequently, the lower volume of C-S-H as well as weaker C-S-H result in a weaker binding force between the CPB and rock as the sulphate content is increased to 25,000 ppm. This results in the formation of weaker asperities at the interface between CPB and rock, thereby decreasing the peak shear stress of the interface. The sulphate induced inhibition of the cement hydration is experimentally supported by the results of thermal analyses performed on samples with 0 ppm, 5,000 ppm and 25,000 ppm (see Figure 4.61). A comparison of the TG and DTG curves of the cement paste of the CPB samples with different initial sulphate contents shows that their weight loss at 400°C-450°C (due to the decomposition of CH (Pane and Hansen, 2005; Jiang et al., 2016)) is lower as the sulphate content increases. The smaller amount of CH as the sulphate content increases, particularly in 25,000 ppm sample, means lower cement hydration degree, as thus less C-S-H and CH.

From Figure 4.59, it can also be noticed that despite the aforementioned inhibition effect of the sulphate on cement hydration, the shear strength of the interface samples with 25,000 ppm of initial sulphate content is still higher than those of samples with sulphate contents of 5,000 ppm and 0 ppm. This observation suggests that competition exists between the factors of shear strength increase (refinement of pore structure of CPB by expansive minerals) and reduction (inhibition of cement hydration, adsorption of sulphate by C-S-H) as sulphate content in CPB is increased.

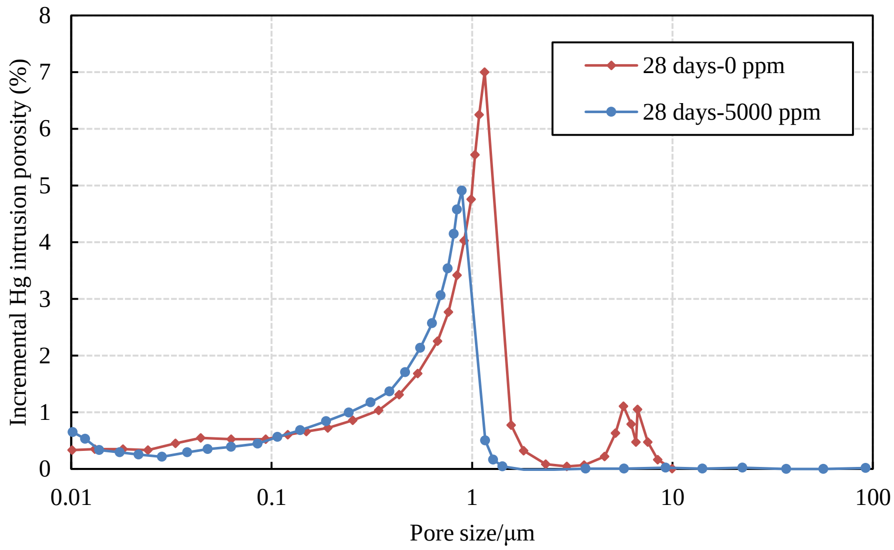

Figure 4.60 Pore size distribution of 28-day samples with sulphate content of 0 ppm and 5,000 ppm

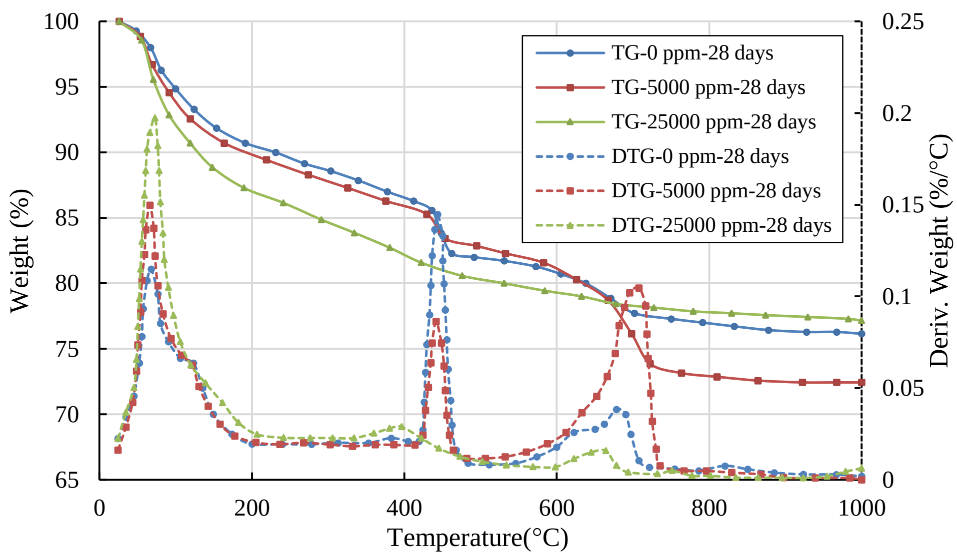

Figure 4.61 TG and DTG diagrams for 28 day -cement paste samples with different initial sulphate contents (0, 5,000 and 25,000 ppm)

4.5.3.2.2 90 days curing time

Figure 4.59 shows that, after being cured for 90 days, all the CPB-rock interfaces experience an increase in shear strength, regardless of the sulphate content. The increase in shear strength with curing time is due to the increased degree of cement hydration as curing time is increased. Indeed, when the curing time of the CPB increases, CPB tends to harden because of the progression of binder hydration. This hardening will lead to stronger asperities on the surface of the CPB, thereby raising the value of the critical stress required to break these asperities (Nasir and Fall, 2008; Fall and Nasir, 2010). Moreover, a higher degree of binder hydration results in a higher cementation binding force between the CPB and the rock surface

(Nasir and Fall, 2008). This obviously means that a higher shear stress will be required to fail these binding forces of the cement. Furthermore, from Figure 4.59 it can be observed that, similar to the results obtained from the tests on 28 day aged interfaces, samples with sulphate have higher shear strength than the sulphate-free samples as well as the shear strength of the 25,000 ppm specimens are lower than that of the 15,000 samples and higher than that of the 5,000 ppm interfaces. The reasons for this behaviour are the same as those described for the 28 day interface specimens.

4.5.3.2.3 150 days curing time

Figure 4.59 shows that the shear strength of the CPB-rock interface samples with 0 ppm and 5,000 ppm of sulphate continues to increase as curing time is increased to 150 days. The mechanisms responsible for this behaviour are already explained above.

In contrast, the samples with sulphate contents of 15,000 ppm and 25,000 ppm suffer from a significant reduction in shear strength. Moreover, the rate of shear strength decrease of samples with 15,000 ppm of sulphate content is lower than that of the latter one. This observed significant drop of strength for the highly sulphated samples (15,000 ppm, 25,000 ppm) and higher drop and strength decrease rate for the samples with 25,000 ppm are the results of the combined effects of the following mechanisms: (i) formation of excessive amounts (with respect to the size of the capillary pores) of expansive minerals, such as ettringite and gypsum, within the pores of CPB due to the reactions of sulphate ions with C_3A and CH, respectively; (ii) sulphate induced inhibition of the cement hydration; (iii) sulphate adsorption on C-S-H.

The precipitation of excessive amounts of ettringite and gypsum within the capillary pores of CPB leads to the fact that excessive pressure will be applied onto the pores of the CPB (Ping and Beaudoin, 1992). A combination of two factors can explain this excessive pressure; namely, (1) a higher sulfate content (15,000 ppm, 25,000 ppm), which leads to formation of more expansive minerals; and (2) the refinement of the pore structure of CPB as the curing time increases from 90 days to 150 days. This pressure, which is higher as the sulphate content increase results in the physical damage (generation of microcracks due to coarsening of the pore structure of the CPB) of the CPB matrix, thereby weakening the asperities on the surface of the CPB, decreasing the contact area between the CPB and the rock, and lowering the cementation binding force between the CPB and the rock surface. Subsequently, the interface shear strength of the highly sulphated decreases. This sulphate-attack induced physical damage or coarsening of the pore structure of the CPB that has high sulphate content and cured for 150 days is supported by the results of the SEM analyses performed and pore structure analysis (MIP) presented in Aldhafeeri and Fall (Aldhafeeri and Fall, 2017) and Figure 4.62, respectively. The SEM observation (Aldhafeeri and Fall, 2017) of a 150 days old CPB sample with 25,000 ppm show that there are many cracks formed in the sample with high sulphate content. From Figure 4.62, which illustrates the results of the MIP tests conducted on 150 day old CPB samples with sulphate contents of 0 ppm and 25,000 ppm, it can be clearly seen that the 25,000 ppm sample has a less dense pore structure with a coarser distribution of pores than that of the sample without sulphate.

Moreover, the aforementioned sulphate-inhibition of the cement hydration in the highly sulphated specimens results in the formation of fewer hydration products (e.g., C-S-H), which eventually lead to the decrease of the interface shear strength. C-S-H is the key contributor to the strength of any Portland cement-based materials (Gani, 1997). Also, fewer cement hydration products leads to coarser pore structure (Figure 4.62) of the CPB, and thus strength decrease as explained previously. This argument of sulphate-induced inhibition of cement hydration is in agreement with the results of XRD analyses performed on 150 day old CPB samples with a relatively low (5,000 ppm) and high (25,000 ppm) sulphate content, as presented in Figure 4.63. It can be observed that the 25,000 ppm sample still has unreacted C_2S and C_3S, whereas none of these minerals are present in the 5,000 ppm sample. This means that the 25,000 ppm has not fully hydrated or its hydration degree is lower than that of the 5,000 ppm.

Furthermore, it is well-documented that sulphate ions can be adsorbed by C-S-H and a higher sulphate content leads to a higher adsorption of sulphate by C-S-H (Jelenić et al., 1977; Barbarulo, 2002; Fall and Pokharel, 2010). This would result in the formation of C-S-H of lower quality within the highly sulphated samples, thereby resulting in their strength reduction since the strength of portland cement-bound materials is mainly determined by C-S-H (Jelenić et al., 1977; Barbarulo, 2002; Divet and Randriambololona, 1998; Fall and Pokharel, 2010) as discussed above.

A closer look at the values of shear strength of the 150 day old samples presented in Figure 4.59 also reveals that the strength of the 5,000 ppm interface specimen is higher than that of the sulphate-free and other sulphated samples. This higher strength is due to (1) the refinement of the pore structure of the 5000 ppm CPB induced by the precipitation of sufficient (but not excessive) amount of ettringite and gypsum within the CPB pores as discussed previously and demonstrated in numerous previous studies (Fall and Benzaazous, 2005; Pokharel and Fall, 2013), and (2) the absence or low sulphate-induced inhibition of cement hydration at a sulphate content of 5,000 ppm. This absence or low inhibition effect is consistent with the results of XRD analyses presented in Figure 4.63. It can be noticed that there is no unreacted C_2S and C_3S in the 5,000 ppm sample, while the 25,000 ppm show unreacted C_2S and C_3S. These observations indicate that, similar to the curing times of 28 and 90 days, there is also at 150 days a competition exists between interface strength increasing (formation of more hydration products (e.g., C-S-H with time; refinement of the pore structure due to precipitation of sufficient amount of expansive minerals within CPB pores) and decreasing (sulphate induced inhibition of cement hydration, formation of C-S-H of lower quality due to sulphate adsorption, coarsening and microcraking of the CPB matrix due to precipitation of excessive amount of expansive minerals) factors. The magnitude of their effect, or in other words, the dominant factors that influence the strength (decreasing or increasing) of the studied specimens, depends on the initial sulfate content and curing time.

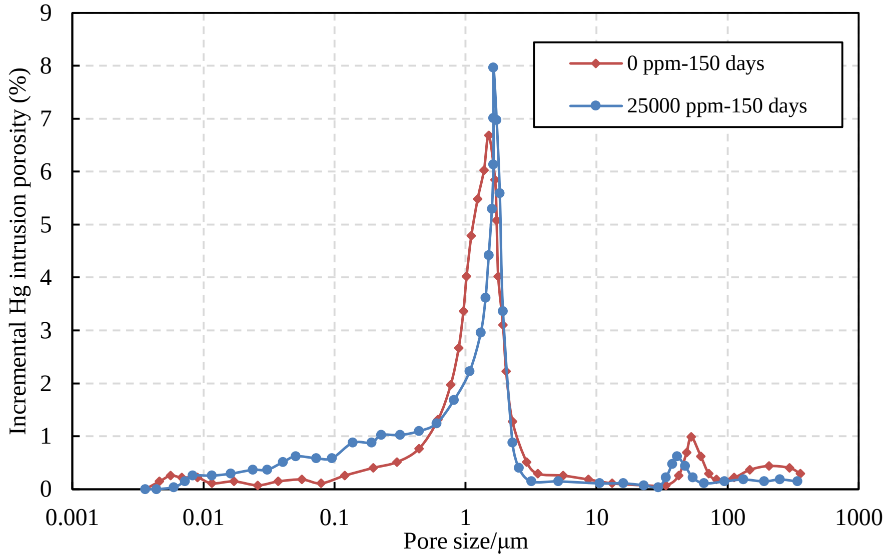

Figure 4.62 Pore size distribution of 150-day samples with sulphate content of 0 ppm and 25,000 ppm

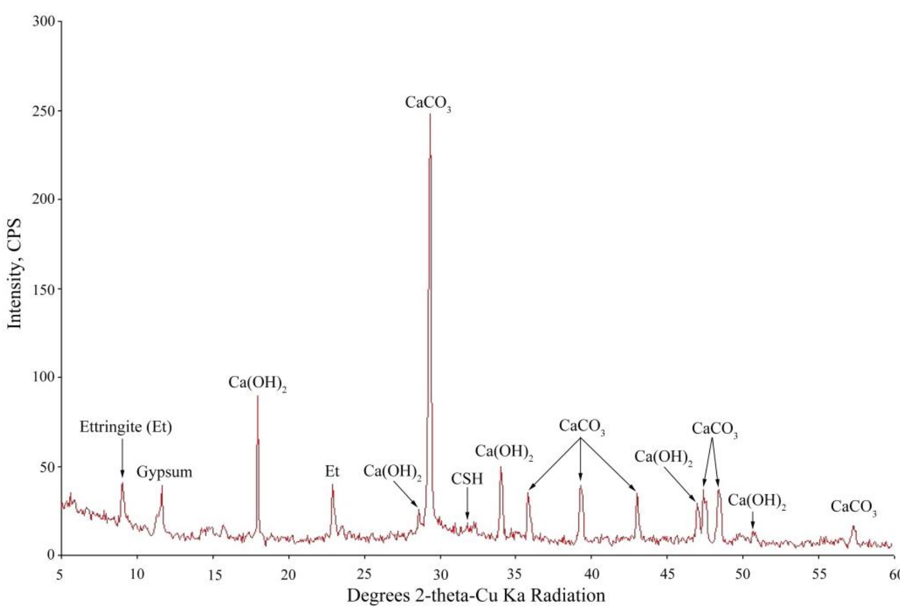

(a) 5,000 ppm

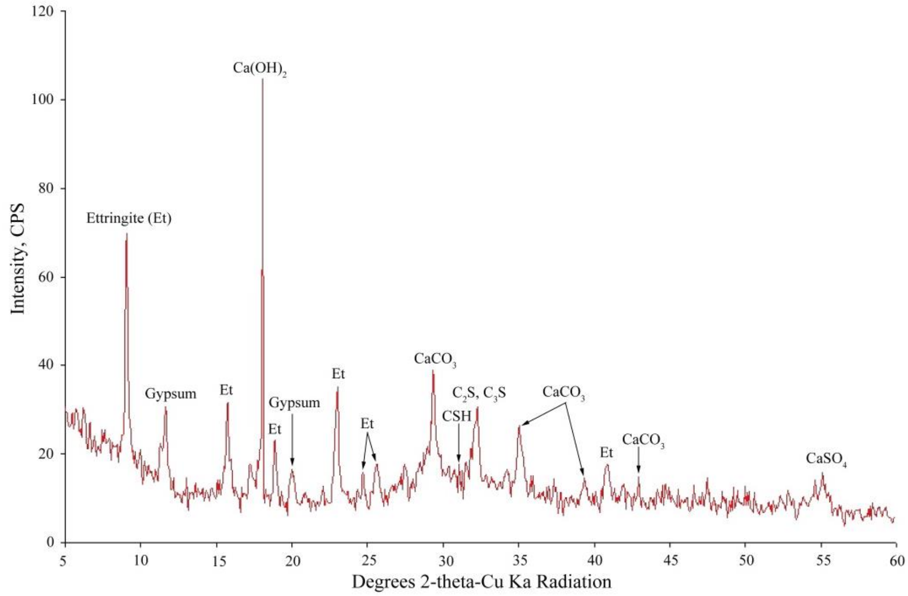

(b) 25,000 ppm

Figure 4.63 XRD result of cement paste (a) 5,000 ppm (b) 25,000 ppm cured for 150days

4.5.3.3 Effect of sulphate on the evolution of the shear strength parameters of CPB-rock interface

The analysis of the data obtained has shown that the shear failure envelope of the interface of the interface samples follows the Mohr-Coulomb failure criterion regardless of the sulphate content and curing time. Therefore, the Mohr-Coulomb failure criterion is adopted here to determine the shear strength parameters (friction angle, adhesion) of the CPB-rock interface. Figure 4.64, which illustrates the time and sulphate dependent evolution of the strength parameters of the CPB-rock interface, indicates that the friction angle and adhesion (or cohesion) of the interface is significantly affected by the curing time and initial sulphate content. It can be clearly observed that both the friction angle and adhesion of samples with 0 ppm and 5,000 ppm of sulphate increase with curing time. This finding is also in agreement with the results of previous studies on CPB-rock interface and cemented soils (Uddin et al., 1997; Nasir and Fall, 2008; Koupouli et al., 2016). The increase in adhesion is due to the increased binding force at the interface, as a result of an enhanced degree of cement hydration (Nasir and Fall, 2008). Whereas the slight increase in friction angle is attributed to stronger asperities formed at the interface between CPB and rock. The stronger asperities which form interlocking structures at the CPB-rock interface are cemented together by small cement hydration products with curing time (Lade and Overton, 1989). This in turn leads to a higher frictional resistance between the tailings and the surface of the rock, thus increasing the friction angle.

However, for samples with 15,000 ppm and 25,000 ppm of sulphate, the adhesion and friction angle show an increase during the first 90 days as well, and then depict a decrease after being cured from 90 days to 150 days. The main mechanisms responsible for this reduction in adhesion and friction angle of highly sulphated samples (15,000 ppm and 25,000 ppm) cured for 150 days are the same as those that cause the drop the strength of the 15,000 ppm and 25,000 ppm samples cured for 150 days. Specifically, the excessive pressure applied by the large amounts of expansive minerals on the pores of the CPB matrix breaks the cemented microstructure between the CPB and rock surface, thereby decreasing the adhesion. The formation of lower amount of C-S-H due to sulphate-induced inhibition and of C-S-H of lower quality due to sulphate adsorption is additional factors that lead to the decrease of the interface adhesion. They also induce the formation of weaker asperities at the surface of CPB thereby decreasing the interface friction angle.

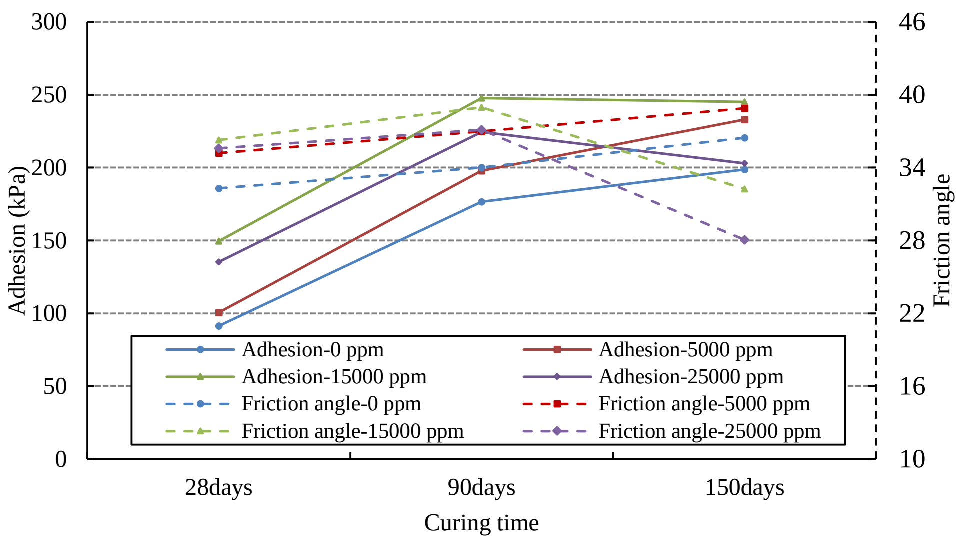

Figure 4.64 Evolution of adhesion and friction angle of CPB-rock interfaces with different initial sulphate contents

4.5.4 Summary and conclusions

This paper presents the experimental results of the effect of initial sulphate content of CPB on the shear behaviour and properties of the interface between rock and CPB cured at advanced ages. The main conclusions are summarized as follows:

- Sulphate has a significant impact on the long-term shear behaviour and strength of the CPB-rock interface. This effect depends on the initial sulphate content and curing time. Simultaneous variations of the initial sulfate content and curing time can have two opposite effects on the shear strength development and shear strength parameters (friction angle, adhesion) of CPB-rock interface. The sulfate can lead to an increase of interface shear strength and shear strength parameters owing to the dominating influence of shear strength-increasing factors. However, shear strength-decreasing factors counteract the beneficial effect of the strength-increasing factors and can induce a reduction of the interface strength and shear strength parameters if their effects outweigh those of the increasing factors.

- The shear strength increasing factors include (1) precipitation of more cement hydration products (particularly, C-S-H) as the curing time increases due to the progress of cement hydration; (2) refinement of the CPB pore structure due to the progress of cement hydration; (iii) refinement of the pore structure of CPB due the precipitation of sufficient amount (but not excessive) of expansive minerals (ettringite, gypsum) within the pores of CPB. The combined effect of these increasing factors lead to the formation of stronger asperities at the surface of CPB, larger contact area between the CPB and the rock, and stronger binding force between the CPB and rock.
- The shear strength decreasing factors are (1) inhibition of cement hydration due to high sulphate content which induces the precipitation of lower amount of hydration products, (2) the formation of excessive amount (with respect to the size of the capillary pores) of expansive minerals within the pores of CPB that leads to physical damage or coarsening of the CPB matrix, (3) adsorption of sulphate by C-S-H that results in the formation of C-S-H of lower quality.
- It is found that there is a competition between the shear strength decreasing and strength-increasing factors. The dominant influencing factors and magnitude of the effect of each influencing factor depend on the curing time and initial sulfate content.
- The initial sulphate content does not significantly affect the contraction behaviour of the studied interface specimens. However, the magnitude of the shear dilation is a function of the curing time and initial sulphate content.

This study will provide useful information for understanding and better assessment of the shear behaviour and strength at the interface between CPB structure and rock mass, which is critical for the design of safe and cost-effective backfill structures.

Acknowledgements

The authors would like to thank the Natural Sciences and Engineering Research Council of Canada (NSERC), the University of Ottawa and the China Scholarship Council. Also the authors would like to thank Mr. Jean Claude Celestin and Mr. Jiwei Bian for their kind help.

4.5.5 References

Aldhafeeri Z, Fall M (2017) Sulphate induced changes in the reactivity of cemented tailings backfill. Int. J. Miner. Process. 166:13-23.

Amaratunga LM, Yaschyshyn DN (1997) Development of a high modulus paste fill using fine gold mill tailings. Geotech. Geol. Eng. 15(3):205-219.

Aubertin M, Li L, Arnoldi S, Belem T, Bussière B, Benzaazoua M, Simon R (2003) Interaction between backfill and rock mass in narrow stopes. Soil and rock America 1:1157-1164.

Barbarulo R (2002) Comportement des matériaux cimentaires: actions des sulfates et de la temperature. Ph.D. Dissertation, Université Laval, Canada; (in French)

Bentur A (1976) Effect of gypsum on the hydration and strength of C3S Pastes. Journal of the American Ceramic Society, 59(5-6):210-214.

Benzaazoua M, Fall M, Belem T (2004) A contribution to understanding the hardening process of cemented pastefill. Miner. Eng. 17(2):141-152.

Bing B, Cohen MD (2000) Does gypsum formation during sulphate attack on concrete lead to expansion. Cem. Concr. Res. 30(1):117–123.

Brackebusch FW (1994) Basic of paste backfill system. Miner. Eng. 46:1175-1178.

Buckby T, Black S, Coleman ML, Hodson ME (2003) Fe-sulphate-rich evaporative mineral precipitates from the Rio Tinto, southwest Spain. Mineral. Mag. 67:263-278.

De Souza E, Dirige AP (2001) Procedures for the design of sillmats with paste backfill. The 38th US Symposium on Rock Mechanics (USRMS), Washington, D.C.

De Souza E, Dirige AP (2002) An integrated approach for the design of stable mine backfill sillmats. WIT Transactions on Engineering Sciences DOI: 10.2495/DM020301.

Divet L, Randriambolona R (1998) Delayed ettringite formation: the effect of temperature and basicity on the interactions of sulphate and C–S–H phase. J. Cem. Concr. Res. 28(3):357-363.

Fall M, Samb SS (2009) Effect of high temperature on strength and microstructural properties of cemented paste backfill. Fire Saf. J. 44(4):642-651.

Fall M, Benzaazoua M (2005) Modelling the effect of sulphate on strength development of paste backfill and binder mixture optimization. Cem. Concr. Res. 35(2):301-314.

Fall M, Célestin JC, Pokharel M, Touré M (2010) A contribution to understanding the effects of curing temperature on the mechanical properties of mine cemented tailings backfill. Eng. Geol. 114(3-4):397-413.

Fall M, Nasir O (2010) Mechanical behaviour of the interface between cemented tailings backfill and retaining structures under shear loads. Geotech. Geol. Eng. 28(6):779-790.

Fall M, Pokharel M (2010) Coupled effects of sulphate and temperature on the strength development of cemented tailings backfills: Portland cement-paste backfill. Cem. Concr. Compos. 32:819-828.

Fang K, Fall M (2018a) Effects of curing temperature on the shear behaviour of cemented paste backfill-rock interface. Int. J. Rock Mech. Min. Sci. 112, 184-192.

Fang K, Fall M (2018b) Chemically induced changes in the shear behaviour of the interface between rock and tailings backfill undergoing cementation. Rock. Mech. Rock. Eng. 1-16

Fu Y, Ding J, Beaudoin J (1997) Expansion of Portland cement mortar due to internal sulfate attack. Cem. Concr. Res. 27(9):1299-1306.

Gani MSJ (1997) Cement and Concrete. Chapman & Hall, London, UK.

Grice T (2001) Recent mine developments in Australia. Proceeding of the 7th International Symposium on Mining with Backfill (MINEFILL), 351–357.

Hassani F, Archibal J (1998) Mine backfill. Canadian Institute of mine, Metallury and Petroleum, Canada.

Husem M, Gozutok S (2005) The effects of low temperature curing on the compressive strength of ordinary and high performance concrete. Constr. Build. Mater. 19(1):49–53.

Jelenić I, Panović A, Halle R, Gaćeša T (1977) Effect of gypsum on the hydration and strength development of commercial Portland cements containing alkali sulfates. Cem. Concr. Res, 7:239-245.

Jiang HQ, Fall M, Cui L (2016) Yield stress of cemented paste backfill in sub-zero environments: experimental results. Miner. Eng. 92:141-150.

Kesimal A, Yilmaz E, Ercikdi B, Alp I, Deveci H (2005) Effect of properties of tailings and binder on the short-and long-term strength and stability of cemented paste backfill. Mater. Lett. 59(28):3703-3709.

Koupouli NJ, Belem T, Rivard P, Effenguet H (2016) Direct shear tests on cemented paste backfill-rock wall and cemented paste backfill-backfill interfaces. J. Rock. Mech. Geotech. Eng. 8(4):472-479.

Lade PV, Overton DD (1989) Cementation effects in friction materials. Journal of Geotechnical Engineering, 115(10):1373-1387.

Li WC, Fall M (2016) Sulphate effect on the early age strength and self-desiccation of cemented paste backfill. Constr. Build. Mater. 106:296-604.

Li WC, Fall M (2018) Strength and self-desiccation of slag-cemented paste backfill at early ages: Link to initial sulphate concentration. Cem. Concr. Compos. 89:160-168.

Marston A (1930) The theory of external loads on closed conduits in the light of latest experiments. Highway research board proceedings, Ames Iowa.

Nasir O, Fall M (2008) Shear behaviour of cemented pastefill-rock interfaces. Eng. Geol. 101:146-153.

Nonnet E, Lequeux N, Boch P (1999) Elastic properties of high alumina cement castables from room temperature to 1600°C. J. Eur. Ceram. Soc. 19(8):1575-1583.

Pakalnis R, Caceres C, Clapp K, Morin M, Brady T, Williams T, MacLaughlin M (2005) Design spans-underhand cut and fill mining. 107th CIM-AGM, Toronto, Canada.

Pane I, Hansen W (2005) Investigation of blended cement hydration by isothermal calorimetry and thermal analysis. Cem. Concr. Res, 35(6):1155–1164.
Pelisser F, Gleize PJP, Mikowski A (2012) Effect of the Ca/Si Molar Ratio on the Micro/nanomechanical Properties of Synthetic C-S-H Measured by Nanoindentation. J. Phys. Chem. C. 116(32):17219–17227
Pirapakaran K, Sivakugan N (2007) A laboratory model to study arching within a hydraulic fill stope. Geotech. Test. J. 30(6):1-8.
Ping X, Beaudoin JJ (1992) Mechanism of sulphate expansion. I: Thermodynamic Principle of Crystallization Pressure. Cem. Concr. Res. 22(4):631-640.
Pokharel M, Fall M (2013) Combined influence of sulphate and temperature on the saturated hydraulic conductivity of hardened cemented paste backfill. Cem. Concr. Compos. 38:21-28.
Ramlochan T, Zacarias P, Thomas M, Hooton R (2003) The effect of pozzolans and slag on the expansion of mortars cured at elevated temperature: Part I: Expansive behaviour. Cem. Concr. Res. 33(6):807-814.
Saiang D, Malmgren L, Nordlund E (2005) Laboratory tests on shotcrete-rock joints in direct shear, tension and compression. Rock Mech. Rock Eng. 38(4):275-297.
Simms P, Grabinsky M (2009) Direct measurement of matrix suction in triaxial tests on early-age cemented paste backfill. Canadian Geotechnical Journal 46(1):93-101.
Swedenborg S (2001) Rock mechanical effects of cement grouting in hard rock. Ph.D. Dissertation, Chalmers University of Technology, Sweden.
Tagawa H (1984) Thermal decomposition temperatures of metal sulfates. Thermochim. Acta. 80(1):23-33.
Tian HM, Chen WZ, Yang DS, Yang JP (2015) Experimental and numerical analysis of the shear behaviour of cemented concrete-rock joints. Rock. Mech. Rock. Eng. 48(1):213-222.
Tse R, Cruden DM (1979) Estimating joint roughness coefficients. Int. J. Rock Mech. Min. Sci. 16(5):303-307.
Tzouvalas G, Dermatas N, Tsimas S (2004) Alternative calcium sulfate-bearing materials as cement retarders: Part I. Anhydrite. Cem. Concr. Res. 34(11):2113-2118.
Uddin K, Balasubramaniam AS, Bergardo DT (1997) Engineering behaviours of cement-treated Bangkok soft clay. Geotechnical Engineering Journal 28(1):89-119.
Wang Y, Fall M (2016) Initial temperature-dependence of strength development and self-desiccation in cemented paste backfill that contains sodium silicate. Cem. Concr. Compos. 67:101-110.
Yilmaz E, Kesimal A, Ercidi B (2004) Strength development of paste backfill simples at Long term using different binders. Proceedings of 8th symposium MineFill04, China.
Yilmaz E, Benzaazoua M, Belem T, Bussiere B (2009) Effect of curing under pressure on compressive strength development of cemented paste backfill. Miner. Eng. 22(9-10):772-785.
Zhou Q, Glasser F (2001) Thermal stability and decomposition mechanisms of ettringite at <120 C. Cem. Concr. Res. 31(9):1333–1339.

4.6 Paper VI: Shear Behaviour of Rock-Tailing Backfill Interface: Effect of cementation, rock type, and rock surface roughness

Published in *Geotechnical and Geological Engineering*, 2020, doi.org/10.1007/s10706-020-01586-x.

Kun Fang, Mamadou Fall

Abstract

Determination of interface shear behaviour is critical for the design of many geotechnical structures. With the purpose of studying the effects of interface roughness on the evolution of peak shear stress and properties of the interface between cemented paste backfill (CPB) and rock, a series of direct shear tests are conducted on interface samples with various roughness values. The obtained results show that roughness has a significant effect on the shear characteristics of a CPB-concrete interface. For a certain curing time, the roughness can increase the shear strength due to the increased size of the interlocking structure. In addition, the shear strength, shear dilation, and adhesion of the interface also increase with curing time, which is ascribed to the raised degree of cement hydration. However, according to the revised Barton's equation, the effective friction angle of interface with roughness experiences a decreasing tendency with time, despite the increasing tendency of the friction angle of the smooth interface. In other words, the interface asperity contributes more to the evolution of adhesion, and the contribution of friction angle to the shear strength is partially offset. The findings in this study enrich the understanding of the effects of mechanical factors on the interface behaviour and also have practical importance to the design of the underground CPB structures.

4.6.1 Introduction

Cemented paste backfilling, a relatively newly developed mine backfilling method, has been widely adopted and used extensively by many mines worldwide (Brackebusch, 1994; Hassani and Archibald, 1998; Fall and Benzaazoua, 2003; Fang and Fall, 2018). Cemented paste backfill (CPB) is made of tailings (soils or waste generated in a mine processing plant), water, and hydraulic binder. The main purpose of cemented paste backfilling technology is to guarantee the stability of the underground mining space and, thus provide a safe working environment for mine workers. Besides, the cemented paste backfilling technology is regarded as an environmental-friendly mining method for the underground disposal of tailings, which are a main source of acid mine drainage (AMD). In addition to the safety and environmental benefits, cemented paste backfilling can also bring economic benefits to a mine. The support of a backfilling body underground allows complete exploitation of ore body and then improves the recovery ratio. The aforementioned advantages of cemented paste backfilling technology mainly explain its popularity in mining operations worldwide.

The underground CPB structure and its schematic diagram are depicted in Figure 4.65, which shows that the priority of the geomechanical design of the CPB structure is to ensure its mechanical stability. Otherwise, the failure of CPB structures can result in financial ramifications and even fatalities. This mechanical stability is a function of the shear characteristics or behaviour of the CPB-rock interface, as briefly discussed below.

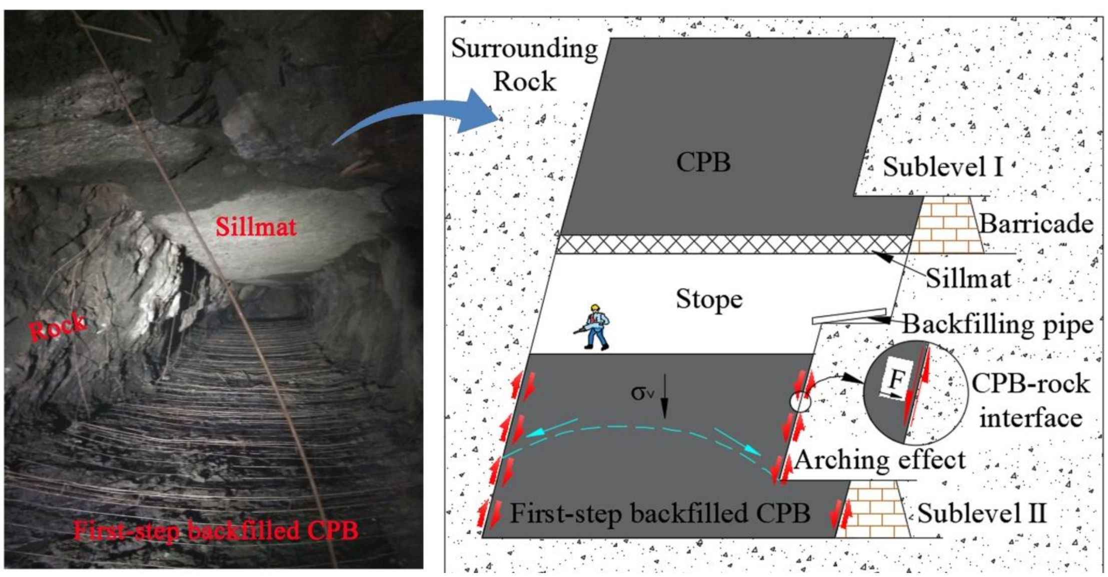

Figure 4.65 Underground CPB structure and its schematic diagram

In general, the bonded interface between dissimilar materials is often a weak link in terms of mechanical stability (Dong et al., 2017), and Nasir and Fall (2008) have concluded that both the adhesion and the friction angle of the CPB body are higher than those of the CPB-rock interface with a smooth surface.

Moreover, the occurrence of an arching effect, which is a result of shear stress redistribution and CPB consolidation, is also related to the interface shear performance or characteristics. In other words, the arching effect can transfer the overlying stress to surrounding rock via the interface, thereby decreasing the vertical stress within the CPB mass (Terzaghi, 1943; Pirapakaran and Sivakugan, 2007; Yang et al., 2015). Helinski et al. (2010) and Cui and Fall (2017) also observed this phenomenon experimentally and numerically, as shown in Figure 4.66. The backfilling process in-situ is divided into several steps, and the initial stress monitored by the bottom sensor increases with the filling operation, which is in good agreement with the development of self-weight stress (Figure 2). However, after the initial backfilling process (from the first day to the second day), the measured stress experiences a slight decrease (from the second day to the fifth day), and this reduction in stress is because of the stress redistribution, which means the occurrence of the arching effect. After the beginning of the second-step filling (fifth day), the measured stress at the bottom depicts a gradual increase, and the increasing rate is significantly lower than the expected increasing rate of self-weight stress. This means that the total stress induced by the overlying CPB body was mainly transferred to the surrounding rock through the arching effect. However, if arching is not present, the condition described in Figure 4.66 would require a CPB body with a minimum strength of 480 kPa to ensure its mechanical stability. This means a large amount of cement would be needed to achieve the required minimum strength, and consequently, the cost of the CPB would be significantly increased (Grice, 2001; Fall and Benzaazoua, 2005; Kuganathan, 2005). The binder can represent up to 75% of the CPB cost (Grice 2001; Fall et al. 2010). Therefore, the mechanical behaviour, especially the shear resistance capacity of the interface, is extremely important for a safer and more economical design of CPB structures.

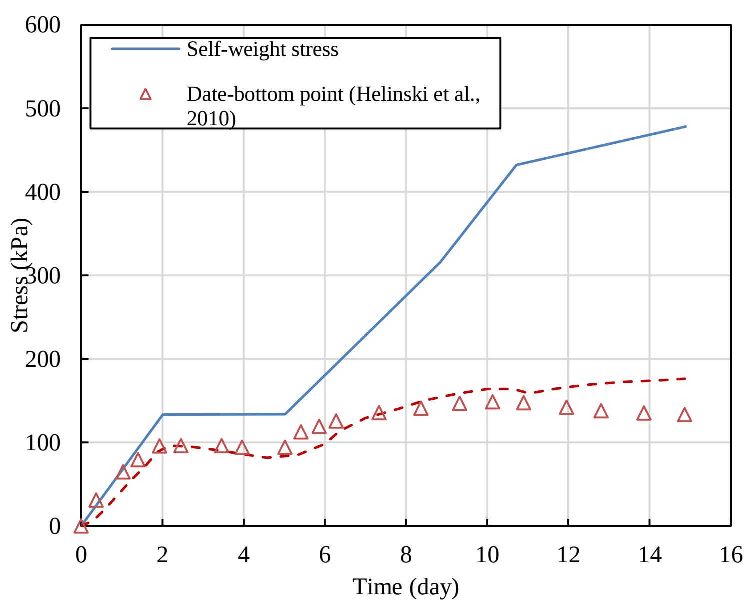

Figure 4.66 Arching effects in CPB structure: Measured and predicted total stress vs. time; self-weight stress vs time (adapted from Cui and Fall 2017)

A limited number of experimental studies have been conducted on the mechanical properties of the CPB-rock interface (e.g., Fall and Nasir, 2010; Manaras et al., 2011; Koupouli et al., 2016; Fang and Fall, 2018, 2019, 2020). These studies have concluded that the shear behaviour of the interface is affected by several factors, such as normal stress, temperature, content of sulphate ions, and drainage condition. Despite the contributions of the aforementioned previous studies to understand the CPB-rock interface shear behaviour or properties better, a fundamental comprehension of the shear characteristics of the CPB-rock interface is still far from complete. Most of the previous studies on the CPB-rock interface consider only one type of rock, namely granite. However, given the different geological conditions of mines in different places, the type of rocks around the stope varies with each other. This means that the effect of different types of rocks on the shear behaviour or properties of CPB-rock is still unknown or not well understood. Moreover, the effect of the rock surface roughness on the shear characteristics of the CPB-rock interface as well as the coupled effect of rock surface roughness and degree of cementation on the interface shear behaviour were ignored in the previous studies. In the field, the surface of the rock adjacent to or surrounding the CPB body can have various degrees of roughness. The surface of rock can also be characterized with various asperities, as shown in Figure 4.65. Even though the interaction between geo-materials and rock with asperity surface has been extensively studied (Seidel and Haberfield, 2002; Wang et al., 2015; Bahaaddini et al., 2015; He et al., 2017; Han et al., 2018), the knowledge of the shear performance of the interface between CPB and rough rock remains unknown. Moreover, the results of previous studies on the behaviour of the interface of rock with asperities and other geo-materials are not directly transferable to the CPB-rock interface because CPB is different from the other geo-materials.

Considering the facts mentioned above, the major purpose of this research is to experimentally investigate the influence of rock surface roughness and CPB curing times as well as the rock type on the shear characteristics of CPB-rock interface, which is important for a thorough evaluation of the geomechanical stability of CPB structures in the practice.

The present paper is organized as follows. Firstly, surface parameters used to evaluate surface roughness are introduced and discussed. Then, the experimental program conducted in this research is described. A large number of direct shear tests are conducted on interface samples with different interface roughness values. Subsequently, the obtained results are presented and discussed with respect to the influence of the rock type, rock surface roughness, combined effect of surface roughness and degree of cementation. Finally, the conclusions are presented.

4.6.2 Surface Parameters to Estimate Joint Roughness Coefficient

The difficulty in expressing the influence of the complex geometry of the asperity surface on the interface shear mechanical behaviour is addressed by introducing a simple coefficient, namely, joint roughness coefficient (JRC), which is initiated by Barton (1973) for evaluating the strength of rock joints with roughness:

$$\tau = \sigma \tan\left[\text{JRC } \log(\text{JCS}/\sigma) + \varphi_b\right] \tag{4-9}$$

where τ is the shear strength, σ is the applied normal stress, JCS is the compressive strength of the joint, and φ_b is the basic (residual) friction angle. Usually, according to Mohr-Coulomb criterion, the whole part $\left[\text{JRC } \log(\text{JCS}/\sigma) + \varphi_b\right]$ is regarded as the friction angle. Herein, Barton specifically divided the friction angle into basic friction angle and the contribution of interface asperities. To determine the JRC of the targeted profile, ten surfaces with various JRC values (ranging from 0-20, where 0 means the smoothest and 20 refers to the roughest profile) were provided by Barton and Choubey (1977), as shown in Figure 4.67. The ISRM commission suggested that the JRC value of the targeted profile can then be determined by comparing it with the following standard surfaces (Brown, 1981).

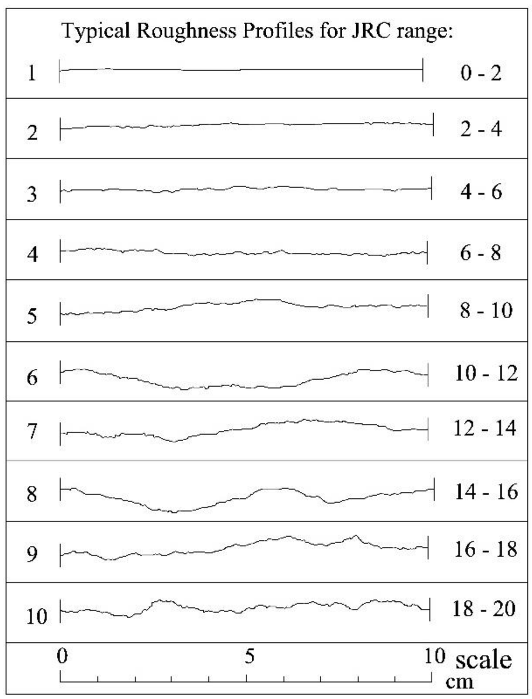

Figure 4.67 Standard roughness profiles and their JRC values (Barton and Choubey 1977)

However, the determination of JRC value by visible comparison is inevitably considered as subjective. Hence, to evaluate the JRC value objectively and quantitatively, many surface parameters have been proposed. Tse and Cruden (1979) proposed several surface parameters, such as RMS (root mean square roughness index), CLA (arithmetical mean deviation roughness index), Z_2 (root mean square of the first deviation of the surface), MSV (mean square value roughness index), and SF (structure function of the profile) to estimate the JRC of a rock surface. But after analysing the correlation coefficient of eleven regression equations, they finally adopted Z_2 and SF to describe the JRC. However, Yu and Vayssade (1991) and Yang et al. (2001) found that the amplification of the surface would affect the evaluation of the JRC. Moreover, they also found the JRC is sensitive to the sampling interval. Therefore, they digitized ten standard profiles and adopted 200 discrete data points along the surface with different intervals, and finally improved the correlation coefficient of the regression equation. The ratio of the true length of profile to its projected length, R_p, was also proposed by EI-Soudani (1978) and related to JRC by Maerz et al. (1990). Another surface parameter, RL, which is similar to R_p, was developed by Yu and Vayssade (1991) to evaluate the JRC value. The aforementioned surface parameters and their relevant regression equations are summarized in Table 4.9.

Table 4.9 Surface parameters and regression equations

Surface parameter	Calculation	Regression equation	Correlation coefficient	Reference
SF	$SF = \frac{1}{L}\sum (y_{i+1} - y_i)^2 \Delta x$	$JRC = 37.28 + 16.58 \log SF$	0.984	Tse and Cruden (1979)
Z_2	$Z_2 = \left[\frac{1}{L}\sum \frac{(y_{i+1} - y_i)^2}{x_{i+1} - x_i}\right]^{1/2}$	$JRC = 32.2 + 32.47 \log Z_2$	0.986	Tse and Cruden (1979)
		$JRC = 32.69 + 32.98 \log Z_2$	0.993	Yang et al. (2001)
R_p	$R_p = \frac{\sum_1^n \sqrt{(x_{i+1} - x_i)^2 + (y_{i+1} - y_i)^2}}{\sum_1^n (x_{i+1} - x_i)}$	$JRC = 558.68\sqrt{R_p} - 557.13$	0.951	EI-Soudani (1978); Maerz et al. (1990)
RL	$RL = \frac{\sum_1^n \sqrt{(x_{i+1} - x_i)^2 + (y_{i+1} - y_i)^2}}{\sum_1^n (x_{i+1} - x_i)} - 1$	$JRC = 63.69\sqrt{RL} - 2.31$	0.982	Yu and Vayssade (1991)

Herein, the parameter Z_2, is employed to evaluate the JRC value. To prepare CPB-rock interface samples with different roughness values, some concrete bases with three different roughness measures, as shown in Figure 4.68, are produced in this study. To accurately determine the JRC of concretes, a highly precise linear variable displacement transformer (LVDT) is used to survey the coordinates along the centerline at the concrete surface. The results of measured coordinates along the centerline are presented in Figure 4.69. Thereafter, the following two estimation equations are adopted to calculate the JRC value (Yu and Vayssade, 1991):

$$Z_2 = \left[\frac{1}{L} \sum \frac{(y_{i+1} - y_i)^2}{x_{i+1} - x_i} \right]^{1/2} \tag{4-10}$$

$$JRC = 32.69 + 32.98 \log Z_2 \tag{4-11}$$

where L is the nominal length of the digitized joint profile, and (x_i, y_i) are the coordinates of the discrete points. According to Eqs. (2) and (3), and the geometry of the prepared samples, the JRCs of the concrete surface prepared are calculated as 0, 6.5 and 16.6, respectively.

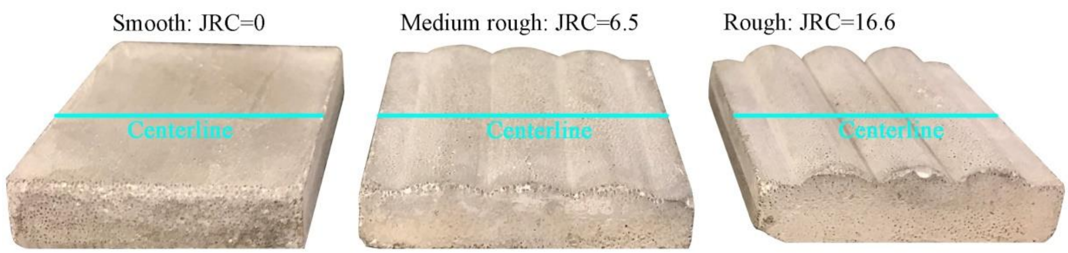

Figure 4.68 Prepared concrete samples with three different JRC values

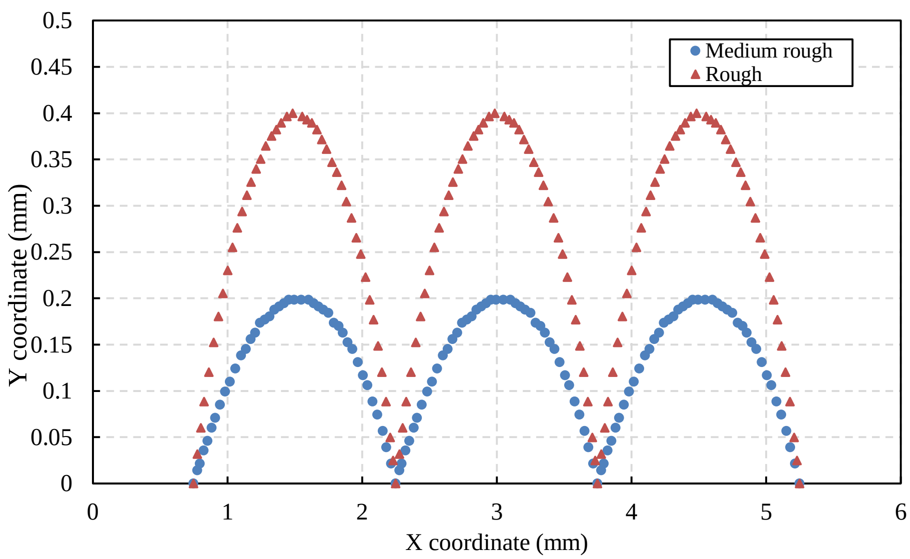

Figure 4.69 Coordinates along the centerline

4.6.3 Experimental Program

4.6.3.1 Material used

Synthetic tailings (silica tailings (ST)) were used as tailings materials. The ST are essentially made of quartz, which is the predominant mineral found in natural tailings from Canadian hard rock mines. Besides, given the pure component of ST (with 99.8% S_iO_2), the adoption of ST can then avoid uncertainties in the results due to natural tailings, which can often interact with the cement hydration. Hence, the CPB part of the samples used in this paper are all produced by mixing ST, binder, and tap water. The Portland cement type I (PCI), a proportion of 4.5%, is used as the binder in this research. Meanwhile, the water-cement ratio is controlled as 7.35.

For the rock part of the samples, two kinds of rocks (e.g., marble and granite) and concrete are adopted. The use of concrete allows an easier preparation of rock surfaces with different roughness by using special plastic molds. The uniaxial compressive strength (UCS) of the marble ranges from 60 MPa to 80 MPa, while that of granite (160 MPa) is much higher, which is noted in previous studies by the authors (Fang and Fall 2018, 2019). In contrast, the concrete (with a strength of 38 MPa) is made of Portland cement type I (PCI), fine sand, and water with the weight ratio of 4:2:1.

4.6.3.2 Samples preparation and test plans

4.6.3.2.1 Samples preparation

The marble and granite are cut into small cuboid pieces with dimensions of 60×60×15 mm; the length and width are exactly the same as those of the direct shear box. To produce a concrete base with the same size, the mixed material (PCI: fine sand: water = 4:2:1) is cast into a plastic model (with three different levels of roughness) to form concrete. After being cured for 150 days (it is assumed that cement hydration is almost completed after 150 days), the concrete samples are then ready for producing CPB-concrete interface samples.

A B20F mixer is used to mix and stir the prepared materials (e.g., ST, PCI, and tap water), and to ensure the materials are fully mixed, the mixing process usually last 7 minutes. The obtained paste is then poured into a plastic container (with an inner size of 60×60×30 mm), in which the marble, granite or concrete has already been set. Thereafter, the air or oxygen in the CPB is squeezed out by manual vibration, and then the whole container is covered with a plastic film (to avoid evaporation). Some typical CPB-rock samples with different rock types and interface roughness are shown in Figure 4.70.

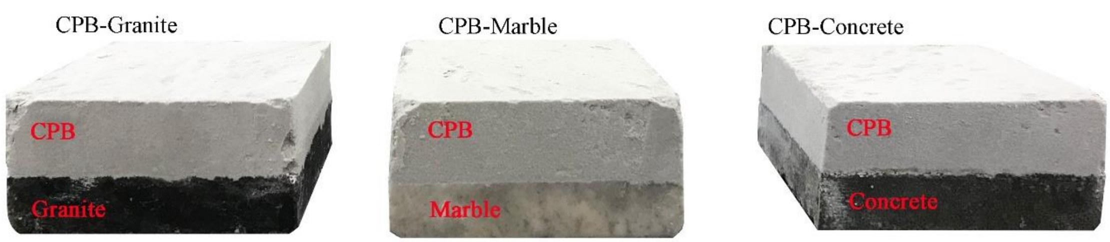

(a) Samples made with different types of rocks (JRC=0, curing for 1 day)

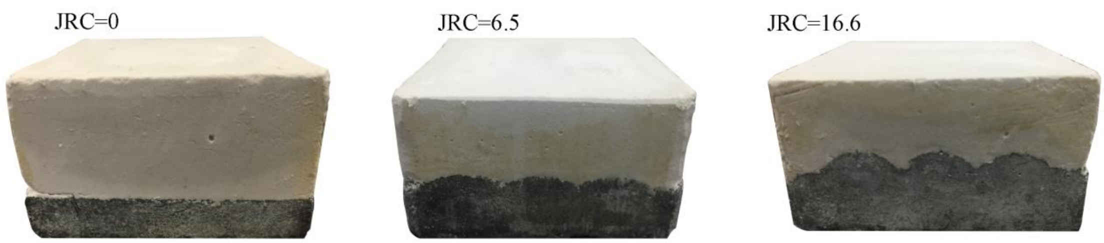

(b) Samples with different interface roughness (with concrete base, cured for 28 days)

Figure 4.70 Examples of prepared CPB-rock interface samples

4.6.3.2.2 Testing plan

To determine the effects of rock types on the interface shear behaviour, the surface of the rocks (marble, granite, and concrete) are first polished smoothly, and then the interface samples are produced and cured for 1 day. Thereafter, three constant normal stresses, as shown in Table 10, are applied to the samples during the tests. Besides, to investigate the change in the shear characteristics of the CPB-rock interface with different roughness values and cementation degrees, the interface samples with JRC values of 0, 6.5 and 16.6 are also tested after being cured for 1, 7, and 28 days. To confirm the repeatability of the results, each test is repeated three times. The experimental details are provided in Table 4.10.

Table 4.10 Experiment details

PCI content (%)	Water-cement ratio	Curing time	Normal stress (kPa)	Rock type	Interface roughness
4.5	7.35	1 day	50	Marble, Granite, Concrete	0
4.5	7.35	1 day	100	Marble, Granite, Concrete	0
4.5	7.35	1 day	150	Marble, Granite, Concrete	0
4.5	7.35	1 day	50	Concrete	0, 6.5, 16.6
4.5	7.35	1 day	100	Concrete	0, 6.5, 16.6
4.5	7.35	1 day	150	Concrete	0, 6.5, 16.6
4.5	7.35	7 days	50	Concrete	0, 6.5, 16.6
4.5	7.35	7 days	100	Concrete	0, 6.5, 16.6
4.5	7.35	7 days	150	Concrete	0, 6.5, 16.6
4.5	7.35	28 days	50	Concrete	0, 6.5, 16.6
4.5	7.35	28 days	100	Concrete	0, 6.5, 16.6
4.5	7.35	28 days	150	Concrete	0, 6.5, 16.6

4.6.3.2.3 Test setup

A direct shear device is employed to conduct the direct shear tests according to ASTM D3080-04. Figure 4.71 shows the configuration of the direct shear device. It can be observed from the figure that a load cell is installed and connected to the upper shear box to measure the shear force, while two LVDTs are adopted for displacement measurement. After the perpendicular application of the designed normal stress on the top of the samples, the lower shear box moves horizontally with a rate of 0.5 mm per minute. During the test, the upper shear box is maintained stationary. A computer software, Labview, is used to record the data of the tests.

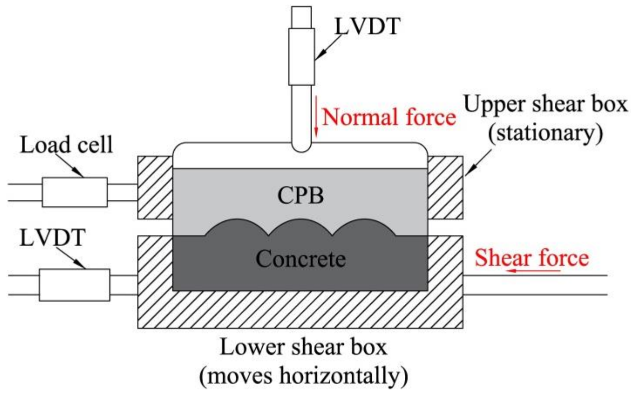

Figure 4.71 Configuration of direct shear test device

4.6.3.3 Microstructural analyses

Two main microstructural analyses, including thermal analysis and scanning electron microscope (SEM), are used here to investigate the progress of the cement hydration as well as the microstructure of the interface, respectively. The thermal analysis is conducted on cement paste of CPB (with w/c= 1 to simulate the high water content of CPB) with a Q5000IR thermogravimetric analyzer, which can record the weight loss of cement paste with the temperature increasing to 1000°C. In contrast, the SEM observation is performed on intact interface samples with a Hitachi 3500-N microscope, which allows the analysis of the texture and the pore structure at the interface microscopically. Prior to the above-mentioned two tests, samples are all subjected to a drying process (at a temperature of 45°C for 4 days).

4.6.4 Results and Discussions

Typical results of the direct shear tests are presented and discussed in this section. The effect of the rock type on the interface shear performance is briefly introduced in section 4.1, while the influences of roughness and cementation are addressed in section 4.2, respectively.

4.6.4.1 Influence of the type of rock on interface shear performance

Figure 4.72 presents the shear behaviour of the interface samples with different rock bases of granite, marble, and concrete (cured for 1 day). The results show that the shear curves of all samples show a similar tendency, and rock type has limited effects on both shear strength and dilation. The shear displacement-shear stress curve first depicts an increase up to peak shear stress (strain hardening behaviour), followed by a slight decrease (strain softening behaviour). Besides, the shear strength varies from 70 kPa to 82 kPa for samples with different type rocks (with a normal stress of 100 kPa). In terms of the normal displacement of interface samples, all samples (conducted under normal stresses of 50 kPa and

100 kPa) first experience an initial contraction, as can be seen from the figures in the right column of Figure 4.72. This initial contraction is attributed to the inherent compressibility of CPB, and the compressibility of the early-age samples decreases with time (Fang and Fall, 2018). The study conducted by Nasir and Fall (2008) also indicated the same contraction behaviour. Thereafter, it shows a slight dilation until the shear stress reaches its peak value (shear strength). The magnitude of shear dilation is associated with the degree of cement hydration, whose mechanism is introduced in detail below. For subsequent shear displacement beyond the point with the highest shear dilation, the shear displacement-normal displacement curve is then characterized by continuous contracting behaviour. In contrast, the high normal stress (150 kPa) restricts the normal displacement at the interface, and as a result, the shear displacement-normal displacement curves all depict contraction behaviours, regardless of the type of rock.

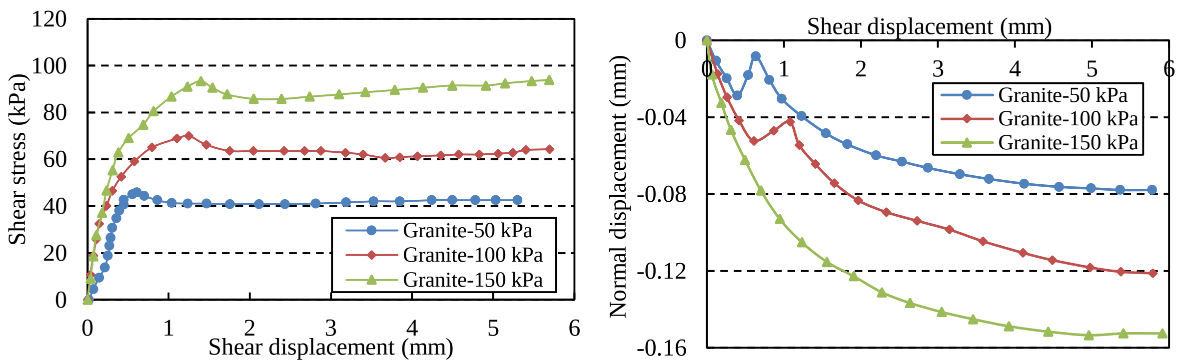

(a)

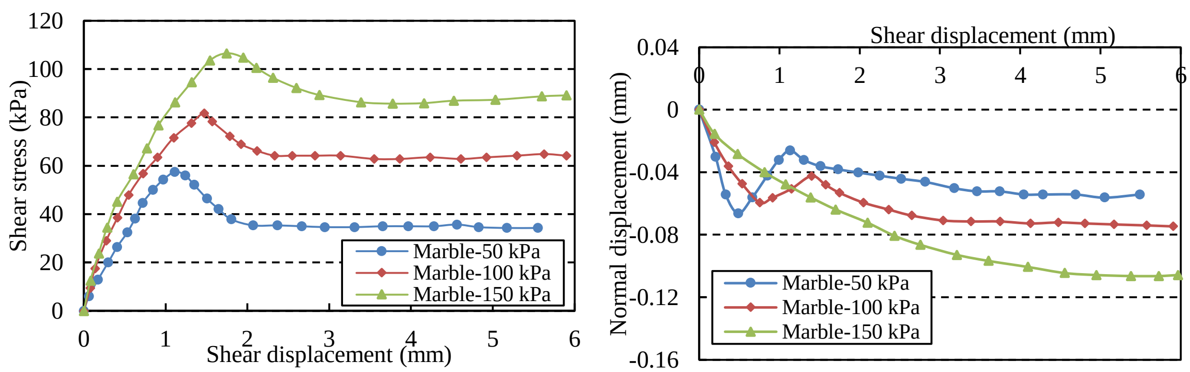

(b)

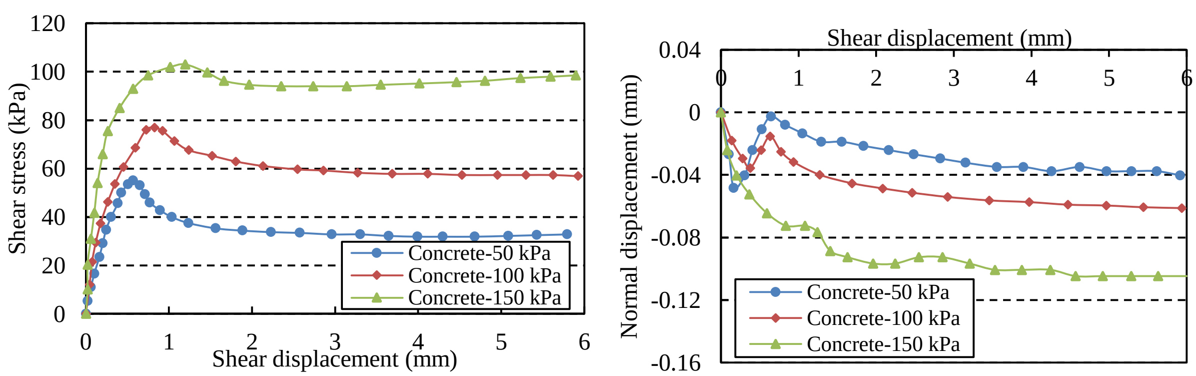

(c)

Figure 4.72 Evolution of shear stresses and normal displacements of interface samples produced with different rock types: (a) Granite, (b) Marble (c) Concrete (with a curing time of 1 day)

The evolution of shear strength with normal stresses of the corresponding interface samples is shown in Figure 4.73, based on which, the shear envelopes can be easily obtained by linear regression fitting. Because the R^2 of the three fitted linear regression lines are all close to 1, the Mohr-Coulomb criterion is then adopted to describe the shear failure envelopes of the interface samples. Hence, the shear strength parameters of the interface are easily derived, which are also indicated in the figure. The results show that the difference in the mechanical properties (e.g., shear strength, friction angle) of the interface samples made with different rocks is insignificant, especially the friction angle. This observation means that the type of rocks has limited influence on the shear properties of the interface.

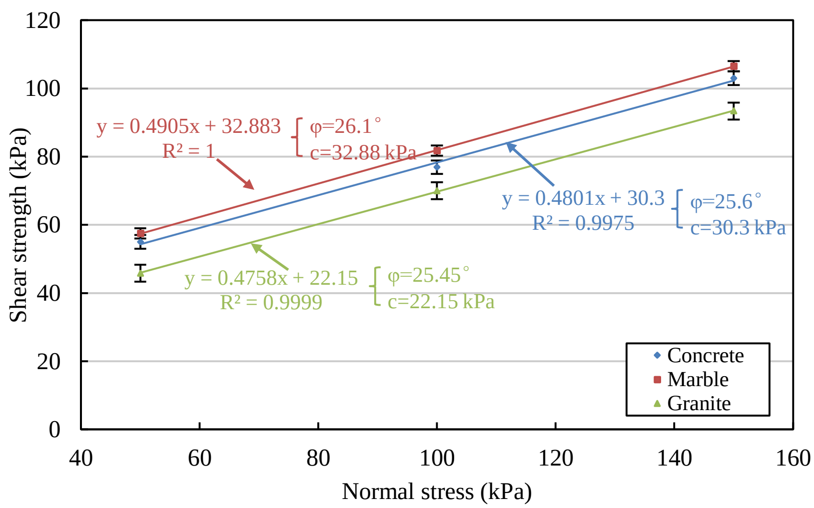

Figure 4.73 Shear envelops of the interface between CPB and different type of rocks (cured for 1 day)

The failure of the interface between CPB and different types of rock is because of the existence of the interfacial transition zone (ITZ), which is also observed in many studies on other geotechnical structures involving cementitious material (Breton et al., 1993; Ke et al., 2010). The ITZ is characterized by high porosity. This phenomenon is also known as the “wall” effect (Diamond and Huang, 2001; Scrivener et al., 2004). The formation of the ITZ is due to the penetration of cement paste into the pore structure; this ITZ then bonds CPB and rock together. The result of SEM analyses, as presented in Figure 4.74, attests to this argument. The interface crack is clearly observed, which is marked by a red dashed line in the figure. Besides, between the interface and granite, a thin layer of ITZ is also observed. This result of SEM analyses also agrees with the interface model proposed by He et al. (2017) on the interface between new and old concrete. Moreover, the results of SEM analysis (×1500, presented in the right of Figure 10) on granite, marble, and mature concrete show a similar observation, which are all characterized by a denser structure. This reconfirms the limited effects of rock type on the interface shear performance.

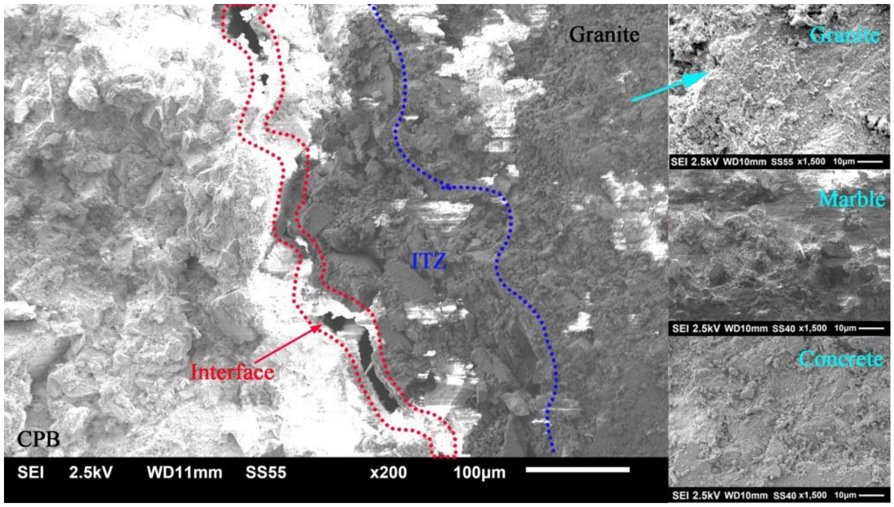

Figure 4.74 SEM images of the interface

4.6.4.2 Influence of roughness and cementation on the interface shear behaviour

4.6.4.2.1 Influence of interface roughness

The shear characteristics of the CPB-concrete samples with three various roughness measures (e.g., JRC = 0, 6.5, 16.6) are shown in Figure 4.75. Obviously, from the figure, it can be observed that the shear strength of the interface samples is considerably affected by the interface roughness. Specially, the peak shear stress rises with the increasing roughness, and this observation is in agreement with the conclusions made by Chen et al. (2015) and Fang and Fall (2019). For instance, for samples conducted under 50 kPa normal stress, the shear strength of smooth interface sample is 55 kPa, while those of samples with roughness of JRC = 6.5 and JRC = 16.6 are 67 kPa and 76 kPa, respectively. The slight rise in shear strength with rougher interfaces is because of the increasing size of the asperity at the interface. In other words, the interlocking structure becomes larger as the roughness of the concrete surface increases. This argument is macroscopically attested to by the interface pictures taken after the direct shear test, as shown in Figure 4.78. The size of the interlocking structure of the rough interface sample (JRC = 16.6) is larger than that of the medium rough interface (JRC = 6.5), as indicated in Figure 4.78, for example, $L2 > L1$. However, the shear strength of the sample with a JRC of 6.5 is 21.3% higher than that obtained from the tests performed with a smooth interface (conducted with 50 kPa normal stress). In contrast, for the test with an even rougher surface (JRC = 16.6), the increase in the peak shear stress with respect to the sample with a JRC of 6.5 is less than 14.4%. In other words, the increased stress is not proportional to the difference in roughness, and the difference in shear strength for the medium rough surface with respect to the smooth surface is higher than that between the medium rough and the roughest surface. This phenomenon is also observed by the study on the sand-steel interface conducted by Han et al. (2018). The significant difference in shear strength (comparison between smooth and medium rough interface samples) indicates the strength of the interlocking structure contributes a lot to the shear strength of the interface. In contrast, the comparatively smaller difference in shear strength between the medium rough and the rough interface means the size of the interlocking structure has a less significant influence on the evolution of the shear strength.

Similar to the normal displacement of the smooth interface introduced in Section 4.1, the interface samples with roughness also experience contraction due to the inherent compressibility of CPB at first. Thereafter, most interface samples experience obvious dilation (with the exception of samples conducted with 150 kPa normal stress), and the magnitude of the shear dilation is closely related to the interface roughness. Take the samples conducted with 50 kPa normal stress as examples, the shear dilation of the interface samples with JRC = 0, 6.5, and 16.6 are 0.05 mm, 0.2 mm and 0.24 mm, respectively. In addition, the magnitude of shear dilation of interface samples decreases significantly with normal stress, and this reduction in the amount of shear dilation is owing to the suppression of normal stress on relative separation at the interface. In other words, before the further increase in normal displacement, the major asperities at the interface cannot sustain the increasing normal stress, and then failure occurs. The continuous contraction-less pronounced shear dilation of interface samples subjected to 150 kPa normal stress is also attributed to this mechanism. Another interesting phenomenon is that the smooth interface samples suffer from contracting behaviour for subsequent shear displacement beyond the point with the highest shear dilation, whereas the interfaces with rougher surface experience a continuous increase in shear dilation, and this is especially obvious for samples sheared at lower normal stresses (e.g., 50 kPa).

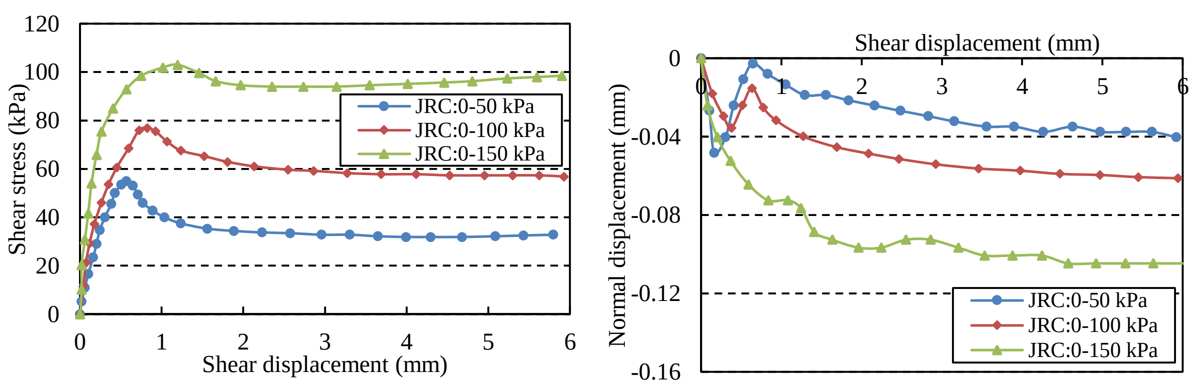

(a)

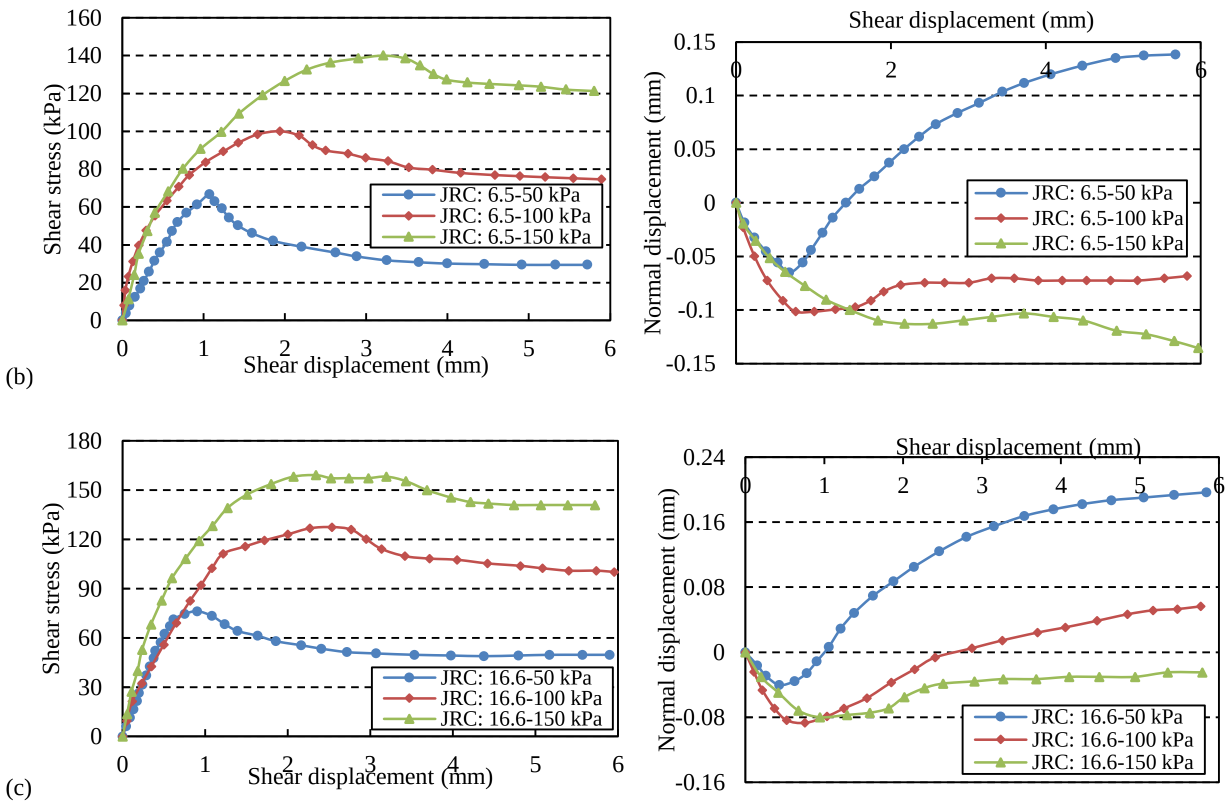

Figure 4.75 Evolution of shear stresses and normal displacements with shear displacements at curing time of 1 day: (a) JRC=0, (b) JRC=6.5 (c) JRC=16.6

4.6.4.2.2 Combined influence of cementation and surface roughness

Figs. 4.75-4.77 show the effects of cementation on the shear performance of CPB-concrete samples with different interface roughness values, and Figure 4.79 presents the evolution of peak shear stress with time. It is observed from the figures that both peak shear stress and normal displacement are influenced by the curing time and interface roughness. For example, the CPB-concrete interface cured for 28 days has the highest shear strength, followed by samples cured for 7 days, and 1 day, regardless of interface roughness. Besides, the shear stiffness of the interface sample also increases with curing time. These time-dependent changes are consistent with conclusions drawn by other researchers (Nasir and Fall, 2010; Koupouli et al., 2016). Actually, the curing time-induced increases in shear strength and shear stiffness are due to the progress of cement hydration in CPB. It is known that calcium silicate hydrate (C-S-H), a bonding phase in cementitious materials, is a major product of cement hydration, the degree of which raises with curing time (Taylor, 1964; Gani, 1997; Pokharel and Fall, 2013). As a result, the quantity of C-S-H also increases with time, thereby leading to high shear strength at the CPB-concrete interface. The rising amounts of C-S-H with time are supported by the results of thermal analysis on cement paste cured for 7 days and 28 days, as shown in Figure 4.80. The weight change at a temperature of 30°C-200°C in the figure is owing to the dehydration of C-S-H and gypsum (Sha et al., 1999; Jiang et al., 2016), while the weight loss range from 400°C to 450°C is due to the disintegration of calcium hydroxide (Nonnet et al., 1999; Zhou and Glasser, 2001). The higher weigh loss of the 28-day sample at a temperature from 30°C to 200°C (in comparison to the date of the 7-day sample) means larger amounts of C-S-H are generated in the long-cured sample. In addition to the shear strength, it can also be noted from Figure 4.75-4.77 that the magnitude of initial contraction decreases with curing time, while the shear dilation increases with curing time. This observed reduction in initial contraction and increase in shear dilation is also because of the raised degree of cement hydration. Specifically, the cement hydration process consumes large amounts of water, and this then decreases the water content in the CPB; as a result, the effective stress is increased. On the other hand, the precipitation of expansive minerals (e.g., gypsum, ettringite) with time refines the capillary pore, which decreases the compressibility. The larger shear dilation with time is owing to the development in both size and strength of asperity.

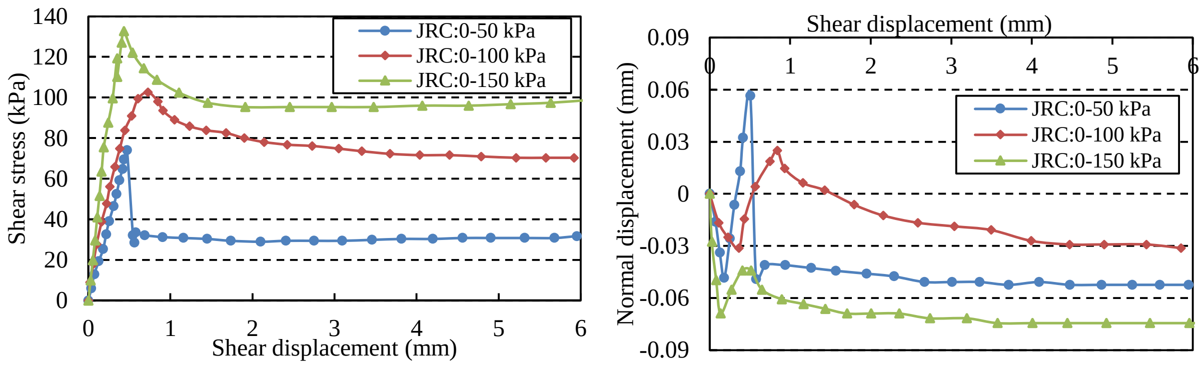

(a)

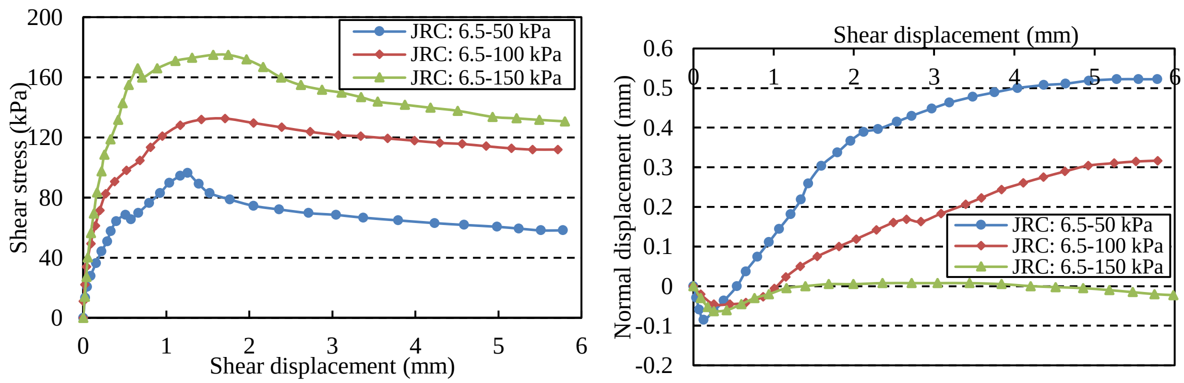

(b)

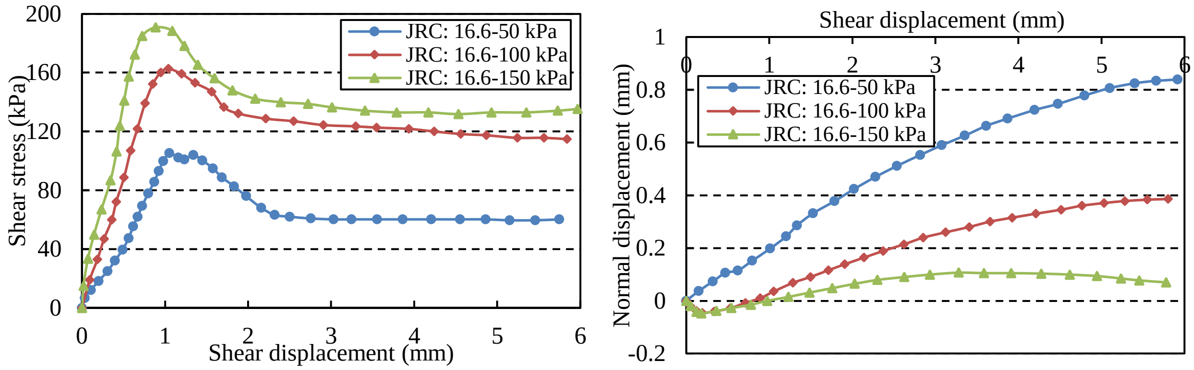

(c)

Figure 4.76 Evolution of shear strength and normal displacements with shear displacements at curing time of 7 days: (a) JRC=0, (b) JRC=6.5, (c) JRC=16.6

The results presented in Figure 4.75-4.77 also show that the interface samples with roughness, especially those sheared at high normal stress, tend to experience two peak shear stresses during the shear test. This is very obvious for long-cured samples, as shown in Figure 4.77(b). The first peak stress—which is in the same vein as the stress peak that occurred in the smooth interface—is because of the loss of the binding force between CPB and concrete. To some degree, this effect is similar to the wall effect of the cement grains against the aggregate, and this phenomenon is regarded as the loss of adhesion. Saiang et al. (2005) also observed the same phenomenon in their study on the interface between concrete and rock. The second peak in shear stress is attributed to the failure of the interlocking structure. Specifically, as a consequence of the relative motion of the asperity at the non-cemented CPB-concrete interface, the shear dilation is increased. Besides, the contacting area between CPB and concrete is decreased. Consequently, the normal stress keeps increasing with shear dilation until reaching the strength of the major asperity at the interface. Thereafter, the failure of the interlocking structure corresponds to the second peak stress.

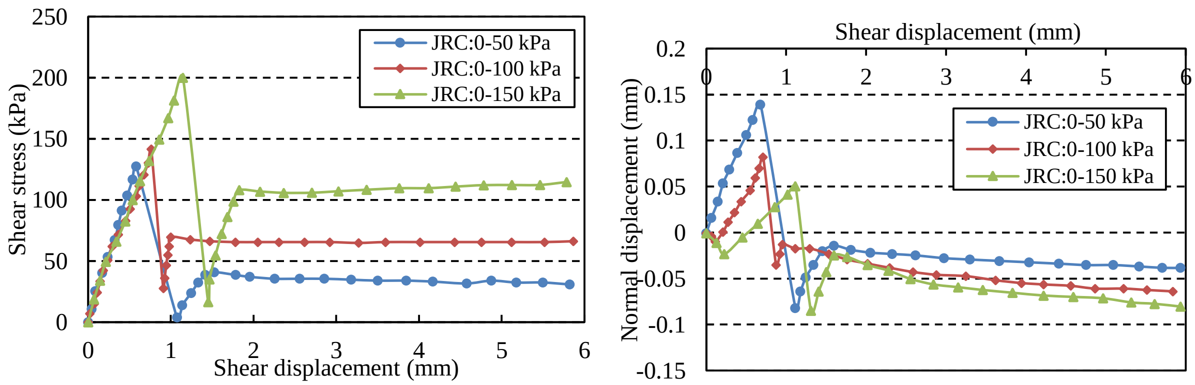

(a)

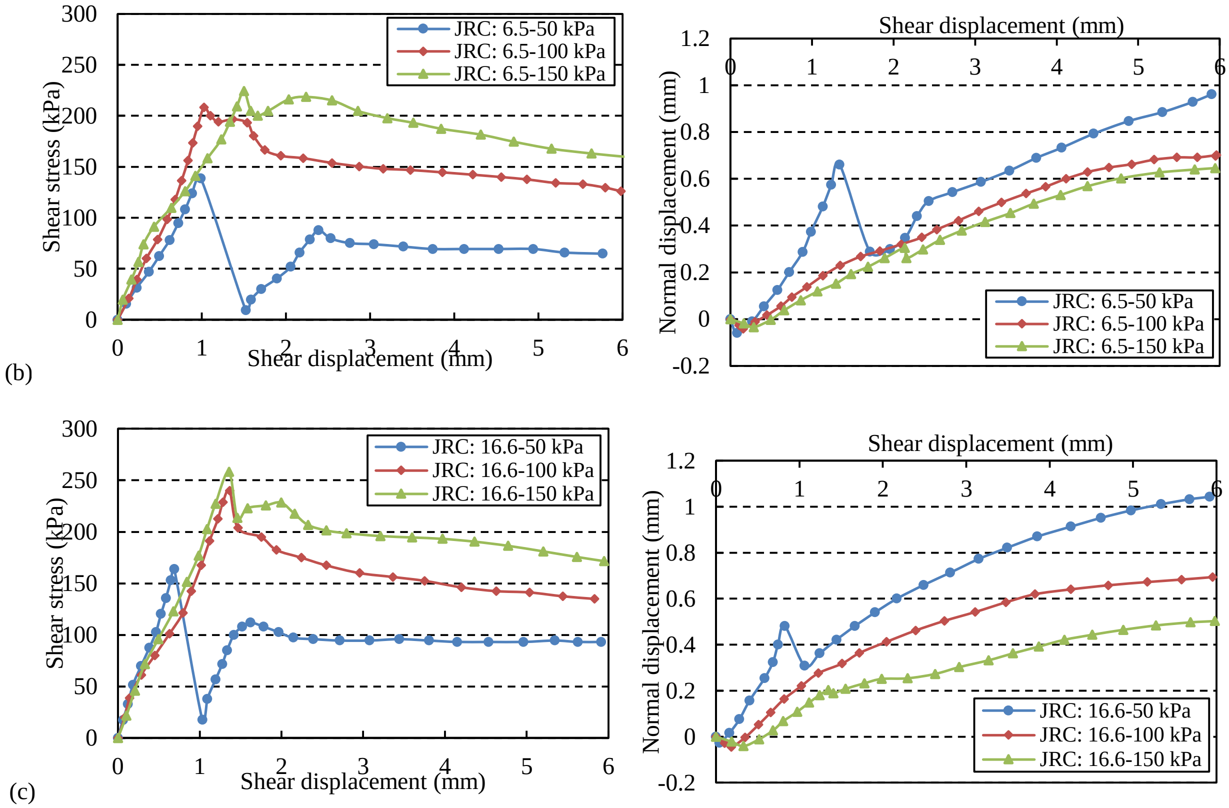

Figure 4.77 Evolution of shear strength and normal displacements with shear displacements at curing time of 28 days: (a) JRC=0, (b) JRC=6.5 (c) JRC=16.6.

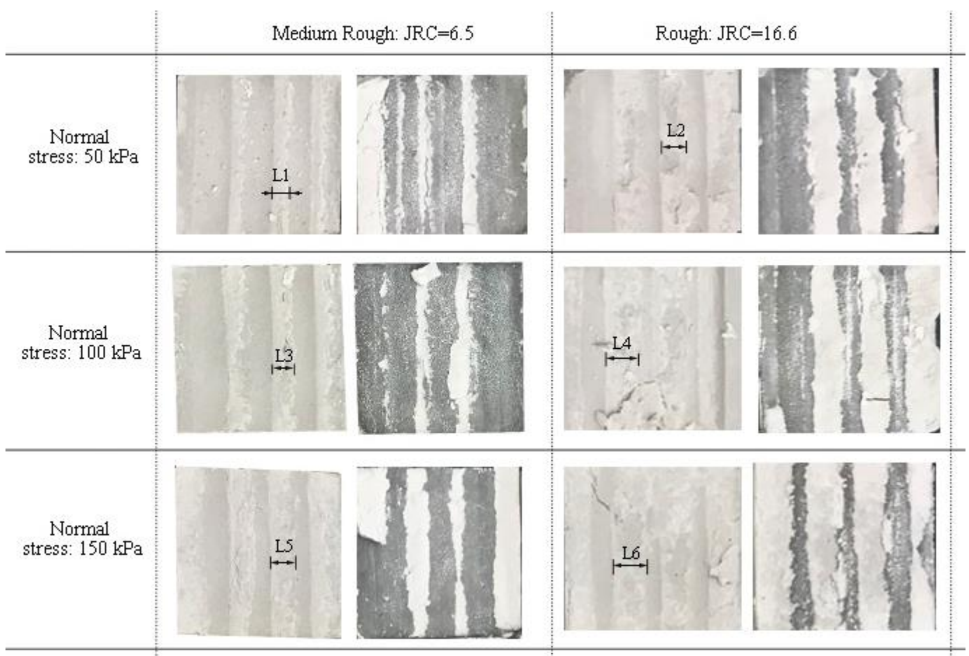

Figure 4.78 Pictures of interface of samples after direct shear test (cured for 7 days)

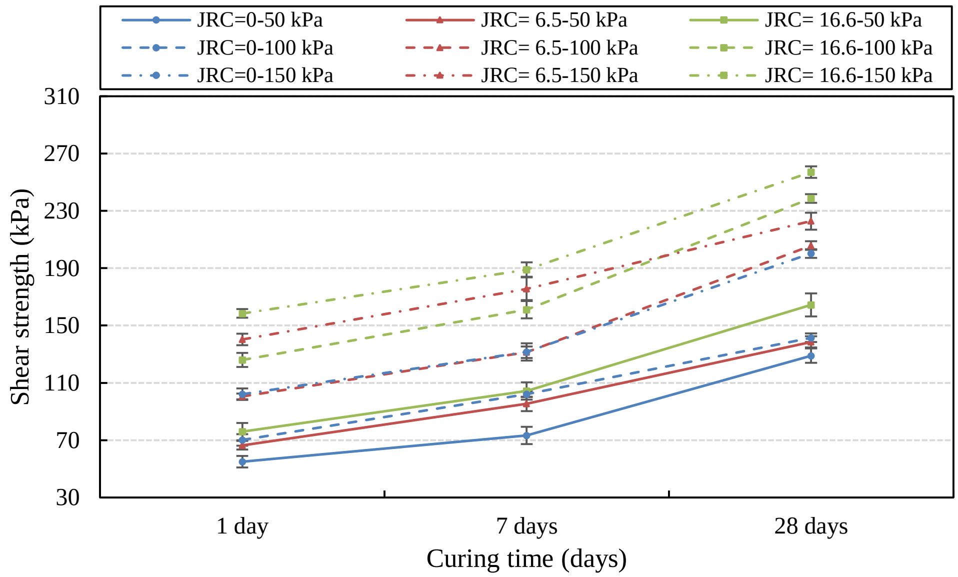

Figure 4.79 Evolution of peak shear stress of CPB-concrete interface with time

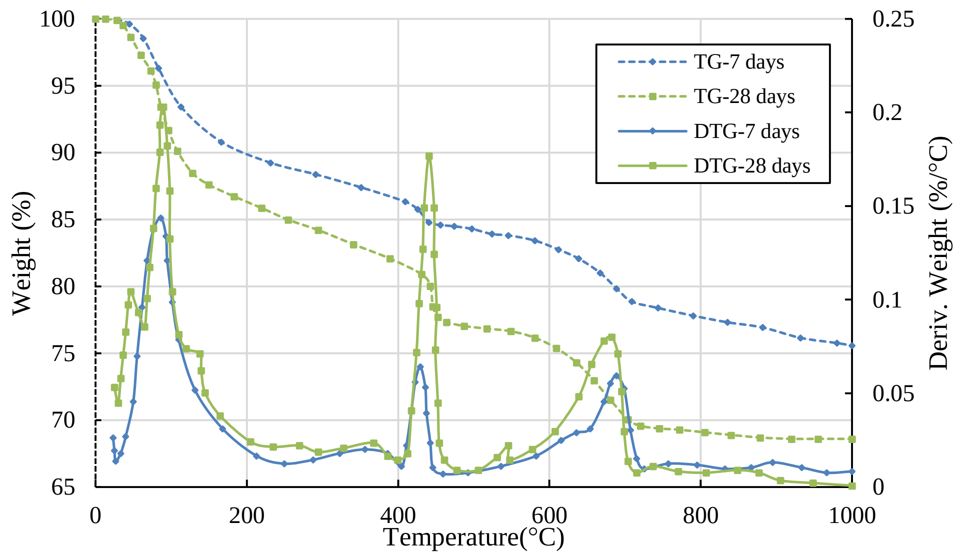

Figure 4.80 Results of TG and DTG analyses on CPB (cured for 7 and 28 days)

It can also be observed from Figs. 4.75-4.77 that the shear dilation increases with curing time, regardless of interface roughness. For the smooth CPB-concrete interface conducted with 50 kPa normal stress, the shear dilation increases from 0.05 mm on the first day to 0.14 mm on the twenty-eighth day. In contrast, the shear dilation of the roughest interface samples (JRC=16.6) rises from 0.24 mm to 1.07 mm during the same curing period. The increased shear dilation of the CPB-concrete interface with time is due to (i) the refined pore structure of CPB, and (ii) the stronger interlocking structure, as results of the raised degree of cement hydration, which was discussed previously.

4.6.4.3 Evolution of mechanical properties of CPB-concrete interface with different roughness

Given the significant effects of interface roughness on the evolution of the mechanical strength of rock joints, Barton (1973) took the roughness into consideration and proposed Eq. (1) to estimate the shear strength of rough rock joints. However, Manaras et al. (2011) found the shear strength derived from Barton's equation is lower compared to measured samples. Considering the significant role of adhesion in predicting the shear strength of cementitious materials, a revised version of Barton's equation is adopted here to deduce the shear properties of the CPB-concrete interface:

$$\tau = \sigma \tan\left[\text{JRC } \log(\text{JCS}/\sigma) + \varphi_b\right] + c \tag{4-12}$$

where c is the adhesion of the interface. The JCS value here is the UCS of the CPB, which is also associated with the degree of binder hydration. According to the tests conducted by Fall et al. (2010), the UCS of standard CPB samples cured for 1 day, 7 days, and 28 days are 150 kPa, 444 kPa and 624 kPa, respectively. Therefore, based on the data on the shear strength-normal stress at the interface, the shear strength envelopes of the interface samples can be obtained, and then the mechanical parameters of the interface (e.g., friction angle, adhesion) can be deduced.

Figure 4.81 presents the evolution of shear parameters (e.g., friction angle, adhesion) of the studied rough interface. The figure shows that these properties are significantly affected by time. Specifically, the adhesion of the interface increases with curing time, as a result of the increasing degree of binder hydration (Nasir and Fall, 2008; Fang and Fall, 2018). Besides, the rougher interface tends to experience higher adhesion, regardless of curing time. The roughness-induced increase in adhesion is due to the increased contact area between CPB and concrete. In contrast, the evolution of the friction angle is complex. For the smooth interface (JRC=0), the friction angle rises with curing time, which coincides with the conclusion made by Nasir and Fall (2008) and Fang and Fall (2019). However, for the interface sample with roughness, the evolution of the friction angle varies with the failure criterion adopted. In other words, if the Mohr-Coulomb failure criterion is used, the friction angle presents an increasing tendency with time, the value of which is shown in Table 4.11. However, the effective friction angle depicts a decreasing tendency in the first 7 days by adopting a revised Barton's equation, as shown in Figure 4.81. In other words, the roughness contributes a lot to the development of the friction angle, and after extracting the contribution caused by roughness, the effective friction angle decreases with time.

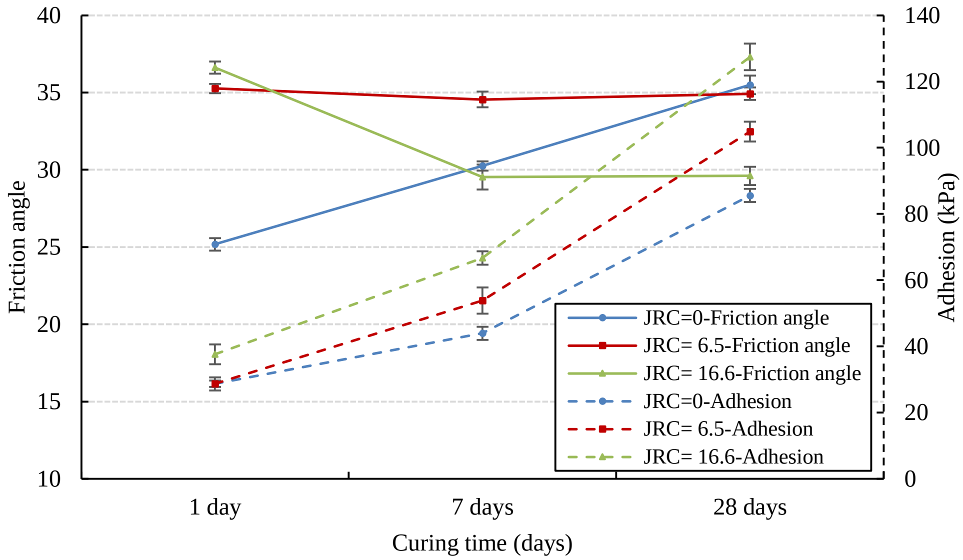

Figure 4.81 Evolution of the adhesion and effective friction angle of the CPB-concrete interface

Table 4.11 Evolution of friction angle (according to Mohr-Coulomb criterion)

Interface roughness	Friction angle		
	1 day	7 days	28 days
Smooth (JRC=0)	25.2	30.3	35.5
Medium rough (JRC=6.5)	36.4	38.8	40.1
Rough (JRC=16.6)	39.5	40.3	42.8

4.6.5 Summary and conclusions

The paper presents the experimental results of the direct shear tests on the interface between CPB and surrounding rock (with different roughness values). The following conclusions are made:

- Three kinds of rocks or materials (e.g., granite, marble, and concrete) are used as the rock part of the interface samples. The results of direct shear tests on 1-day interface samples show that all samples experience similar shear behaviour, regardless of the type of rock used. Besides, the effect of the type of rock on the friction angle and the shear strength of the interface are also limited.
- Surface parameter, Z_2, is adopted to estimate the surface roughness in this study, and three kinds of concrete with different roughness values (e.g., JRC=0, JRC=6.5 and JRC=16.6) are produced to investigate the contribution of roughness to the interface shear strength. It is found that the shear strength of the rough interface increases with roughness. This increase in shear strength is due to the larger interlocking structure with more roughness. However, the increased stress is not proportional to the difference in roughness.

- The peak shear stress and shear dilation of the interface samples increase with curing time, as a result of the raised degree of binder hydration. The specific mechanisms are (1) a large amount of moisture was consumed by binder hydration; (2) some expansive products (e.g., ettringite) of cement hydration refine the pore structure at the interface; (3) the increasing amount of C-S-H enhances the binding force at the interface, thereby increasing the strength of the interlocking structure.
- The adhesion of the interface samples increases with both curing time and roughness. The curing time-induced increase in adhesion is due to the increased degree of cement hydration with time, while the roughness-induced increase is because of the larger contact area between CPB and concrete. Meanwhile, the friction angle of the smooth interface also depicts a rising tendency with time. However, with respect to the interface with roughness, the effective friction angle decreases with time.

Acknowledgements

The University of Ottawa, the Natural Sciences and Engineering Research Council of Canada (NSERC), and the China Scholarship Council (CSC) are acknowledged by the authors for their support. Also, the authors want to thank Mr. Glenn for his help on the SEM analysis.

4.6.6 References

Bahaaddini M, Hagan PC, Mitra R, Hebblewhite BK (2015) Parametric study of smooth joint parameters on the shear behaviour of rock joints. Rock. Mech. Rock. Eng. 48:923–940.
Barton N (1973) Review of a new shear strength criterion for rock joints. Eng. Geol. 7(4):287-332.
Barton N, Choubey V (1977) The shear strength of rock joints in theory and practice. Rock mechanics. 10(1):1-54.
Brackebusch FW (1994) Basics of paste backfill systems. Min. Eng. 46:1175-1178.
Breton D, Carles-Gibergues A, Ballivy G, Grandet J (1993) Contribution to the formation mechanism of the transition zone between rock-cement paste. Cem. Concr. Res. 23(2):335-346.
Brown ET (1981) Rock characterization testing and monitoring (ISRM suggested methods). Oxford: Pergamon.
Chen X, Zhang J, Xiao Y, Li J (2015) Effect of roughness on shear behaviour of red clay-concrete interface in large-scale direct shear tests. Can. Geotech. J. 52:1122–1135.
Cui L, Fall M (2017) Multiphysics modeling of arching effects in fill mass. Comput. Geotech. 83:114-131.
Cui L, Fall M (2016) An evolutive elasto-plastic model for cemented paste backfill. Computers & Geotechnics 71:19-29.
Diamond S, Huang J (2001) The ITZ in concrete–a different view based on image analysis and SEM observations. Cem. Concr. Compos. 23(2-3):179-188.
Dong W, Yang D, Zhou X, Kastiukas G, Zhang B (2017) Experimental and numerical investigations on fracture process zone of rock–concrete interface. Fatigue. Fract. Eng. M. 40(5):820-835.
EI-Soudani SM (1978) Profilometric analysis of fractures. Metallography, 11:247-336.
Fall M, Benzaazoua M (2003) Advances in predicting performance properties and cost of paste backfill. Int. Conf. Tailings & Mine Waste, Colorado, USA, 12-15.
Fall M, Benzaazoua M (2005) Modeling the effect of sulphate on strength development of paste backfill and binder mixture optimization. Cem. Concr. Res., 35(2):301-314.
Fall M, Célestin JC, Pokharel M, Touré M (2010) A contribution to understanding the effects of temperature on the mechanical properties of cemented mine backfill. Eng. Geol. 14(3-4):397-413.

Fall M, Nasir O (2010) Mechanical behaviour of the interface between cemented tailings backfill and retaining structures under shear loads. Geotech. Geo. Eng. 28:779–790.

Fang K, Fall M (2018) Effects of curing temperature on the shear behaviour of cemented paste backfill-rock interface. Int. J. Rock. Mech. Min. 112:184-192.

Fang K, Fall M (2019) Chemically induced changes in the shear behaviour of the interface between rock and tailings backfill undergoing cementation. Rock. Mech. Rock. Eng. 52(9):3047-3062.

Fang K, Fall M (2020) Effect of curing stress, drainage condition and filling rate on shear behaviour of the interface between cemented paste backfill and rock. Rock. Mech. Rock. Eng. 53(1):325-336.

Gani MSJ (1997) Cement and Concrete. London, UK: Chapman & Hall.

Ghirian A, Fall M, (2014) Coupled thermo-hydro-mechanical-chemical behaviour of cemented paste backfill in column experiments. Part II: Mechanical, chemical and microstructural processes and characteristics. Eng. Geol. 170:11-23.

Ghirian A, Fall M (2013) Coupled thermo-hydro-mechanical-chemical behaviour of cemented paste backfill in column experiments. Part I: Physical, hydraulic and thermal processes and characteristics. Eng. Geol. 164:195-207.

Grice T (2001) Recent mine developments in Australia. Proceedings of the 7th International Symposium on Mining with Backfill (MINEFILL), 351-357.

Han F, Ganju E, Salgado R, Prezzi M (2018) Effects of interface roughness, particle geometry, and gradation on the sand–steel interface friction angle. J. Geotech. Geoenviron. 144(12), 04018096.

Hassani F, Archibal J (1998) Mine backfill. Canadian Institute of Mine, Metallurgy and Petroleum, Canada.

He Y, Zhang X, Hooton R, Zhang X (2017) Effects of interface roughness and interface adhesion on new-to-old concrete bonding. Constr. Build. Mater. 151:582-590.

Helinski M, Fahey M, Fourie A (2010) Behavior of cemented paste backfill in two mine stopes: Measurements and modeling. J. Geotech. Geoenviron. 137(2):171-182.

Jiang HQ, Fall M, Cui L (2016) Yield stress of cemented paste backfill in sub-zero environments: experimental results. Miner. Eng. 92:141-150.

Ke Y, Ortola S, Beaucour A, Dumontet H (2010) Identification of microstructural characteristics in lightweight aggregate concretes by micromechanical modelling including the interfacial transition zone (ITZ). Cem. Concr. Res. 40(11):1590-1600.

Koupouli NJF, Belem T, Rivard P, Effenguet H (2016) Direct shear tests on cemented paste backfill-rock wall and cemented paste backfill-backfill interfaces. Journal of Rock Mechanics and Geotechnical Engineering, 8(4):472-479.

Kuganathan K (2005) "Geomechanics of mine fill" in Y. Potvin, E. Thomas, and A. Fourie (Eds.), Handbook on mine fill, Australian Centre of Geomechanics, 23-49.

Li W, Fall M (2016) Sulphate effect on the early age strength and self-desiccation of cemented paste backfill. Constr. Build. Mater. 106:296-304.

Maerz NH, Franklin JA, Bennett CP (1990) Joint roughness measurement using shadow profilometry. Int. J. Rock. Mech. Min. Sci. Geomech. Abstr. 27(5):329-343.

Manaras E, De-Souza Archibald JF (2011) Strength behaviour and failure mechanisms of backfill–rock mass interfaces. 10th International Conference on Mining with Backfill. The southern African Institute of Mining and Metallurgy, Cape Town, South Africa.

Nasir O, Fall M (2008) Shear behaviour of cemented pastefill-rock interfaces. Eng. Geol. 101(3):146-153.

Nonnet E, Lequeux N, Boch P (1999) Elastic properties of high alumina cement castables from room temperature to 1600°C. J. Eur. Ceram. Soc. 19(8):1575-1583.

Pirapakaran K, Sivakugan N (2007) Arching within hydraulic fill stopes. Geotech. Geol. Eng. 25:25–35.

Pokharel M, Fall M (2013) Combined influence of sulphate and temperature on the saturated hydraulic conductivity of hardened cemented paste backfill. Cem. Concr. Compos. 8:21-28.

Saiang D, Malmgren L, Nordlund E (2005) Laboratory tests on shotcrete-rock joints in direct shear, tension and compression. Rock. Mech. Rock. Eng. 38(4):275-297.

Scrivener KL, Crumbie AK, Laugesen P (2004) The interfacial transition zone (ITZ) between cement paste and aggregate in concrete. Interface science, 12(4):411-421.

Seidel JP, Haberfield CM (2002) Theoretical models for concrete-rock joints subjected to constant normal stiffness direct shear. Int. J. Rock. Mech. Min. Sci., 39:539–553.

Sha W, O'Neill E, Guo Z (1999) Differential scanning calorimetry study of ordinary Portland cement. Cem. Concr. Res. 29(9):1487-1489.

Taylor HFW (1964) The chemistry of cements, vol. 1, 1st ed. London: Academic Press.

Terzaghi K (1943) Theoretical soil mechanics. New York: John Wiley & Sons.

Tse R, Cruden DM (1979) Estimating Joint Roughness Coefficients. Int. J. Rock. Mech. Min. Sci. 16(5):303-307.

Wang Y, Fall M, Wu A (2016) Initial temperature-dependence of strength development and self-desiccation in cemented paste backfill that contains sodium silicate. Cem. Concr. Compos. 67:101-110.

Wang JA, Wang YX, Gao QJ (2015) Behavior of microcontacts in rock joints under direct shear creep loading. Int. J. Rock. Mech. Min. Sci. 78:217-229.

Yang PY, Li L (2015) Investigation of the short-term stress distribution in stopes and drifts backfilled with cemented paste backfill. Int. J. Min. Sci. Tech. 25:721-28.

Yang ZY, Lo SC, Di CC (2001) Reassessing the joint roughness coefficient (JRC) estimation using Z2. Rock. Mech. Rock. Eng. 34:243-251.

Yu XB, Vayssade B (1991) Joint profiles and their roughness parameters. Int. J. Rock. Mech. Min. Sci. Geo. Mech. Abstr. 28:333-6.

Zhou Q, Glasser F (2001) Thermal stability and decomposition mechanisms of ettringite at <120 C. Cem. Concr. Res. 31(9):1333-1339.

Chapter 5 Multiphysics models for CPB-rock interface shear behaviour

5.1 Introduction

Despite the significant progress made in understanding the shear behaviour of the CPB-rock interface, all the previous studies have only investigated the effects of an isolated factor on the shear performance. However, the CPB-rock interface is subjected to Multiphysics conditions after the placement of CPB. Therefore, studying the coupled effects of thermal, hydraulic, mechanical and chemical (THMC) process on the shear performance of CPB-rock interface is important for the reliability of the stability assessment of underground structures. Meanwhile, compared with laboratory tests, mathematical modelling is much more efficient and cost-effective when it refers to the Multiphysics analyses. Hence, the CZM is adopted in this chapter to numerically describe the shear behaviour of the interface between the CPB-rock interface. Speciafically, an equivalent chemical age is proposed to describe the different effects of sulphate ions on the mechanical properties of the CPB-rock interface. Thereafter, a chemo-elastic CZM is developed to describe the shear behaviour of the interface samples with various sulphate contents. The introduction of the chemo-elastic CZM and the numerical simulation results are presented in section 5.2. Similarly, to capture the shear behaviour of the interface samples subjected to different thermal conditions, an equivalent thermal age is proposed as well in section 5.3. Besides, the influence of the temperature on the evolution of the fracture toughness of the CPB-rock interface is also experimently investigated. The good agreement between experimental results and the modeling outputs confirms the predictability of the thermal-chemo-mechanical CZM.

5.2. Paper VII: A Coupled Chemo-Elastic Cohesive Zone Model for Backfill-Rock Interface

Published in *Computers and Geotechnics*, 2020, 125: 103666

Kun Fang, Liang Cui, Mamadou Fall

Abstract

To date, only a very few number of models are available to study the shear characteristics of the backfill-rock interface, and none of them have incorporated the effect of the interactions between sulphate ions and cement hydration on the interface shear behaviour. Therefore, a coupled chemo-elastic cohesive zone model (CZM) has been developed to simulate the shear characteristics of the cemented paste backfill (CPB)-rock interface that contains sulphate ions at the early ages. To quantitatively address the influence of sulphate on binder hydration at the early ages, the concept of equivalent chemical age is proposed and integrated into a binder hydration model. Besides, the interface shear properties, fracture toughness as well as shear stiffness are expressed as a function of the equivalent chemical age. By implementing the developed model in COMSOL Multiphysics, the results of the numerical simulation are found to be agree with the experimental results. The validated results confirm the capability of the developed model to describe the shear characteristics of the interface that contains sulphate ions. The developed model will contribute to improving the assessment of the shear behaviour of the CPB-rock interface in the field, thus leading to a more economical design of safe CPB structures.

Keywords: cemented paste backfill; tailings; cohesive zone model; interface; rock; mine

5.2.1 Introduction

Cemented paste backfill (CPB) has been extensively used in many mines worldwide since the 1970s (Brackebusch, 1994; Fall and Benzaazoua, 2005; Yilmaz et al., 2014; Jiang et al., 2016). After pumping the cemented backfill into underground mine cavities (stopes), finding ways to maintain the geotechnical stability of these CPB structures is a key task for engineers and researchers. Given that mechanical stability is an important design criterion of CPB structures, many investigations have been conducted to assess the development of their mechanical strength, which is a key parameter required to assess the mechanical stability of CPB. However, most of the previous studies on the mechanical strength or properties mainly focus on the changes in the uniaxial compressive strength (UCS) of the CPB material or mass (Yilmaz et al., 2003; 2013; 2014; Kesimal et al., 2005; Ercikdi et al., 2009; Wang et al., 2016; Ghirian and Fall, 2016; Jiang and Fall, 2017; Cao et al., 2018; 2019; Xue et al., 2018; Yilmaz, 2018;). However, the peak shear stress and shear behaviour of CPB-rock interface are also other key factors that influence the geotechnical stability of backfill structures. The interface shear characteristics significantly influence the arching effect in backfill structures, which is a common phenomenon in narrow backfill structures as a result of stress redistribution (Aubertin et al., 2003; Pirapakaran and Sivakugan, 2007; Cui and Fall, 2017). Due to the arching phenomenon, the backfill structure can sustain the weight of the overlying strata to a greater extent. Therefore, the required bearing capacity of the designed structure can be significantly decreased. This in turn decreases the amount of cement consumed, thereby reducing the cost of the backfill structure (Cui and Fall, 2016; Jiang et al., 2019), which subsequently leads to considerable financial benefits for the mine. However, only a few studies have investigated the changes in the peak shear stress and shear behaviour of the interface under different conditions (Nasir and Fall, 2008; Koupouli et al., 2016; Fang and Fall, 2018; 2019; 2020). Most of these previous studies have carried out experimental investigations. While they have significantly contributed to give useful insight into the shear performance of the CPB-rock interface and arching effect in cemented backfill structures, constitutive modelling of the CPB-rock interface still remains largely absent. Until now, only a few numerical analyses have been conducted to simulate the mechanical behaviour of the CPB-rock interface (Cui and Fall, 2017; 2018; Pierce, 2001; Helinski et al., 2007). However, none have proposed constitutive modelling of the interface behaviour of the rock and paste backfill that is undergoing cementation. Moreover, no constitutive modelling studies have been done to address the coupled effects of sulphate ions and cementation (cement hydration) on the shear characteristics of the young CPB rock interface. It is therefore necessary to address this knowledge gap since field CPB is usually rich in sulphate ions (Li and Fall, 2018) and, once placed in the mine cavity in the field, the CPB properties change due to the progression of binder hydration. Moreover, it is well acknowledged that the progression of the binder hydration and/or the sulphate reactions can considerably affect the mechanical properties of CPB and the

CPB-rock interface as shown in many previous experimental studies (Ercikdi et al., 2009; Fang and Fall, 2019; Li and Fall, 2018; Fall and Nasir, 2010) and discussed below.

Figure 5.1 shows an example of a CPB-rock interface sample after a direct shear test (DST), and an interfacial transition zone, which contains numerous micro fractures, can be clearly observed at the CPB-rock interface. The emergence of micro fractures can be deterred by adding natural and/or artificial fibres when preparing CPB (Cao et al., 2019; Xue et al., 2020; Xu et al., 2019). However, to analytically describe the interface behaviour (without fibres), the initiation and propagation of cracks along the interface must be evaluated. Previous studies (Regueiro and Borja, 2001; Grueschow and Rudnicki, 2005; Kakogiannou et al., 2016) have found that the fracture propagation behaviour of geomaterials is sensitive to changes in the confining pressure. Specifically, many different types of geomaterials that are subjected to a low confining pressure show quasi-brittle failure (Borja et al., 2000), which is mainly controlled by the surface energy of the crack walls of the geomaterial. In contrast, the ductile behaviour of geomaterials becomes more apparent when the confining pressure is significantly increased (Choo and Sun, 2018). Consequently, the formation of a plastic zone near the crack tip and the associated plastic dissipation can further enhance the material toughness. Hence, fracturing is one of the main failure mechanisms of geomaterials and structural components.

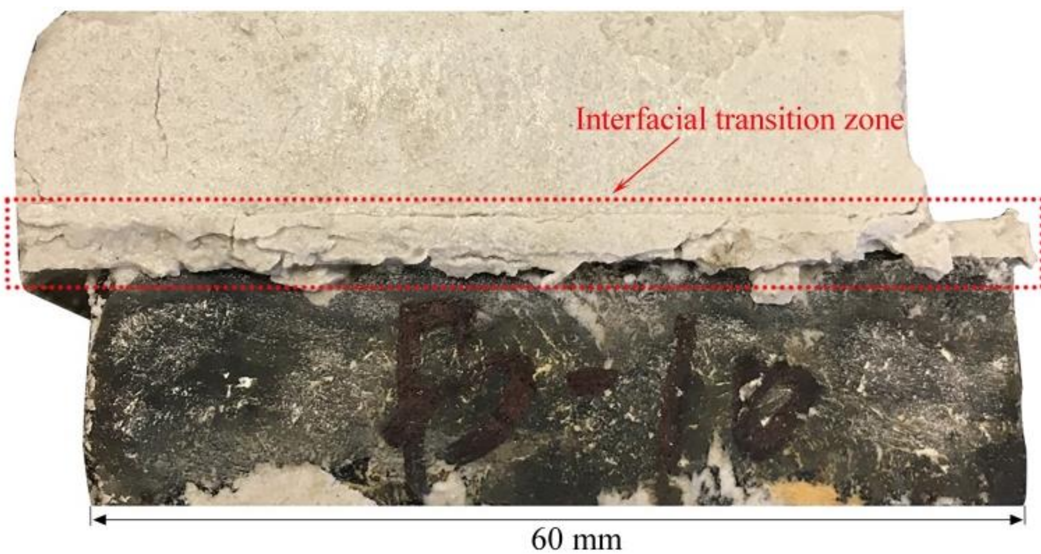

Figure 5.1 Fractured zone shown at CPB-rock interface after direct shear test (sample without sulphate; cured for 1 day)

The numerical simulation of fractures is usually based on two approaches, namely, the discrete and continuum approaches. However, a common drawback of the former is that the discretization must change the topology because of fracture propagation. In other words, the mesh-sensitivity of the propagation always requires the use of a regularization method during the modelling (Bouchard et al., 2003). In contrast, the latter approach, which uses for instance, gradient damage, phase field and cohesive zone models, not only needs to consider stiffness degradation due to fracture propagation, but also resolve mesh-sensitivity by using nonlocal damage functions (Choo and Sun, 2018; Gatuingt and Pijaudier-Cabot, 2002; Einav et al., 2007; Lyakhovsky et al., 2015; Miehe et al., 2010). Among these models, the cohesive zone model (CZM) is especially applicable for modeling delamination, debonding, and more generally, fracture initiation and propagation on material interfaces. The CZM originated from the Barenblatt-Dugdale (BD) model based on work by Barenblatt (Barenblatt, 1959; 1962) and Dugdale (Dugdale, 1960), which has been extensively used to analyze fracture development. Presently, smeared and interface cohesive elements are the two main approaches used to implement CZMs (Li et al., 2006; Aoki and Suemasu, 2003). However, the potential convergence difficulties that could emerge with smeared cohesive elements (Xie and Waas, 2006) means that interface cohesive elements are commonly used instead to simulate interface failure with the CZM.

Despite the tremendous contributions of previous studies in modelling fracture initiation and propagation with CZMs, none have investigated the effect of cement hydration or the coupled effect of cement hydration and sulphate ions on the mechanical response of the CPB-rock interface. Thus, it is timely to address this research gap for the reasons mentioned above and since cement hydration (curing time) and sulphate ions both significantly influence the shear behaviour of the CPB-rock interface as evidenced in previous experimental studies (Koupouli et al., 2016; Fang and Fall, 2019). As an example, Figure 5.2 shows the changes in the shear stress-shear displacement curves of the CPB-rock interface with curing time. It can be noticed that the shear strength rises with time as a result of the enhancement of the cement hydration degree. In addition, the interface shear parameters (e.g., interface adhesion and shear stiffness) as well as softening behaviour change with curing time. Moreover, a good number of experimental studies have demonstrated that sulphate ions can slow down the cement hydration in the young CPB and thus reduce the strength and shear strength of the CPB material and CPB-rock interface, respectively (Fang and Fall, 2019; Fall and Pokharel 2010; Pokharel and Fall, 2013). This is evidenced by Figure 5.3, which shows the experimental results of the effect of CPB sulphate contents. The shear stress is plotted against the shear displacement of the interface sample which has been cured for 7 days (Fang and Fall, 2019). It is obvious that the 7 day-CPB-rock interface samples with a lower sulphate content have a higher shear strength than those with a higher initial sulphate content. However, it should be noted that a low or moderate sulphate content could slightly improve the shear strength of the interface at the early ages (≤ 7 days) because of the formation of swelling products , such as gypsum or ettringite (not excessive), in the pores of the CPB (Fang and Fall, 2019).

Hence, the objective of this work is to develop an evolutive interface constitutive model that can analytically describe the changes in the behaviour of the young CPB-rock interface and quantitatively incorporate the coupled effect of binder hydration and sulphate ions.

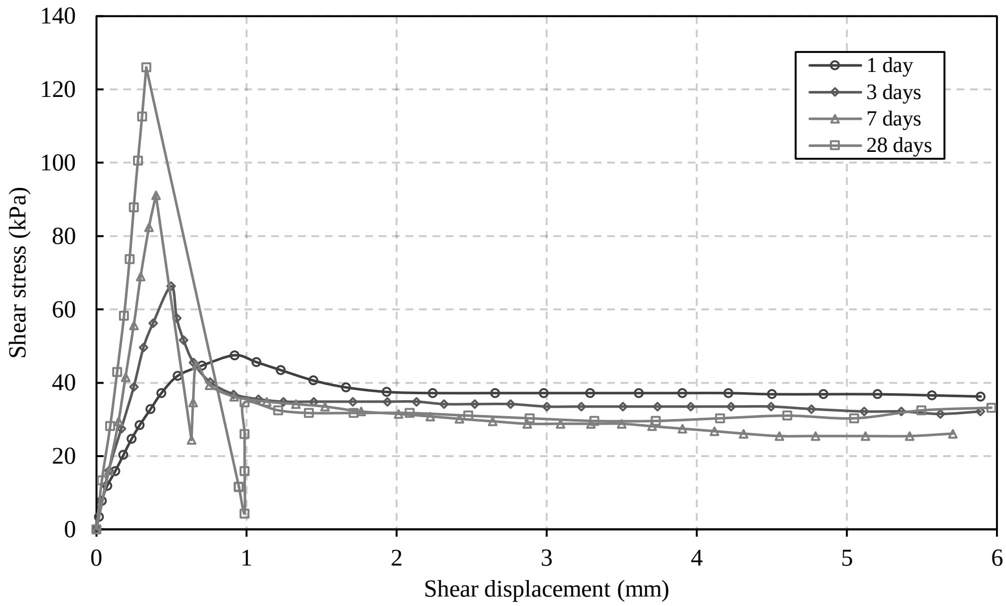

Figure 5.2 Effect of progression of cement hydration (or degree of cement hydration) or curing time on development of shear stress-shear displacement at CPB-rock interface (normal stress = 50 kPa, sulphate content = 0 ppm) (Fang and Fall, 2019)

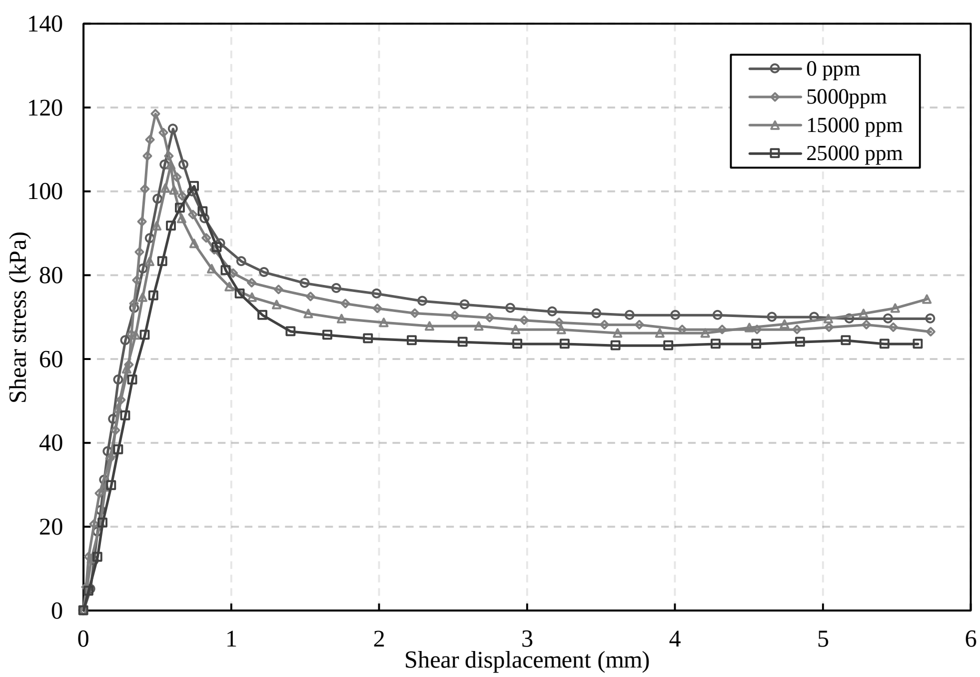

Figure 5.3 Effect of sulphate contents of CPB on shear stress vs shear displacements in CPB-rock interface cured for 7 days (normal stress = 100 kPa) (Fang and Fall, 2019)

5.2.2 Formulation of coupled chemo-elastic cohesive zone model

The bond of the interface between dissimilar materials is often weak in terms of the mechanical stability, and cohesive zone modeling is regarded to be a suitable method for simulating potential fractures at a bimaterial interface (Dong et al., 2007). Moreover, modifications are made to a binder hydration model to incorporate the effects of sulphate ions and binder hydration on the interface behaviour, and the modified model is then coupled to the elastic CZM. The modified binder hydration model is described in Section 5.2.1, and the formulation of the interface constitutive relation and the failure criterion that governs the interface behaviour is presented in Section 5.2.2.

5.2.2.1 Binder hydration model

It can be observed in Figure 5.2 that the shear behaviour and properties of the CPB-rock interface are very time-dependent due to the advancement of binder hydration. Therefore, it is important to quantitatively assess the extent of binder hydration in CPB and its impact on the shear behaviour and properties of the interface. To accurately characterize the progression of the cement hydration, a normalized variable proposed by De Schutter (1999) called the degree of binder or cement hydration, which is a ratio of the reacted cement fraction over total cement amount, is adopted in this study:

$$\xi(\mathrm{t}_e) = \xi_u \exp\left[-\left(\frac{\kappa}{t_e} \right)^{\varsigma} \right] \tag{5-1}$$

where $\xi(\mathrm{t}_e)$ is the degree of cement hydration, t_e denotes the chronological curing age of the CPB-rock samples, and κ and ς represent time and the shape parameter, respectively. According to research conducted by Schindler (2004), the unknown parameters in Eq. (5-1) are determined to be: $\kappa = 1.4$, $\varsigma = 0.394$ and $\xi_u = 1$, in which ξ_u refers to the ultimate degree of cement hydration, which is related to the weight proportion (with respect to the total weight of the cement, fly ash and slag) of the mineral admixture and water-cement (w/c) ratio (Kjellsen et al., 1991; Cui and Fall, 2016):

$$\xi_u = \frac{1.031 \times w/c}{0.194 + w/c} + 0.5 \times \vartheta_{FA} + 0.3 \times \vartheta_s \tag{5-2}$$

where ϑ_{FA} refers to the weight proportion of the fly ash while ϑ_s represents the weight fraction of slag. Note that the ultimate degree of cement hydration equals to 1 when the w/c ratio is larger than 6.258. But for CPB with a high binder content (e.g., 10-12%), the w/c ratio will be lower than 6.2. This means the ultimate degree of cement hydration can never reach 1, regardless of the age of CPB. However, no matter what the w/c ratio is, the cement hydration degree is a function of time, as presented in Eq. (5-1).

Also note that Eq. (5-1) is proposed to characterize the progression of the chemical reaction of cement paste that does not contain sulphate ions. However, sulphate ions are frequently present in CPB (Cui and Fall, 2018), and numerous experimental studies have found that sulphate ions can hinder the binder hydration (Bian et al., 2019; Aldhafeeri and Fall, 2017; Kesimal et al., 2004), which in turn substantially impacts the shear behaviour and parameters of the CPB-rock interface at the early ages (Fang and Fall, 2019). The effect of the coupled chemo-mechanical process on the shear performance of the interface is shown in Figure 5.4. Aside from the influence of the sulphate ions on inhibiting cement hydration, their presence can also lead to the production of ettringite (Liu et al., 2019). This can either refine or coarsen (depending on the amount of ettringite) the microstructure of the interface, thereby affecting its shear strength (Fang and Fall, 2019). Despite the two aforementioned negative effects, the major contribution of the chemical process on the mechanical process is the bonding force between the rock and CPB, which is a consequence of the increase in degree of cement hydration.

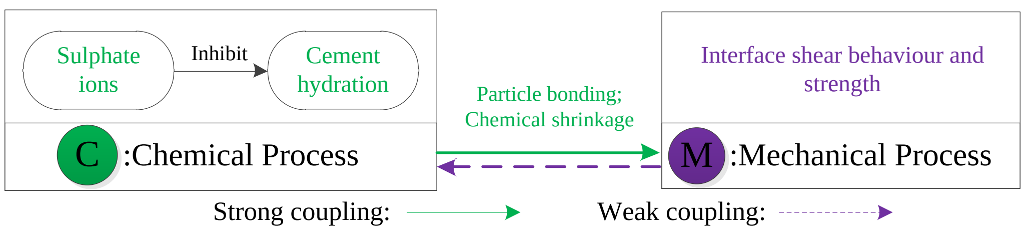

Figure 5.4 Schematic representation of coupled chemo-mechanical process

Therefore, modification of the binder hydration model is required to describe the cementation in CPB with sulphate at the early ages (up to 28 days). In this study, the concept of equivalent chemical age is proposed to evaluate the effects of a chemical factor, that is, sulphate ions, on cement hydration. The equivalent chemical age is regarded as the duration of the curing time with the reference sulphate content that would lead to the same maturity as the curing time with other sulphate contents. The concept enables the conversion of a given curing history for sulphate content vs. time at the early ages to an equivalent chemical age of curing for a reference sulphate content as follows:

$$t_e^j(\chi) = A_j t_e^2 + B_j t_e + C_j \tag{5-3}$$

where $t_e^j(\chi)$ is the equivalent chemical age for a reference sulphate content, χ denotes the sulphate content, and A_j, B_j and C_j are the chemical parameters. The subscript j represents adhesion c, the friction angle φ and elastic stiffness K.

Therefore, the equation for estimating the binder hydration degree (by taking the effect of the sulphate ions into consideration) is as follows:

$$\xi(\mathrm{t}_e) = \xi_u \exp\left[-\left(\frac{\kappa}{A_j t_e^{\ 2} + B_j t_e + C_j}\right)^{\varsigma}\right] \tag{5-4}$$

This modified binder hydration model (Eq. 5-4) is adopted to evaluate the effect of chemical reactions on the material properties and behaviour of the interface. A discussion on the development of a predictive function for each material property is presented in Section 5.2.2.2.

5.2.2.2 Interface constitutive model

5.2.2.2.1 Bilinear cohesive law

The bilinear cohesive law, which was proposed by Camanho et al. (2003), is one of the most commonly used traction separation laws (TSLs) in CZMs. The bilinear cohesive law was developed based on the debonding process in interlaminar cracking. The tearing of the interlaminar structure in the normal direction is called Mode I failure, while the debonding caused by shear stress is known as Mode II failure. Mode III fractures are in the same vein as Mode II, but result from out-of-plane shear stress, as stated in Abrate et al. (2015). Given the failure mechanism of the CPB-rock interface in DSTs (Fang and Fall, 2019), only Modes I and II are considered in this study. Figure 5.5 presents the bilinear constitutive laws of pure Modes I (Figure 5.5(a)) and II (Figure 5.5(b)). In the following, subscript *i* denotes a value of 1 and 2.

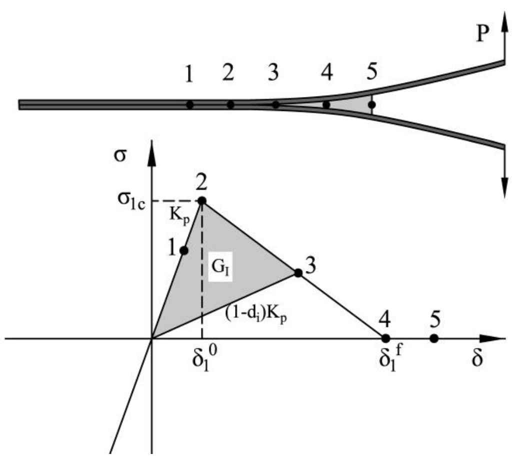

(a) Mode I

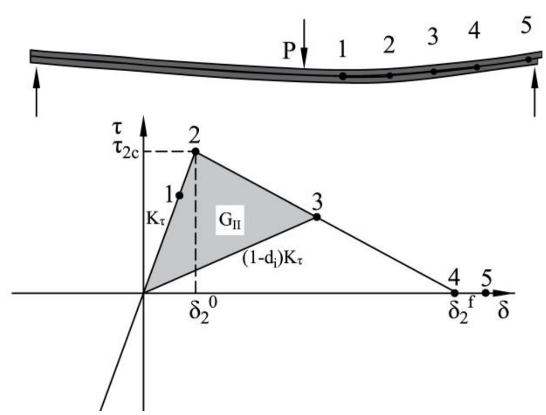

(b) Mode II

Figure 5.5 Bilinear cohesive zone model (G_{I} and G_{II} denotes strain energy release rate of Modes I and II, respectively; K_p: stiffness in the normal direction; K_τ: shear stiffness; d_i: damage parameter; δ_i^0: critical relative displacement; and δ_i^f : final relative displacement) (Xie and Waas, 2006)

The bilinear cohesive law is characterized by three stages, as shown in Figure 5.5. In the first stage (with a displacement less than the critical relative displacement δ_i^0), the traction increases with relative movement, and no damage occurs. After the first stage, a softening period follows, which is characterized by the emergence of damage. Besides, given the accumulation of the damage, the traction also displays a declining tendency with relative movement. The last period (with a displacement greater than the final relative displacement δ_i^f) refers to the complete loss of cohesive strength after maximum relative displacement takes place. In the first stage, traction is assumed to be linearly elastic up to the maximum stress, regardless whether it is Mode I or II. Hence, the stiffness in the normal direction K_p, which is equal to the penalty stiffness P_n, is defined as:

$$K_p = \frac{\sigma_{1c}}{\delta_1^0} \tag{5-5}$$

where δ_1^0 is the critical displacement when the maximum tensile stress σ_{1c} is reached (i.e., the onset of the debonding process). Similarly, for pure Mode II, the shear stiffness is defined by the critical displacement δ_2^0 which corresponds to the peak shear stress τ_{2c} :

$$K_\tau = \frac{\tau_{2c}}{\delta_2^0} \tag{5-6}$$

The relationship between shear and normal stiffness can be defined through a stiffness coefficient n_τ (Comsol, 2018) as follows:

$$K_\tau = n_\tau K_p = \frac{1-2\nu}{2(1-\nu)} K_p \tag{5-7}$$

where ν is the Poisson's ratio. Therefore, the penalty stiffness factor is then formulated as an equation of the Poisson's ratio ν and shear stiffness K_τ:

$$P_n = K_p = \frac{2(1-\nu)K_\tau}{1-2\nu} \tag{5-8}$$

Since the shear stiffness and Poisson's ratio of the CPB-rock interface are time-dependent properties, and the changes are also related to the degree of cement hydration, the penalty stiffness factor is therefore a variable that changes with time. In order to thoroughly determine the influence of the chemical factor on cement hydration, a series of DSTs on CPB-rock samples were conducted by Fang and Fall (2019). Through the obtained data from the DSTs done on CPB-rock samples, the development of the interfacial shear stiffness with time was determined and is presented in Figure 6.

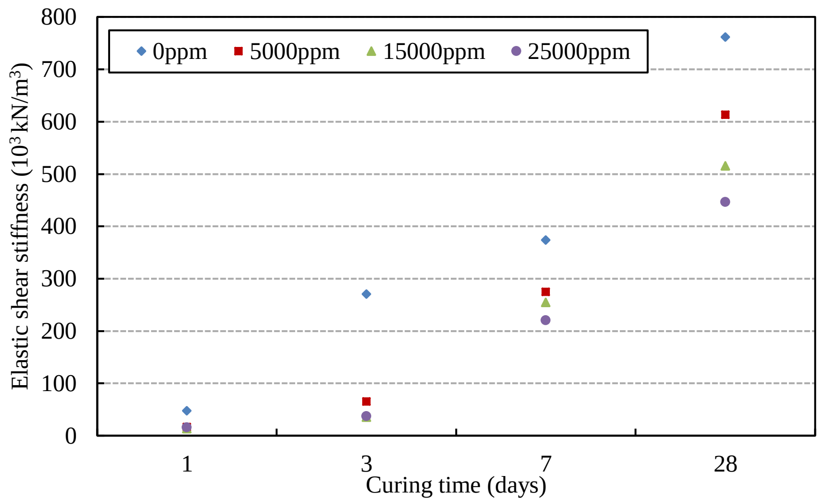

Figure 5.6 Changes in shear stiffness of interface with different sulphate contents

According to the concept of equivalent chemical age and the experimental results presented in Figure 5.6, the chemical parameters A_K, B_K and C_K (in terms of shear stiffness, shown in Eq. 5-3) for calculating the shear stiffness of the CPB-rock interface are expressed as:

$$\begin{cases} A_K = \alpha_{K1}\chi^3 + \alpha_{K2}\chi^2 + \alpha_{K3}\chi + \alpha_{K4} \\ B_K = \beta_{K1}\chi^3 + \beta_{K2}\chi^2 + \beta_{K3}\chi + \beta_{K4} \\ C_K = \lambda_{K1}\chi^3 + \lambda_{K2}\chi^2 + \lambda_{K3}\chi + \lambda_{K4} \end{cases} \tag{5-9}$$

where $\alpha_{K1} = -3\times10^{-14}$, $\alpha_{K2} = 8\times10^{-10}$, $\alpha_{K3} = -2\times10^{-6}$, $\alpha_{K4} = -0.0596$, $\beta_{K1} = 7\times10^{-13}$, $\beta_{K2} = -2\times10^{-8}$, $\beta_{K3} = 2\times10^{-5}$, $\beta_{K4} = 2.7104$, $\lambda_{K1} = -3\times10^{-12}$, $\lambda_{K2} = 1\times10^{-7}$, $\lambda_{K3} = -1.4\times10^{-3}$, $\lambda_{K4} = 2.1231$, in this study. The shear stiffness K_τ is then written as:

$$K_\tau = d_1 \times t_e^K (\chi)^{d_2} \tag{5-10}$$

Based on the data obtained by Fang and Fall (2019), d_1 and d_2 are determined to be $d_1 = 14.11$ and $d_2 = 1.1579$, respectively, in this study. The Poisson's ratio also changes with the progression of binder hydration, and as a result of the increased stiffness, the Poisson's ratio of the CPB as well as cement all show a trend of decline with time (Galaa et al., 2011; Bittnar, 2006). Considering the positive effects of cement hydration on the changes in the Poisson's ratio, an exponential equation is proposed by Cui and Fall (Cui and Fall, 2017) to describe the development of the Poisson's ratio with cement hydration:

$$\nu = 0.5\exp(c_1\xi) + c_2\xi^{c_3}\exp(c_4\xi^{c_5}) \tag{5-11}$$

Given the comparison between the measurements and predicted Poisson's ratio (Cui and Fall, 2017), the equation is proven to be highly capable of predicting the changes in the Poisson's ratio and thus adopted in this study. Substituting Eq. (5-10) into Eq. (5-8), the penalty stiffness factor is expressed as:

$$P_n = \frac{2d_1(1-\nu)t_e^K(\chi)^{d_2}}{1-2\nu} \tag{5-12}$$

As mentioned earlier, softening behaviour is observed when the tension or shear traction at the interface reaches the tensile or shear strength. Meanwhile, damage is assumed to have occurred and thereby leads to stiffness degradation. The damage function is a scalar function of the maximum relative displacement which has occurred between the two boundaries. Complete failure of the interface occurs when the relative displacement reach its maximum value, δ_1^f and δ_2^f, shown as Point 4 in Figure 5.5. Due to the presence of the damage function d_i, the constitutive behaviour of Modes II and II is written as (Alfano and Crisfield, 2001; Zhu et al., 2015):

$$\sigma_i = \begin{cases} K\delta_i, & \delta_i \le \delta_i^0 \\ (1-d_i)K\delta_i, & \delta_i^0 \le \delta_i < \delta_i^f \\ \sigma_{res}, & \delta_i \ge \delta_i^f \end{cases} \tag{5-13}$$

$$d_i = \frac{\delta_i^f(\delta_i - \delta_i^0)}{\delta_i(\delta_i^f - \delta_i^0)} \tag{5-14}$$

where σ_{res} represents the residual strength of the interface, which is determined by the normal stress σ and friction angle φ (i.e., $\sigma_{res} = \sigma \tan\varphi$).

To evaluate the changes in the scalar damage variable, the relative displacements δ_i^0 and δ_i^f are needed. However, it should be noted that due to the complexities of the stress state at the interface, mixed-mode fractures can be found. Hence, it is important to address the combination of the two traction components when interface delamination and debonding are investigated. Correspondingly, it is necessary to define the relative displacement, δ_m^0 and δ_m^f (subscript m denotes the mixed mode), associated with mixed-mode fractures along the interface. Figure 5.7 illustrates the stress-relative displacement curves that correspond to Modes I and II, and the mixed-mode fracturing process based on the bilinear cohesive law.

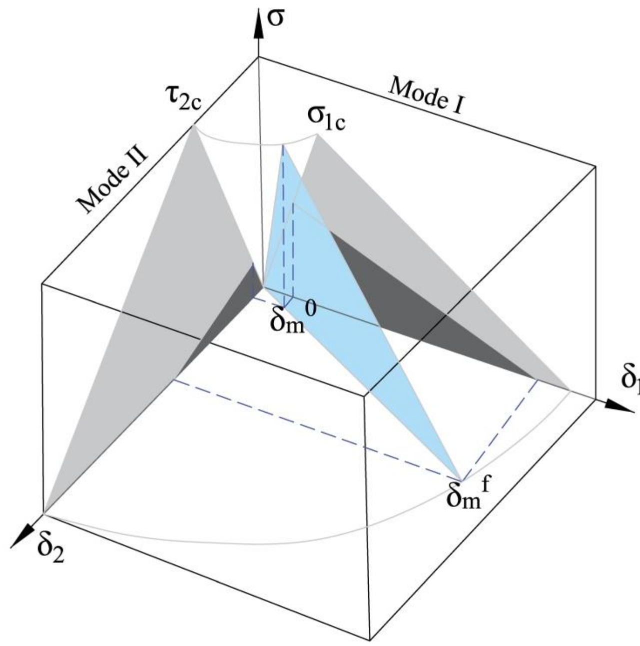

Figure 5.7 Modes I, II, and mixed-mode fracturing process based on bilinear cohesive law

2.2.2 Critical relative displacement

As a measure of the amount of displacement in the adhesive layer, the relative displacement from the mixed-mode fracturing δ_m is determined from the displacement in the normal direction δ_1 and the tangential displacement δ_2 with appropriate weighting factors:

$$\delta_m = \sqrt{\langle \delta_1 \rangle^2 + {\delta_2}^2} \tag{5-15}$$

where the notation

$$\langle x \rangle = \begin{cases} x, & \text{if } x \geq 0 \\ 0, & \text{if } x < 0 \end{cases} \tag{5-16}$$

is used. Thus, δ_m is insensitive to changes in the compressive displacement. Since the bilinear cohesive law is adopted in this study, the critical displacement, δ_m^0, corresponds to the peak stress the interface can sustain. As a result, the onset of delamination along the interface is determined by the interface tensile strength, σ_{1c}, and shear strength, τ_{2c}, by using the following damage criterion (Camanho and Matthews, 1999):

$$\left(\frac{\langle \sigma_1 \rangle}{\sigma_{1c}} \right)^2 + \left(\frac{\tau_2}{\tau_{2c}} \right)^2 = 1 \tag{5-17}$$

According to Eqs. (5) and (6), the critical relative displacement δ_m^0 of the mixed-mode fracture can then be determined with:

$$\delta_m^0 = \delta_1^0\delta_2^0\sqrt{\frac{(\delta_1)^2+(\delta_2)^2}{(\delta_1)^2(\delta_2^0)^2+(\delta_2)^2(\delta_1^0)^2}} \tag{5-18}$$

In accordance with the Mohr-Coulomb failure criterion, the shear strength of the CPB-rock interface is determined by its adhesion and friction angle. Based on the results in Fang and Fall (2019), the changes in the friction angle and adhesion of the interface with different sulphate contents and time are shown in Figure 5.8.

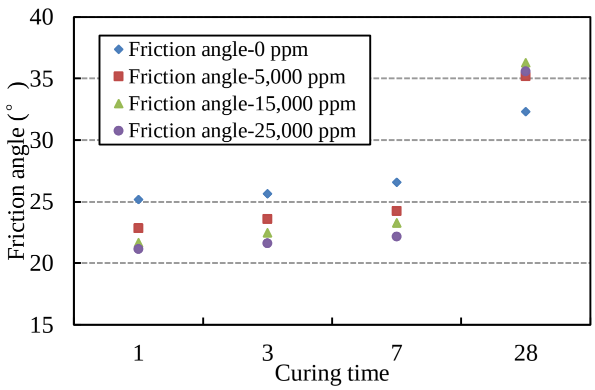

(a) Friction angle

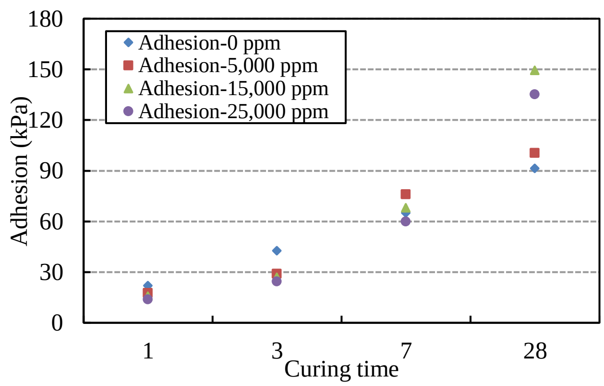

(b) Adhesion

Figure 5.8 Evolution of shear strength properties of interface with time

The chemical parameters (Figure 5.8(a)) in terms of the friction angles A_φ, B_φ and C_φ are determined to be:

$$\begin{cases} A_\varphi = \alpha_{\varphi1}\chi^3 + \alpha_{\varphi2}\chi^2 + \alpha_{\varphi3}\chi + \alpha_{\varphi4} \\ B_\varphi = \beta_{\varphi1}\chi^3 + \beta_{\varphi2}\chi^2 + \beta_{\varphi3}\chi + \beta_{\varphi4} \\ C_\varphi = \lambda_{\varphi1}\chi^3 + \lambda_{\varphi2}\chi^2 + \lambda_{\varphi3}\chi + \lambda_{\varphi4} \end{cases} \tag{5-19}$$

where $\alpha_{\varphi1} = 2\times10^{-14}$, $\alpha_{\varphi2} = -7\times10^{-10}$, $\alpha_{\varphi3} = 6\times10^{-6}$, $\alpha_{\varphi4} = -1\times10^{-15}$, $\beta_{\varphi1} = -5\times10^{-13}$, $\beta_{\varphi2} = 2\times10^{-8}$, $\beta_{\varphi3} = -9\times10^{-5}$, $\beta_{\varphi4} = 0.4768$, $\lambda_{\varphi1} = -3\times10^{-13}$, $\lambda_{\varphi2} = 4\times10^{-8}$, $\lambda_{\varphi3} = -1.1\times10^{-3}$, and $\lambda_{\varphi4} = 8.9287$ in this study. Figure 5.9 shows the regression line of the friction angle of the interface samples against the different sulphate contents. From the figure, it can be noted that there is an exponential relationship between the friction angle and equivalent curing time (with a reference sulphate content of 15,000 ppm). The exponential function of the friction angle is expressed as:

$$\varphi = a_1 e^{a_2 t_e^{\varphi}(\chi)} \tag{5-20}$$

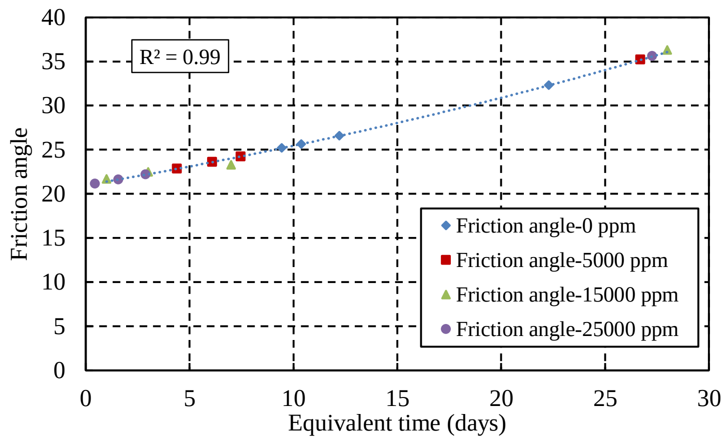

Figure 5.9 Regression line of friction angle of CPB-rock interface with various sulphate contents

The R^2 of the regression line of the friction angle of the interface with 15,000 ppm of sulphate is 0.99, as shown in Figure 5.9, and the friction angle of the other samples that contain sulphate at an equivalent curing time is in good agreement with the regression line. According to the regression results based on the experimental data, $a_1 = 20.964$ and $a_2 = 0.0194$.

Similarly, the adhesion of the interface specimens with various amounts of sulphate can also be expressed as a function of the equivalent curing age. Based on the experimental results shown in Figure 5.8(b), the chemical parameters in terms of the adhesion A_c, B_c and C_c are expressed as:

$$\begin{cases} A_c = \alpha_{c1}\chi^3 + \alpha_{c2}\chi^2 + \alpha_{c3}\chi + \alpha_{c4} \\ B_c = \beta_{c1}\chi^3 + \beta_{c2}\chi^2 + \beta_{c3}\chi + \beta_{c4} \\ C_c = \lambda_{c1}\chi^3 + \lambda_{c2}\chi^2 + \lambda_{c3}\chi + \lambda_{c4} \end{cases} \tag{5-21}$$

where $\alpha_{c1} = 1\times10^{-14}$, $\alpha_{c2} = 5\times10^{-10}$, $\alpha_{c3} = -4\times10^{-6}$, $\alpha_{c4} = -0.0119$, $\beta_{c1} = 7\times10^{-14}$, $\beta_{c2} = -7\times10^{-9}$, $\beta_{c3} = 1\times10^{-4}$, $\beta_{c4} = 0.6257$, $\lambda_{c1} = -3\times10^{-13}$, $\lambda_{c2} = 2\times10^{-8}$, and $\lambda_{c3} = -3\times10^{-4}$, $\lambda_{c4} = 1.1151$, in this study. The adhesion of the CPB-rock interface is then determined by using:

$$c = b_1 \times ln(t_e^c(\chi)) - b_2 \tag{5-22}$$

The regression line of the adhesion of the interface is shown in Figure 5.10. Based on the experimental data, $b_1 = 41.381$ and $b_2 = 0.9188$ are adopted here.

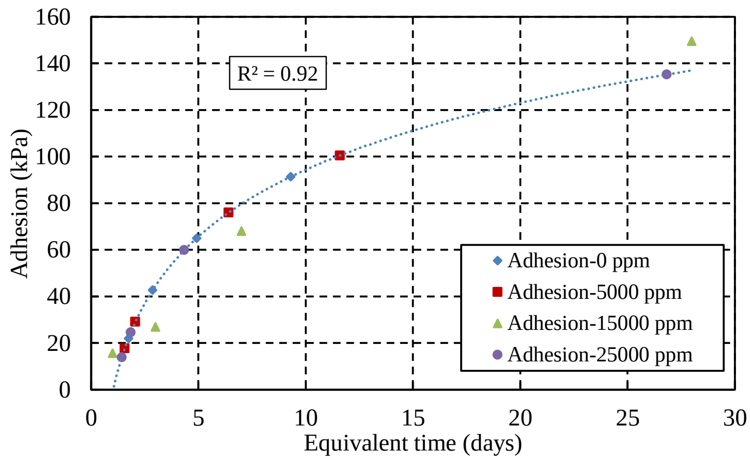

Figure 5.10 Regression line of adhesion of CPB-rock interface with various amounts of sulphate contents

Therefore, the time-dependent evolution of the shear strength of the interface samples with different sulphate concentrations are expressed as:

$$\tau = c + \sigma_n \tan(\varphi) = \left[b_1 \times ln(t_e^c(\chi)) - b_2 \right] + \sigma_n \tan(a_1 e^{a_2 t_e^{\varphi}(\chi)}) \tag{5-23}$$

As shown in Eq. (5-23), both adhesion and friction are responsible for the development of the interface shear strength. However, in comparison with the tensile strength, the interface shear strength τ_{2c} denotes the resistance of materials to shear stress and thus, is only related to the adhesion of the interface. Therefore, it is reasonable to assume that the shear strength of pure Mode II is equal to the adhesion of the interface:

$$\tau_{2c} = c = b_1 \times ln(t_e^c(\chi)) - b_2 \tag{5-24}$$

According to the generalized Von Mises theory, the tensile strength of the interface can be determined by using:

$$\sigma_{1c} = \sqrt{3}\tau_{2c} = \sqrt{3}b_1 \times ln(t_e^c(\chi)) - \sqrt{3}b_2 \tag{5-25}$$

2.2.3 Final relative displacement

The final relative displacement δ_m^f identifies the boundary between the damage and fractured zones in this study. To identify the initiation of fractured zone at the interface, the fracture toughness of the interface is calculated. Fracture toughness refers to the resistance in advancing the fracture, which is calculated by using the critical energy release rate, G_{ic}. In this study, the Benzeggagh-Kenane (B-K) fracture criterion (Benzeggagh and Kenane, 1996) is adopted.

$$G_{\mathrm{I\,c}} + (G_{\mathrm{II\,c}} - G_{\mathrm{I\,c}})\left(\frac{G_{\mathrm{II}}}{G_{\mathrm{I}} + G_{\mathrm{II}}}\right)^{\eta} = G_{\mathrm{I}} + G_{\mathrm{II}} \tag{5-26}$$

where η represents the mode mixity exponent which is defined by the ratio of the relative shear displacement and relative normal displacement. $G_{\mathrm{I\,c}}$ and $G_{\mathrm{II\,c}}$ denote the critical energy release rate of Modes-I and II respectively, which can be determined by referring to the area beneath the stress-relative movement curves, as shown in Figure 5.5:

$$\begin{cases} \int_0^{\delta_1^f} \sigma_{1c} d\delta = G_{\mathrm{I\,c}} \\ \int_0^{\delta_2^f} \tau_{2c} d\delta = G_{\mathrm{II\,c}} \end{cases} \tag{5-27}$$

In addition, the critical energy release rate is linked to the fracture toughness of Modes I ($K_{\mathrm{I\,c}}$) and II ($K_{\mathrm{II\,c}}$):

$$\begin{cases} G_{\mathrm{I\,c}} = \dfrac{{K_{\mathrm{I\,c}}}^2}{E'} \\ G_{\mathrm{II\,c}} = \dfrac{{K_{\mathrm{II\,c}}}^2}{E'} \end{cases} \tag{5-28}$$

with

$$E' = \begin{cases} E, & \text{plane stress} \\ \dfrac{E}{1-\nu^2}, & \text{plane strain} \end{cases} \tag{5-29}$$

where E refers to the Young's modulus. The critical energy release rate is an important parameter for the implementation of the constitutive model of the interface. The strain energy release rates G_{I} and G_{II}, which are represented by the shaded area in Figure 5.5, can be expressed as:

$$G_{\mathrm{I}} = \frac{\delta_1 - \delta_1^0}{\delta_1^f - \delta_1^0} G_{\mathrm{I\,c}} \tag{5-30}$$

$$G_{\mathrm{II}} = \frac{\delta_2 - \delta_2^0}{\delta_2^f - \delta_2^0} G_{\mathrm{II\,c}} \tag{5-31}$$

Then, based on the B-K fracture criterion, the final relative displacement δ_m^f can be explicitly expressed as (Comsol, 2018):

$$\delta_m^f = \frac{2\left[(\delta_1)^2 + (\delta_2)^2\right]}{\delta_m^0 K_p \left[(\delta_1)^2 + n_\tau (\delta_2)^2\right]} \left[G_{\mathrm{I\,c}} + (G_{\mathrm{II c}} - G_{\mathrm{I\,c}}) \left(\frac{n_\tau (\delta_2)^2}{(\delta_1)^2 + n_\tau (\delta_2)^2} \right)^{\eta} \right] \tag{5-32}$$

Determining the fracture toughness in this study will be discussed in Section 5.2.3.

5.2.3 Determination of fracture toughness of Modes I ($K_{\mathrm{I\,c}}$) and II ($K_{\mathrm{II c}}$)

As discussed in Section 5.2.2.2, fracture toughness is important for finding the final relative displacement. However, due to the complexities associated with the interface between CPB and rock, no investigations have been conducted to determine the fracture toughness of Modes I and II. Therefore, to establish the predictive functions of fracture toughness, numerous semi-circular bending (SCB) tests have been conducted in this study. The SCB test (schematically shown in Figure 5.11) is recommended by the International Society for Rock Mechanics and Rock Engineering (ISRM) to determine the fracture toughness of a brittle material (Chong and Kuruppu, 1984; Chang et al., 2002; Wong et al., 2019). For the SCB method, Mode I occurs when the crack angle α' equals to 0, and Mode II at different crack angles, which depends on the sample dimensions (i.e., a / R and S / R, where *a* denotes the notch length, *S* the half of span length, and *R* the radius of the sample) (Lim et al., 1993; Ayatollahi and Aliha, 2004). Herein, the ratios a / R and S / R are set to be 0.4 and 0.5, respectively.

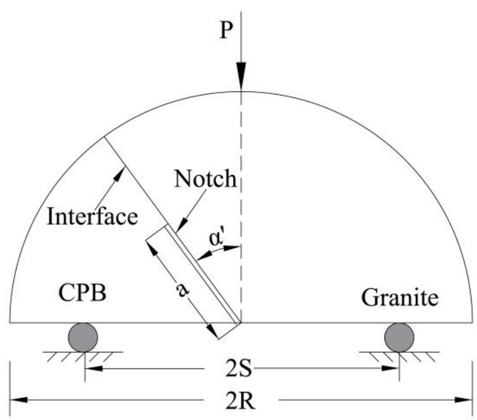

Figure 5.11 Semi-circular bending test

To prepare the samples, granite (rock) was first cut into a circular shape (with dimensions of 98 mm × 20 mm; diameter x thickness). Thereafter, the crack angle was determined according to the type of mode, as shown in Figure 5.11 (e.g., $\alpha' = 0^\circ$ for Mode I and $\alpha' = 45^\circ$ for Mode II). The prepared granite was then placed into a semi-circular container (with a radius of 49 mm). The other half of the sample consisted of CPB with different sulphate concentrations (0 ppm, 5000, 15,000, and 25,000 ppm). To prepare the CPB, silica tailings and Portland cement type I (PCI) were mixed with tap water. Details of the mixture recipe are summarized in Table 5.1. Before pouring the cemented paste into the container, a clapboard (19.6 mm × 20 mm; length x height) was placed along the edge of the granite to produce a 19.6 mm-length notch, as shown in Figure 5.11. Then the prepared samples were wrapped with plastic film and cured at 20°C for 1 day, and 3, 7, and 28 days. Finally, SCB tests were conducted on the semi-circular samples after being cured for a certain number of days.

Table 5.1 Mixture recipe of CPB samples in this study

Tailings	Water	Water-cement ratio	PCI content (%)	Sulphate content (ppm)	Curing time (days)
Silica tailings	Distilled water	7.35	4.5	0, 5000, 15,000, and 25,000	1, 3, 7, and 28

The specific calculations of the fracture toughness, $K_{\mathrm{I\,c}}$ and $K_{\mathrm{II\,c}}$, are (Ayatollahi and Aliha, 2006):

$$K_{\mathrm{I\,c}} = \frac{P\sqrt{\pi a}}{2Rt} Y_{\mathrm{I}}\left(\alpha', \frac{a}{R}, \frac{S}{R}\right) \tag{5-33}$$

$$K_{\mathrm{II\,c}} = \frac{P\sqrt{\pi a}}{2Rt} Y_{\mathrm{II}}\left(\alpha', \frac{a}{R}, \frac{S}{R}\right) \tag{5-34}$$

where P is the normal peak load in the SCB test, R and t are the radius and thickness of the sample, a is the length of the notch, α' means the angle between the vertical direction and crack, and Y_{I} and Y_{II} are geometry factors that are determined by α', a/R and S/R (Ayatollahi and Aliha, 2004; 2006). For the cementitious material, the fracture toughness of the CPB-rock interface varies depending on the curing time. According to the data obtained from the SCB tests, the fracture toughness of the interface with different amounts of sulphate in Modes I and II can then be expressed as:

$$K_{\mathrm{I\,c}} = h_1 e^{h_2 t_e^{K_{\mathrm{I\,c}}}(\chi)} \tag{5-35}$$

$$K_{\mathrm{II\,c}} = m_1 \times ln(t_e^{K_{\mathrm{II\,c}}}(\chi)) + m_2 \tag{5-36}$$

where h_1, h_2 and m_1, and m_2 are determined to be $h_1 = 2.2844$, $h_2 = 0.0481$, $m_1 = 7.0884$, and $m_2 = -2.8809$, in this study. Similarly, the chemical parameters in terms of the fracture toughness of Modes I and II are expressed as:

$$\begin{cases} A_{K_{\mathrm{Ic}}} = \alpha_{K_{\mathrm{Ic}}1}\chi^3 + \alpha_{K_{\mathrm{Ic}}2}\chi^2 + \alpha_{K_{\mathrm{Ic}}3}\chi + \alpha_{K_{\mathrm{Ic}}4} \\ B_{K_{\mathrm{Ic}}} = \beta_{K_{\mathrm{Ic}}1}\chi^3 + \beta_{K_{\mathrm{Ic}}2}\chi^2 + \beta_{K_{\mathrm{Ic}}3}\chi + \beta_{K_{\mathrm{Ic}}4} \\ C_{K_{\mathrm{Ic}}} = \lambda_{K_{\mathrm{Ic}}1}\chi^3 + \lambda_{K_{\mathrm{Ic}}2}\chi^2 + \lambda_{K_{\mathrm{Ic}}3}\chi + \lambda_{K_{\mathrm{Ic}}4} \end{cases} \tag{5-37}$$

$$\begin{cases} A_{K_{\mathrm{IIc}}} = \alpha_{K_{\mathrm{IIc}}1}\chi^3 + \alpha_{K_{\mathrm{IIc}}2}\chi^2 + \alpha_{K_{\mathrm{IIc}}3}\chi + \alpha_{K_{\mathrm{IIc}}4} \\ B_{K_{\mathrm{IIc}}} = \beta_{K_{\mathrm{IIc}}1}\chi^3 + \beta_{K_{\mathrm{IIc}}2}\chi^2 + \beta_{K_{\mathrm{IIc}}3}\chi + \beta_{K_{\mathrm{IIc}}4} \\ C_{K_{\mathrm{IIc}}} = \lambda_{K_{\mathrm{IIc}}1}\chi^3 + \lambda_{K_{\mathrm{IIc}}2}\chi^2 + \lambda_{K_{\mathrm{IIc}}3}\chi + \lambda_{K_{\mathrm{IIc}}4} \end{cases} \tag{5-38}$$

where $\alpha_{K_{\mathrm{Ic}}1} = -2\times10^{-14}$, $\alpha_{K_{\mathrm{Ic}}2} = 9\times10^{-10}$, $\alpha_{K_{\mathrm{Ic}}3} = -9\times10^{-6}$, $\alpha_{K_{\mathrm{Ic}}4} = -8\times10^{-4}$, $\beta_{K_{\mathrm{Ic}}1} = 6\times10^{-13}$, $\beta_{K_{\mathrm{Ic}}2} = -3\times10^{-8}$, $\beta_{K_{\mathrm{Ic}}3} = 3\times10^{-4}$, $\beta_{K_{\mathrm{Ic}}4} = 0.4054$, $\lambda_{K_{\mathrm{Ic}}1} = -4\times10^{-12}$, $\lambda_{K_{\mathrm{Ic}}2} = 1\times10^{-7}$, $\lambda_{K_{\mathrm{Ic}}3} = -9\times10^{-4}$, $\lambda_{K_{\mathrm{Ic}}4} = 2.8227$ and $\alpha_{K_{\mathrm{IIc}}1} = -3\times10^{-15}$, $\alpha_{K_{\mathrm{IIc}}2} = 1\times10^{-10}$, $\alpha_{K_{\mathrm{IIc}}3} = -9\times10^{-7}$, $\alpha_{K_{\mathrm{IIc}}4} = -0.008$, $\beta_{K_{\mathrm{IIc}}1} = -4\times10^{-14}$, $\beta_{K_{\mathrm{IIc}}2} = -2\times10^{-9}$, $\beta_{K_{\mathrm{IIc}}3} = 6\times10^{-5}$, $\beta_{K_{\mathrm{IIc}}4} = 0.6957$, $\lambda_{K_{\mathrm{IIc}}1} = 3\times10^{-13}$, $\lambda_{K_{\mathrm{IIc}}2} = -2\times10^{-9}$, $\lambda_{K_{\mathrm{IIc}}3} = -1\times10^{-4}$, and $\lambda_{K_{\mathrm{IIc}}4} = 1.4025$ in this study.

5.2.4 Model validation and sensitivity analysis

To demonstrate the predicting performance of the developed chemo-elastic CZM, the predicted results are validated against a series of experimental findings obtained in this study and from published research works. Moreover, to further assess the characteristics and performance of the developed model, a sensitivity analysis was conducted by varying the model input parameters, including the sulphate content and fracture toughness. The proposed model was implemented in a commercial finite element (FE) code program called COMSOL Multiphysics, which can be used to conduct a wide range of analyses, such as static, time-dependent, and parametric analyses, as well as other issues through coupled multiphysics processes (Comsol, 2018).

To investigate the behaviour of the CPB-rock interface, DSTs on CPB-rock samples are considered to be standard and have been widely used in previous studies (Nasir and Fall, 2008; Koupouli et al., 2016; Fang and Fall, 2018). Therefore, the numerical studies are conducted on the CPB-rock samples with the granite (rock) cut into small cuboids for both model validation and the sensitivity analysis in this paper. Specifically, the geometric model of the sample consists of two parts; see Figure 5.12. The upper half of the model is the CPB, while the lower half represents the granite. The boundary (in blue) between the CPB and rock is the interface. The size of the model is 60×60×60 mm, which is similar to the sample size used in previous laboratory experiments (Fang and Fall, 2018; 2019; 2020).

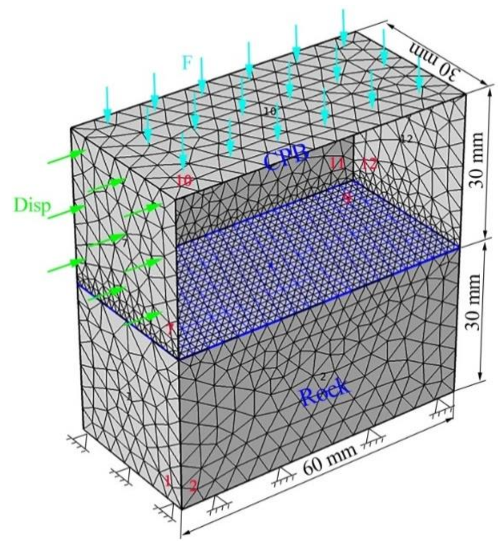

Figure 5.12 Finite element mesh and boundary conditions of CPB-rock interface

In conducting the DSTs on the CPB-rock samples, a direct shear device which contains a shear box was used. The shear box consists of two parts, namely upper container and lower container, as described in (Fang and Fall, 2018). A horizontal load was applied on either the upper or lower half, which allowed a symmetrical distribution of stress and displacement that is relative to the center of the vertical plane along the shearing direction. Therefore, to decrease the degrees of freedom and enhance the computational efficiency, only half of CPB-rock sample was simulated and a symmetrical boundary was applied to the front side, which was marked as Planes 2 and 8. To capture the normal stress, a uniform stress boundary condition was applied to the top plane of the sample (i.e., Plane 10). Moreover, the shearing was simulated by applying load-control or displacement control boundary conditions in the horizontal direction. However, compared to a load control boundary condition, a prescribed displacement boundary condition allows further analysis (Comsol, 2018). Therefore, a prescribed displacement boundary condition was applied to Plane 7. A fixed constraint was applied to the bottom plane. The contact interfaces of the rock and CPB were marked as Planes 4 and 9, respectively.

5.2.4.1 Model validation

In this section, three case studies are used to validate the predicting performance of the proposed CZM in capturing the shear behaviour of the interface samples. The validation is carried out by comparing the numerical simulation results and experimental data obtained from previous studies done by the authors of this paper and in other published work (Nasir and Fall, 2008; Koupouli et al., 2016; Fall and Nasir, 2010). The parameters of these three cases, which were determined based on the experimental results in (Fang and Fall, 2019), are listed in Table 5.2.

Table 5.2 Input parameters of cohesive zone model

Parameter \ Sulphate content-time	Case Study 1	Case Study 2			Case Study 3			
	0 ppm-1day	0 ppm-1day	0 ppm-3days	0 ppm-7days	0 ppm-1day	5000 ppm-3days	15,000 ppm-7days	25,000 ppm-28days
Fracture toughness of Mode I $K_{\mathrm{I}c}$ ($kPa\sqrt{m}$)	2.66	2.66	2.75	3.04	2.66	2.69	3.06	7.10
Fracture toughness of Mode II $K_{\mathrm{II}c}$ ($kPa\sqrt{m}$)	4.34	4.34	6.50	8.86	4.34	6.24	10.14	17.84
Elastic shear stiffness (10^3 kN/m^3)	47.7	47.7	85.2	270.5	47.7	65.2	255.1	446.7
Penalty stiffness P_n (10^3 kN/m^3)	274.0	274.0	394.0	960.4	274.0	317.5	1082.5	1354.7
Shear strength in pure mode τ_{2c} (kPa)	22.0	22.0	42.7	65.0	22.0	29.1	68.0	135.2
Tensile strength in pure mode σ_{1c} (kPa)	38.1	38.1	73.9	112.6	38.1	50.3	112.3	234.2
Friction angle φ	25.2	25.2	25.6	26.6	25.2	23.6	23.3	35.6
Normal to shear ratio n_τ	0.174	0.174	0.216	0.282	0.174	0.205	0.236	0.330

5.2.4.1.1 Case Study 1: Simulation of shear performance of interface under different normal stresses

The in-situ characteristics and behaviour of the CPB-rock interface differ from each other. Nasir and Fall (2008) conducted a series of DSTs to experimentally model the influence of self-weight on the shear properties of the CPB-rock interface. The three normal stresses applied to the samples were 100 kPa, 150 kPa and 200 kPa. Based on the data and the Mohr-Coulomb criterion, the peak shear stress of the interface sample under a normal stress of 50 kPa was also obtained (Nasir and Fall, 2008). Herein, the shear characteristics of the interface samples were numerically simulated with normal stresses of 50 kPa, 100 kPa, and 150 kPa.

The numerical results of the shear stress distribution and changes in shear stress when the samples are subjected to normal stresses of 50, 100 kPa, and 150 kPa are illustrated in Figure 5.13. From the figure, the peak shear stress of the interface is found to be closely related to the normal stress, and with an increase in the normal stress (from 50 kPa to 150 kPa), the shear strength increases from 44.3 kPa to 91.8 kPa, respectively. In addition, the shear stress-shear displacement curves show similar trends in the changes, regardless of the amount of normal stress applied. The shear behaviour is initially characterized with an increase in shear stress followed by softening behaviour. Moreover, the results of the numerical simulation and experiment, as shown in Figure 5.14, indicate that the predicted peak shear stress of the interface agree with the results obtained by Nasir and Fall (2008) and Fang and Fall (2019).

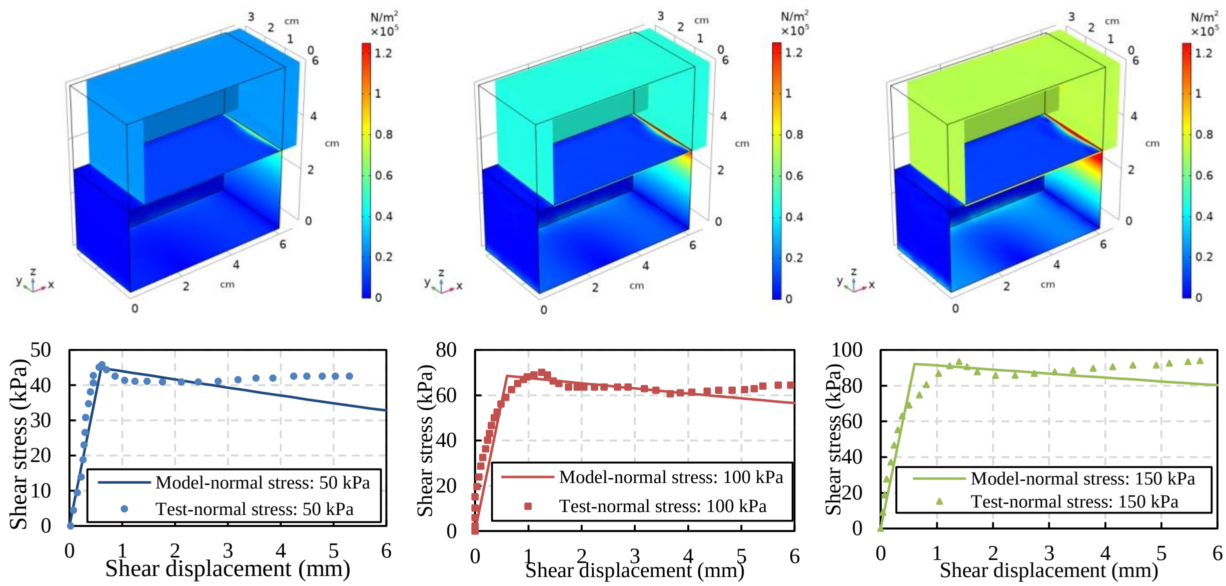

(a) Normal stress: 50 kPa (b) Normal stress: 100 kPa (c) Normal stress: 150 kPa

Figure 5.13 Shear stress changes in interface sample under different normal stresses (curing time: 1 day)

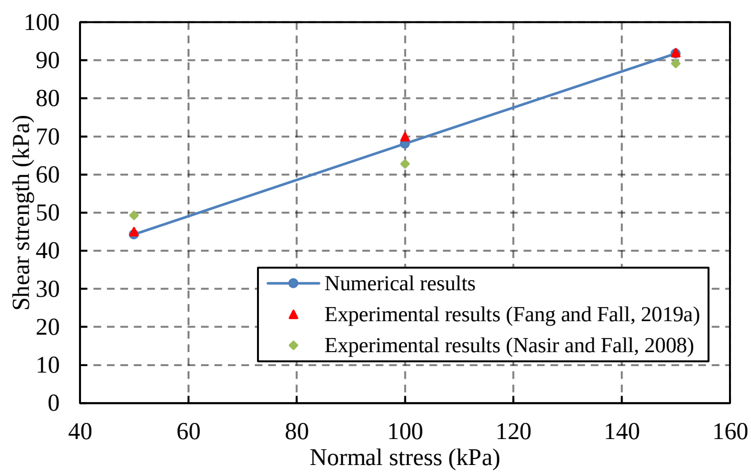

Figure 5.14 Comparison of shear strength of interface: numerical simulation vs. experiment (curing time: 1 day, sulphate content: 0 ppm)

5.2.4.1.2 Case Study 2: Effect of curing time

It is widely acknowledged that the mechanical properties of cementitious material change with time (Fall et al., 2010; Neville, 2011). Nevertheless, only a few experimental studies have been conducted on the changes in the shear properties of the CPB-structure interface with time. The studies include experiments performed by Fall and Nasir (2010) who show that the shear strength of the CPB-brick interface increases from 65.6 kPa to 101.85 kPa from the first to the seventh day of curing. Koupouli et al. (2016) studied the influence of cement content on the shear strength of CPB-granite samples, and the shear strength of samples with time are shown in Figure 5.15. The effect of time on the changes in the shear strength of the interface is numerically investigated in this study. The results of the numerical simulation are shown in Figure 5.15. It can be observed that the shear strength of the interface sample increases from 68.3 kPa to 112.7 kPa with a normal stress of 100 kPa from the first to the seventh day. Moreover, it is found that the simulated changes in shear strength with time agree with the experimental results.

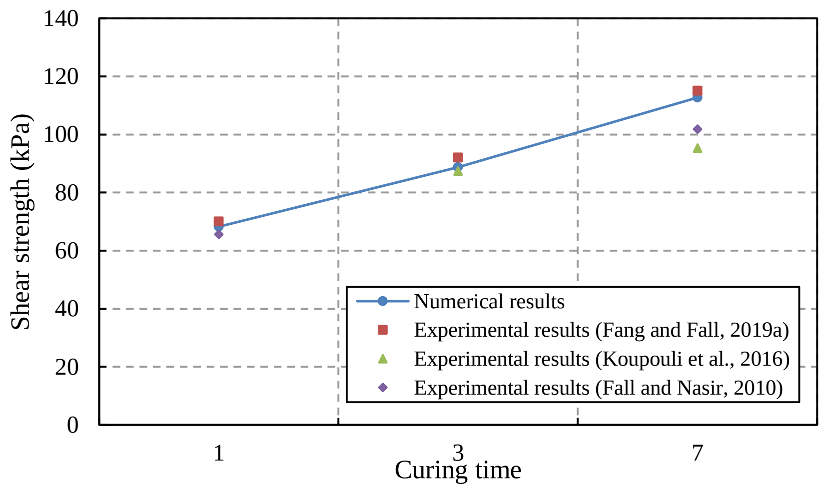

Figure 5.15 Comparison of the shear strength of interface obtained from numerical simulation and laboratory tests (Normal stress: 100 kPa, sulphate content: 0 ppm)

5.2.4.1.3 Case Study 3: Effects of sulphate ions and time on development of shear stress of interface

The impact of sulphate ions on the shear characteristics of the CPB-rock interface with time is described in Fang and Fall (2019). To produce interface samples with sulphate contents of 5000 ppm, 15,000 ppm and 25,000 ppm, a certain amount of $FeSO_4{\cdot}7H_2O$ was added to the water before mixing in the tailings and cement. After the samples were prepared with different amounts of sulphate, they were wrapped with plastic film and cured at 20°C for 1 day, 3, 7, 28, 90 and 150 days. Thereafter, all of the samples were subjected to DSTs (ASTM D3080-04).

Herein, a series of tests were also carried out to numerically simulate the shear performance of the samples with different sulphate contents. The numerical results of the shear stress distribution of the interface are shown in Figure 5.16 (with a displacement of 6 mm), while the changes in shear stress obtained through numerical simulations and experiments are compared in Figure 5.17.

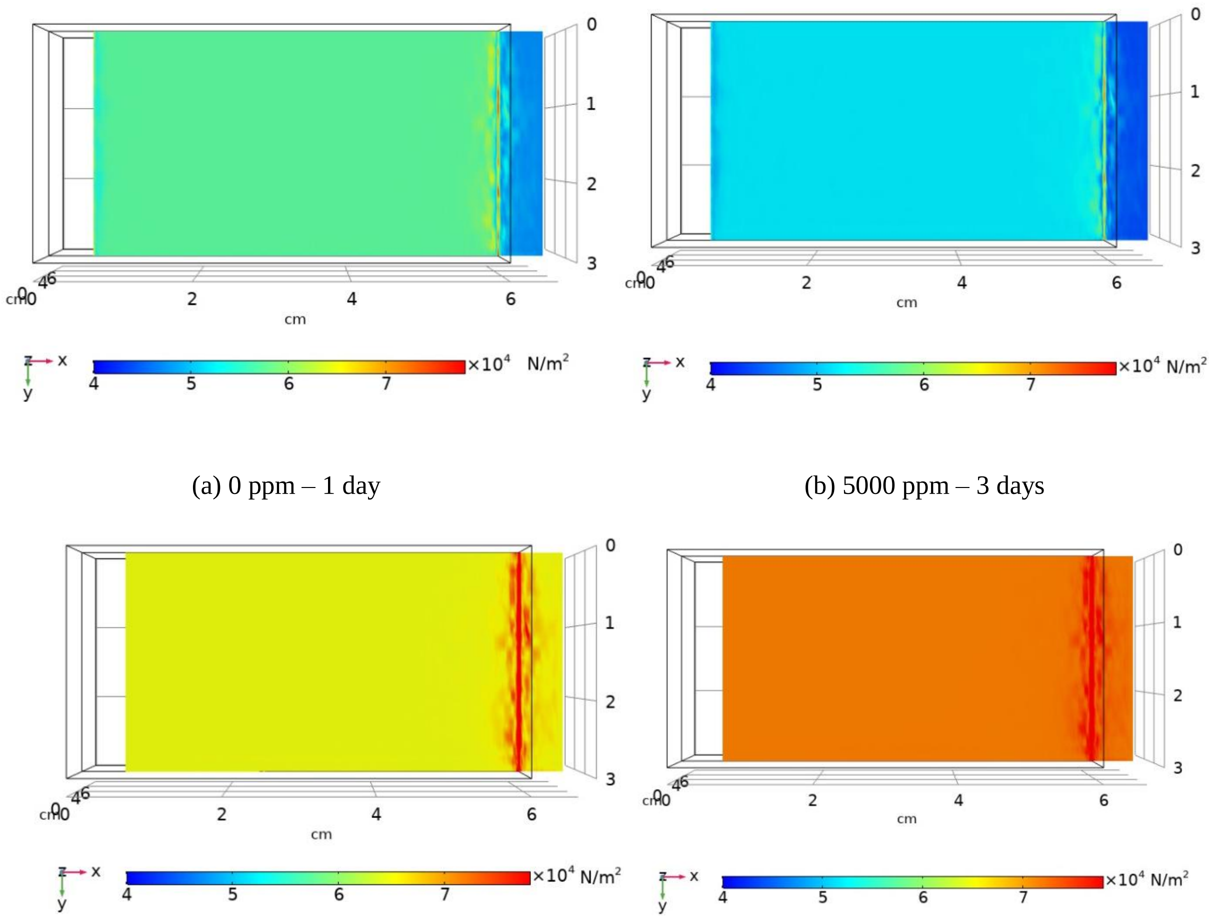

(a) 0 ppm – 1 day

(b) 5000 ppm – 3 days

(c) 15,000 ppm – 7 days

(d) 25,000 ppm – 28 days

Figure 5.16 Shear stress changes in interface (at normal stress of 100 kPa)

The changes in the shear stress of the interface samples plotted in Figure 5.16 show that the shear stress generally increases with time, which is in good agreement with the experimental results (Fang and Fall, 2019). It is obvious from Figure 5.17 that both the shear stiffness and shear strength increase with time, regardless of the sulphate content. The change in shear stiffness and shear strength is attributed to the enhancement of the degree of cement hydration (Nasir and Fall, 2008). However, a comparison made between the 1-day sample with no sulphate and 3-day sample with 5000 ppm of sulphate showed an insignificant difference in shear strength. This demonstrates the inhibiting effect of sulphate on binder hydration, which echoes the findings in previous studies (Li and Fall, 2018; Hassani and Archibald, 1998; Tzouvalas et al., 2004). Besides, the shear stress-shear displacement curves presented in Figure 5.17 show a substantial difference with respect to the strain hardening/softening behaviour of the interface. For samples cured for 1 day and 3 days, the strain softening behaviour is less pronounced. However, for samples cured for 7 and 28 days, the softening behaviour is greatly reduced with increases in the shear stiffness. A similar pattern was also mentioned in (Saiang et al., 2005; Tian et al., 2015). The numerical simulation results (shear stress vs shear displacement) of the CPB-rock interface shown in Figure 5.17 are consistent with the experimental results in Fang and Fall (2019).

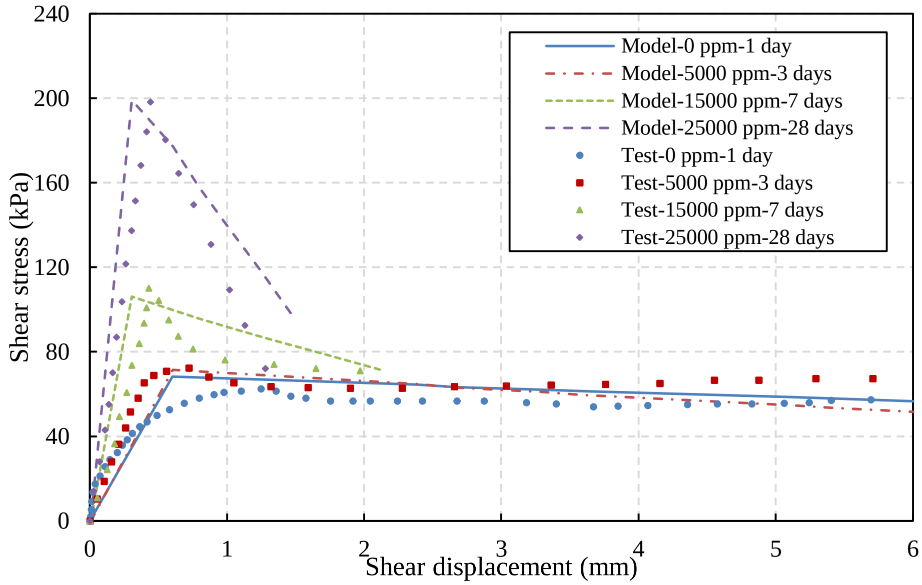

Figure 5.17 Shear stress vs shear displacement of CPB-rock interface (at normal stress of 100 kPa)

5.2.4.2 Sensitivity analysis of proposed model

A sensitivity analysis allows parameters that largely influence the output of the proposed model to be identified, especially the constant parameters. In terms of previous CPB models, the predicted results are sensitive to the mix components (e.g., binder type, w/c ratio, and cement content) (Cui and Fall, 2017). For example, Cui and Fall (2017) found that the increases in the cement content can reduce the pressure on barricades, thereby increasing the stability of the underground structures. To examine the plausibility of the proposed CZM in this study, a sensitivity analysis is conducted with respect to the sulphate content and fracture toughness.

5.2.4.2.1 Effect of sulphate ions

As an frequent component found in mine tailings, sulphate ions considerably affect the progression of binder hydration, thereby influencing the mechanical properties of CPB structures (Fang and Fall, 2019; Pokharel and Fall, 2013). For very early-age samples, the cement particles in the CPB are mainly isolated from the water by ettringite, which is a product of the reaction between tricalcium aluminate and sulphate ions (Li and Fall, 2016; Yilmaz and Fall, 2017). As a result, cement hydration is considerably inhibited, and the inhibition effect becomes more intense with the sulphate content (Fang and Fall, 2019). Consequently, the pore water pressure remains high in the CPB. Therefore, less consolidation is observed with sulphate content. Meanwhile, the adsorption of the sulphate by calcium silicate hydrate (C-S-H) leads to the formation of C-S-H gel, which reduces the binding capacity of the cement (Jelenić et al., 1997). On the other hand, a moderate sulphate content (e.g., 5000 ppm) in the CPB can result in the formation of large amounts (but not excessive) of ettringite, which in turn decreases the capillary pores and then increases the mechanical strength. In other words, the two opposite effects of the sulphate ions have a competing effect on the changes in the strength of the CPB. Hence, it is necessary to numerically investigate the influence of sulphate on the behaviour of the interface through the developed model in this study. In the sensitivity analysis case, the shear behaviour of the 7-day interface samples with various sulphate contents is numerically simulated with the proposed model. Some of the parameters inputted into the model are listed in Table 5.3, and the simulation results are presented in Figure 5.18.

The modelling results in Figure 5.18 depict that the shear strength and the shear stiffness of the 7-day interface samples varies with the sulphate content. To be specific, both the shear strength and the shear stiffness of the interface with sulphate content of 5000 ppm are higher than those of samples with 0 ppm and 15000 ppm of sulphate, while the 25000 ppm sample has the lowest shear strength. This is in agreement with the experimental results in Fang and Fall (2019). Compared with sulphate-free sample, the higher shear strength of 5000 ppm interface is because of the precipitation of appropriate quantity of gypsum and ettringite (Fall et al., 2005). The expanded contacting area between CPB and rock, as a result of refinement of microstructure by cement hydration conducts, increases the possibility for C-S-H to migrate and then to bind the interface together. The lower shear strength of the highly sulphated interface is because of the increasing thickness of the diffusion barrier around cement particles, which makes it longer for water to have access to cement particles (Fang and Fall, 2019). Meanwhile, according to the slopes of the plotted softening behaviour, the softening behaviour of the interface samples is also sensitive to the sulphate content. It can be observed in Figure 5.18 that the sample with 25,000 ppm of sulphate has the most obvious softening behaviour, which is the result of the inhibition effect, as mentioned above. Therefore, this case study validates the ability of the developed model to capture the experimental observations in terms of the effect of sulphate on the behaviour of the short-term CPB-rock interface.

Table 5.3 Parameters of samples (with different sulphate contents) after 7 days of curing

Sulphate content-time / Parameter	0 ppm	5000 ppm	15,000 ppm	25,000 ppm
Fracture toughness of Mode I K_{Ic} ($kPa\sqrt{m}$)	3.04	3.57	3.06	2.16
Fracture toughness of Mode II K_{IIc} ($kPa\sqrt{m}$)	8.86	10.51	10.14	5.85
Elastic shear stiffness (10^3 kN/m^3)	270.5	275.1	255.1	220.4
Shear strength in pure mode τ_{2c} (kPa)	65	76	68.0	59.8
Tensile strength in pure mode σ_{1c} (kPa)	112.6	131.6	117.8	103.6
Friction angle φ	26.6	24.2	23.3	22.1
Normal to shear ratio n_{τ}	0.282	0.258	0.236	0.221
Penalty stiffness P_n (10^3 kN/m^3)	960.4	1066.3	1082.2	996.5

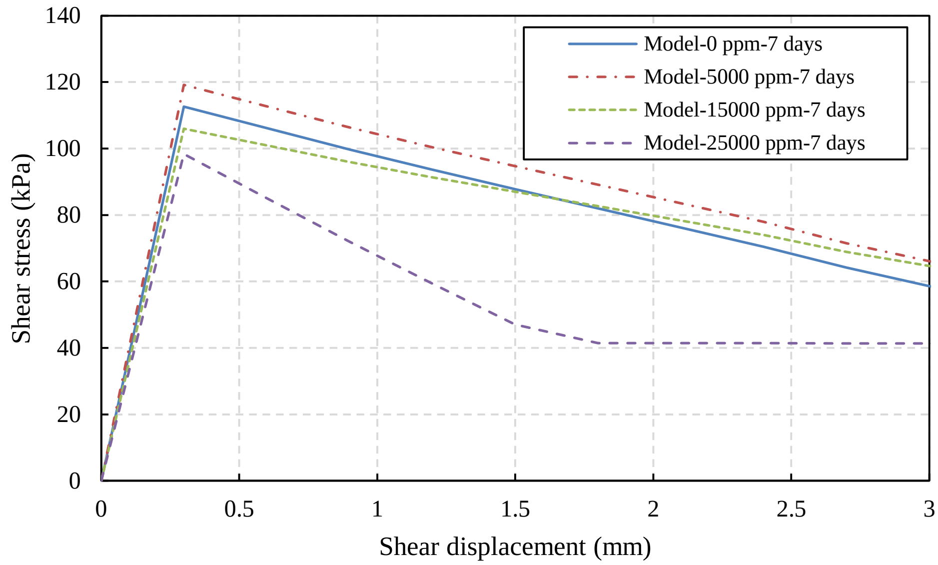

Figure 5.18 Sensitivity of proposed CZM to sulphate content

5.2.4.2.2 Effect of fracture toughness

As mentioned in Section 5.2.3, the fracture toughness of pure Modes I and II are time-dependent, which is related to the degree of cement hydration. Hence, to verify the ability of the proposed model to predict the shear performance of the interface, it is important for the CZM to respond to changes in the fracture toughness. Four numerical studies were conducted to examine the sensitivity of the proposed CZM to different levels of fracture toughness. The parameters were based on 7-day samples with 15,000 ppm of sulphate, and the only variable was fracture toughness. The numerical results are presented in Figure 5.19. As can be seen from the figure, the changes in the fracture toughness of pure Mode II, K_{IIc}, significantly affect the softening behaviour of the samples. In other words, the softening behaviour becomes less pronounced with increasing K_{IIc}. In contrast, the fracture toughness of pure Mode I, K_{Ic}, has no influence on the softening behaviour, which further proves that the shear behaviour of the targeted interface samples is mainly attributed to the shear properties.

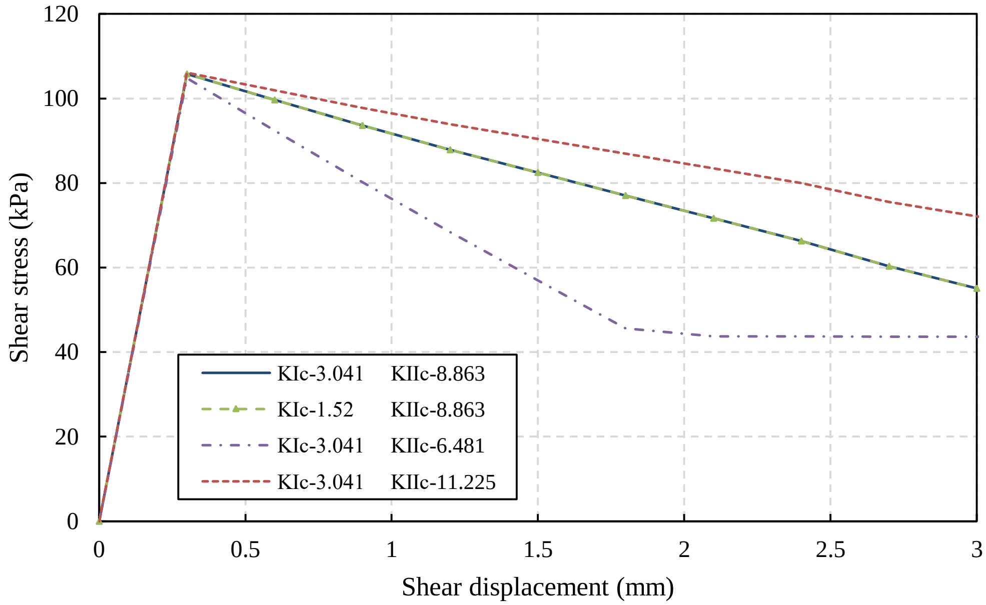

Figure 5.19 Sensitivity of proposed CZM to fracture toughness

5.2.5 Conclusions

In this paper, a coupled chemo-elastic CZM has been developed and the influence of time and sulphate ions on the shear performance of the interface that is undergoing cementation is presented and discussed. The following conclusions are thus made:

- Given the prevalence of sulphate ions in CPB systems, a chemo-elastic CZM is proposed to capture the shear performance of the CPB-rock interface prepared with various amounts of sulphate ions at the early ages. This model not only takes into consideration the influence of sulphate ions on the shear strength changes of the interface, but can also capture the time-dependent softening behaviour.
- The concept of equivalent chemical age is proposed here to quantitatively evaluate the evolution of the mechanical properties of the interface with different amounts of sulphate. The equation for estimating the degree of binder hydration is then modified. Besides, the shear properties, such as adhesion, friction angle and shear stiffness, are expressed as functions of the equivalent chemical age.
- Similar results (including shear behaviour and strength) obtained by numerical simulation and laboratory-scale tests validate the ability of the proposed chemo-elastic CMZ to capture the shear performance of sulphate-bearing CPB-rock interfaces. Furthermore, the numerical results also attest to the inhibiting effect of sulphate ions on the cement hydration of the CPB-rock interface at the early ages.

- The good predicting performance of the chemo-elastic CZM model shows that this model can be a useful tool for conducting analyses on the CPB-rock interface after placement of CPB in the stopes. The model can also help to assess the stability of CPB structures from the early to advanced ages. Therefore, the coupled chemo-elastic CZM is an invaluable tool for designing safe and cost-effective backfill structures.

The chemo-elastic CZM put forward in this paper can describe the shear performance of the CPB-rock interface with different sulphate contents ideally. This will contribute to the prediction of the bearing capacity of underground CPB structures. However, the CPB-rock interface in field is usually exposed to Multiphysics conditions. Therefore, a better understanding of the evolution of the interface fracture toughness under different conditions, as well as the development of a coupled thermo-hydro-mechanical-chemical model to demonstrate the shear behaviour of the CPB-rock interface are required in the future.

Acknowledgements

This study acknowledges the University of Ottawa, the China Scholarship Council and the Natural Sciences and Engineering Research Council of Canada for their financial support. The authors would also like to thank Mr. Guanlong Guo and Mr. Jianxiong Yang for their kind help.

5.2.6 References

Abrate S, Ferrero JF, Navarro P (2015) Cohesive zone models and impact damage predictions for composite structures. Meccanica, 50(10):2587-2620.
Aldhafeeri A, Fall M (2017) Sulphate induced changes in the reactivity of cemented tailings backfill. Int. J. Miner. Process. 166(10):13-23.
Alfano G, Crisfield MA (2001) Finite Element Interface Models for the Delamination Analysis of Laminated Composites: Mechanical and Computational Issues. Int. J. Numer. Methods Eng. 50:1701–1736.
Aoki Y, Suemasu H (2003) Damage analysis in composite laminates by using an interface element. Adv. Compos. Mater. 12:13–21.
Ayatollahi M, Aliha M (2004) Fracture parameters for a cracked semi-circular specimen. Int. J. Rock. Mech. Min. Sci. 41:20-25.
Ayatollahi M, Aliha M (2006) On determination of mode II fracture toughness using semi-circular bend specimen. Int. J. Solids Struct. 43(17):5217-5227.
Aubertin M, Li L, Arnoldi S, Belem T, Bussière B, Benzaazoua M, Simon R (2003) Interaction between backfill and rock mass in narrow stopes. Soil and rock America, 1:1157-1164.
Barenblatt GI (1959) The formation of equilibrium cracks during brittle fracture. General ideas and hypotheses. Axially-symmetric cracks. J. Appl. Math. Mech. 23:622–636.
Barenblatt GI (1962) The mathematical theory of equilibrium cracks in brittle fracture. Advances in applied mechanics, 7:55–129.
Benzeggagh ML, Kenane M (1996) Measurement of mixed-mode delamination fracture toughness of unidirectional glass/epoxy composites with mixed-mode bending apparatus. Compos. Sci. Technol. 56(4):439-449.
Bian JW, Fall M, Haruna S (2019) Sulphate induced changes in rheological properties of fibre-reinforced cemented paste backfill. Mag. Concr. Res. 1-10.
Bittnar Z (2006) Microstructure-based micromechanical prediction of elastic properties in hydrating cement paste. Cem. Concr. Res. 36(9):1708–1718.
Borja RI, Regueiro RA, Lai TY (2000) FE modeling of strain localization in soft rock. J. Geotech. Geoenviron. Eng. 126(4):335-343.

Bouchard PO, Bay F, Chastel Y (2003) Numerical modelling of crack propagation: Automatic remeshing and comparison of different criteria. Comput. Methods Appl. Mech. Eng. 192:3887–3908.
Brackebusch FW (1994) Basic of paste backfill system. Miner. Eng. 46:1175-1178.
Camanho PP, Matthews FL (1999) Delamination onset prediction in mechanically fastened joints in composite laminates, J. Compos. Mater. 33:906-927.
Camanho PP, Davila CG, De Moura M (2003) Numerical simulation of mixed-mode progressive delamination in composite materials. J. Compos. Mater. 37(16):1415-1438.
Cao S, Yilmaz E, Song W (2019) Fiber type effect on strength, toughness and microstructure of early age cemented tailings backfill. Constr. Build. Mater. 223:44-54.
Cao S, Yilmaz E, Song W (2018) Dynamic response of cement-tailings matrix composites under SHPB compression load. Constr. Build. Mater. 186:892-903.
Cao S, Yilmaz E, Xue G, Song W (2019) Assessment of acoustic emission and triaxial mechanical properties of rock-cemented tailings matrix composites. Adv. Mater. Sci. Eng. 6742392, https://doi.org/10.1155/2019/6742392.
Chang SH, Lee CI, Jeon S (2002) Measurement of rock fracture toughness under modes I and II and mixed-mode conditions by using disc-type specimens. Eng. Geol. 66:79–97.
Chong KP, Kuruppu MD (1984) New specimen for fracture toughness determination for rock and other materials. Int. J. Fract. 26:R59–R62.
Choo J, Sun W (2018) Coupled phase-field and plasticity modeling of geological materials: From brittle fracture to ductile flow. Comput. Methods Appl. Mech. Eng. 330:1-32.
COMSOL (2018) Comsol Multiphysics 5.4 http://www.comsol.com.
Cui L, Fall, M (2016) Mechanical and thermal properties of cemented tailings materials at early ages: Influence of initial temperature, curing stress and drainage conditions. Constr. Build. Mater. 125:553-563.
Cui L, Fall M (2016) An evolutive elasto-plastic model for cemented paste backfill. Comput. Geotech. 71:19-29.
Cui L, Fall M (2017) Modeling of pressure on retaining structures for underground fill mass. Tunnelling Underground Space Technol. 69:94-107.
Cui L, Fall M (2017) Multiphysics modeling of arching effects in fill mass. Comput. Geotech. 83:114-131.
Cui L, Fall M (2018) Modeling of self-desiccation in a cemented backfill structure. Int. J. Numer. Anal. Methods Geomech. 42(3):558-583.
De Schutter G (1999) Hydration and temperature development of concrete made with blast-furnace slag cement. Cem. Concr. Res. 29(1):143-149.
Dong W, Yang D, Zhou X, Kastiukas G, Zhang B (2017) Experimental and numerical investigations on fracture process zone of rock–concrete interface. Fatigue Fract. Eng. Mater. Struct. 40(5):820-835.
Dugdale DS (1960) Yielding of steel sheets containing slits. J. Mech. Phys. Solids 8:100–104.
Einav I, Houlsby GT, Nguyen GD (2007) Coupled damage and plasticity models derived from energy and dissipation potentials. Int. J. Solids Struct. 44(7–8):2487–2508.
Ercikdi B, Kesimal A, Cihangir F, Deveci H, Alp I (2009) Cemented paste backfill of sulphide-rich tailings: Importance of binder type and dosage. Cem. Concr. Compos. 31(4):268-274.
Fall M, Benzaazoua M (2005) Modeling the effect of sulphate on strength development of paste backfill and binder mixture optimization. Cem. Concr. Res. 35(2):301-314.
Fall M, Benzaazoua M, Ouellet S (2005) Experimental characterisation of the influence of mill tailings fineness and density on the quality of cemented paste backfill. Miner. Eng. 18(1):41-44.
Fall M, Celestin JC, Pokharel M, Toure M (2010) A contribution to understanding the effects of curing temperature on the mechanical properties of mine cemented tailings backfill. Eng. Geol. 114(3-4):397-413.
Fall M, Nasir O (2010) Mechanical behaviour of the interface between cemented tailings backfill and retaining structures under shear loads. Geotech. Geol. Eng. 28(6):779-790.
Fall M, Pokharel M (2010) Coupled effects of sulphate and temperature on the strength development of cemented tailings backfills: Portland cement-paste backfill. Cem. Concr. Compos. 32:819-828.
Fang K, Fall M (2018) Effects of curing temperature on the shear behaviour of cemented paste backfill-rock interface. Int. J. Rock Mech. Min. Sci. 112:184-192.
Fang K, Fall M (2019) Chemically induced changes in the shear behaviour of the interface between rock and tailings backfill undergoing cementation. Rock Mech. Rock Eng. 52(9):3047-3062.
Fang K, Fall M (2020) Shear behaviour of the interface between rock and cemented backfill: effect of curing stress, drainage condition and backfilling rate. Rock Mech. Rock Eng. 53(1):325-336.
Galaa AM, Thompson BD, Grabinsky MW, Bawden WF (2011) Characterizing stiffness development in hydrating mine backfill using ultrasonic wave measurements. Canadian Geotechnical Journal, 48(8):1174–87.

Gatuingt F, Pijaudier-Cabot G (2002) Coupled damage and plasticity modelling in transient dynamic analysis of concrete. Int. J. Numer. Anal. Methods Geomech. 26(1):1-24.
Ghirian A, Fall M (2016) Strength evolution and deformation behaviour of cemented paste backfill at early ages: effect of curing stress, filling strategy and drainage. International journal of mining science and technology, 26(5):809-817
Grueschow E, Rudnicki JW (2005) Elliptic yield cap constitutive modeling for high porosity sandstone. Int. J. Solids Struct. 42(16-17):4574-4587.
Haiqiang J, Fall M, Cui L (2016) Yield stress of cemented paste backfill in sub-zero environments: experimental results. Miner. Eng. 92:141-150.
Hassani F, Archibald J (1998) Mine backfill. Canadian Institute of mine, Metallury and Petroleum, Canada.
Helinski M, Fourie A, Fahey M, Ismail M (2007) Assessment of the self-desiccation process in cemented mine backfills. Canadian Geotechnical Journal, 44(10):1148–56.
Jelenić I, Panović A, Halle R, Gaćeša T (1997) Effect of gypsum on the hydration and strength development of commercial Portland cements containing alkali sulphates. Cem. Concr. Res. 7(3):239-245.
Jiang H, Fall M (2017) Yield stress and strength of cemented tailings backfill in sub-zero environments: Slag- paste backfill. Journal of Sustainable Cement-Based Materials, 6(5):314-331
Jiang H, Qi Z, Yilmaz E, Han J, Qiu J, Dong C (2019) Effectiveness of alkali-activated slag as alternative binder on workability and early age compressive strength of cemented paste backfills. Constr. Build. Mater. 218:689-700.
Kakogiannou E, Sanavia L, Nicot F, Darve F, Schrefler BA (2016) A porous media finite element approach for soil instability including the second-order work criterion. Acta Geotech. 11(4):805-825.
Kjellsen KO, Detwiler RJ, Gjørv OE (1991) Development of microstructures in plain cement pastes hydrated at different temperatures. Cem. Concr. Res. 21(1):179-189.
Kesimal A, Yilmaz E, Ercikdi B, Alp I, Deveci H (2005) Effect of properties of tailings and binder on the short-and long-term strength and stability of cemented paste backfill. Mater. Lett. 59(28):3703-3709.
Kesimal A, Yilmaz E, Ercikdi B (2004) Evaluation of paste backfill mixtures consisting of sulphide-rich mill tailings and varying cement contents. Cem. Concr. Res. 34(10):1817-1822.
Koupouli NJ, Belem T, Rivard P, Effenguet H (2016) Direct shear tests on cemented paste backfill–rock wall and cemented paste backfill–backfill interfaces. J. Rock Mech. Geotech. Eng. 8(4):472-479.
Li S, Thouless M, Waas A, Schroeder J, Zavattieri P (2006) Mixed-mode cohesive-zone models for fracture of an adhesively bonded polymer–matrix composite. Eng. Fract. Mech. 73(1):64-78.
Li WC, Fall M (2018) Strength and self-desiccation of slag-cemented paste backfill at early ages: Link to initial sulphate concentration. Cem. Concr. Compos. 89:160-168.
Li W, Fall M (2016) Sulphate effect on the early age strength and self-desiccation of cemented paste backfill. Constr. Build. Mater. 106:296-304.
Lim I, Johnston I, Choi S (1993) Stress intensity factors for semi-circular specimens under three-point bending. Eng. Fract. Mech. 44(3):363-382.
Liu L, Zhu C, Qi C, Zhang B, Song KI (2019) A microstructural hydration model for cemented paste backfill considering internal sulfate attacks. Constr. Build. Mater. 211:99-108.
Lyakhovsky V, Zhu W, Shalev E (2015) Visco-poroelastic damage model for brittle-ductile failure of porous rocks. J. Geophys. Res. B: Solid Earth. 120(4):2179-2199.
Miehe C, Welschinger F, Hofacker M (2010) Thermodynamically consistent phase-field models of fracture: Variational principles and multi-field FE implementations. Int. J. Numer. Methods Eng. 83(10):1273-1311.
Nasir O, Fall M (2008) Shear behaviour of cemented pastefill-rock interfaces. Eng. Geol. 101(3):146-153.
Neville AM (2011) Properties of concrete, 5th Edition: Longman London.
Pierce ME (2001) Stability analysis of paste backfill exposures at Brunswick mine. In: 2nd International FLAC symposium, Lyon, 147-56, France.
Pirapakaran K, Sivakugan N (2007) A laboratory model to study arching within a hydraulic fill stope. Geotech. Test J. 30(6):1-8.
Pokharel M, Fall M (2013) Combined influence of sulphate and temperature on the saturated hydraulic conductivity of hardened cemented paste backfill. Cem. Concr. Compos. 38:21-28.
Regueiro RA, Borja RI (2001) Plane strain finite element analysis of pressure sensitive plasticity with strong discontinuity. Int. J. Solids Struct. 38(21):3647-3672.
Saiang D, Malmgren L, Nordlund E (2005) Laboratory tests on shotcrete-rock joints in direct shear, tension and compression. Rock Mech. Rock Eng. 38(4):275-297.
Schindler AK (2004) Effect of temperature on hydration of cementitious materials. ACI. Mater. J. 101(1):72-81.

Tian HM, Chen WZ, Yang DS, Yang JP (2015) Experimental and numerical analysis of the shear behaviour of cemented concrete-rock joints. Rock Mech. Rock Eng. 48(1):213-222.
Tzouvalas G, Dermatas N, Tsimas S (2004) Alternative calcium sulfate-bearing materials as cement retarders: Part I. Anhydrite. Cem. Concr. Res. 34:2113-2118.
Wang Y, Fall M, Wu A (2016) Initial temperature-dependence of strength development and self-desiccation in cemented paste backfill that contains sodium silicate. Cem. Concr. Compos. 67:101-110.
Wong LNY, Guo TY, Lam WK, Ng JYH (2019) Experimental Study of Cracking Characteristics of Kowloon Granite Based on Three Mode I Fracture Toughness Methods. Rock Mech. Rock Eng. 1-19.
Xie D, Waas AM (2006) Discrete cohesive zone model for mixed-mode fracture using finite element analysis. Eng. Fract. Mech. 73(13):1783-1796.
Xu X, Fall M, Alainachi I, Fang K (2019) Characterisation of fibre-reinforced backfill/rock interface through direct shear tests. Geotechnical Research, 1-15.
Xue G, Yilmaz E, Song W, Cao S (2018) Compressive strength characteristics of cemented tailings backfill with alkali-activated slag. Applied Sciences, 8(9):1537.
Xue G, Yilmaz E, Song W, Cao S (2020) Fiber length effect on strength properties of polypropylene fiber reinforced cemented tailings backfill specimens with different sizes. Constr. Build. Mater. 241:118113.
Yilmaz E, Fall M (2017) Paste tailings management: Springer.
Yilmaz T, Ercikdi B, Karaman K (2014) Assessment of strength properties of cemented paste backfill by ultrasonic pulse velocity test. Ultrasonics, 54(5):1386-1394.
Yilmaz E, Kesimal A, Deveci H, Ercikdi B (2003) The factors affecting the performance of paste backfill: physical, chemical and mineralogical characterization. In First Engineering Sciences Congress for Young Researcher (MBGAK'03), Istanbul.
Yilmaz E (2018) Stope depth effect on field behaviour and performance of cemented paste backfills. Int. J. Min. Reclam. Environ. 32(4):273-296.
Yilmaz E, Belem T, Benzaazoua M (2013) Study of physico-chemical and mechanical characteristics of consolidated and unconsolidated cemented paste backfills. Mineral Resources Management, 29(1):81-100.
Zhu W, Yang L, Guo J, Zhou Y, Lu C (2015) Determination of interfacial adhesion energies of thermal barrier coatings by compression test combined with a cohesive zone finite element model. Int. J. Plast. 64:76-87.

5.3 Paper VIII: A coupled thermo-chemo-mechanical cohesive zone model for cemented paste backfill-rock interface

Published in *Engineering Fracture Mechanics*, 2021, 244(2), 107546

Kun Fang, Mamadou Fall, Liang Cui

Abstract

A thermo-chemo-mechanical cohesive zone model (CZM) is proposed to study the coupled effects of temperature and cement hydration on the shear behaviour of the interface between cemented paste backfill (CPB) and rock. To quantitatively evaluate the thermal effect on cement hydration, an equivalent thermal age is put forward to describe the contribution of temperature to the mechanical properties. The interface shear strength properties (e.g., adhesion and friction angle) are then formulated with the equivalent thermal age. Besides, the evolution of the fracture toughness (including modes I and II) of the CPB-rock interface cured at different temperatures is experimentally investigated and incorporated into the CZM. The proposed thermo-chemo-mechanical CZM is validated against the measured data from the direct shear test on the CPB-rock specimens cured at three different temperatures (2°C, 20°C and 35°C) and different times (1, 3, 7 and 28 days). The good agreement between the predicted results and the laboratory measurements confirms the predictability of the thermo-chemo-mechanical CZM. The results of the sensitivity analysis indicate that the proposed CZM is sensitive to the variations in friction angle, adhesion and modes I and II fracture toughness.

5.3.1 Introduction

An annual production of more than five billion tons of tailings was produced all over the world by mining activities and ore beneficiation processes (Mudd and Boger, 2013), and the surface disposal of such a large amount of tailings not only pollutes the water and land, but also poses a significant threat to local communities (Buckby et al., 2003; Fang and Fall, 2020). As a new mining and tailings-management method, cemented paste backfill (CPB) has been adopted by many mines worldwide (Landriault, 1995). Besides the environmental and safety benefits mentioned above, another advantage of CPB is that the mixture of tailings, hydraulic binder and water can fill the underground voids (as a result of mining operation), thereby ensuring the stability of underground structures. However, the stress level and its spatial distribution in CPB mass are controlled by the CPB-rock interface behaviour (Aubertin et al., 2003). Specifically, the vertical settlement due to the consolidation process triggers the interface responses and causes the development of interface resistance, which in turn affects the magnitude and spatial distribution of stress in CPB mass (i.e., arching occurs in CPB, especially in the narrow stopes) (Cui and Fall, 2017). The occurrence of the arching effect can decrease the vertical stress up to 35% of the overburden stress due to self-weight (Helinski et al., 2010), thus reducing the amount of cement required. This reduced amount of cement can significantly decrease the investment cost of CPB (Grice, 2001; Jiang et al., 2019). Moreover, the bi-material interface is generally acknowledged to be a weak plane when determining the failure of laminated structures (Dong et al., 2017). Based on the previous study performed by Nasir and Fall (2008), it has been found that the adhesion and the friction angle of the CPB-rock interface are lower than the counterparts of CPB if the rock surface is relatively smooth. For example, as shown in Figure 5.20, the interface between CPB and granite can be clearly observed by the scanning electron microscopy. The resultant weak CPB-rock interface will affect the behaviour and the performance of the CPB structure. In short, the investigation of the shear performance of the CPB-rock interface will contribute to a safer CPB design and at the same time, with a lower cost.

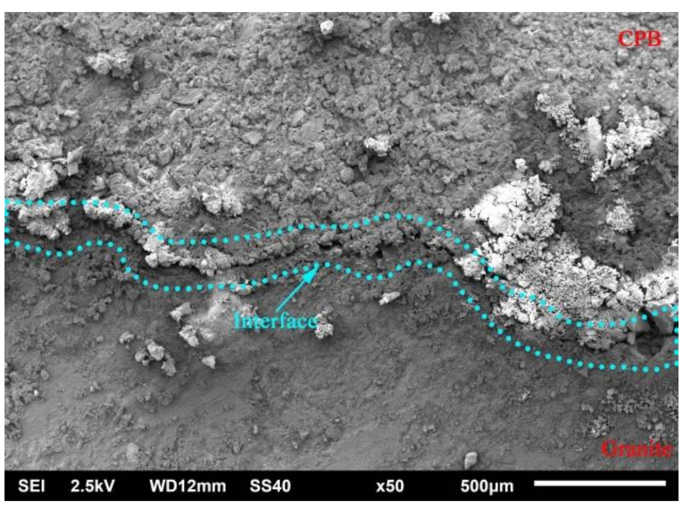

Figure 5.20 SEM image of the CPB-rock interface

The shear property/behaviour of the CPB-rock interface is affected by many factors, such as temperature, cement and sulphate content, overlying stress, and surface morphology (Nasir and Fall, 2008; Koupouli et al., 2016; Fang and Fall, 2018, 2019, 2020). In spite of the significant contributions of these studies towards understanding the shear performance of the CPB-rock interface, none of them has investigated the coupled effects of different influencing factors on the CPB-rock interface behaviour. For example, the mechanical strength of the CPB-rock interface is sensitive to thermal condition (Fang and Fall, 2018). Given the many sources of thermal load (e.g., seasonal variation, the heat generated by cement hydration, geothermal gradient), it is necessary to assess the shear response of the CPB-rock interface under different thermal conditions. However, the variation in temperature will affect the rate of cement hydration, which is characterized as an exothermic process. As the cement hydration proceeds, more heat will be generated (Ghirian and Fall, 2013). In addition, the degree of cement hydration is related to the curing time. A common scenario is that the amount of the products caused by the cement hydration increases with time, and large amounts of them will change the microstructure of CPB. This in turn affects the thermal conductivity of CPB (Neville, 2011; Celestin and Fall, 2009). Consequently, the shear strength of the CPB-rock interface varies with thermal (e.g., temperature, thermal conductivity (involves with time)) and chemical (cement hydration) conditions as well as with time. The effects of curing temperature and time on the evolution of the shear strength of the CPB-rock interface have already been experimentally revealed by Fang and Fall (2018), and typical results are shown in Figure 5.21. It can be noted that, for a given normal stress, the shear strength of the CPB-rock interface is significantly affected by the curing temperature and time. Therefore, the coupled effects of thermal (T, temperature), chemical (C, cement hydration) and mechanical (M, stress) on the shear behaviour of the CPB-rock interface are important to the stability assessment of CPB structures. Even though some numerical studies have been carried out on the interface so far (Helinski et al., 2007; Cui and Fall, 2017, 2018), the coupled effects of thermal, chemical and mechanical factors on the shear characteristics of the CPB-rock interface still remain unexplored.

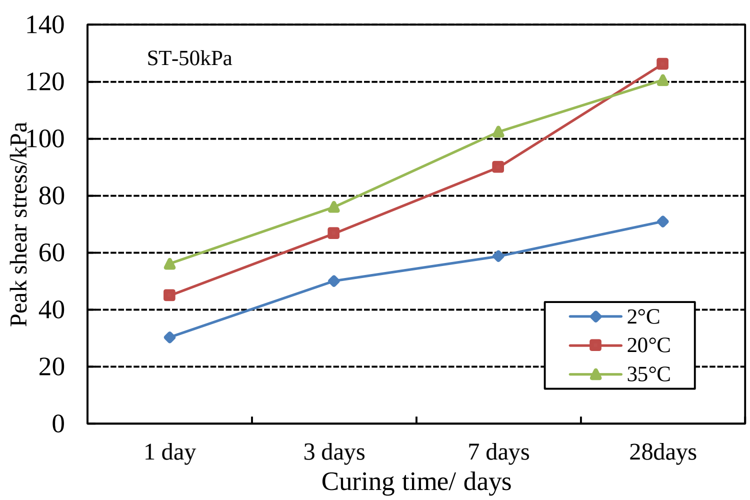

Figure 5.21 Evolution of the shear strength of the CPB-rock interface (Fang and Fall, (2018))

To address these technology deficiencies, the cohesive zone model (CZM, initially proposed by Barenblatt (1962)), is adopted in this study to capture the shear behaviour of the CPB-rock interface. It is well known that the CZM is an effective way to simulate fracture initiation and propagation within sandwich structures (Xie and Waas, 2006; Dimitri et al., 2015). It assumes that there is a cohesive damage zone before the fracture path, and when the critical energy release rate is reached, decohesion takes place. Therefore, the main objective of this study is to (i) develop a CZM-based interface constitutive model in which the coupled effects of thermal, chemical and mechanical on the behaviour of the CPB-rock interface are fully considered; (II) numerically simulate the shear behaviour of the CPB-rock interface with CZM.

5.3.2 Formulation of the coupled thermo-chemo-mechanical cohesive zone model

This section is organized as follows: the coupled thermal, chemical and mechanical processes that take place at the CPB/rock interface are firstly introduced in section 5.3.2.1. Subsequently, the modified binder hydration model based on the equivalent thermal age is described in section 5.3.2.2. Finally, section 5.3.2.3 focuses on the formulation of the interface constitutive relation and the failure criterion governing the interface behaviour.

5.3.2.1 Coupled thermal, chemical and mechanical processes

Once being mixed and placed underground, the shear behaviour of the CPB-rock interface is subjected to multiphysics conditions. Figure 5.22 illustrates the thermal (T), chemical (C) and mechanical (M) factors that inevitably exert effects on it. The evolutions of the interface shear properties (e.g., adhesion, friction angle) and behaviour are dominated by the coupled TCM processes as discussed below.

5.3.2.1.1 Thermal processes

As mentioned above, there are many sources of heat in underground mine backfills. The variation in temperature can mainly contribute to a change in the rate of the cement hydration and the intensity of self-desiccation (Poole et al., 2007; Wu et al., 2013). Generally, a change in the self-desiccation intensity affects the evolution of volumetric water content (VWC) as well as the matrix suction at the interface. Lower VWC and higher matrix suction bring about an increase in the peak shear stress of the CPB-rock interface (Fang and Fall, 2018). Similarly, an appropriate increase in temperature benefits to the acceleration of cement hydration, thereby enhancing the shear strength of the early ages interface. In contrast, for advanced aged interface samples, a higher temperature could result in a crossover effect, which leads to a coarsened pore structure as well as a non-uniform microstructure (Neville, 2011). Accordingly, the shear strength of the CPB-rock interface decreases (Fang and Fall, 2018). However, this study mainly focuses on the positive contribution of the temperature to the shear strength development of the interface samples at early ages.

5.3.2.1.2 Chemical processes

The cement hydration is an important process in changing the mechanical properties of CPB, and the most significant effect is the bonding force between particles, as a result of the generation of calcium silicate hydrate (C-S-H) (Nasir and Fall, 2008; Fang and Fall, 2020). In addition to the particle bonding, the occurrence of chemical shrinkage (because of a less volume of cement hydration products) is another effect that the chemical process has on the mechanical process (as shown in Figure 5.22). Moreover, the heat released by cement hydration can change the thermal condition, which can result in thermal strain in CPB. Other products of cement hydration, especially expansive minerals (not excessive amount), such as ettringite and gypsum, lead to the refinement of the microstructure of CPB. This pore refinement can increase the bonded area between CPB and rock, which increases the shear strength of the CPB-rock interface as well. Also, the finer capillary structure can significantly affect the thermal conductivity (Abbasy, 2009).

5.3.2.1.3 Mechanical processes

A higher self-weight stress can decrease the VWC in drained CPB rapidly, and this reduced VWC is beneficial to the increase in the shear strength at the CPB-rock interface (Fang and Fall, 2019). In addition, the self-weight stress of CPB leads to the presence of volumetric deformation, which in reverse affects the evolution of the porosity of CPB. Because of the inverse relationship between thermal conductivity and pore structure (porosity), the volumetric deformation will effectuate a change in the thermal conductivity (Celestin and Fall, 2009; Cui and Fall, 2015). Moreover, a higher self-weight stress is associated with a higher horizontal stress (which is equivalent to the normal stress in the direct shear tests) applied on the CPB-rock interface. According to the Mohr-Column failure criterion, an increase in the normal stress leads to an improvement in the shear strength of frictional materials.

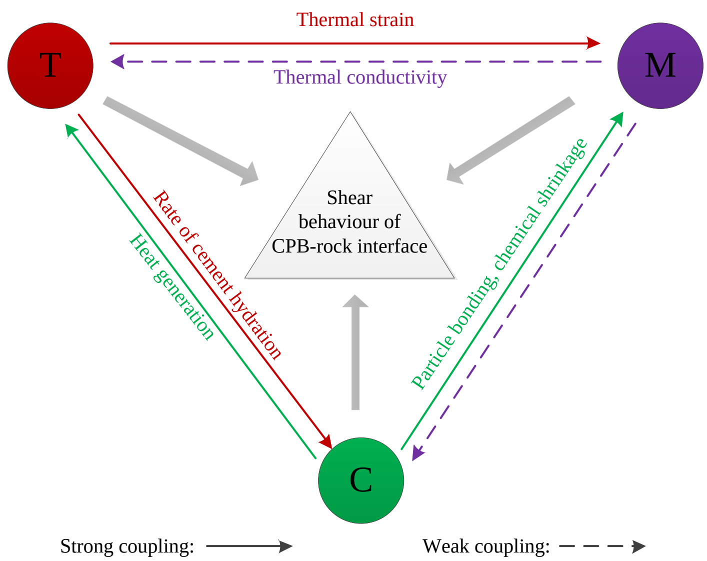

Figure 5.22 Coupled effects of TCM processes on CPB-rock interface

5.3.2.2 Model of cement hydration degree

Most of the mechanical properties of the CPB-rock interface are time-dependent, including fracture toughness, friction angle, and adhesion. It is then necessary to determine the relationship between cement hydration and time. To quantitatively evaluate the process of cement hydration with time, a normalized variable, known as binder hydration degree $\xi(\mathrm{t}_e)$, has been put forth (Schuttera, 1999; Schindler, 2004):

$$\xi(\mathrm{t}_e) = \xi_u \exp\left[-\left(\frac{\kappa}{t_c}\right)^{\varsigma}\right] \tag{5-39}$$

where κ and ς refer to the time and shape parameter, which are empirically determined as $\kappa = 1.4$, $\varsigma = 0.394$ by the test conducted by Schindler (2004). ξ_u means the ultimate degree of cement hydration, while t_c refers to the chronological curing time. The ultimate degree of cement hydration is written as Eq.(5-40) (Wu et al., 2012; Cui and Fall, 2015):

$$\xi_u = \frac{1.031 \times w/c}{0.194 + w/c} + 0.5 \times \vartheta_{FA} + 0.3 \times \vartheta_s \tag{5-40}$$

where w/c represents the water-cement ratio, ϑ_{FA} and ϑ_s indicate the weight fraction of fly ash and furnace slag in the binder. In this study, these two values equal to 0, because cement is the only binder used to produce CPB samples. The binder hydration model, as demonstrated in Eq.(5-39) can only describe the evolution of the cement hydration degree with cement hydration progression, and neglect the contribution of temperature on the shear strength properties. Therefore, to capture the positive effect of temperature, an equivalent thermal age according to the Arrhenius rate theory is put forward. It is used to convert the curing time of samples cured at any temperature T_c to an equivalent curing time when cured at a temperature of T_r.

$$t_e^{\xi}\left(T\right)=f_{\xi}(t_c) \tag{5-41}$$

where $t_e^{\xi}\left(T\right)$ means the equivalent thermal age for samples cured at different temperatures, and the subscript ξ refers to the shear strength properties, including mode I and mode II fracture toughness K_{Ic}, K_{IIc}, friction angle φ, and adhesion c. The cement hydration model can then be formulated as:

$$\xi(\mathrm{t}_e)=\xi_u \exp\left[-\left(\frac{\kappa}{f_{\xi}(t_c)}\right)^{\varsigma}\right] \tag{5-42}$$

5.3.2.3 Interface constitutive model

The schematic diagram of the CZM is shown in Figure 5.23. The domain Ω_1 and Ω_2 in Figure 5.23(a) stand for CPB and rock, respectively. The interface between the two domains is the potential fracture path. The subdomain Ω_3, which is magnified in Figure 5.23(b), represents the cohesive damage zone. It can be seen from the figure that the fracture process is mainly composed of four periods: (I) – OA, it refers to an intact state of the interlaminar structure; (II) – AB, linear elastic response prevails in this period and the tensile/shear stress increases along with the relative movement. However, no damage occurs in this phase; (III) –BC, when the traction increases to σ_{ic} (corresponding to a displacement of δ_i^0), it means the commencement of decohesion. With the further increase in displacement, damage takes place. Moreover, the stress decreases due to the accumulation of the damage; (IV) –CD, the last period is characterized by a complete loss of cohesive strength. The critical energy release rate, G_{jc}, which represents the area beneath the traction separation curve (shade zone, as shown in Figure 5.23(b)), can be derived by the fracture toughness (Lim et al., 1993). The fracture toughness refers to the capacity of the interlaminar structure to resist fracture propagation. The subscript j represents I and II, and they refer to mode I (decohesion of the structure due to tensile stress) and mode II (sliding because of shear stress) respectively (Abrate et al., 2015).

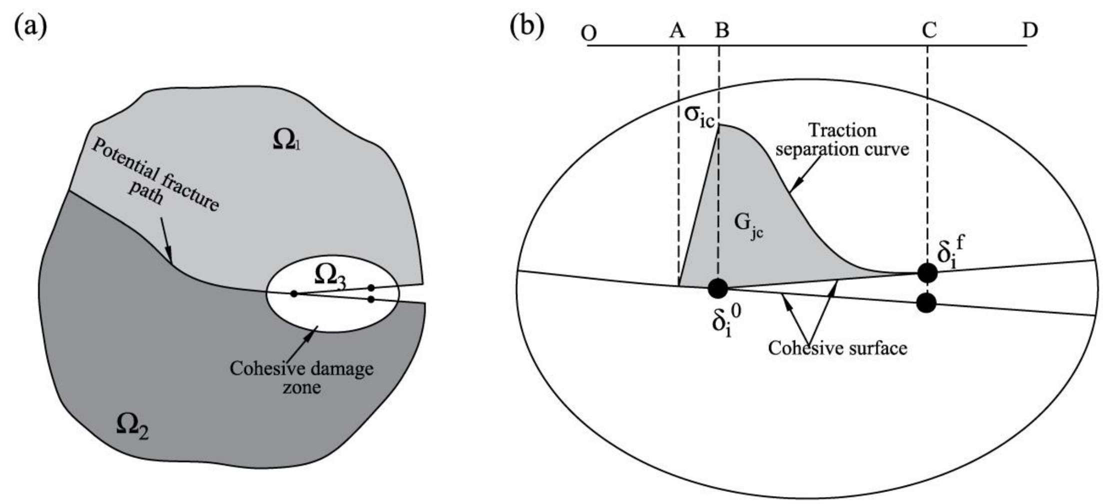

Figure 5.23 Schematic diagram of the cohesive zone model

To determine the constitutive behaviour of the CPB-rock interface, the traction separation relationship is required. Several traction separation laws (TSLs) have been applied to describe the fracture propagation (e.g., Tvergaard and Hutchinson, 1992; Xu and Needleman, 1993; Camanho et al., 2003; Davila et al., 2009). For example, the exponential and polynomial TSLs, as presented in Figure 5.24, were firstly proposed by Needleman (1987, 1990) to simulate the decohesion in metal matrices. Tvergaard and Hutchinson (1992) adopted a trapezoidal TSL to calculate the crack growth resistance. In contrast, Geubelle and Baylor (1998) utilized a bilinear TSL to simulate the initiation and propagation of cracks in thin composite plates. As is shown in Figure 5.24, the polynomial and exponential TSLs differ from the linear TSL in that the decreasing part of the curve is demonstrated by a curve, which is characterized by a zero slope in both ends. The trapezoidal TSL experiences a constant stress after peaking at the critical stress, and this allows describing the plastic region in geomaterial. The comparison of different TSLs is explicitly introduced by Chandra et al. (2002).

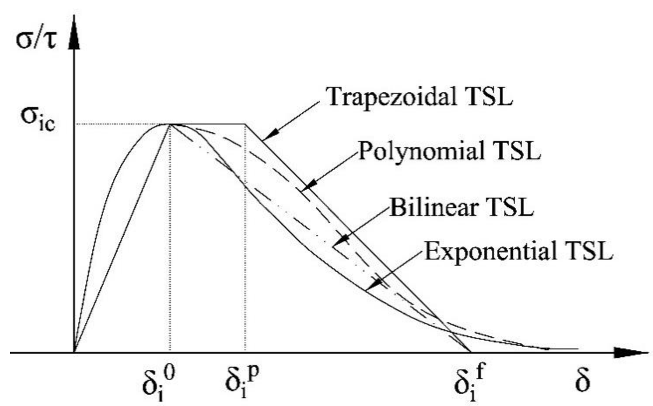

Figure 5.24 Typical traction separation laws

Considering the linear shear stress-shear displacement curve obtained by direct shear test, the bilinear TSL is used to simulate the shear characteristics of the CPB-rock interface in this study. Correspondingly, the equation of the traction separation relationship of either mode I or mode II can be written as:

$$\sigma_i = \begin{cases} K\delta_i, & \delta_i \le \delta_i^0 \\ (1-d_i)K\delta_i, & \delta_i^0 \le \delta_i < \delta_i^f \\ \sigma_{res}, & \delta_i \ge \delta_i^f \end{cases} \tag{5-43}$$

where K means the tensile (K_p) and shear (K_τ) stiffness of mode I and mode II. The subscript i is used to distinguish these two modes, and for mode I, i equals to 1, while for mode II, i refers to 2. σ_{res} represents the residual strength of the interface and d_i is the damage function, which is a function of relative displacement (Comsol, 2018):

$$d_i = min\left(1,\ max\left(0, \frac{\delta_i^0}{\delta_i}\left(1+\left(\frac{\delta_i-\delta_i^0}{\delta_i^f-\delta_i^0}\right)^2 \times \left(2\times\left(\frac{\delta_i-\delta_i^0}{\delta_i^f-\delta_i^0}\right)-3\right)\right)\right)\right) \tag{5-44}$$

where δ_i^0 and δ_i^f represent the critical and final relative displacement as indicated in Figure 5.23 and Figure 5.24. The relationship between the two stiffnesses in Eq.(5-43) is expressed as:

$$K_\tau = n_\tau K_p \tag{5-45}$$

where n_τ is a function of Poisson's ratio ν, $n_\tau = (1-2\nu)/2(1-\nu)$.

For interlaminar structure, the penalty factor P_n equals to the stiffness in the normal direction of the adhesive layer (Comsol, 2018). According to the Eq.(5-45), the penalty factor then can be formulated as:

$$P_n = K_p = \frac{2(1-\nu)K_\tau}{1-2\nu} \tag{5-46}$$

The Poisson's ratio is relevant to the cement hydration degree (Galaa et al., 2011; Cui and Fall, 2016), and the shear stiffness of the CPB-rock interface is also found to be a time-dependent property (Fang and Fall, 2018).

The shear stiffness can then be estimated as:

$$K_\tau = f_1 \times t_e^K(T) + f_2 \tag{5-47}$$

with

$$t_e^K(T) = f_K(t_c) = A_K t_c + B_K \tag{5-48}$$

$$\begin{cases} A_K = \alpha_{K1}T^2 + \alpha_{K2}T + \alpha_{K3} \\ B_K = \beta_{K1}T^2 + \beta_{K2}T + \beta_{K3} \end{cases} \tag{5-49}$$

where $t_e^K(T)$ is the equivalent age of sample (in terms of shear stiffness) and f_i ($i = 1, 2$), A_K, B_K, α_{Ki} ($i = 1, 2, 3$), β_{Ki} ($i = 1, 2, 3$) denote the fitting parameters. Through regression analysis of the experimental data shown in Figure 5.25, $f_1 = 0.5627$, $f_2 = -12.08$ $\alpha_{K1} = 1.1227$, $\alpha_{K2} = -24.651$, $\alpha_{K3} = 45.81$, $\beta_{K1} = -1.3625$, $\beta_{K2} = 34.016$, and $\beta_{K3} = -62.582$ are determined in this study. The obtained shear stiffness of the interface and predicted data with time are presented in Figure 5.25. It is noticed that the contribution of temperature to the shear stiffness acquisition can be well demonstrated by the predicted equation.

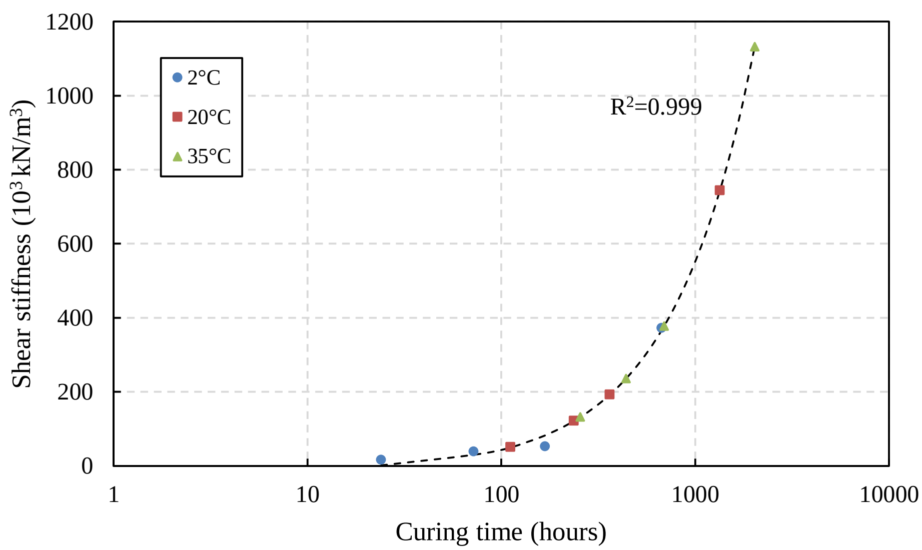

Figure 5.25 Evolution of shear stiffness of CPB-rock interface with time

Substitute Eq.(5-47) into Eq.(5-46), the penalty factor is then formulated as:

$$P_n = \frac{2(1-\nu)\left[f_1 \times t_e^K(T) + f_2 \right]}{1-2\nu} \tag{5-50}$$

The fracture process of an interlaminar structure is usually a result of the combination of pure mode I and mode II. Taking the direct shear test of the CPB-rock interface as an example, not only the lateral displacement, the shear dilation can also be observed clearly (Fang and Fall, 2018). Therefore, the determination of the critical relative displacement δ_m^0 and final relative displacement δ_m^f of the mixed mode (subscript m denotes the mixed mode) is important to the investigation of interface delamination and decohesion. Because the relative displacement δ_m of the mixed mode is a weighted combination of pure mode I and mode II, the δ_m is then expressed as:

$$\delta_m = \sqrt{\langle \delta_1 \rangle^2 + {\delta_2}^2} \tag{5-51}$$

with

$$\langle x \rangle = \begin{cases} x, & \text{if } x \geq 0 \\ 0, & \text{if } x < 0 \end{cases}$$

where δ_1 and δ_2 mean the relative displacement of mode I and mode II respectively. The relative displacement of mixed mode is insensitive to compressive displacement, this is why the Macaulay bracket $\langle x \rangle$ is used in Eq.(5-51).

To predict the delamination of the mixed mode, the following criterion was proposed by Mohammadi et al. (1998) and Camanho and Matthews (1999):

$$\left(\frac{\langle \sigma_1 \rangle}{\sigma_{1c}} \right)^2 + \left(\frac{\tau_2}{\tau_{2c}} \right)^2 = 1 \tag{5-52}$$

where σ_{1c} and τ_{2c} refer to the tensile and shear strength of mode I and mode II. The critical relative displacement of mixed mode δ_m^0 then can be expressed as:

$$\delta_m^0 = \delta_1^0 \delta_2^0 \sqrt{\frac{(\delta_1)^2 + (\delta_2)^2}{(\delta_1)^2 (\delta_2^0)^2 + (\delta_2)^2 (\delta_1^0)^2}} \tag{5-53}$$

To determine the tensile and shear strength in Eq. (5-52), Fang and Fall (2018) conducted a series of direct shear tests on CPB-rock samples cured at different temperatures, and the development of the shear properties of the interface with time is presented in Figure 5.26.

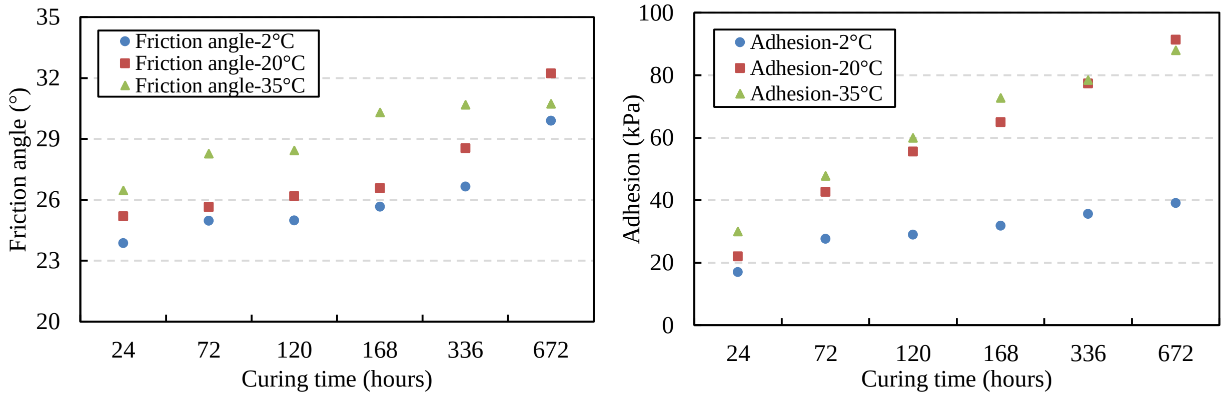

(a) Friction angle (b) Adhesion

Figure 5.26 Evolution of adhesion and friction angle of CPB-rock interface

It can be noticed from the figure that the evolution of friction angle and adhesion of the CPB-rock interface is affected by the cement hydration, and a higher temperature contributes to the improvement of the interface properties. The evolution of the friction angle of the interface samples then can be expressed as an exponential function:

$$\varphi = c_1 e^{c_2 t_e^{\varphi}(T)} \tag{5-54}$$

Based on the experimental results, c_1 and c_2 were determined as $c_1 = 24.053$, $c_2 = 0.0003$ in this study, $t_e^{\varphi}(T)$ means the equivalent age of the sample (in terms of the friction angle) cured at different temperatures:

$$t_e^{\varphi}(T) = f_{\varphi} = A_{\varphi} t_c + B_{\varphi} \tag{5-55}$$

The fitting parameters A_{φ} , B_{φ} are functions of temperature:

$$\begin{cases} A_{\varphi} = \alpha_{\varphi1} T^2 + \alpha_{\varphi2} T + \alpha_{\varphi3} \\ B_{\varphi} = \beta_{\varphi1} T^2 + \beta_{\varphi2} T + \beta_{\varphi3} \end{cases} \tag{5-56}$$

where $\alpha_{\varphi1} = -0.0018$, $\alpha_{\varphi2} = 0.0544$, $\alpha_{\varphi3} = 0.8984$, $\beta_{\varphi1} = 0.5309$, $\beta_{\varphi2} = -4.7723$, $\beta_{\varphi3} = 7.4209$ in this study. The comparison between the experimental data and the predicted friction angle of the CPB-rock interface cured at different temperatures is shown in Figure 5.27, and the predicted results of the friction angle are found to be in good agreement ($R^2 = 0.95$) with the experimental data.

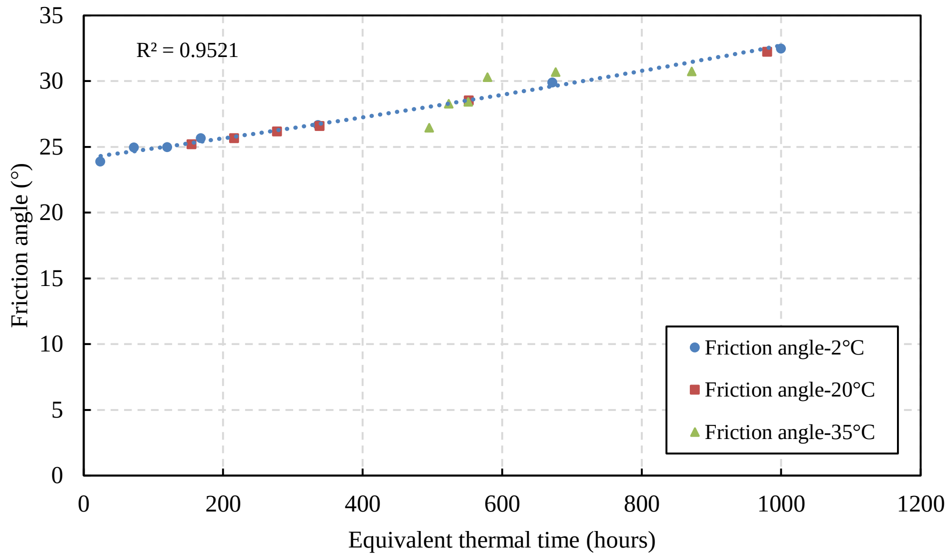

Figure 5.27 Estimated equation of the friction angle of the CPB-rock interface cured at different temperatures

Given the experimental results shown in Figure 5.26(b), the prediction of the adhesion of the interface samples (cured at different temperatures) can be expressed as a function of temperature as well:

$$c = e_1 \ln\left[t_e^c(T)\right] + e_2 \tag{5-57}$$

where e_1 and e_2 are the fitting parameters and were determined as $e_1 = 6.477$, $e_2 = -2.0071$ according to the experimental data. $t_e^c(T)$ represents the equivalent age of the samples (in terms of adhesion) cured at different temperatures, and it can be depicted as:

$$t_e^c(T) = f_c = A_c t_c^{B_c} \tag{5-58}$$

A_c, B_c are functions of temperature as well:

$$\begin{cases} A_c = \alpha_{c1}T^2 + \alpha_{c2}T + \alpha_{c3} \\ B_c = \beta_{c1}T^2 + \beta_{c2}T + \beta_{c3} \end{cases} \tag{5-59}$$

where $\alpha_{c1} = 0.0017$, $\alpha_{c2} = -0.0935$, $\alpha_{c3} = 1.18$, $\beta_{c1} = -0.0048$, $\beta_{c2} = 0.2309$, $\beta_{c3} = 0.5573$. The high consistence of the predicted adhesion and the obtained laboratory data shown in Figure 5.28 indicates that the logarithmic function Eq.(5-57) can well capture the evolution of adhesion of the CPB-rock interface cured at different temperatures.

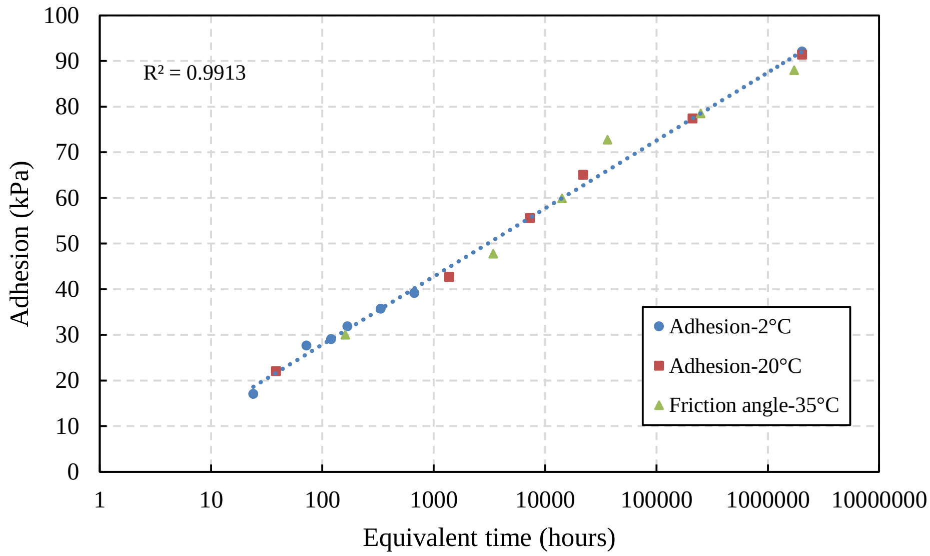

Figure 5.28 Estimated equation of the adhesion of the CPB-rock interface cured at different temperatures

Herein, the shear strength of pure mode II τ_{2c} is assumed to be the same as the adhesion of the interface. After reaching the final relative displacement δ_i^f , the shear resistance of Mode II is caused by the friction angle at the interface. Therefore, the shear and residual strengths of the interface are then determined as:

$$\tau_{2c} = c = e_1 \ln\left[t_e^c(T)\right] + e_2 \tag{5-60}$$

$$\sigma_{res} = \sigma \tan(c_1 e^{c_2 t_e^{\varphi}(T)}) \tag{5-61}$$

The determination of the final relative displacement of the mixed mode depends on the selected failure criterion. Herein, Benzeggagh-Kenane (B-K) criterion (Benzeggagh and Kenane, 1996), which is expressed in Eq. (5-62), is adopted in this study.

$$G_{\mathrm{I\,c}} + (G_{\mathrm{II\,c}} - G_{\mathrm{I\,c}})\left(\frac{G_{\mathrm{II}}}{G_{\mathrm{I}} + G_{\mathrm{II}}}\right)^{\eta} = G_{\mathrm{I}} + G_{\mathrm{II}} \tag{5-62}$$

where η means the mode mixity exponent. G_{I} and G_{II} are the strain energy release rate, and they are associated with the critical energy release rate (Camanho et al., 2003):

$$G_{\mathrm{I}} = \frac{\delta_1 - \delta_1^0}{\delta_1^f - \delta_1^0} G_{\mathrm{I\,c}}; \quad G_{\mathrm{II}} = \frac{\delta_2 - \delta_2^0}{\delta_2^f - \delta_2^0} G_{\mathrm{II\,c}} \tag{5-63}$$

Therefore, the final relative displacement of the mixed mode is then detailed as:

$$\delta_m^f = \frac{2\left[(\delta_1)^2 + (\delta_2)^2\right]}{\delta_m^0 K_p \left[(\delta_1)^2 + n_\tau(\delta_2)^2\right]}\left[G_{\mathrm{I\,c}} + (G_{\mathrm{II c}} - G_{\mathrm{I\,c}})\left(\frac{n_\tau(\delta_2)^2}{(\delta_1)^2 + n_\tau(\delta_2)^2}\right)^\eta\right] \tag{5-64}$$

The critical energy release rates, $G_{\mathrm{I\,c}}$ and $G_{\mathrm{II c}}$ in Eq. (5-63), are related to the fracture toughness of mode I ($K_{\mathrm{I\,c}}$) and mode II ($K_{\mathrm{II c}}$) (Lim et al., 1993), which are specifically determined by semi-circular bending (SCB) tests introduced in section 5.3.3.

5.3.3 Fracture toughness determination

Modes I and II fracture toughness, which represent the capacity of elements to resist fracture initiation (Kuruppu et al., 2014; Wong et al., 2019), are of high importance in determining the final relative displacement introduced above. In this part, the fracture toughness of the CPB-rock interface is experimentally tested. Based on the obtained results, two predictive functions for the Modes I and II fracture toughness of the interface cured at different temperatures are then established.

5.3.3.1 Experimental tests

Owing to the cement hydration progress, the fracture toughness of the CPB-rock interface also evolves with time. Therefore, the determination of the fracture toughness of the interface samples cured at different temperatures is important to the accurate simulation of the shear behaviour of the interface. For brittle material, four main methods are recommended by the International Society for Rock Mechanics and Rock Engineering for the determination of fracture toughness, specifically, semi-circular bend (SCB), chevron bend (CB), cracked chevron notched Brazilian disc (CCNBD) and short rod (SR) test (ISRM, 2007). In this study, the SCB, which was initially developed by Chong and Kuruppu (1984), was adopted to determine the fracture toughness of the CPB-rock interface. The schematic diagram of the SCB test of the CPB-rock interface is shown in Figure 5.29.

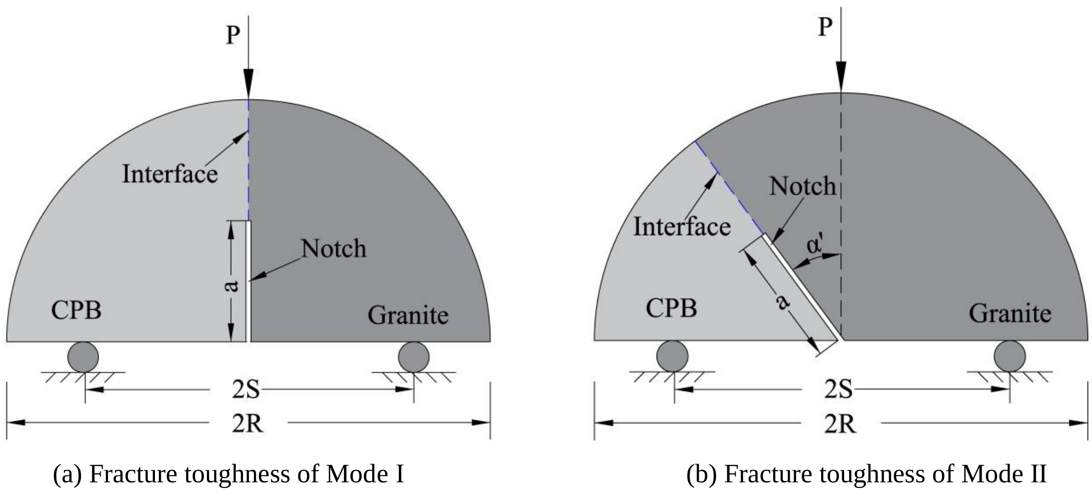

(a) Fracture toughness of Mode I (b) Fracture toughness of Mode II

Figure 5.29 Schematic diagram of the SCB test of the CPB-rock interface

As presented in Figure 5.29(a), mode I occurs when there is a notch right at the interface between CPB and granite. In contrast, mode II can be achieved at different crack angles (Figure 5.29(b)), and is determined by the following two ratios: a/R and S/R (Lim et al., 1993; Ayatollahi and Aliha, 2004). The relationship between the crack angle α' and a/R as well as S/R for pure mode II is shown in Figure 5.30. In this study, a value of $a/R=0.4$ and $S/R=0.493$ are chosen, and then the crack angle is decided as $\alpha'=45^{\circ}$. In addition, since the radius of the sample is $R=49\ mm$, the lengths of the half span of the two rollers and the crack are $S=24.16\ mm,\ a=19.6\ mm$.

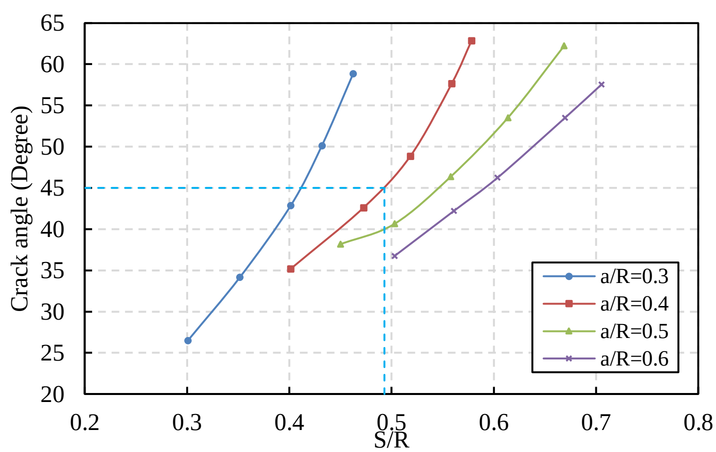

Figure 5.30 Relationship between crack angle α' and a/R, S/R (Ayatollahi and Aliha, 2006)

To prepare the interface sample, a core drill (model DD 150-U) was first used to cut the granite into a circular shape. The size of the core bit is 101.6 mm in diameter and 431.8 mm in height. Thereafter, by using a special rock cutter, the core granite was sliced into a disc sample with a thickness of 20 mm. For the measurement of mode I fracture toughness, the rock disc sample was cut into four pieces evenly, while for measuring the mode II fracture toughness, a rock sector with a centre angle of 135° is produced. The obtained two types of rock samples were then placed into a plastic circular container (with an inner diameter of 98 mm, a height of 20 mm), as shown in Figure 5.31. A thin clapboard was set along the central diameter with the purpose of separating the two samples. In addition, before pouring the prepared CPB (the recipe and the production of CPB are elaborately described in Fang and Fall (2018)) into the container, another two short clapboards were adopted to produce the artificial crack between CPB and granite. To make sure the clapboard would be extracted out easily, the surfaces were initially lubricated with oil. Manual vibration was also applied on the samples for the removal of entrapped air bubbles, which ensures that CPB and rock contact with each other thoroughly. After being cured at three temperatures of 35°C (oven), 20°C (room temperature) and 2°C (refrigerator) for 1 day, 3, 7, and 28 days, the samples were exposed to SCB test which is performed in accordance with ASTM E399-83.

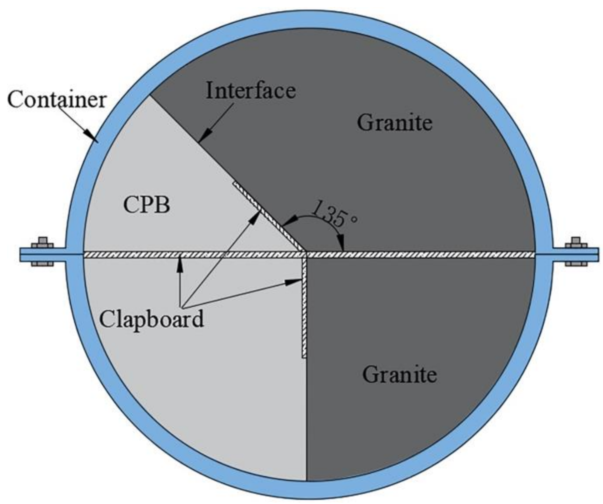

Figure 5.31 Sample preparation

5.3.3.2 Predictive functions of the fracture toughness

With the peak load P obtained by the SCB test, the fracture toughness of mode I and mode II can thus be calculated with the following equation (Ayatollahi and Aliha, 2006):

$$K_{\mathrm{I\,c}} = \frac{P\sqrt{\pi a}}{2Rt} Y_{\mathrm{I}}\left(\alpha', \frac{a}{R}, \frac{S}{R}\right) \tag{5-65}$$

$$K_{\mathrm{II\,c}} = \frac{P\sqrt{\pi a}}{2Rt} Y_{\mathrm{II}}\left(\alpha', \frac{a}{R}, \frac{S}{R}\right) \tag{5-66}$$

where t is the thickness of specimen, Y_{I} and Y_{II} are geometry factor, expressed as functions of α', a/R and S/R. For mode I, Y_{I} is expressed as (Wong et al., 2019):

$$Y_{\mathrm{I}} = -1.297 + 9.516 \times \frac{S}{R} - \left(0.47 + 16.457 \times \frac{S}{R}\right) \times \frac{a}{R} + \left(1.071 + 34.401 \times \frac{S}{R}\right) \times \left(\frac{a}{R}\right)^2 \tag{5-67}$$

while Y_{II} is usually decided by the numerical values based on α', a/R and S/R (Ayatollahi and Aliha, 2004). The calculated modes I and II fracture toughness of the CPB-rock interface cured at different temperatures are presented in Figure 5.32.

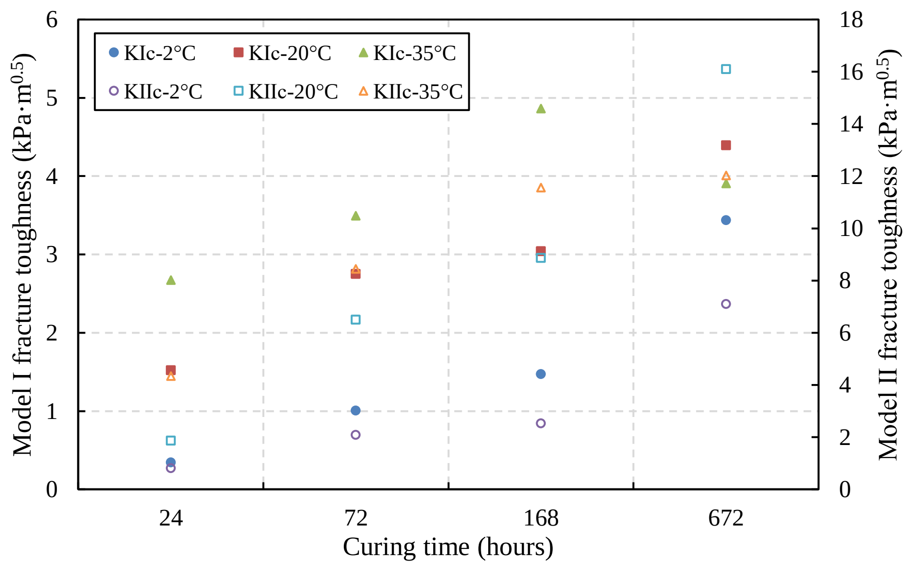

Figure 5.32 Fracture toughness of the CPB/rock interface cured at different temperatures vs curing times

According to the obtained experimental results, the evolution of mode I fracture toughness with time (cured with different thermal conditions) can be expressed as:

$$K_{\mathrm{Ic}} = m_1 \ln\left[t_e^{K_{\mathrm{Ic}}}(T)\right] + m_2 \tag{5-68}$$

where m_1 and m_2 are determined as $m_1 = 0.9179$, $m_2 = -2.815$ through a regression analysis, $t_e^{K_{\mathrm{Ic}}}(T)$ is the equivalent age of the samples cured at different temperatures, and can be expressed as a function of chronological curing time:

$$t_e^{K_{\mathrm{Ic}}}(T) = A_{K_{\mathrm{Ic}}} t_c + B_{K_{\mathrm{Ic}}} \tag{5-69}$$

while $A_{K_{\mathrm{Ic}}}$ and $B_{K_{\mathrm{Ic}}}$ are the functions of temperature:

$$\begin{cases} A_{K_{\mathrm{Ic}}} = \alpha_{K_{\mathrm{Ic}}1} T^2 + \alpha_{K_{\mathrm{Ic}}2} T + \alpha_{K_{\mathrm{Ic}}3} \\ B_{K_{\mathrm{Ic}}} = \beta_{K_{\mathrm{Ic}}1} T^2 + \beta_{K_{\mathrm{Ic}}2} T + \beta_{K_{\mathrm{Ic}}3} \end{cases} \tag{5-70}$$

where $\alpha_{K_{\mathrm{Ic}}1} = 0.0447$, $\alpha_{K_{\mathrm{Ic}}2} = -0.8308$, $\alpha_{K_{\mathrm{Ic}}3} = 2.483$, $\beta_{K_{\mathrm{Ic}}1} = -1.391$, $\beta_{K_{\mathrm{Ic}}2} = 33.553$, $\beta_{K_{\mathrm{Ic}}3} = -61.543$. Similarly, the mode II fracture toughness can be estimated with the following equation:

$$K_{\mathrm{IIc}} = n_1 \ln\left[t_e^{K_{\mathrm{IIc}}}(T)\right] + n_2 \tag{5-71}$$

$$t_e^{K_{\mathrm{IIc}}}(T) = A_{K_{\mathrm{IIc}}} t_c^{B_{K_{\mathrm{IIc}}}} \tag{5-72}$$

$$\begin{cases} A_{K_{\mathrm{IIc}}} = \alpha_{K_{\mathrm{IIc}}1} T^2 + \alpha_{K_{\mathrm{IIc}}2} T + \alpha_{K_{\mathrm{IIc}}3} \\ B_{K_{\mathrm{IIc}}} = \beta_{K_{\mathrm{IIc}}1} T^2 + \beta_{K_{\mathrm{IIc}}2} T + \beta_{K_{\mathrm{IIc}}3} \end{cases} \tag{5-73}$$

where $n_1 = 1.837$, $n_2 = -5.6333$, $\alpha_{K_{\mathrm{IIc}}1} = 0.0023$, $\alpha_{K_{\mathrm{IIc}}2} = -0.1041$, $\alpha_{K_{\mathrm{IIc}}3} = 1.199$, $\beta_{K_{\mathrm{IIc}}1} = -0.0027$, $\beta_{K_{\mathrm{IIc}}2} = 0.1308$, $\beta_{K_{\mathrm{IIc}}3} = 0.7491$. The comparison between the experimental and estimated modes I and II fracture toughness of the CPB-rock interface is shown in Figure 5.33.

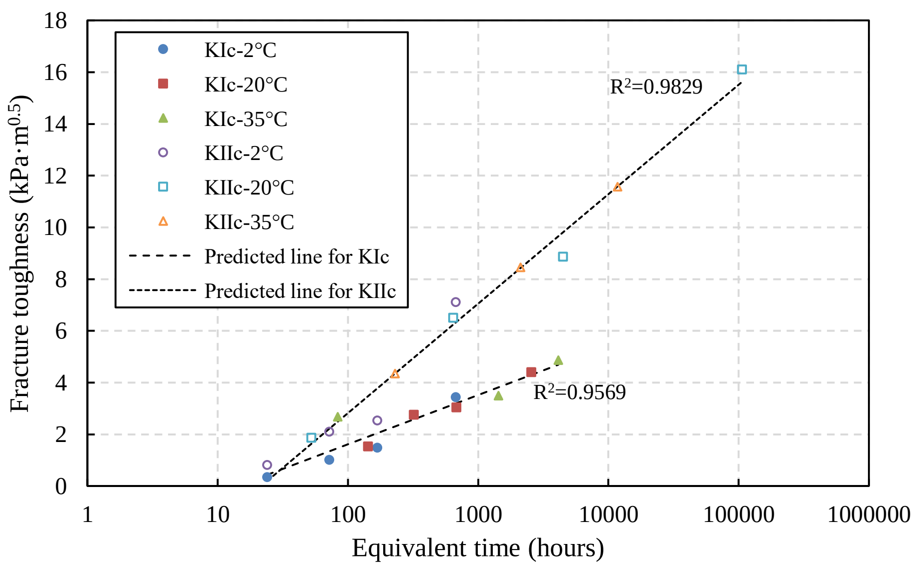

Figure 5.33 Comparison between the experimentally obtained fracture toughness and the predicted values

5.3.4 Model validation and applications

The proposed model was implemented into a finite element method code, COMSOL Multiphysics. To validate the predictive ability of the developed model, the shear strength and shear performance of the

CPB-rock interface at different temperatures are simulated, and the numerical simulation results are compared with the experimental data.

5.3.4.1 Model validation

5.3.4.1.1 Numerical models and parameters

A 3-D model with a size of 60×60×60 mm is built, and the size is almost the same with the samples used for the direct shear test (Fang and Fall, 2018). The model consists of two parts, namely CPB and rock, as shown in Figure 5.34. The normal stress in the direct shear test is indicated as F, which is applied on plane 10. Besides, the plane 7 is applied with a prescribed displacement of 6 mm, while planes 2 and 8 (plane 8 is set invisible to show the inner interface) are the symmetrical ones. To avoid nonphysical oscillations, the mesh at the destination side of the interface (plane 9, CPB) should be at least two times finer than that at source (plane 4, rock). In this study, the maximum element size at plane 4 is 0.075 mm, while that at plane 9 is 0.0375 mm.

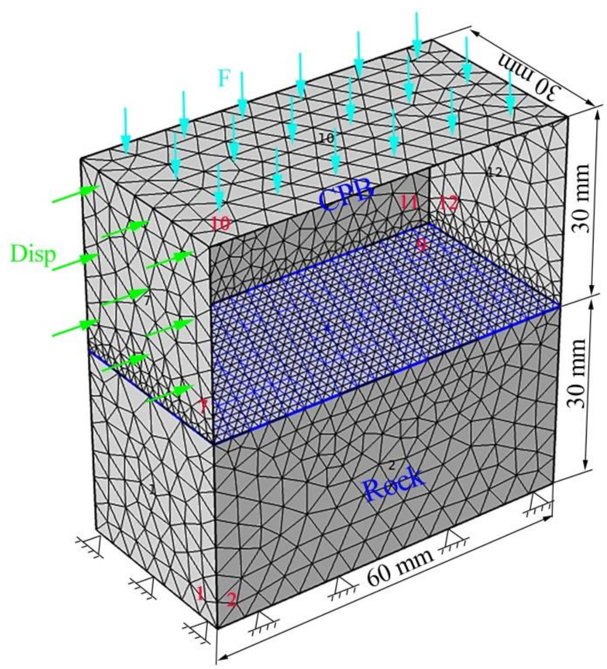

Figure 5.34 Three-dimensional model of the CPB-rock interface

Two cases are simulated to validate the predictability of the proposed model in this section. Since there are no studies on the thermal effect on the shear characteristics of the CPB-rock interface published by other anthors, the validation is carried out by comparing the numerical simulation results with the results of experimental tests conducted by the authors. Model parameters for these two cases are tabulated in Table 5.4.

Table 5.4 Input parameters of CZM

Parameters \ Temperature- Curing time	Case study 1			Case study 2			
	2°C - 3days	20°C - 3days	35°C - 3days	20°C - 1day	20°C - 3days	20°C - 7days	20°C - 28days
Fracture toughness of mode I $K_{\mathrm{I}c}$ ($kPa\sqrt{m}$)	1.01	2.75	3.49	1.52	2.75	3.04	4.39
Fracture toughness of mode II $K_{\mathrm{II}c}$ ($kPa\sqrt{m}$)	2.09	6.50	8.45	1.86	6.50	8.86	16.1
Elastic shear stiffness (10^3 kN/m^3)	38.1	121.5	235.3	50.7	121.5	192.4	743.8
Penalty stiffness P_n (10^3 kN/m^3)	236.9	543.8	873.9	291.1	543.8	683.2	2142
Pure shear strength τ_{2c} (kPa)	27.6	42.7	47.8	22	42.7	65	91.3
Pure tensile strength σ_{1c} (kPa)	47.9	73.9	82.7	38.1	73.9	112.6	158.2
Friction angle φ	24.6	25.6	28.3	25.2	25.6	26.6	32.2
Normal to shear ratio n_τ	0.160	0.223	0.269	0.174	0.223	0.281	0.347

5.3.4.1.2 Cases study 1: Effect of temperature on the shear strength of the CPB-rock interface

As mentioned in the introduction section, the variation in temperature is a common situation that CPB structures will go through, and many previous studies have concluded that the mechanical behaviour of CPB is sensitive to thermal changes (Aldhafeeri et al., 2016; Wang et al., 2016; Fang and Fall, 2018). To numerically investigate the difference in the shear behaviour and strength of the CPB-rock interface with temperature, the samples cured at temperatures of 2°C, 20°C and 35°C for three days are simulated.

The numerical results of the shear strength of the CPB-rock interface with temperature are displayed in Figure 5.35 and Figure 5.36, respectively. It can be observed that the model can simulate the contribution of temperature to the shear strength of the CPB-rock interface: with the temperature increasing from 2°C to 20°C and 35°C, the shear strength rises from 50 kPa to 66 kPa and 76 kPa, respectively (with a normal stress of 50 kPa). This increase in the shear strength with temperature is due to the acceleration effect of temperature on the rate of the cement hydration (Fall et al., 2010; Fang and Fall, 2018).

The comparison of the shear strength of the CPB-rock interface obtained from experimental test and numerical simulation is illustrated in Figure 5.36. As expected, the result indicates that the temperature can significantly improve the shear strength of the CPB-rock interface. In addition, the estimated shear strengths of the CPB-rock interface are in good agreement with the experimental test conducted by Fang and Fall (2018), regardless of the curing temperature and the applied normal stress. This means the proposed model is able to predict the shear strength of the CPB-rock interface accurately.

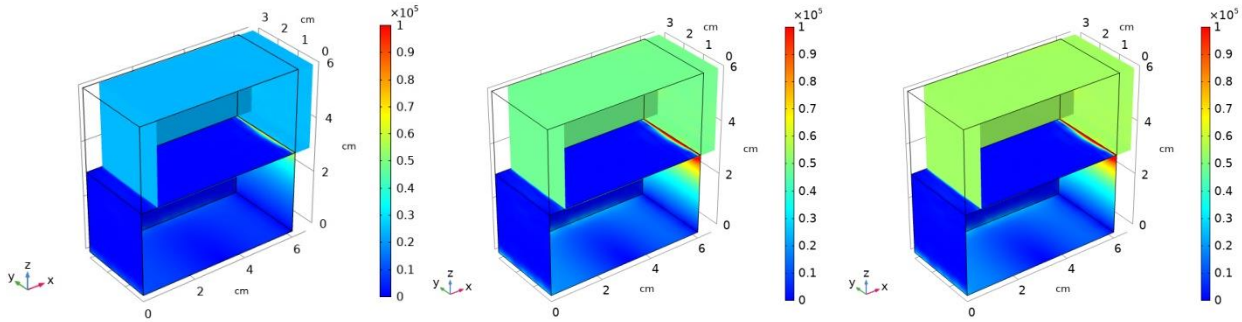

(a) Temperature: 2°C (b) Temperature: 20°C (c) Temperature: 35°C

Figure 5.35 Shear performance of the CPB-rock interface under different temperature (curing time: 3 days; normal stress: 50 kPa)

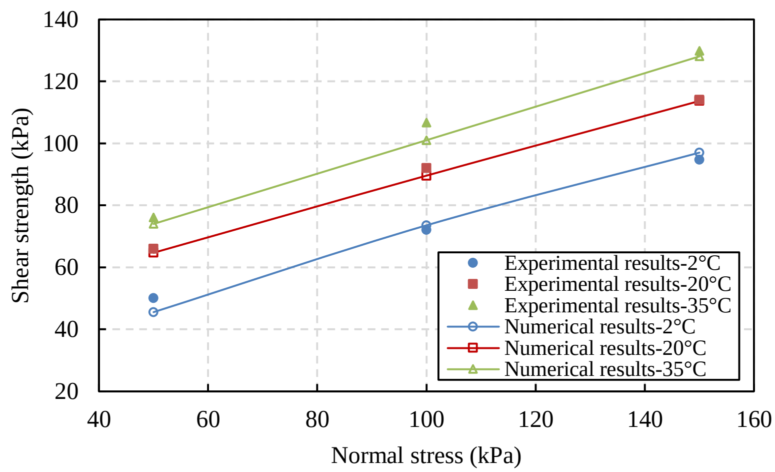

Figure 5.36 Comparison of shear strength obtained from numerical simulation and experimental test (curing time: 3 days)

5.3.4.1.3 Cases study 2: Effect of curing time on the shear behaviour of the CPB-rock interface

With the passage of time, the mechanical properties of CPB evolve with the cement hydration (Kesimal et al., 2005; Ouellet et al., 2007; Yilmaz et al., 2015). Similarly, the shear strength properties of the CPB-rock interface were also experimentally attested to be related to the ages of samples (Nasir and Fall, 2008; Koupouli et al., 2016; Xu et al., 2019). Therefore, to elaborate on the evolution of the time-dependent parameters, it is necessary to analyze the shear characteristics of the CPB-rock interface with time. Herein, the shear behaviour of the interface samples cured at a temperature of 20°C for 1 day, 3, 7 and 28 days are numerically simulated. The shear stress-shear displacement curves of the CPB-rock interface with time are shown in Figure 5.37.

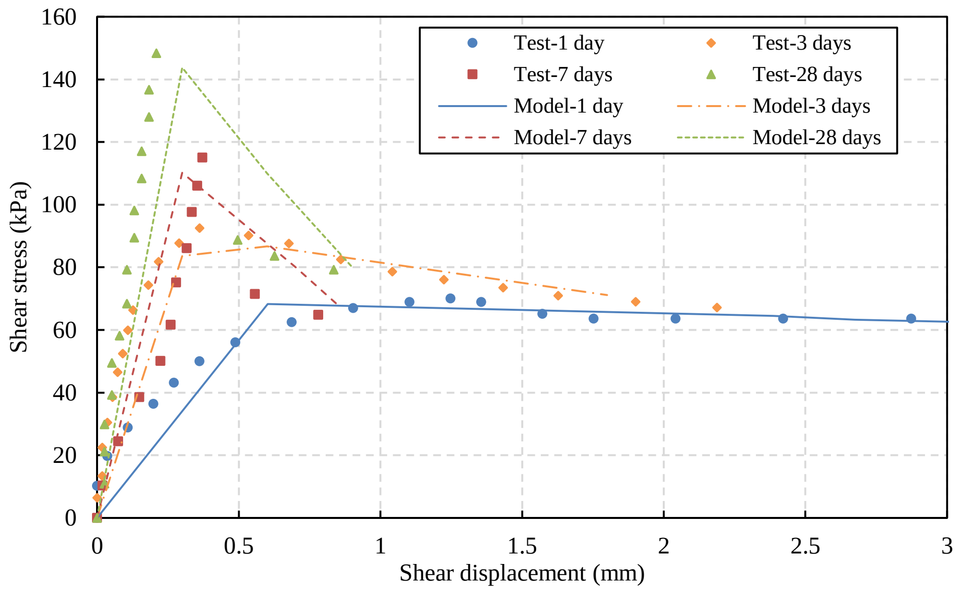

Figure 5.37 Comparison of the shear behaviour of the CPB-rock interface obtained from numerical simulation and experimental test (normal stress: 100 kPa)

The numerical simulation result in Figure 5.37 illustrates an increasing tendency of the shear stiffness and the shear strength with time, which is mainly attributed to the improvement of the matrix suction and the increasing amount of C-S-H, as a result of the cement hydration progression. In addition, the higher peak shear stress with time observed in Figure 5.37 is because of the increasing amount of gypsum and C-S-H generated by cement hydration (Metha, 1986; Pokharel and Fall, 2013). Firstly, the precipitation of the gypsum refines the pore structure of CPB, and this will enlarge the contacting area between CPB and rock. Meanwhile, the larger amount of C-S-H enhances the bonding force between CPB and rock. Moreover, compared with early-age interface samples, the shear stress-shear displacement curves of the samples cured for 7 days and 28 days are pronounced in softening behaviour. This is ascribed to the contribution of cement hydration to the development of the fracture toughness, namely, modes I and II fracture toughness increase with curing time, as introduced in section 5.3.3.2. In a word, both the shear strength and the shear behaviour of the CPB-rock interface obtained by numerical simulation and experimental testing depict good agreement, which proves the predictability of the proposed thermal-chemo-mechanical CZM.

5.3.4.2 Sensitivity analysis

Sensitivity analysis is an effective method to testify the response of a numerical model to the changes of certain determining factors. For example, adhesion & friction angle, fracture toughness, and shear stiffness are several important parameters in terms of this thermal-chemo-mechanical CZM. Making sure the consistency of other parameters is necessary when conducting a sensitivity analysis so as to investigate the sensitivity of the model to the target parameter precisely. In this study, to validate the reliability of the suggested thermal-chemo-mechanical CZM, a series of sensitivity analyses were performed regarding the adhesion & friction angle, modes I and II fracture toughness of the CPB-rock interface.

5.3.4.2.1 Effect of adhesion & friction angle of the interface

By affecting the cement hydration progression, the variation in temperature has a significant influence on the evolution of the mechanical properties of CPB, among which, friction angle and cohesion are the most important ones (Yilmaz et al., 2003; Wang et al., 2016). The existence of friction angle and adhesion at the interface are the causes of the shear resistance at the CPB-rock interface. To date, the development of these two properties of the CPB-rock interface under Multiphysics conditions has only been experimentally investigated by the authors (Fang and Fall, 2018, 2019, 2020). To analyze the response of the proposed CZM to the variation in friction angle and adhesion, CPB-rock interface samples cured at 20°C for 3 days were chosen for the sensitivity analysis. Figure 5.38 shows the shear stress-shear displacement curves (with different friction angle and adhesion) obtained by numerical simulation.

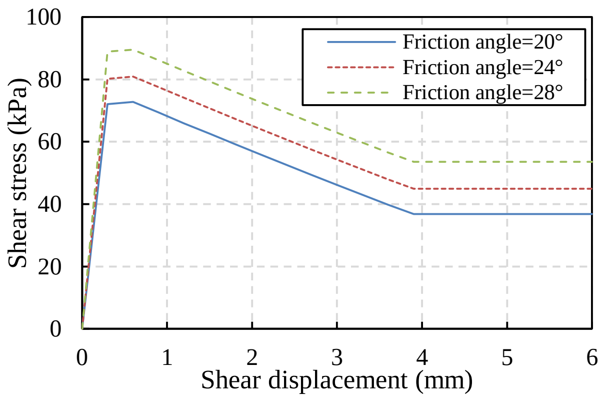

(a) Effect of friction angle (adhesion = 40 kPa)

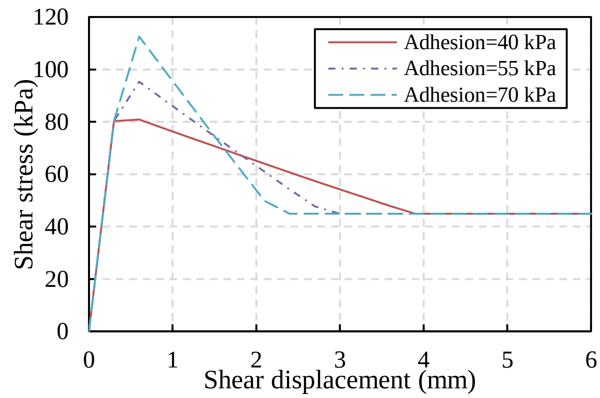

(b) Effect of adhesion (friction angle = 24°)

Figure 5.38 Sensitivity of the chemo-chemo-mechanical CZM to the change in adhesion & friction angle of the interface (normal stress: 100 kPa)

With the adhesion rising from 40 kPa to 55kPa and 70 kPa, the peak shear stress increases from 81 kPa to 95 kPa and 113 kPa, as can be clearly seen from Fig 5.38(b). In addition, the change in the adhesion has no effect on the residual strength of the interface sample, as expected. Instead, the residual strength is mainly determined by the friction angle. Specifically, it increases from 37 kPa to 54 kPa when the friction angle rises from 20° to 28° (Fig 5.38(a)). To sum up, the evolution of the friction angle and adhesion has significant effects on the shear behaviour of the interface sample, which can be well captured by the proposed CZM.

5.3.4.2.2 Effect of mode II fracture toughness

The fracture toughness of the CPB-rock interface is temperature/time-dependent as well, as indicated in Eq.(5-68) and Eq.(5-71). The direct shear test is mainly characterized by an in-plane shearing mode. As a result, the shear stress-shear displacement curves of the CPB-rock interface are majorly dominated by the mode II fracture toughness (Fang et al., 2020). As it is well known, the shear behaviour of the CPB-rock interface in field usually involves load transformation. Consequently, the arching effect, which is related to the stress redistribution, is a normal phenomenon encountered both in laboratory test and field measurement (Terzaghi, 1943; Cui and Fall, 2017). Taking the arching effect into consideration is important to the design of many geotechnical structures, such as retaining walls, tunnels, and CPB structures (Take and Valsangkar, 2001; Goel and Patra, 2008; Fahey et al., 2009). Therefore, it is necessary to verify the sensitivity of the proposed chemo-chemo-mechanical CZM to the change in the mode II fracture toughness. In this case, three numerical studies were performed, and except for the mode II fracture toughness, all other input parameters were determined based on the interface sample cured at 20°C for 7 days.

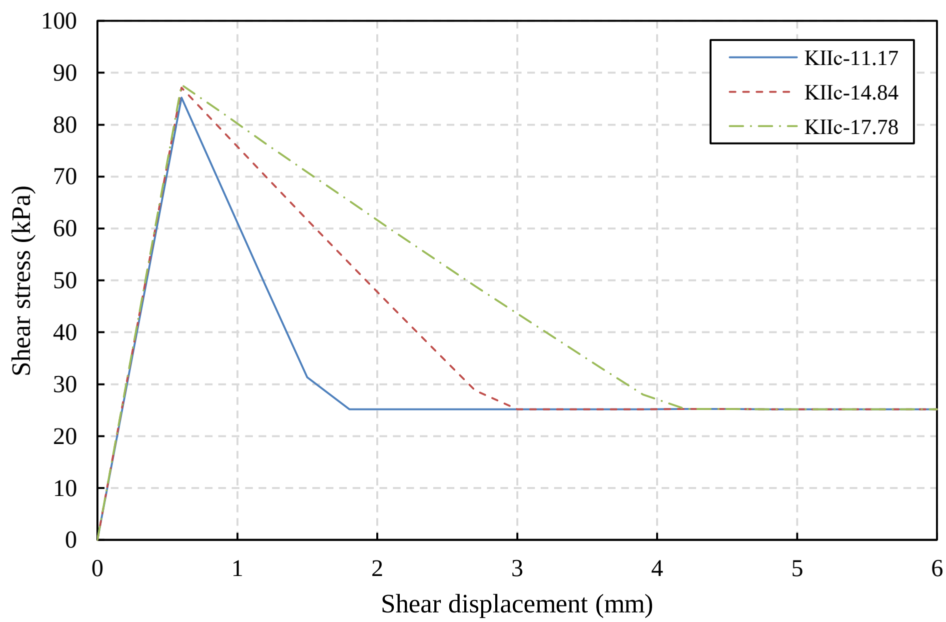

Figure 5.39 Sensitivity of the proposed CZM to mode II fracture toughness (normal stress: 50 kPa)

The numerical results shown in Figure 5.39 indicate that the change in mode II fracture toughness will mainly affect the softening behaviour of the CPB-rock interface. This is because as the mode II fracture toughness increases, the critical energy release rate rises (Fang et al., 2020). As a result, the softening behaviour becomes less obvious. In addition, the peak shear stress also experience a gradual improvement as the mode II fracture toughness increases from 11.17 $kPa\sqrt{m}$ to 17.78 $kPa\sqrt{m}$. It is because the mode II fracture toughness represents the capacity of structures to resist shear failure (Kuruppu et al., 2014). Moreover, the variation in the mode II fracture toughness has no effects on the development of the residual strength, as observed in Figure 5.39. This observation supports the argument that the residual strength is related to the friction angle, as introduced above. In a nutshell, this case proves the sensitivity of the proposed CZM to the change in mode II fracture toughness.

5.3.4.2.3 Effect of mode I fracture toughness

The underground CPB structure is subject to complex stress conditions. For example, when the adjacent ore body was mined out, the CPB is exposed to lateral earth pressure. In this condition, the tensile strength will exert considerable effects on the shear characteristics of the CPB-rock interface. To fully capture the shear behaviour of the interface under complex stress state, it is necessary for the thermo-chemo-mechanical CZM to respond to the variation in mode I fracture toughness. With the purpose of addressing the resistance of direct shear tests to mode I fracture toughness, a tensile test is numerically conducted. The geometry of the test sample is shown in Figure 5.40. An initial crack is observed at the interface, and the length of the crack is 34 mm. Besides, a pulling force F_1 is applied on the edge of CPB while another force F_2 is acting at the center of the model. Moreover, a prescribed displacement (6 mm) and a fixed constraint are applied on the left edge and the bottom plane, respectively.

Another three numerical analyses with different mode I fracture toughness are conducted as well. The mode I fracture toughness is determined as 2.7 $kPa\sqrt{m}$, 4.3 $kPa\sqrt{m}$ and 6.7 $kPa\sqrt{m}$ respectively, while the other parameters are the same with 3-day interface sample, as indicated in Table 5.4. The evolution of the force F_1 with vertical displacement and the ultimate crack length (vertical displacement at the edge equals to 6 mm) are presented in Figure 5.41.

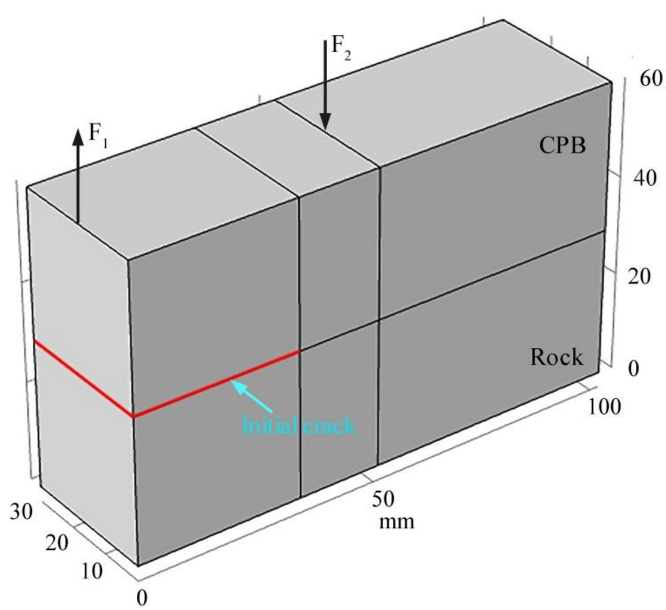

Figure 5.40 Geometry of the model

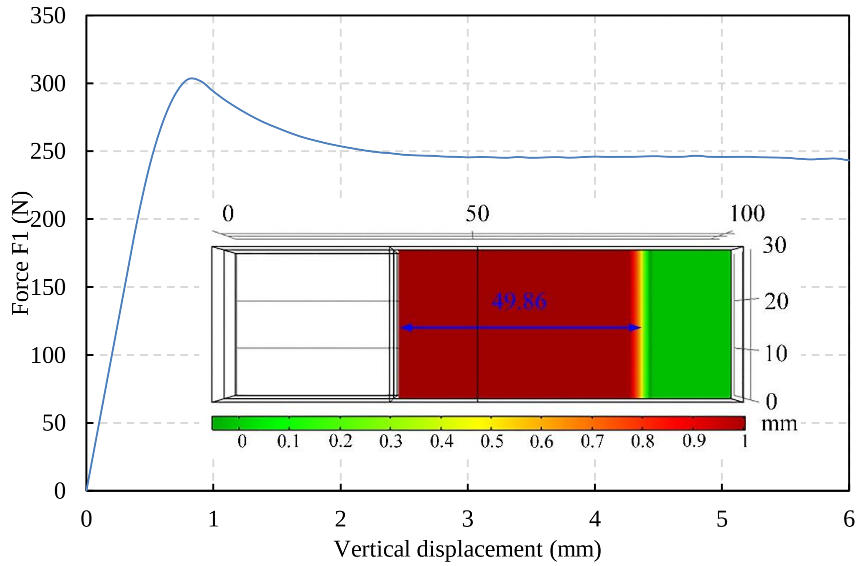

(a) Test 1 ($K_{\mathrm{Ic}} = 2.7\ kPa\sqrt{m}$)

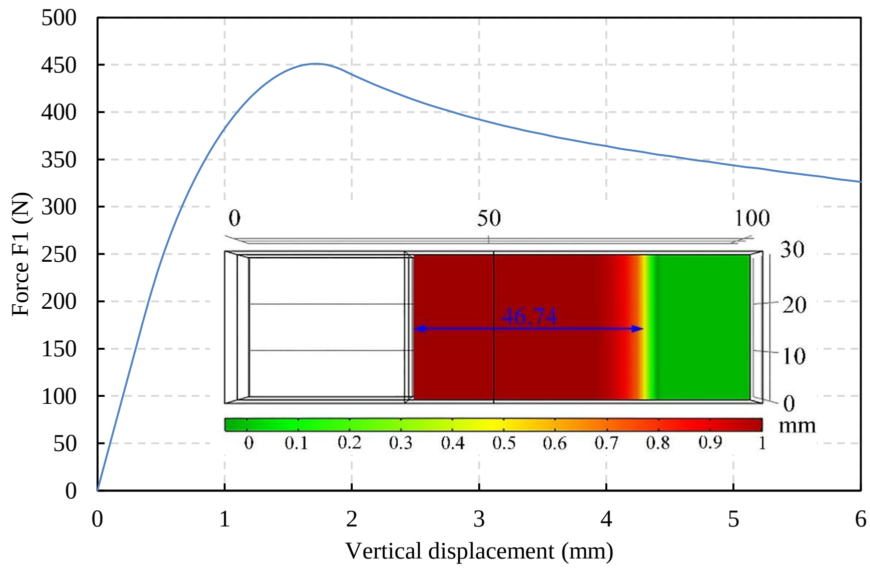

(b) Test 2 ($K_{\mathrm{Ic}} = 4.3\ kPa\sqrt{m}$)

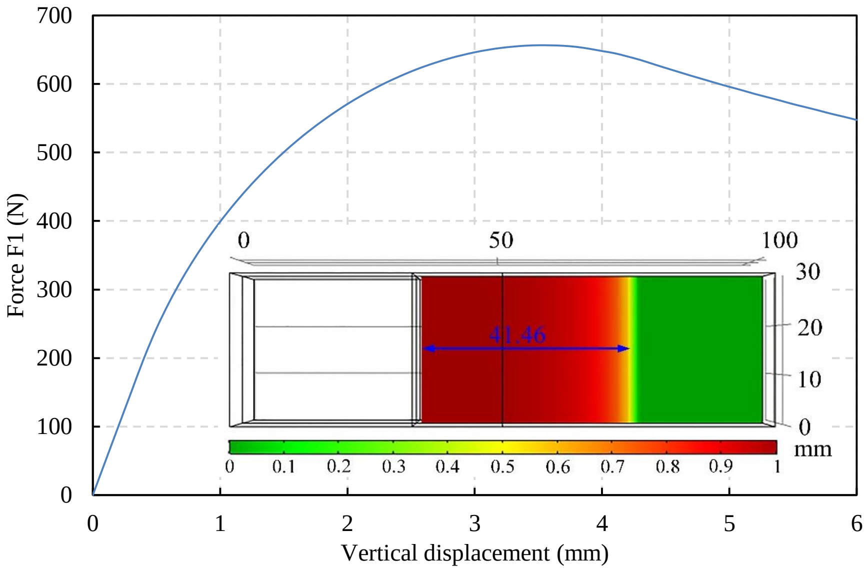

(c) Test 3 ($K_{\mathrm{I}c} = 6.7\ kPa\sqrt{m}$)

Figure 5.41 Numerical results with different mode I fracture toughness

A higher mode I fracture toughness represents a higher capacity of interlaminar structures to resist the tensile failure (Kuruppu et al., 2014). This argument is clearly supported by the obtained numerical results: the peak force of F_1 experiences a significant improvement from 303 N to 656 N as the mode I fracture toughness ascends from 2.7 $kPa\sqrt{m}$ to 6.7 $kPa\sqrt{m}$. Besides, the critical vertical displacement at which F_1 peaks varies with mode I fracture toughness. In detail, the critical vertical displacement is 0.8 mm in the first test, and it goes up to 3.5 mm when the mode I fracture toughness increases to 6.7 $kPa\sqrt{m}$. Moreover, it can be observed from Figure 5.41 that with the increase in the mode I fracture toughness, the ultimate crack length decreases from 49.86 mm to 41.46 mm. It means the proposed thermo-chemo-mechanical CZM has the ability to demonstrate the experimental results in response to the change in the mode I fracture toughness.

5.3.5 Summary and conclusion

A thermo-chemo-mechanical CZM is proposed in this paper to analyze the coupled effects of thermal, chemical and mechanical conditions on the shear behaviour of the CPB-rock interface. The following conclusions are reached:

- A concept of equivalent thermal age is firstly suggested. The evolutions of time-dependent parameters (e.g., adhesion and friction angle) of the CPB-rock interface are then described as functions of the equivalent thermal age. Finally, a thermo-chemo-mechanical CZM is put forward to describe the shear behaviour of the CPB-rock interface cured at different temperatures.

- The fracture toughness (including mode I and mode II) of the CPB-rock interface cured at temperatures of 2°C, 20°C and 35°C is also experimentally investigated with SCB testing. Thereafter, predictive equations based on the equivalent thermal age are developed to predict the evolution of the modes I and II fracture toughness.
- By implementing the bilinear separation law into CZM, the shear behaviour of the CPB-rock interface cured for different times are well captured. In addition, the shear strengths of the interface under different thermal conditions obtained by numerical simulations are in good agreement with the experimental results.
- The sensitivity analyses indicate that the proposed CZM is sensitive to the variations in friction angle, adhesion and modes I and II fracture toughness.

The thermo-chemo-mechanical CZM can be used to predict the bearing capacity of the CPB-rock interface at different temperatures, and this will help to design safe CPB structures in the field.

Acknowledgements

The University of Ottawa, the China Scholarship Council as well as the Natural Sciences and Engineering Research Council of Canada are greatly acknowledged for their financial support.

5.3.6 Reference

Abbasy F (2009) Thermal Conductivity of Mine Backfill. Concordia University, Montreal, Quebec, Canada.

Abrate S, Ferrero JF, Navarro P (2015) Cohesive zone models and impact damage predictions for composite structures. Meccanica, 50(10):2587-2620.

Aldhafeeri Z, Fall M, Pokharel M, Pouramini Z (2016) Temperature dependence of the reactivity of cemented paste backfill. Appl. Geochem. 72:10-19.

Ayatollahi M, Aliha M (2004) Fracture parameters for a cracked semi-circular specimen. Int. J. Rock Mech. Min. Sci. 41:20-25.

Ayatollahi M, Aliha M (2006) On determination of mode II fracture toughness using semi-circular bend specimen. Int. J. Solids Struct. 43(17):5217-5227.

Aubertin M, Li L, Arnoldi S, Belem T, Bussière B, Benzaazoua M, Simon R (2003) Interaction between backfill and rock mass in narrow stopes. Soil and rock America, 1:1157-1164.

Barenblatt GI (1962) The mathematical theory of equilibrium cracks in brittle fracture. Advances in applied mechanics, 7:55-129.

Belem T, Harvey A, Simon R, Aubertin M (2004) Measurement and prediction of internal stresses in an underground opening during its filling with cemented fill. Proceedings of the 5th Int. Symp. on Ground support in Mining and Underground Construction. Villaescusa & Potvin (eds.), 28-30 September 2004, Perth, Western Australia, Australia, Tayler & Francis Group, London, pp. 619-630.

Buckby T, Black S, Coleman ML, Hodson ME (2003) Fe-sulphate-rich evaporative mineral precipitates from the Rio Tinto, southwest Spain. Mineral. Mag. 67(2):263-278.

Camanho PP, Matthews FL (1999) Delamination onset prediction in mechanically fastened joints in composite laminates, J. Compos. Mater. 33:906–927.

Camanho PP, Davila CG, De Moura M (2003) Numerical simulation of mixed-mode progressive delamination in composite materials. J. Compos. Mater. 37(16):1415-1438.

Celestin JCH, Fall M (2009) Thermal conductivity of cemented paste backfill material and factors affecting it. International Journal of Mining Reclamation and Environment, 23(4):274-290.

Chandra N, Li H, Shet C, Ghonem H (2002) Some issues in the application of cohesive zone models for metal–ceramic interfaces. Int. J. Solids Struct. 39(10):2827-2855.
Chong K, Kuruppu M (1984) New specimen for fracture toughness determination for rock and other materials. Int. J. Fract. 26(2):R59-R62.
Comsol (2018) Comsol Multiphysics 5.4 <http://www.comsol.com>.
Cui L, Fall M (2015) A coupled thermo–hydro-mechanical–chemical model for underground cemented tailings backfill. Tunnelling Underground Space Technol. 50:396-414.
Cui L, Fall M (2016) An evolutive elasto-plastic model for cemented paste backfill. Comput. Geotech. 71:19-29.
Cui L, Fall M (2017) Multiphysics modeling of arching effects in fill mass. Comput. Geotech. 83:114-131.
Cui L, Fall M (2018) Modeling of self-desiccation in a cemented backfill structure. Int. J. Numer. Anal. Methods Geomech. 42(3):558-583.
Davila CG, Rose CA, Camanho PP (2009) A procedure for superposing linear cohesive laws to represent multiple damage mechanisms in the fracture of composites. Int. J. Fract. 158:211–223.
De Schuttera G (1999) Hydration and temperature development of concrete made with blast-furnace slag cement. Cem. Concr. Res. 29(1):143-149.
Dimitri R, Trullo M, De Lorenzis L, Zavarise G (2015) Coupled cohesive zone models for mixed-mode fracture: A comparative study. Eng. Fract. Mech. 148:145-179.
Dong W, Yang D, Zhou X, Kastiukas G, Zhang B (2017) Experimental and numerical investigations on fracture process zone of rock–concrete interface. atigue Fract. Eng. Mater. Struct. 40(5):820-835.
Fahey M, Helinski M, Fourie A (2009) Some aspects of the mechanics of arching in backfilled stopes. Can. Geotech. J. 46(11):1322–36.
Fall M, Célestin J, Pokharel M, Touré M (2010) A contribution to understanding the effects of curing temperature on the mechanical properties of mine cemented tailings backfill. Eng. Geol. 114(3):397-413.
Fang K, Fall M (2018) Effects of curing temperature on the shear behaviour of cemented paste backfill-rock interface. Int. J. Rock Mech. Min. Sci. 112:184-192.
Fang K, Fall M (2019) Chemically induced changes in the shear behaviour of the interface between rock and tailings backfill undergoing cementation. Rock Mech. Rock Eng. 52(9):3047-3062.
Fang K, Fall M (2020) Shear behaviour of the interface between rock and cemented backfill: effect of curing stress, drainage condition and backfilling rate. Rock Mech. Rock Eng. 53(1):325-336.
Fang K, Cui L, Fall M (2020) A Coupled Chemo-Elastic Cohesive Zone Model for Backfill-Rock Interface. Comput. Geotech. (under review).
Galaa AM, Thompson BD, Grabinsky MW, Bawden WF (2011) Characterizing stiffness development in hydrating mine backfill using ultrasonic wave measurements. Can. Geotech. J. 48(8):1174–1187.
Geubelle PH, Baylor J (1998) Impact-induced delamination of laminated composites: a 2D simulation. Composites Part B Engineering, 29(5):589–602.
Ghirian A, Fall M (2013) Coupled thermo-hydro-mechanical-chemical behaviour of cemented paste backfill in column experiments. Part I: Physical, hydraulic and thermal processes and characteristics. Eng. Geol. 164:195-207.
Goel S, Patra N (2008) Effect of arching on active earth pressure for rigid retaining walls considering translation mode. Int. J. Geomech. 8(2):123–33.
Grice T (2001) Recent mine developments in Australia. Proceedings of the 7th International Symposium on Mining with Backfill (MINEFILL), 351-357.
Helinski M, Fourie A, Fahey M, Ismail M (2007) Assessment of the self-desiccation process in cemented mine backfills. Can. Geotech. J. 44(10):1148–56.
Helinski M, Fahey M, Fourie A (2010) Behavior of cemented paste backfill in two mine stopes: Measurements and modeling. J. Geotech. Geoenviron. Eng. 137(2):171-182.
ISRM (2007) The complete ISRM suggested methods for rock characterization, testing and monitoring: 1974–2006. In: Ulusay R, Hudson JA (eds) Suggested methods prepared by the commission on testing methods. International Society for Rock Mechanics, Compilation Arranged by the ISRM Turkish National Group, Ankara, Turkey.
Jiang H, Qi Z, Yilmaz E, Han J, Qiu J, Dong C (2019) Effectiveness of alkali-activated slag as alternative binder on workability and early age compressive strength of cemented paste backfills. Constr. Build. Mater. 218:689-700.
Kesimal A, Yilmaz E, Ercikdi B, Alp I, Deveci H (2005) Effect of properties of tailings and binder on the short-and long-term strength and stability of cemented paste backfill. Mater. Lett. 59(28):3703-3709.
Koupouli NJ, Belem T, Rivard P, Effenguet H (2016) Direct shear tests on cemented paste backfill–rock wall and cemented paste backfill-backfill interfaces. J. Rock Mech. Geotech. Eng. 8(4):472-479.

Kuruppu M, Obara Y, Ayatollahi M, Chong K, Funatsu T (2014) ISRM-suggested method for determining the mode I static fracture toughness using semi-circular bend specimen. Rock Mech. Rock Eng. 47(1):267-274.

Landriault DA (1995) Paste backfill mix design for Canadian underground hard rock mining, Proc. of the 97th Annual General Meeting of the CIM Rock Mechanics and Strata Control Session, Halifax, Nova Scotia.

Lim I, Johnston I, Choi S (1993) Stress intensity factors for semi-circular specimens under three-point bending. Eng. Fract. Mech. 44(3):363-382.

Metha PK (1986) Concrete: Structure, Properties and Materials. Prentice-Hall Inc, Englewood Cliffs, N.J.

Mohammadi S, Owen DRJ, Peric D (1998) A Combined Finite/Discrete Element Algorithm for Delamination Analysis of Composites. Finite Elem. Anal. Des. 28:321–336.

Mudd G, Boger D (2013) The ever growing case for paste and thickened tailings—towards more sustainable mine waste management. Journal of Australasian Institute of Mining and Metallurgy, 2:56-59.

Nasir O, Fall M (2008) Shear behaviour of cemented pastefill-rock interfaces. Eng. Geol. 101(3):146-153.

Needleman A (1987) A continuum model for void nucleation by inclusion debonding. J. Appl. Mech. 54:525-531.

Needleman A (1990) An analysis of tensile decohesion along an interface. J. Mech. Phys. Solids, 38:289-324.

Neville AM (2011) Properties of concrete, 5th Edition: Longman London, 362 pp.

Ouellet S, Bussière B, Aubertin M, Benzaazoua M (2007) Microstructural evolution of cemented paste backfill: Mercury intrusion porosimetry test results. Cem. Concr. Res. 37(12):1654-1665.

Pokharel M, Fall M (2013) Combined influence of sulphate and temperature on the saturated hydraulic conductivity of hardened cemented paste backfill. Cem. Concr. Compos. 38:21-28.

Poole JL, Riding KA, Folliard KJ, Juenger MC, Schindler AK (2007) Methods for calculating activation energy for Portland cement. ACI Mater. J. 104:303–311.

Schindler AK (2004) Effect of temperature on hydration of cementitious materials. ACI Mater. J. 101(1):72-81.

Take W, Valsangkar A (2001) Earth pressures on unyielding retaining walls of narrow backfill width. Can. Geotech. J. 38(6):1220-30.

Terzaghi K. (1943) Theoretical soil mechanics. Wiley.

Tvergaard V, Hutchinson JW (1992) The relation between crack growth resistance and fracture process parameters in elastic-plastic solids. J. Mech. Phys. Solids, 40:1377–1397.

Wang Y, Fall M, Wu A (2016) Initial temperature-dependence of strength development and self-desiccation in cemented paste backfill that contains sodium silicate. Cem. Concr. Compos. 67:101-110.

Wong LNY, Guo TY, Lam WK, Ng JYH (2019) Experimental Study of Cracking Characteristics of Kowloon Granite Based on Three Mode I Fracture Toughness Methods. Rock Mech. Rock Eng. 1-19.

Wu D, Fall M, Cai SJ (2012) Coupled Modeling of Temperature Distribution and Evolution in Cemented Tailings Backfill Structures that Contain Mineral Admixtures. Geotech. Geol. Eng. 30(4):935-961.

Wu D, Fall M, Cai SJ (2013) Numerical modelling of thermally and hydraulically coupled processes in hydrating cemented tailings backfill columns. Int. J. Min. Reclam. Env. 28:173–199.

Xie D, Waas AM (2006) Discrete cohesive zone model for mixed-mode fracture using finite element analysis. Eng. Fract. Mech. 73(13):1783-1796.

Xu X, Needleman A (1993) Void nucleation by inclusion debonding in a crystal matrix. Modell. Simul. Mater. Sci. Eng. 1:111–132.

Xu X, Fall M, Alainachi I, Fang K (2019) Characterisation of fibre-reinforced backfill/rock interface through direct shear tests. Geotechnical Research, 1-15.

Yilmaz E, Belem T, Bussière B, Mbonimpa M, Benzaazoua M (2015) Curing time effect on consolidation behaviour of cemented paste backfill containing different cement types and contents. Constr. Build. Mater. 75:99-111.

Yilmaz E, Kesimal A, Deveci H, Ercikdi B (2003) The factors affecting the performance of paste backfill; physical, chemical and mineralogical characterization. First Engineering Sciences Congress for Young Researcher (MBGAK003), Istanbul, 2003.

Chapter 6 Synthesis of the results and implication for CPB design

6.1 Introduction

The principal objective of CPB structure design is to ensure the safety of sustainable backfill operations and reduce the operating cost as much as possible. Given that the utilization of the arching effect (which is closely related to the shear behaviour of the CPB-rock interface) can decrease the overlying stress, the required strength of CPB and the barricade can be reduced. This means that the amount of cement consumed for the preparation of CPB can be decreased. Considering that the cost can be mitigated from 75% to 42% when the cement content drops from 9 wt.% to 3 wt.% (De Souza et al., 2003; Fall and Benzaazoua, 2003), it is promising to address the evolution of the shear strength properties of the interface. Therefore, the shear behaviour of the CPB-rock interface under multiphysics conditions is experimentally and numerically investigated in this study. The obtained experimental results of the shear strength properties of the CPB-rock interface, which are discussed in detail in Chapters 4 and 5, are firstly synthesized in section 6.2. Thereafter, a summary of the features and application of findings are provided in section 6.3. Lastly, the model application is demonstrated in section 6.4.

6.2 Shear behaviour of the CPB-rock interface under different loading conditions

The stability of CPB structures is affected by the mechanical strength of CPB, including the UCS of the CPB body and the shear strength of the CPB-rock interface. The shear strength of the interface tends to be one of the dominant factors in stability analysis, and the interaction between CPB and rock is associated with the external loading conditions or influencing factors, such as thermal, hydraulic, mechanic and chemical factors, based on which the interface behaviours are summarized as below.

The variation in temperature mainly comes from heat transfer and generation. The heat transfer can be further classified as heat advection (as a result of pore fluid flow) and heat conduction (as a result of temperature gradient), while the heat generation is due to the exothermic reaction of the cement hydration. The column tests conducted by Ghirian and Fall (2013; 2014) found that the heat released by the cement hydration can increase the temperature by 3°C to 5°C in CPB column (1.6 m height, 20 cm diameter) and this process dominates the change in temperature in the first 3 days (Qi and Fourie, 2019). In the field, the heat generated by the binder hydration can increase the temperature of the CPB mass by 30°C or more than this value (Fall et al. 2010). After that, the heat transfer between CPB and rock becomes the major contributor to the temperature variation. The experimental results shown in Section 4.3 indicate that both the shear strength and the shear strength properties (e.g., friction angle and adhesion) mainly increase with temperature (with an exception of the samples cured at 35°C for 28 days), as a result of the increased rate/degree of cement hydration and the enhanced self-desiccation. On the one hand, a higher rate/degree of the cement hydration corresponds to large amounts of cement hydration products, such as C-S-H, CH, and ettringite. The increasing quantity of C-S-H is beneficial to the acquisition of the binding force at the interface. Meanwhile, the precipitation of other products extends the contacting area between CPB and rock, which also contributes to a rise in the binding force. On the other hand, the enhanced self-desiccation with temperature helps to the increase in the effective stress at the interface. Besides, the increasing matrix suction at the interface also increases the peak shear stress and the shear strength parameters of the CPB-rock interface. In contrast, the lower shear strength of the interface samples cured at 35°C for 28 days is ascribed to the occurrence of the cross-over effect. In addition to the mechanical strength, the shear contraction experiences a decreasing tendency with temperature. The decreasing shear contraction is because of the finer pore structure of CPB, as a result of higher rate of the cement hydration. With respect to the interface samples cured for longer than 7 days, shear dilation increases with temperature as well. The pronounced shear dilation with temperature is due to the stronger asperity at the interface.

The chemical process or factor can be investigated from two aspects, namely the evolution of the cement hydration with time, and the effect of sulphate ions on the cement hydration. The volumetric deformation, which is a result of the cement hydration, is an important trigger to the consolidation of CPB, also known as the chemical shrinkage. The specific mechanism of the chemical shrinkage is that fewer products are generated than those being consumed. The obtained results in Section 4.2 and 4.5 indicate that the shear contraction of the samples decreases with the curing time regardless of the sulphate contents. The same phenomenon is also observed in Section 4.3. However, as for the effects of sulphate ions on the shear behaviour of the interface, it can be seen that for early-age samples (≤ 3 days), the shear contraction becomes more pronounced with increasing sulphate content because of the inhibition of sulphate ions on the cement hydration. Consequently, the majority of the water remained in CPB is drained away upon the normal stress is applied. After being cured for a longer period (≥ 28 days), the differently sulphated interface samples experience similar shear contractions. In contrast, the shear dilation occurs and usually increases with sulphate content. The decreasing shear dilation of the samples cured for 150 days is due to the physical damage caused by the excessive amount of expansive minerals. In terms of the influence of sulphate ions on the shear strength properties, it varies with curing time and initial sulphate content. For very early-age samples (≤ 3 days), the presence of sulphate ions can decrease the shear strength of the interface samples, and the negative effects become obvious with higher sulphate contents. However, after being cured for 7 days, the samples with 5000 ppm sulphate content present the highest shear strength.

The precipitation of an appropriate amount of expansive minerals leads to a finer pore structure at the interface. However, the highly sulphated samples show a lower shear strength compared with sulphate-free samples. The sulphate-induced reduction in the shear strength is attributed to two mechanisms: (i) a stronger inhibition effect of sulphate on cement hydration, and (ii) adsorption of sulphate by C-S-H. With the passage of time, the samples with 15000 ppm sulphate content appear the highest shear strength after 28 days and 90 days. The competing effects exist between the factors of shear strength increase (refinement of the pore structure of CPB, precipitation of more hydration products) and decrease (inhibition of cement hydration; sulphate absorption by C-S-H) as the initial sulphate content of the CPB increases.

After the placement of CPB into stopes, the magnitude of its self-weight affects the consolidation as well as the stress at the CPB-rock interface. Traditionally, the vertical stress in CPB is assumed to be equal to the self-weight of the overlying CPB body. The field test and numerical simulation conducted by Helinski et al. (2010) and Cui and Fall (2017) found that the vertical stress inside CPB is far lower than the self-weight of itself, which is known as the arching effect in CPB design. To investigate the effect of CPB's weight on the shear behaviour of the interface, certain stress is applied to simulate the self-weight in laboratory tests. Besides the self-weight of CPB, the consolidation is related to the drainage condition, which is determined by the property of the surrounding rock mass, especially its permeability. Therefore, to investigate the potential shear performance of the CPB-rock interface in the field, the effects of different curing stresses and drainage conditions on the interface shear behaviour are studied in Section 4.4. For interface samples cured under drained conditions, the increasing curing stress leads to a higher shear strength because of the stronger matrix suction as well as the lower thermal conductivity at the interface. For undrained samples, the mechanism of a higher curing stress to the improvement in the shear strength properties is ascribed to the rearrangement of particles. The degree of cement hydration rises with the curing stress as well. A higher curing stress and drained condition contribute to a decrease in the compressibility of the CPB. As a result of lower PWP and stronger asperities at the interface, the samples cured at a higher curing stress and/or in drained conditions experience obvious shear dilation during direct shear testing. The comparison between the results in Section 4.3 and Section 4.4 indicates that the application of the curing stress leads to the occurrence of shear dilation.

The shear behaviour of the interface samples with different rock bases is analyzed in Section 4.6, and it is found that the type of rock has a limited effect on the shear strength and performance of the interface. However, the interface roughness affects the shear behaviour and the shear strength properties of the interface samples significantly. For samples with a rough interface, the shear behaviour mainly depicts shear dilation, the increase of which is more pronounced with higher JRC value. The prominent shear dilation is a result of a larger asperity at the interface. Besides, both the shear strength and the adhesion of the interface increase with roughness, owing to a larger contacting area between the CPB and the concrete base.

The evolution of shear properties (shear strength, adhesion, and friction angle) of the CPB-rock interface under various loading conditions is presented in Table 6.1.

Table 6.1 Evolution of shear strength, adhesion and friction angle of the CPB-rock interface

<table>
<tr><th>Multiphysical factors</th><th>Shear strength</th><th>Adhesion and friction angle</th></tr>
<tr><td>Chemical
(short-term)</td><td>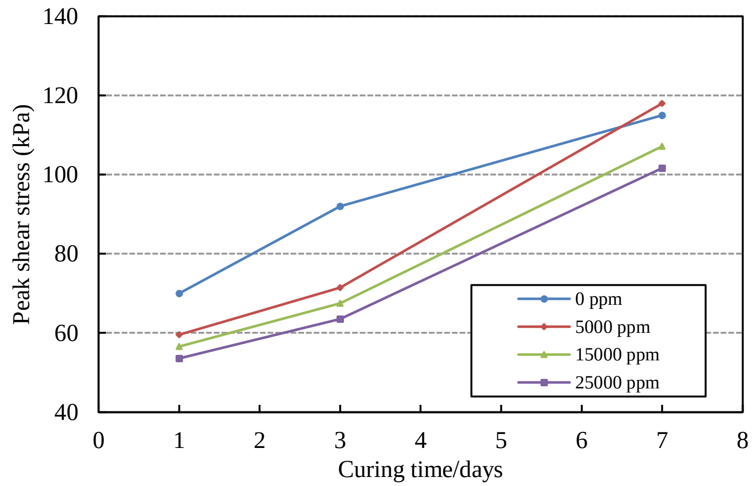
</td><td>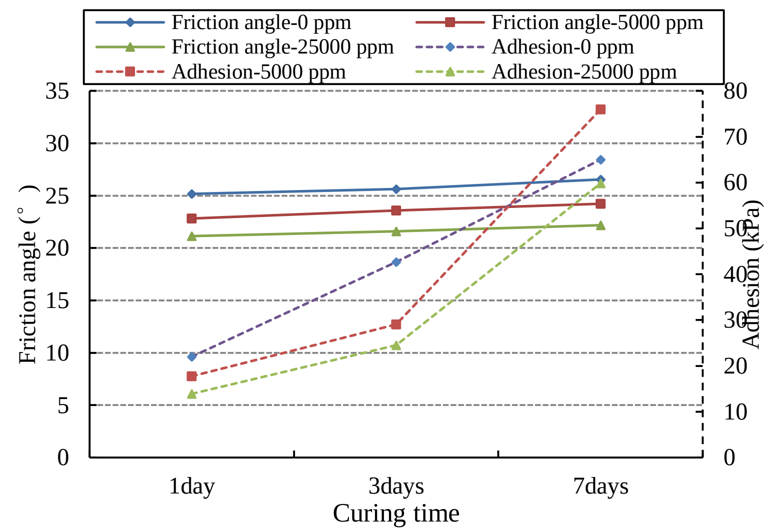
</td></tr>
<tr><td>Chemical
(long-term)</td><td>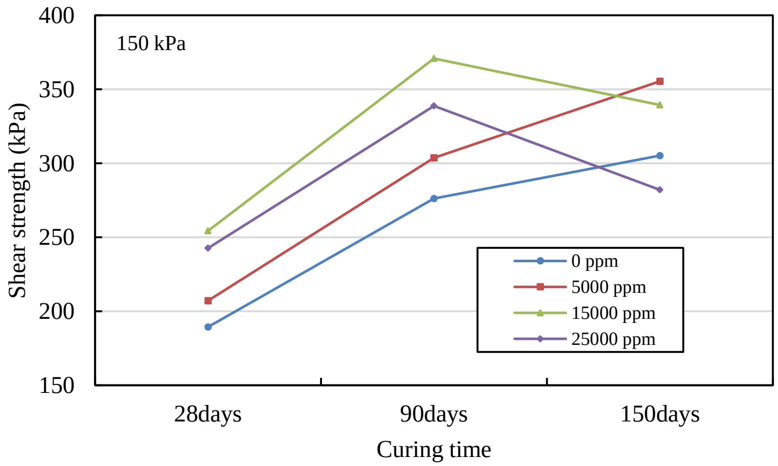
</td><td>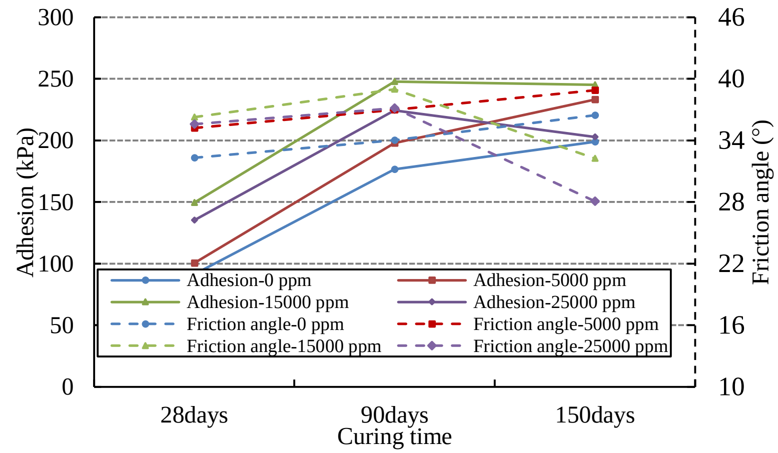
</td></tr>
</table>

Thermal

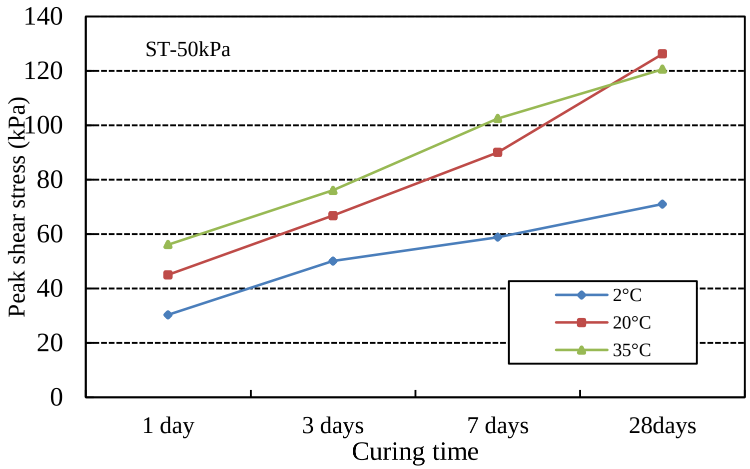

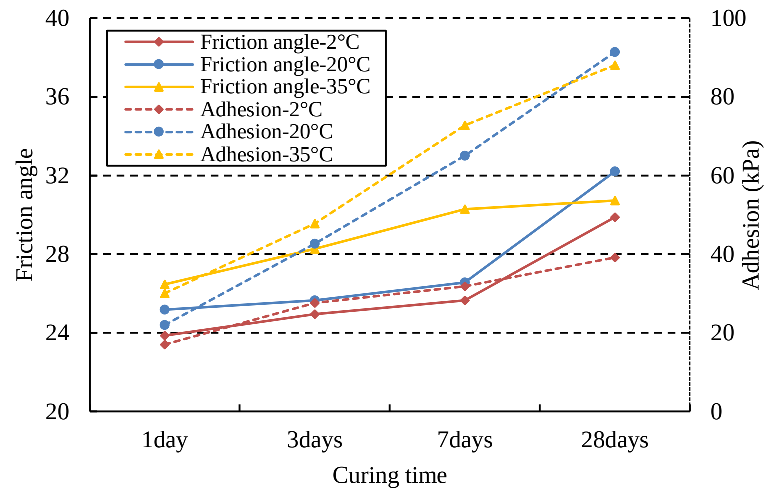

Mechanical and hydraulic

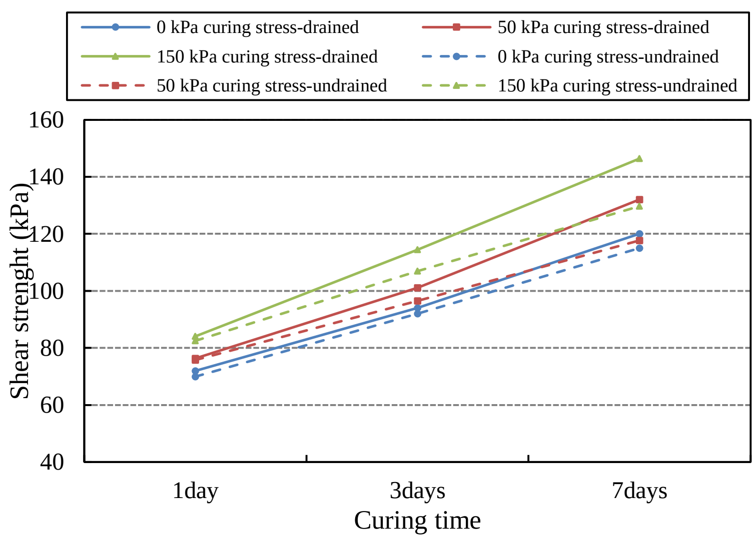

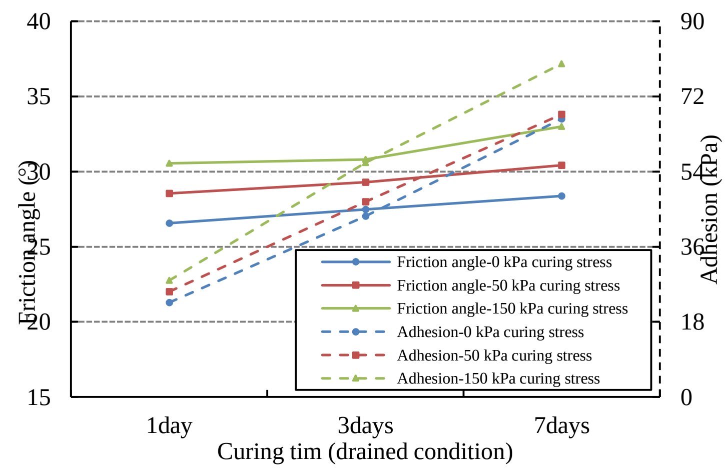

<table>
<tr>
<td></td>
<td></td>
<td>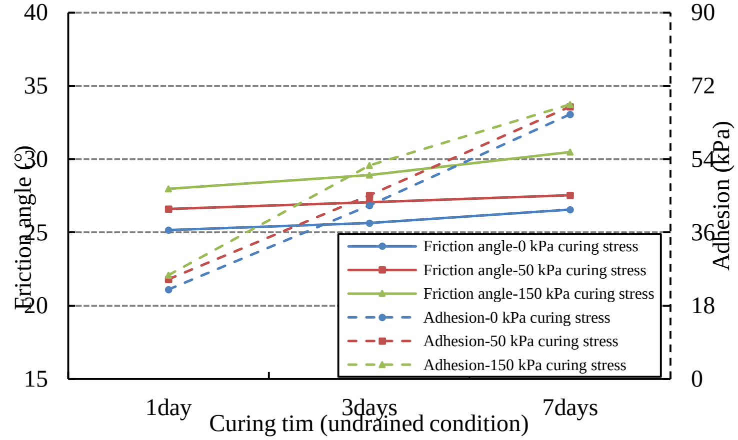
</td>
</tr>
<tr>
<td>Surface morphology</td>
<td>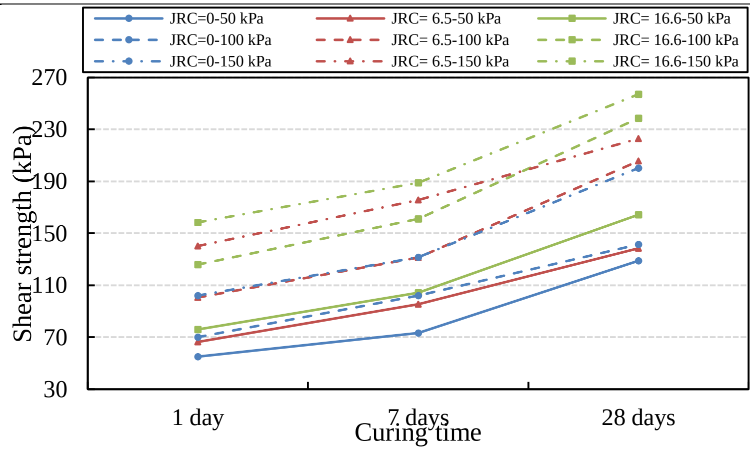
</td>
<td>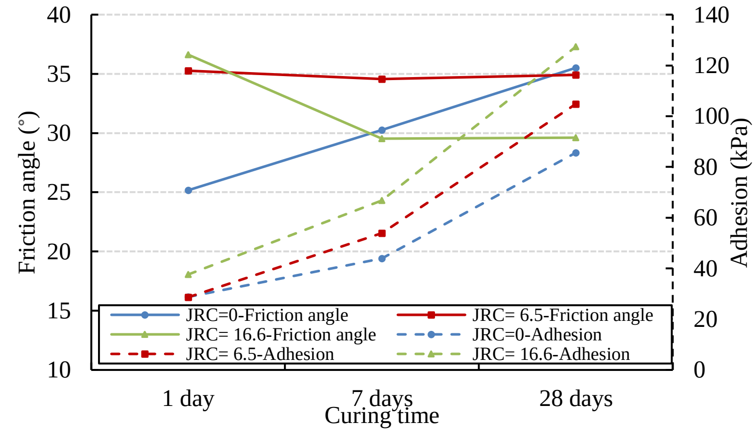
</td>
</tr>
</table>

6.3 Features and potential application of the findings to CPB design

6.3.1 Effect of chemical factor

The main effects of chemical factor on the shear performance of the CPB-rock interface include:

1. The chemical processes or factors can be further classified into two aspects, (i) the evolution of the cement hydration with time; and (ii) the influence of sulphate ions on the cement hydration;
2. The degree of the cement hydration increases with time. Therefore, the evolution of the shear strength of the CPB-rock interface is positively associated with time;
3. For early-age interface samples, the presence of sulphate ions inhibits the cement hydration, and the inhibition effect enhances with sulphate contents; for advanced-age samples, the slight increase in sulphate content benefits the acquisition of the shear strength.

Given the positive effect of the low sulphate content on the shear strength development of the CPB-rock interface, the dosage of the cement can be decreased, still adhering to the strength requirement. This is beneficial to the design optimization (in terms of the investment cost). As for the mine process water with high sulphate content, mines can lower the sulphate content by mixing it with fresh water. Thereafter, it can be used for the preparation of CPB. Otherwise, this highly sulphated content water will weaken the shear strength of the CPB-rock interface, therefore diminishing the stability of the CPB structure as well as increasing its design cost.

6.3.2 Effect of thermal factor

The primary features of temperature on the shear strength of the CPB-rock interface are summarized as:

1. The rate of cement hydration increases with temperature. As a result, more cement hydration products can be generated in a short time, and the required strength of the designed structure can be fast achieved.
2. Higher temperature speeds up the self-dessication which then benefits the fast acquisition of the effective stress and the matrix suction at the interface. Higher effective stress and matrix suction allow engineers to mitigate the amout of cement being used, thereby decreasing the CPB cost.
3. The occurrence of the crossover effect in cementitious materials is related to temperature. It will result in the reduction in the shear strength of the interface. Therefore, a competing effect exists in shear strength increase (acceleration of cement hydration) and decrease (crossover effect) due to the rise in temperature.

The amount of cement used for the CPB preparation can be reduced due to the higher effective stress and matrix suction at the interface as a result of the intense temperature-induced self-dessication. On the other hand, the fast-achieved strength of the CPB-rock interface (due to the acceleration effect of the temperature on the cement hydration) is beneficial to the reduction in the backfilling interval, and this will improve the mining productivity.

6.3.3 Effect of hydraulic and mechanical factors

The contributions of drainage condition and curing stress on the shear strength are listed as follows:

1. Regardless of the drainage condition, the increase in the curing stress benefits the shear strength acquisition of the interface. However, the mechanism resulting in the difference in the shear strength varies with drainage conditions. For drained samples, a higher curing stress contributes a lot to the increase in interface properties (e.g., shear strength, friction angle, and adhesion). This is because of the stronger matrix suction as well as lower thermal conductivity at the CPB-rock interface. For undrained samples, a higher curing stress can increase the degree of the cement hydration as well as rearrange the particles.
2. Compared with undrained condition, the drained condition is beneficial to the shear strength development. Both the effective stress and the matrix suction can be significantly improved due to the drainage of water.

Different sizes of the CPB structures correspond to various normal stresses at the interface. Therefore, the curing stress at the CPB-rock interface evolves with the backfilling height. Higher curing stress generally increases the shear strength properties of the interface. It is more suitable to design a narrow but higher CPB structure. With regards to the properties of the surrounding rock mass, rock with higher hydradulic conductivity will appear stronger interfacial strength. Under this condition, the cement usage can be decreased (compared to rock with lower hydraulic conductivity).

6.3.4 Effect of rock type and interface roughness

The main features of the surface morphology on the shear strength of the CPB-rock interface include:

1. The type of the rock has a limited influence on the shear performance of the interface. However, the interface roughness significantly affects the shear behaviour of the interface.
2. A rough interface can increase the shear strength and dilation because of the bigger asperity and larger contacting area at the interface. Besides, a concept of effective friction angle is proposed for rough interfaces. The estimation equation for the shear strength with JRC is also presented.

Rock type (with similar pore structure) will not affect the shear strength of the CPB-rock interface in the field. However, the shear strength of the CPB-rock interface varies with interface roughness. A rougher surface corresponds to a stronger interface structure. Considering the surface roughness of the surrounding rock mass in CPB design therefore is beneficial to the cost reduction.

6.3.5 Chemo-elastic cohesive zone model for CPB-rock interface

The main features of the developed chemo-elastic CZM include:

1. A concept of chemical-equivalent age is proposed. With the adoption of chemical-equivalent age, the effect of sulphate ions on the cement hydration is incorporated into the estimating equation for the binder hydration;
2. The fracture toughness of the CPB-rock interface with different sulphate contents are experimentally investigated;
3. The shear strength properties of the interface are expressed as a function of chemical-equivalent age. And the developed CZM can well capture the shear behaviour of the differently sulphated interface.

The chemo-elastic CZM can be used to analyze the arching effect in CPB. This will help us to predict the vertical stress and then to design the bearing capacity of the barricade. The shear strength of the interface between the sulphated CPB and rock can be estimated as well.

6.3.6 Coupled chemo-thermo-mechanical cohesive zone model for CPB-rock interface

The features of the coupled chemo-thermo-mechanical CZM for the CPB-rock interface are summarized as follows:

1. A coupled chemo-thermo-mechanical CZM is proposed to simulate the multiphysics processes at the interface;
2. The fracture toughness of the CPB-rock interface cured at different temperatures is experimentally investigated;
3. By implementing the linear traction separation law into CZM, the shear behaviours of the CPB-rock interfaces under different thermal conditions are numerically simulated.
4. The developed model is attested to be sensitive to the variations in both modes I and II fracture toughness.

The proposed CZM can predict the shear behaviour of the CPB-rock interface under coupled chemo-thermo-mechanical loading conditions. This can be utilized to analyze the magnitude of the arching effect in backfilled stopes, thus reducing the cost of CPB structure design.

6.4 Model application

To demonstrate the contribution of the shear resistance at the interface to the spatial stress distribution, the developed chemo-elastic CZM is incorporated with the coupled THMC model (Cui and Fall, 2015) and the consolidation model (Cui and Fall, 2016) to investigate the arching effect in CPB structures. Two cases are studied herein, namely the contribution of the shear resistance of the interface to the stress distribution and the size effect on the occurrence of the arching effect. The properties of the interface cured at a temperature of 20°C for 7 days (as shown in Table 5.4) are used as the input parameters for the modeling.

6.4.1 Effect of the shear resistance on the stress distribution in CPB

The arching effect is an important phenomenon that occurs in backfill structures in mines, and it is closely related to the interface behaviour between CPB and the surrounding rocks. To describe the importance of the shear resistance to the arching effect, the comparison of two studies (with and without CZM) is conducted. A 3-D model of the stope and the surrounding rock is shown in Figure 6.1. The stope has a size of 6 m in length and 8 m in width. In contrast, the length and the height of the drawpoints are both 2 m. The size of the surrounding rock mass is 16 m length × 16 m width × 22 m height. The symmetry boundary is applied on boundaries 2 and 14. Three monitoring lines, namely, AB (A (0,0,2), B (6,0,2)), CD (C (0,0,4), D (6,0,4)), EF (E (0,0,6), F (6,0,6)) are set inside to record the stress distribution. It is well known that the backfilling operation is usually divided into several stages to ensure the stability of the barricade. As a result, the stress distribution evolves with time. Therefore, to analyze the different stress distributions with backfilling height, CPBs with heights of 5 m, 12 m and 20 m are simulated.

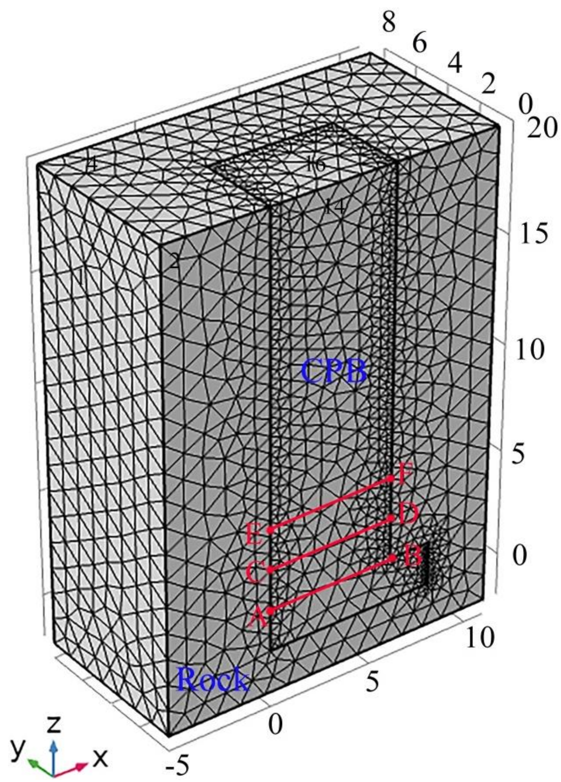

Figure 6.1 3-D model of the simulated stope

The modeling results of the stress distribution are presented in Figure 6.2 and Figure 6.3, with Figure 6.3 incorporating the CZM while the former one not. The comparison between these figures indicates that the

CZM can significantly affect the spatial distribution of stress inside CPB. It can be observed from Figure 6.2 that the stress contour in CPB without incorporating CZM tends to be flat. In contrast, the arching effect occurs in CPBs with CZM, especially in those with a high height. The less obvious arching effect in 5-meter CPB is due to the lower self-weight. In other words, it has the potential to form an arching structure, and if the vertical load is high enough, the arching effect will take place. In addition, the values of the stress at the monitoring line AB without CZM are much higher than those with CZM, which are explicitly shown in Figure 6.4. From the results, it can be seen that, with the same length and width, the increase in height can lead to a higher stress in CPB, whether CZM was adopted or not. However, for the stress in CPB without CZM (taking the stress at point A as an example, as shown in Figure 6.5), it increases linearly from 39.9 kPa to 260.1 kPa when the backfill height rises from 5 m to 20 m, while the stress in CPB with CZM only experiences a slight increase from 34.7 kPa to 66.1 kPa. Besides, after the formation of the arching effect in CPB, the increase in shear stress is not proportional to the increase in self-weight. For example, the stress at point A only increases by 5.2 kPa when the height of the CPB rises from 12 m to 20 m.

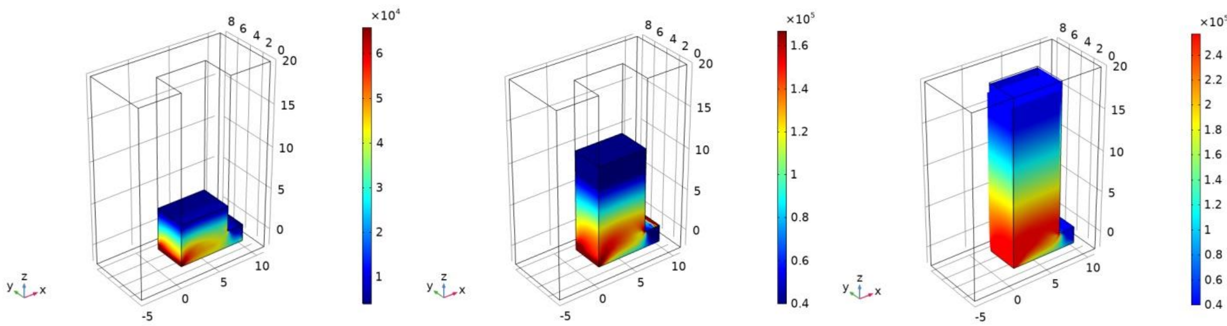

(a) Height: 5 m (b) Height: 12 m (c) Height: 20 m

Figure 6.2 Effect of backfill height on the stress distribution (without CZM)

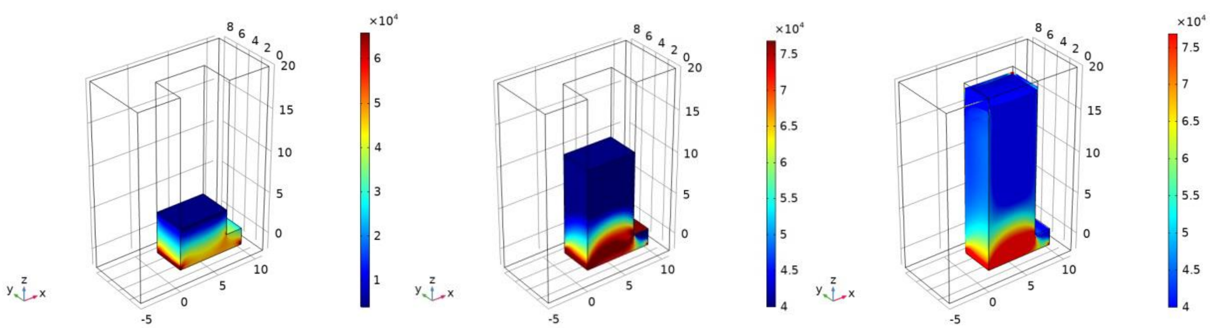

(a) Height: 5 m (b) Height: 12 m (c) Height: 20 m

Figure 6.3 Effect of backfill height on the stress distribution (with CZM)

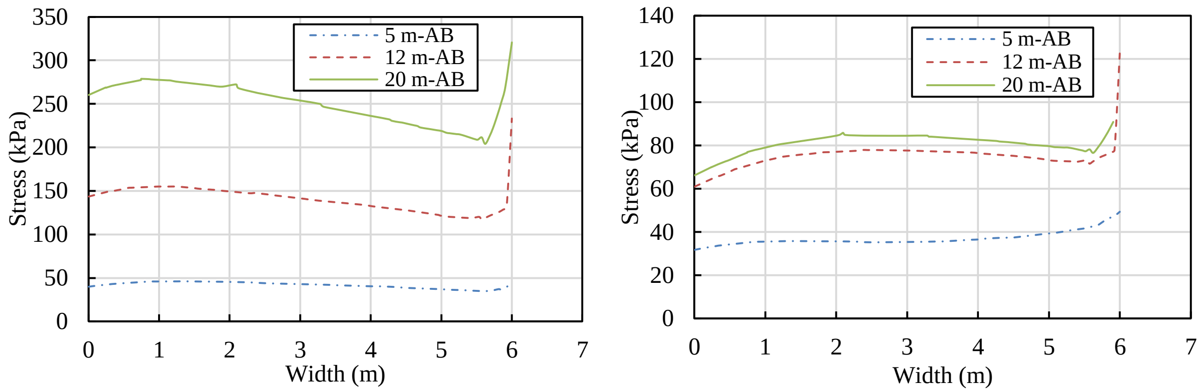

(a) Without CZM

(b) With CZM

Figure 6.4 Stress distributions at the monitoring line AB

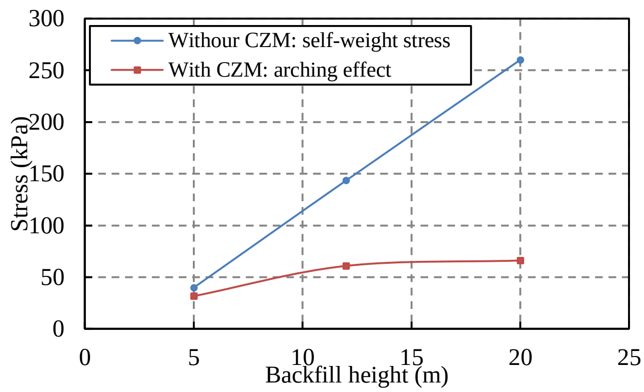

Figure 6.5 Stress evolution with backfilling height (Point A)

The highest stress at point B (with CZM), as shown in Figure 6.6, is because of the stress concentration caused by the existence of the drawpoints. It means further reinforcement is required at point B in the field. Figure 6.6 depicts the stress distribution at different monitoring lines, and from the figure, it can be seen that the stress concentration will vanish with the increase in height. Moreover, the arching effect will become less pronounced with increasing backfilling height. This argument is also supported by the isostress surface of 50 kPa, 60 kPa and 70 kPa in CPB, as shown in Figure 6.7.

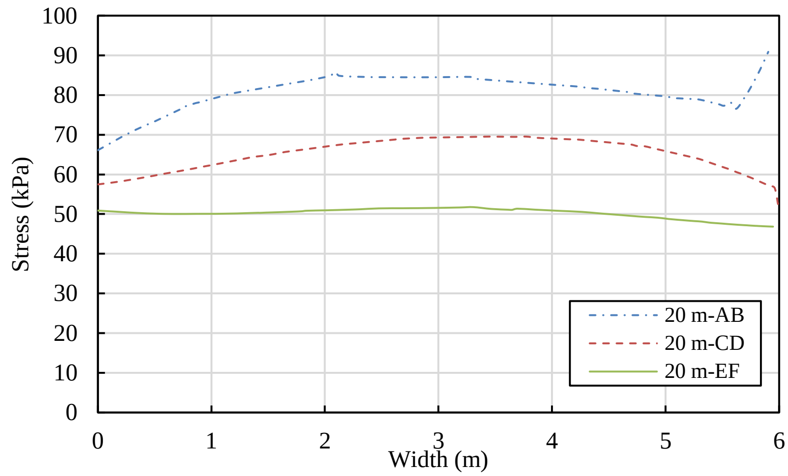

Figure 6.6 Stress distributions at different monitoring lines (with a backfill height of 20 m)

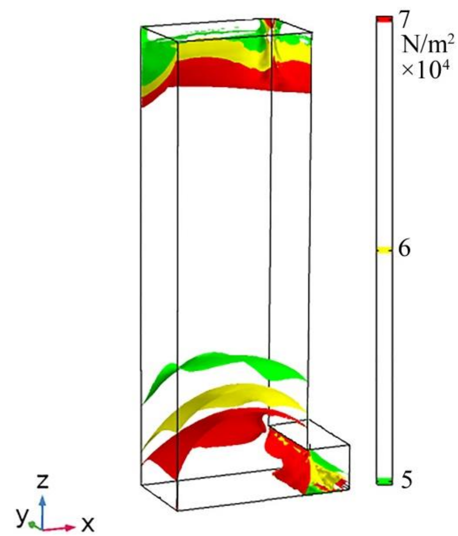

Figure 6.7 Isostress surface of 50 kPa, 60 kPa and 70 kPa (with a backfill height of 20 m)

6.4.2 Effect of the size of the stope on the arching effect

The occurrence of arching effect varies with different stope sizes. To investigate the influence of the size of the stope on the arching effect, CPB bodies with different widths (4 m, 6 m, 8m and 14 m, as shown in Figure 6.8) are simulated numerically by using the CZM. Two monitoring lines A'B' and A'C' (at the same height) are set at the surface of the CPB body. Given the different widths of the CPB body, the coordinates of point A' and C' vary with each other. Specifically, for point A', the coordinates are (0,2,2), (0,3,2), (0,4,2), (0,7,2), while for C', the coordinates are (3,2,2), (3,3,2), (3,4,2), (3,7,2) respectively. In contrast, the coordinates of point B' remain the same, namely (0,0,2).

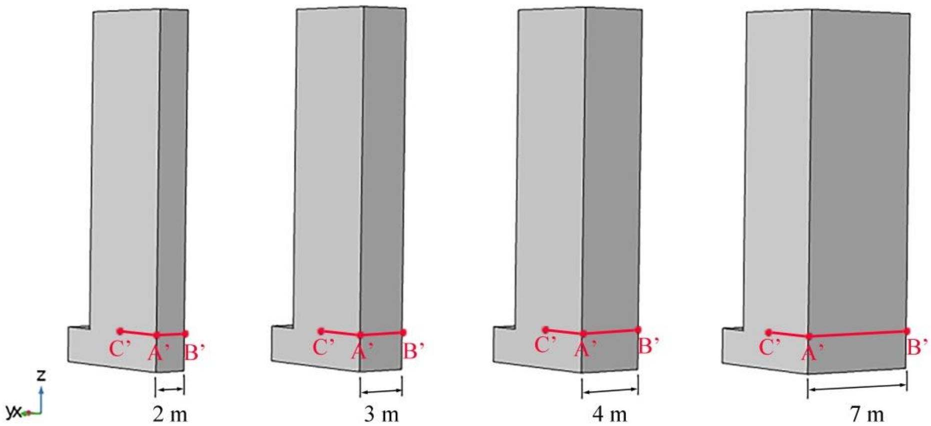

Figure 6.8 3-D model of CPB with different widths

The effects of width on stress distribution at CPB are numerically shown in Figure 6.9. It can be seen from the figure that with the width increasing from 4 m to 14 m, the stress at point B’ rises from 61.1 kPa to 70.6 kPa. Moreover, for CPB with a width less than certain value (8 m in this study), the stresses at line A’B’ keep rising from point A’ to point B’, as illustrated in Figure 6.10. This means the arching effect becomes more obvious with the increase in width. However, for CPB with a width of 14 m, the stress firstly increases from point A’ to point D’. Subsequently, it experiences a slight decrease from point D’ to point B’, as illustrated in Figure 6.10. It indicates that the arching effect becomes less obvious as the width increases. In other words, there is a critical value of width, and when the width is less than that the arching effect becomes more pronounced with width. However, if the width of CPB is larger than the critical value, the arching effect will be less obvious with increasing width. This can also be supported by the comparison of the stresses at lines A’B’ and A’C’, the results of which are shown in Figure 6.11. For the stope with a width of 4 m, the stresses at line A’C’ are generally higher than those at line A’B’ (Figure 6.11(a)). With the width increasing to 6m, the stresses at lines A’B’ and A’C’ are almost the same (Figure 6.11(b)). When the width of the stope reaches 8m, the stresses at line A’B’ exceed those at line A’C’. However, for the stope with a width of 14 m, the stresses at line A’C’ are clearly higher than those at line A’B’ again (Figure 6.11(d)).

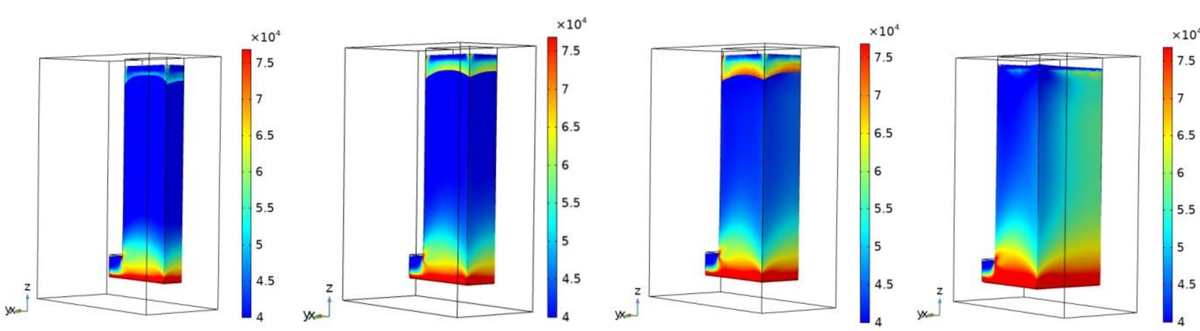

(a) Width: 4 m (b) Width: 6 m (c) Width: 8 m (d) Width: 14 m

Figure 6.9 Effect of backfill width on the stress distribution

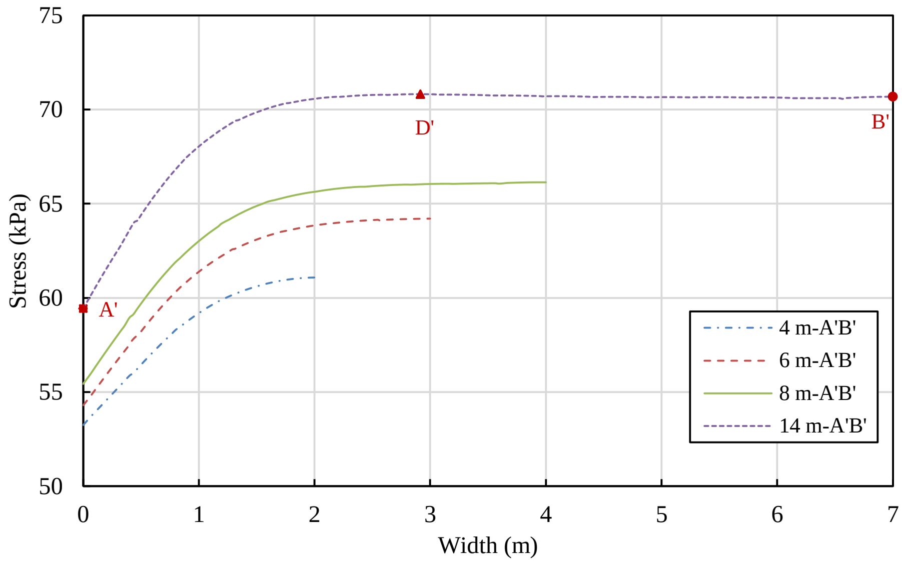

Figure 6.10 Stress distribution at the monitoring line A’B’

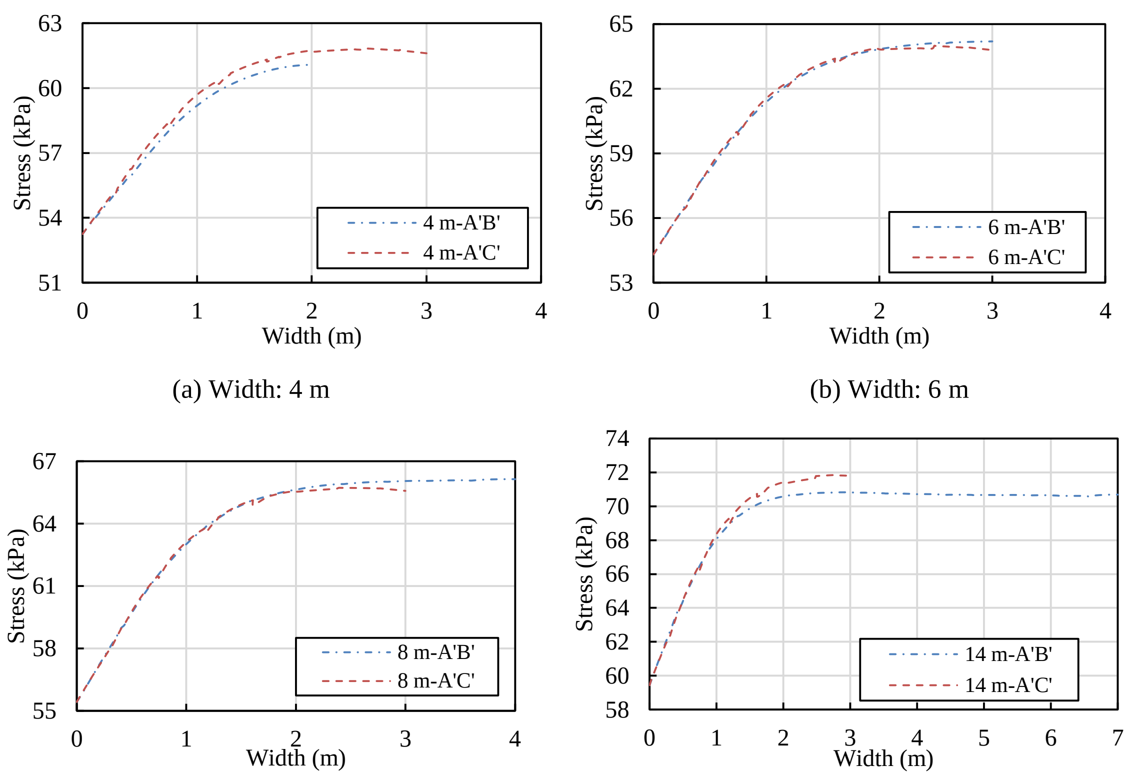

(a) Width: 4 m

(b) Width: 6 m

(c) Width: 8 m

(d) Width: 14 m

Figure 6.11 Comparison of the stress at monitoring line A’B’ and A’C’

6.5 References

De Souza E, Archibald JF, Dirige APE (2003) Economics and perspectives of underground backfill practices in Canadian mining. In: 105th annual general meeting of the Canadian institute of mining, Metallurgy and Petroleum, Montreal, Canada, 15p.

Fall M, Benzaazoua M (2003) Advances in predicting performance properties and cost of paste backfill. In: Proceedings on tailings and mine waste'03, Vail, USA, 73–85.

Cui L, Fall M (2015) A coupled thermo-hydro-mechanical-chemical model for underground cemented tailings backfill. Tunn. Undergr. Sp. Tech. 50:396–414.

Cui L, Fall M (2016) Multiphysics model for consolidation behaviour of cemented paste backfill. Int. J. Geomech. 17(3):2–23.

Chapter 7 Conclusions and recommendations

7.1 General conclusions

The main objective of this study is to investigate the shear behaviour of the CPB-rock interface under multiphysical conditions or factors. A comprehensive understanding of the shear behaviour of the interface is critical to the assessment of the mechanical stability of CPB structure as well as of the arching effect, the utilization of which helps to reduce the amount of cement used, thereby mitigating the operation cost of CPB. To address the evolution of the shear strength properties of the interface, several series of experimental tests concerning the effects of sulphate, temperature, curing stress and drainage conditions, surface morphology on the shear characteristics of the CPB-rock interface were firstly conducted. Thereafter, a chemo-elastic CZM and coupled thermo-chemo-mechanical CZM were proposed to capture the shear behaviour of the CPB-rock interface. Finally, the shear resistance of the interface was proved to be important to the arching effect in CPB. The findings are critical for the design of safe and cost-effective CPB structures. The following conclusions are drawn based on the obtained results.

1. The interaction between CPB and surrounding rock mass plays an important role in the assessment of the stability of CPB structures. Besides, the shear behaviour of the interface is a determining factor in the occurrence of the arching effect.
2. The shear behaviour of the CPB-rock interface varies with different thermal, hydraulic, mechanical, chemical conditions. In addition, the shear strength properties of the interface differ with the curing conditions and times.
3. Sulphate and temperature have significant effects on the shear behaviour and strength of the interface between rock and CPB. The effects can be positive (increase in the interface shear strength) or negative (decrease in the shear strength), which mainly depend on the sulphate content, curing temperature and curing time. In contrast, higher curing stress, drained condition, and rougher interface usually correspond to high shear strength of the CPB-rock interface.
4. Sulphate has a negative effect on the shear strength evolution of very early-age (≤ 3 days) samples due to the inhibition of cement hydration by sulphate ions. However, for samples cured for 7 days, a relatively low amount of sulphate (5000 ppm) leads to a higher interface shear strength (in comparison with sulphate-free samples). This increased shear strength is due to the precipitation of an appropriate amount of expansive minerals in the pore structure of CPB. In contrast, the 7-day samples with higher sulphate content (15000 ppm and 25000 ppm) show a decreasing trend with sulphate contents. The sulphate-induced reduction in shear strength is attributed to two mechanisms: (i) a stronger inhibition effect of sulphate on cement hydration, and (ii) adsorption of sulphate by C-S-H.

For samples cured for 28 days and 90 days, the interface with sulphate content of 15000 ppm shares the highest shear strength due to the refinement of sufficient amount (not excessive) of ettringite. However, the decreasing shear strength of highly sulphated interface is brought about by the physical damage of the CPB matrix.

5. Competing effects exist between the factors of shear strength increase (refinement of the pore structure of CPB, precipitation of more hydration products) and decrease (inhibition of cement hydration; sulphate absorption by C-S-H) as the initial sulphate content of the CPB is increased.
6. The increase in temperature is beneficial to the shear strength acquisition of CPB-rock interface (cured for less than 28 days). It is because the higher temperature improves the rate of cement hydration and self-desiccation. In contrast, due to the crossover effect, the samples cured at 35°C for 28 days show a slightly lower shear strength compared to samples cure at 20°C for 28 days.
7. A higher curing stress leads to a stronger matrix suction as well as lower thermal conductivity at the CPB-rock interface in drained condition, while for interface samples cured in undrained condition, higher curing stress can not only reduce the thermal conductivity but also leads to a denser pore structure. These processes benefit the shear strength acquisition and changes in the adhesion and friction angle at the interface.
8. The type of rocks (marble, granite, cement) has limited effect on the shear strength of the CPB-rock interface. However, the rougher interface is beneficial to the improvement of the shear strength due to the larger contact area between CPB and rock.
9. The shear failure envelops of the interface of the CPB-rock samples follow the Mohr-Coulomb failure criterion, regardless of the sulphate content, curing temperature, curing stress, drainage condition and curing time.
10. The concept of equivalent chemical age can be used to quantitatively evaluate the evolution of the shear strength properties of the CPB-rock interface with different amounts of sulphate ions. The developed chemo-elastic CZM can well capture the shear behaviour of the interface, despite the sulphate contents and ages of the interface structure.
11. The effect of temperature on the shear strength properties of the interface is also incorporated into the CZM to describe the different shear responses under various thermal conditions. The proposed CZMs are sensitive to the variations in friction angle, adhesion and modes I and II fracture toughness.
12. The shear resistance of the CPB-rock interface is critical to the occurrence of the arching effect and the spatial stress distribution in CPB. Therefore, studying the shear behaviour of the interface is important for the design of safer and more cost-effective CPB structures.

7.2 Recommendation for future work

Even though a comprehensive understanding of the shear behaviour of the CPB-rock interface under multiphysical conditions has been made in this study, some research scopes still need further investigation. The following are some recommendations for future work:

1. The rheological and mechanical properties of CPB can be significantly improved by the addition of certain additives, such as plasticizers, fibre and other pozzolanic minerals. Similarly, finding an effective way to reinforce the shear behaviour of the CPB-rock interface is a promising research topic. The shear behaviour reinforcement of the CPB-rock interface has so many advantages. One of the most profound effects is that the arching effect will be enhanced as the shear strength of the CPB-rock interface is reinforced.
2. Fracture toughness is a necessary parameter used in CZM because of its importance in determining the onset of fracture initiation and propagation at a biomaterial interface. For the CPB-rock interface, it mainly refers to modes I (tension mode) and II (in-plane shearing mode) fracture toughness, which are time-dependent parameters due to the cement hydration progression. Therefore, studying the evolutions of the modes I and II fracture toughness of the CPB-rock interface is critical to the stability analysis of underground CPB structures. For example, what is the response of the modes I & II fracture toughness to the variations in temperature, the sulphate attack as well as the drainage conditions? What is the difference in the modes I & II fracture toughness of different cemented backfill-related structures (e.g., CPB, CPB-rock interface, early-age CPB/advanced-age CPB interface)?
3. The shear behaviour of the CPB-rock interface under coupled THMC processes is not fully revealed, and further studies should take this into consideration, expecially from the experimental perspective.
4. The crater blasting technique leads to dynamic loading in underground structures. Therefore, a thorough understanding of the effects of the dynamic loading on the shear behaviour of the CPB-rock interface is crucial to the CPB design. This work should be conducted mainly with the mathematical modelling. For example, will the CZM still be able to capture the shear behaviour of the CPB-rock interface upon the occurrence of the dynamic loading?
5. The mesostructure morphological (grain size distribution, volume fraction) and mechanical properties (stiffness, strength, fracture energy) of tailings particles as well as the cement paste play a critical role in the mechanical behaviour of CPB-rock interface at macro-level. Therefore, the multiscale investigation of the CPB-rock interface is a promising research interest as well. For example, how to predict the macro-level strength of the interface based on the obtained strength of various constituents at multisacle levels? How does fracture occur and propagate at the interface? Is it because of the

failure of the cement paste or that of the tailings particles? When will the dominant fracture change its path from the cement paste to the tailings particles?

Appendixes

Appendix A: Insight into the Mode I and Mode II Fracture Toughness of the Cemented Backfill-Rock Interface: Experimental Results of the Effect of Time, Temperature and Chemistry of the Pore Water

Published in *Construction and Building Materials*, 2020, 262: 120860

Kun Fang, Mamadou Fall

Abstract

Fracture toughness is a key parameter in determining the stability of interlaminar structures. Although many studies have been conducted on the fracture toughness of brittle materials, the evolution of the modes I & II fracture toughness of the interface between the cemented paste backfill (CPB) and rock still remain unknown. Given the significant effect of curing time, temperature and sulphate ions on the binder hydration, it is necessary to study the evolution of the modes I & II fracture toughness of the CPB-rock interface under different thermal and chemical conditions. Therefore, many semi-circular samples (with or without sulphate ions) were produced and cured at 2°C, 20°C, and 35°C for 3 days, 7, 14 and 28 days in this study. Thereafter, all specimens were subjected to the semi-circular bend (SCB) test. The obtained results show that both temperature and sulphate ions have huge effects on the evolution of the modes I & II fracture toughness. Because temperature speeds up the binder hydration as well as the self-desiccation in CPB, the modes I & II fracture toughness rises as the temperature is increased (with an exception of the samples with a curing time of 28 days whose fracture toughness decreases when temperature increases from 20°C to 35°C 0). However, the influences of sulphate ions on the growth of the modes I & II fracture toughness vary with the age of samples and the initial contents of sulphate ions.

A.1 Introduction

Fracture toughness is an important concept in fracture mechanics which represents the capacity of cracked elements to resist the fracture initiation (Kuruppu et al., 2014; Wong et al., 2019). In other words, the onset of fracture propagation in interlaminar structures usually takes place as the stress intensity factor (SIF) achieves their fracture toughness. For various types of decohesion of the biomaterial interface, there are mainly three failure modes, namely, mode I (tension mode), mode II (in-plane shearing mode), and mode III (out-of-plane shearing mode) (Abrate et al., 2015). Investigating the fracture toughness of metal or geomaterials is thus detrimental to the stability analysis of relevant structures. However, the determination methods of fracture toughness vary with materials. In terms of the metal material, Double Cantilevaer Beam (DCB) and End-Notch Flexure (ENF) methods are usually adopted for the determination of the modes I & II fracture toughness, respectively. Besides, with the Mixed-Mode Bending (MMB) test, the fracture toughness of mixed modes (with different mixity ratio) can be easily determined (Reeder and Crews, 1990; Li et al., 2006). As for the brittle material, it is not feasible to obtain the fracture toughness with above-mentioned methods due to the lower tensile strength of geomaterial. Instead, semi-circular bend (SCB), chevron bend (CB), short rod (SR), as well as cracked chevron notched Brazilian disc (CCNBD) methods are the four main methods used to decide the mode I fracture toughness in rock mechanics community (ISRM, 2007; Ayatollahi and Aliha, 2008). Unlike the standard method for the measurement of the mode I fracture toughness, no unified method is available to investigate the mode II fracture toughness so far (Ayatollahi and Aliha, 2006). However, many laboratory tests have been performed to determine the mode II fracture toughness, and among which, SCB and Brazilian disc (BD) are the two methods most frequently used (Lanaro et al., 2009; Aliha and Ayatollahi, 2011).

Cemented paste backfill (CPB), which is characterized as a safer, more economical and environmental-friendly mining method, has been put into practice during the last several decades all over the world (Benzaazoua et al., 2004; Yilmaz et al., 2004). After the placement of prepared mixture (70%-85% tailings, 3%-7% wt% binder, and water) into the underground void, how to ensure the mechanical stability of the structure is the most critical problem facing engineers and mine workers. Because the bonded interface between dissimilar material is always a weak link in terms of the mechanical strength (Dong et al., 2017), the failure of the interlaminar structure is mainly characterized by fracture initiation and propagation (as a result of decohesion). Besides, given that the fracture toughness is the main character to indicate the capacity of the interlaminar structure to resist decohesion (Camanho et al., 2003; Kataoka et al., 2015), it is, therefore, necessary to analyze the fracture toughness of the CPB-rock interface.

Owing to the existence of the cementitious component in cemented paste backfill (CPB), the modes I & II fracture toughness of the interface evolve with time. Therefore, studying the evolution of the fracture toughness plays a significant role in the stability analysis and the design optimization of the CPB structures (Nasir and Fall, 2008; Fang and Fall, 2020). As described in previous studies (Helinski et al., 2010; Koupouli et al., 2016; Fang and Fall, 2018, 2019), the mechanical properties of the CPB-rock interface are affected by various factors, such as the progression of the cement hydration (curing time), thermal (e.g., environmental temperature, cement hydration heat, geothermal gradients), chemical (e.g., sulphate content, tailings reactivity), mechanical (self-weight) and hydraulic (e.g., drainage condition, hydraulic conductivity) conditions. Among which, curing time, temperature and sulphate ions are the most important ones. Firstly, the cement hydration is divided into five phases (according to the heat generated during the progression), and the time-dependent properties (e.g., adhesion, friction angle) evolve with the curing time (Qi and Fourie, 2019). Secondly, there are many sources of heat for the CPB structure: (i) the temperature in the shallow-buried ore body is associated with the geographical location as well as the seasonal change; (ii) while for the deep-buried ore body, the geothermal gradient (with an average value of 3°C/100m) contributes greatly to the variation in the temperature; (iii) the heat generated by the binder hydration change the thermal condition as well. Thirdly, the addition of sulphate ions is mainly used for ore beneficiation processes and to reduce the setting time of the cement. This, in turn, inevitably results in higher sulphate content in tailings. In addition, the variation in temperature and sulphate content imposes a huge effect on the cement hydration progression, thereby affecting the shear performance and properties of the interface significantly (Fang and Fall, 2018, 2019). Specifically, the change in the degree of the binder hydration results in the generation of various quantities of calcium silicate hydrate (C-S-H), gypsum as well as ettringite. These binder hydration products are the main components that contribute to different mechanical features of the interface (e.g., C-S-H improves the interaction force between CPB and rock, while the presence of gypsum and ettringite can refine or coarsen the microstructure, depending on their amounts). Hence, a thorough comprehension of the evolution of the modes I & II fracture toughness of the CPB-rock interface with various curing temperatures and sulphate contents is important for the stability assessment of the CPB structures. However, until now, no studies have addressed the evolution of the fracture toughness of the CPB-rock interface. Therefore, this research is dedicated to the experimental investigation of the modes I & II fracture toughness of the CPB-rock interface under different thermal and chemical conditions (with the adoption of the SCB method).

A.2 Materials and experimental program

A.2.1 Dimensional determination and materials being used

The interface samples for the SCB test (to decide the modes I & II fracture toughness of the CPB-rock interface) are displayed in Figure A-1. From the figure, it is noticeable that the samples consist of CPB and rock, and there exists a notch (with a length of a) at the CPB-rock interface. In addition, two supporting rollers are also observed at the bottom of the sample. The distance between the two supporting rollers is 2S, whereas the diameter of the sample is 2R. At the beginning of the test, a vertical load is applied right at the top (interface) of the sample.

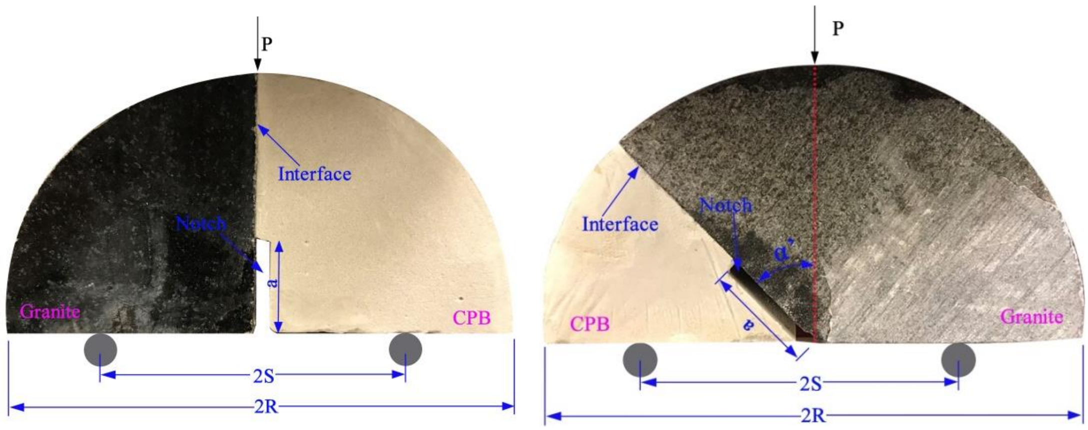

(a) Mode I (b) Mode II

Figure A-1 Interface samples for the SCB test

For the measurement of the mode I fracture toughness, the notch is designed vertically to the edge (Figure A-1(a)), while the mode II can be achieved with different crack angles (Figure A-1(b)), which is determined by the a/R and S/R ratios (Ayatollahi and Aliha, 2004). The relationship between these three parameters is shown in Figure A-2 (Ayatollahi and Aliha, 2006).

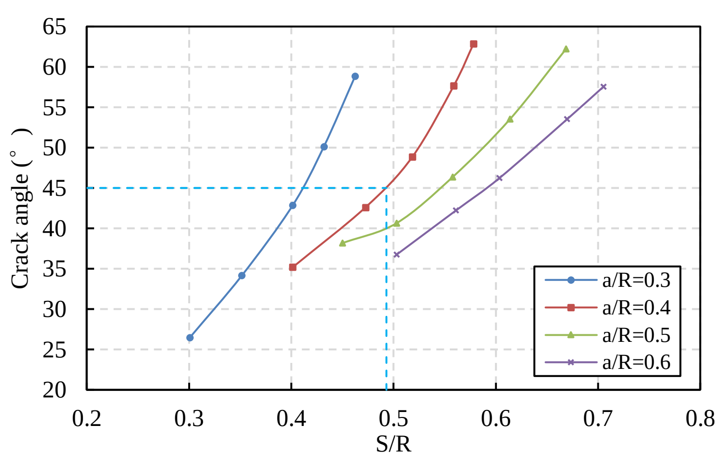

Figure A-2 Relationship between crack angle α' and a/R, S/R (Ayatollahi and Aliha, 2006)

The determinations of the modes I & II fracture toughness, $K_{\mathrm{I}c}, K_{\mathrm{II}c}$ are expressed as (Ayatollahi and Aliha, 2006):

$$K_{\mathrm{Ic}} = \frac{P\sqrt{\pi a}}{2Rt} Y_{\mathrm{I}}\left(\frac{a}{R}, \frac{S}{R}\right) \tag{1}$$

$$K_{\mathrm{IIc}} = \frac{P\sqrt{\pi a}}{2Rt} Y_{\mathrm{II}}\left(\alpha', \frac{a}{R}, \frac{S}{R}\right) \tag{2}$$

where P refers to the peak load during the loading period. t means the thickness of the semi-circular sample. Y_{I} and Y_{II} are the geometry factors, expressed as functions of α', S/R and a/R. Regarding the mode I, Y_{I} is expressed as (Wong et al., 2019):

$$Y_{\mathrm{I}} = 1.297 + 9.516\times\frac{S}{R} - \left(0.47 + 16.457\times\frac{S}{R}\right)\times\frac{a}{R} + \left(1.071 + 34.401\times\frac{S}{R}\right)\times\left(\frac{a}{R}\right)^2 \tag{3}$$

while Y_{II} is usually decided by the numerical values based on α', a/R and S/R (Ayatollahi and Aliha, 2004).

Generally, the thickness of the specimen should be $t \geq 0.8R$ or $t \geq 30\ mm$, however, some researchers also found that the thickness of the specimen has a limited effect on the fracture toughness (Lim et al., 1994; Kuruppu et al., 2014). The length of the notch should be $0.4 \leq a/R \leq 0.6$, and the distance between the two supporting rollers should be $0.5 \leq S/R \leq 0.8$ (ISRM, 2007). In this study, a value of $a/R = 0.4$, $S/R = 0.493$ and the crack angle $\alpha' = 45^{\circ}$ are chosen. Because the radius of the sample is $R = 49\ mm$, the lengths of the half span of the two rollers and the notch are then $S = 24.16\ mm$, $a = 19.6\ mm$.

Due to the large amount of granite in the upper crust of the earth, granite is used as the rock part of the semi-circular sample (Wong et al., 2019). To avoid the influence of roughness on the modes I & II fracture toughness, the surface of the granite, especially the interface, is polished smoothly (Tse and Cruden, 1979). Given the pure composition of silica tailings (ST, 99.8% of which is silicon dioxide) and the homologous particle size distribution of the nature tailings (NT, as shown in Figure A-3), ST is then chosen for the production of CPB part of the sample. The CPB mixture herein is prepared by mixing ST, Portland cement type I (PCI), together with distilled water. The weight proportion of PCI and the water-cement ratio are the same as the recipe used in tests conducted by Fang and Fall (Fang and Fall, 2018).

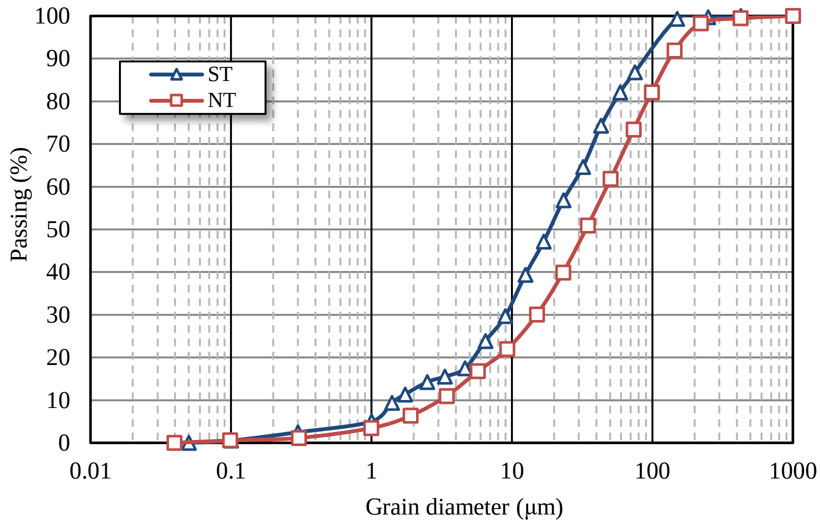

Figure A-3 Comparison of the particle size distribution of ST and NT

To investigate the influence of sulphate ions on the evolution of the modes I & II fracture toughness, CPB mixtures with several sulphate contents (0 ppm, 5000 ppm, 15000 ppm, 25000 ppm) were prepared by adding different amounts of ferrous sulphate to the distilled water (Fang and Fall, 2019).

A.2.2 Sample preparation and testing setup

A.2.2.1 Sample preparation

The granite was firstly shaped into a circle with a core cutter, DD 150-U (along with a core bit with a dimension of 101.6 mm (diameter) × 431.8 mm (height)). By using a special rock cutter, the core granite was then sliced into disc sample with a thickness of 20 mm. To prepare samples for the measurement of the mode I fracture toughness, the disc sample was cut into four pieces evenly. Meanwhile, the granite disc was shaped into a sector with a centre angle of 135° for measuring the mode II fracture toughness. Thereafter, the obtained granite was set into a plastic circular container (with an inner diameter of 98 mm, a height of 20 mm), which was assembled together by two bolts, as shown in Figure A-4. After that, a thin clapboard was set along the central diameter (along with the granite) to divide the container into two parts. This allows us to prepare two semi-circular samples with one container. Another two short clapboards were then set along with the granite as well to produce the artificial crack between CPB and granite. All the surfaces of these three clapboards were lubricated with oil. The CPB was prepared with a food mixer, and the stirring process lasts 7 minutes. The prepared CPB mixture was then poured into the container. After the manual vibration, the whole disc sample was enclosed with plastic film and then placed in an oven (35°C), a curing chamber (20°C) or a freezer (2°C) for curing. For samples with different sulphate contents, they were only cured at a temperature of 20°C. To make sure the repeatability of the SCB test, each test was repeated five times, as suggested by Kuruppu et al. (2014). Thus, a total of 240 semi-circular samples were prepared, and the experimental details are shown in Table A-1.

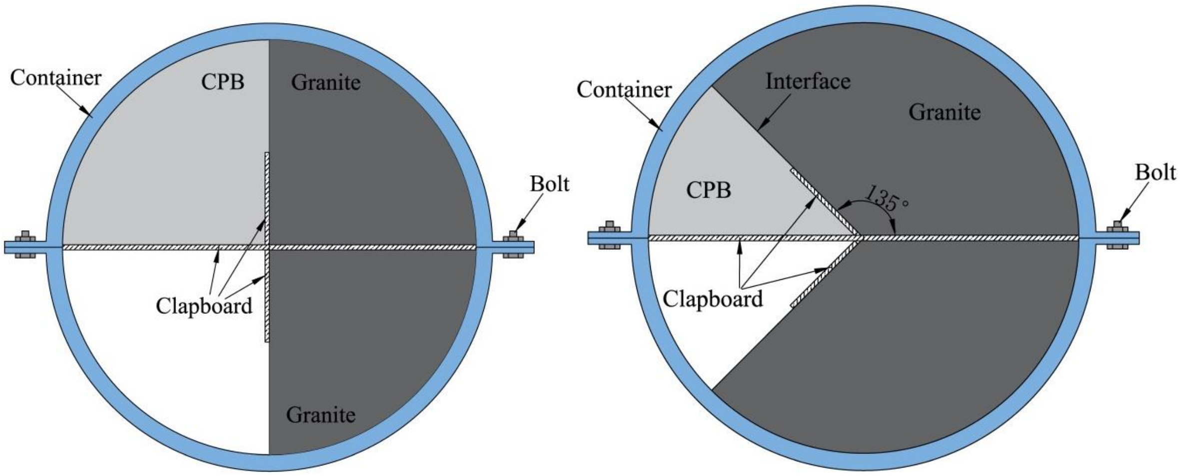

(a) Mode I (b) Mode II

Figure A-4 Preparation procedures of SCB sample

Table A-1 Experiment details for measuring the modes I & II fracture toughness

Influential factor	PCI content (%)	Water-cement ratio	Curing age (days)	Curing temperature (°C)	Sulphate content (ppm)
Temperature	4.5	7.35	3, 7, 14, 28 days	2	0
	4.5	7.35	3, 7, 14, 28 days	20	0
	4.5	7.35	3, 7, 14, 28 days	35	0
Sulphate content	4.5	7.35	3, 7, 14, 28 days	20	5000
	4.5	7.35	3, 7, 14, 28 days	20	15000
	4.5	7.35	3, 7, 14, 28 days	20	25000

A.2.2.2 Test setup

The SCB test of the mode I fracture toughness (ASTM E399-83) was conducted with Digital Tritest 50, the structure of which is illustrated in Figure A-5(a), while the setup for the mode II fracture toughness measurement is shown in Figure A-5(b). A load cell is connected to the loading frame vertically, as can be observed from the figure, and this is for the load measurement during the test. A linear variable differential transformer (LVDT) is used as well for the measurement of vertical displacement. The semi-circular sample was placed at the centre of the platform, and two rollers were adopted for the application of point loading. To prevent the roller from rolling away, two supporting blocks were also used. During the test, all the samples were driven upward at a rate of 0.05 mm per min. A data logger is connected to the computer software (Labview) to record the axial load and displacement.

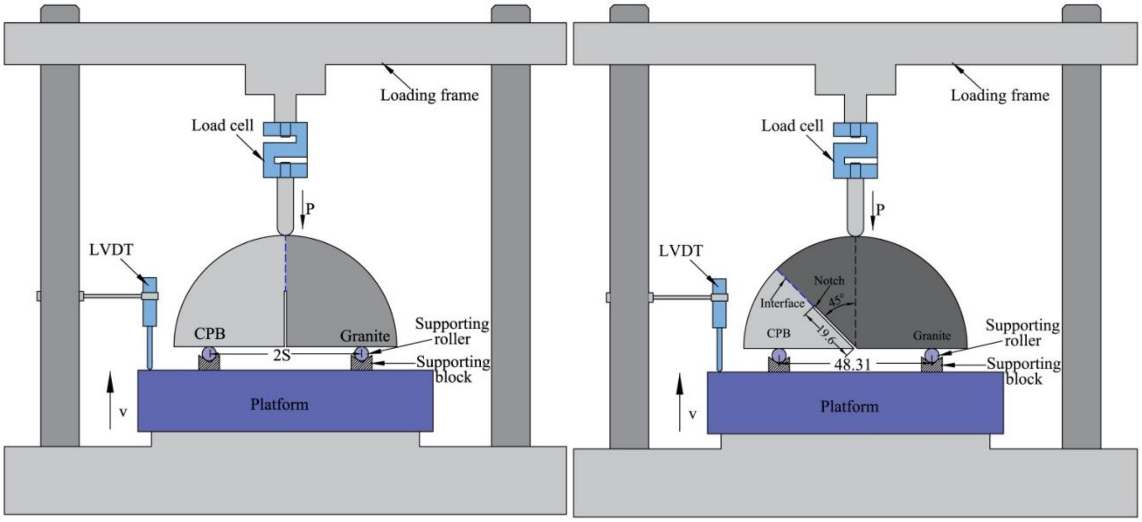

(a) Mode I (b) Mode II

Figure A-5 Setup of the SCB test

A.2.3 Supplementary test

To better illustrate the evolution of the modes I & II fracture toughness under different thermal and chemical conditions, a number of supplementary tests were conducted, including electrical conductivity (EC), volumetric water content (VWC) and matrix suction monitoring, mercury intrusion porosimetry (MIP) test, scanning electron microscopy (SEM) analysis, and thermal analysis (TG/DTG).

The monitoring results of EC value reflect the concentration and movement rate of ions in CPB. Based on the EC evolution, the rate of cement hydration can be easily determined. In contrast, the monitoring results of VWC show the evolution of water content in CPB, and therefore, it is an effective method to assess the degree of self-desiccation. Both the EC and VWC value can be obtained by using the 5TE sensor, which has a VWC and EC measurement from 0%~80% and 0 dS/m~23 dS/m, respectively. However, the matrix suction is monitored with the MPS-6 sensor, and the evolution in matrix suction reflects the degree of self-desiccation in CPB. The data were all collected by adopting an EM50 data logger.

The MIP test was carried out on CPB (according to ASTM D4404-10), with the adoption of Micromeritics AutoPore III 9420 mercury porosimeter. The result of the MIP test demonstrates the porosity and the capillary structure of CPB, and therefore, the effects of the thermal and chemical factors on the refinement/coarsening of the capillary structure can be analyzed.

The SEM analyses were conducted on the interface sample with Hitachi S4800. Prior to the test, the interface sample was firstly dried in an oven (with a temperature of 45°C) for 4 days to eliminate the free water. The SEM images allow us to analyze the cement hydration products as well as the microstructure at the interface.

Unlike the above three tests, the TG/DTG tests were conducted on powdered cement paste (with water-cement ratio of 2) with a Q5000IR thermogravimetric analyzer. The different weight loss/peak at various temperatures corresponds to different amounts of cement hydration products, based on which, the effects of the thermal and chemical factor on the degree/rate of cemented hydration are obtained. Before the test, the sample was dried at 45°C for 4 days as well.

A.3 Results and discussion

A.3.1 Time-dependent evolution of the peak load of the CPB-rock interface

The loading-displacement curves of the three-point bending tests (for determining the modes I & II fracture toughness) are shown in Figure A-6. It is noticeable that the peak load evolves with the curing time. Besides, the samples sustaining higher load experience smaller displacement before failure takes place. This is because stronger interface samples usually correspond to higher stiffness. As a result, it will take less time for the SIF to reach the modes I & II fracture toughness.

For cementitious materials, the evolution of mechanical properties is ascribed to the change in the rate/degree of the cement hydration. Therefore, it is necessary to have a comprehensive understanding of the cement hydration. It is well-known that the ingredients in PCI mainly consist of tricalcium aluminate (C_3A), dicalcium silicate (C_2S), tricalcium silicate (C_3S) and tetracalcium aluminoferrite (C_4AF) (Ouellet et al., 2006; Oliveira et al., 2013), among which, the hydration of C_3A is the first reaction takes place after mixing with water:

$$3CaO \cdot Al_2O_3 + 6H_2O = 3CaO \cdot Al_2O_3 \cdot 6H_2O \tag{A-1}$$

Thereafter, it is followed by the hydration of C_3S and C_4AF, the chemical reaction can be expressed as (A-2) and (A-3), respectively.

$$2(3CaO \cdot SiO_2) + 6H_2O = 3Ca(OH)_2 + 3CaO \cdot 2SiO_2 \cdot 3H_2O \tag{A-2}$$

$$4CaO \cdot Al_2O_3 \cdot Fe_2O_3 + 7H_2O = CaO \cdot Fe_2O_3 \cdot H_2O + 3CaO \cdot Al_2O_3 \cdot 6H_2O \tag{A-3}$$

The initial strength of the interface is mainly determined by the reaction (A-2), namely the amount of C-S-H. Moreover, the hydration of C_2S can also generate C-S-H, which is characterized as the slowest reaction:

$$2(2CaO \cdot SiO_2) + 4H_2O = Ca(OH)_2 + 3CaO \cdot 2SiO_2 \cdot 3H_2O \tag{A-4}$$

Given the products generated by above-mentioned reactions, cement hydration mainly refers to the reactions (A-2) and (A-4), which take up 60% of the hydration reaction (Liu et al., 2019). The increasing amount of cement hydration products then can fill the pore structure between particles, and this will allow C-S-H to migrate and bind the interface together.

The higher peak load with time (as shown in Figure A-6) is attributed to the increased degree of the binder hydration (Metha, 1986; Ercikdi et al., 2009). Specifically, two mechanisms contribute to the higher peak load at the interface: (i) the increasing amount of C-S-H, and (ii) the finer capillary structure. As the age of samples is increased, more C-S-H is generated by reactions (A-2) and (A-4). The large amount of C-S-H with time is experimentally demonstrated by the SEM images of the interface, as presented in Figure A-7. The interface between CPB and rock can be observed clearly, no matter how long the curing time is. However, the comparison between these two SEM images shows that a large quantity of C-S-H is generated at the top of the tailings particle after being cured for 7 days (Figure A-7(b)). In contrast, the surface of the tailings particle cured for 3 days is relatively smooth. On the other hand, the difference in the size of the tailing particle and cement hydration products results in wall effect in CPB. The existence of wall effect inhibits cement grains from gathering together and consequently, a microstructure with a high porosity is formed (Scrivener et al., 2004). However, the increasing amount of cement hydration products with time will refine the pore structure and then decrease the porosity, thereby offsetting the wall effect. This can increase the contacting area between CPB and rock, bringing about an increase in the binding force (Fall et al., 2005).

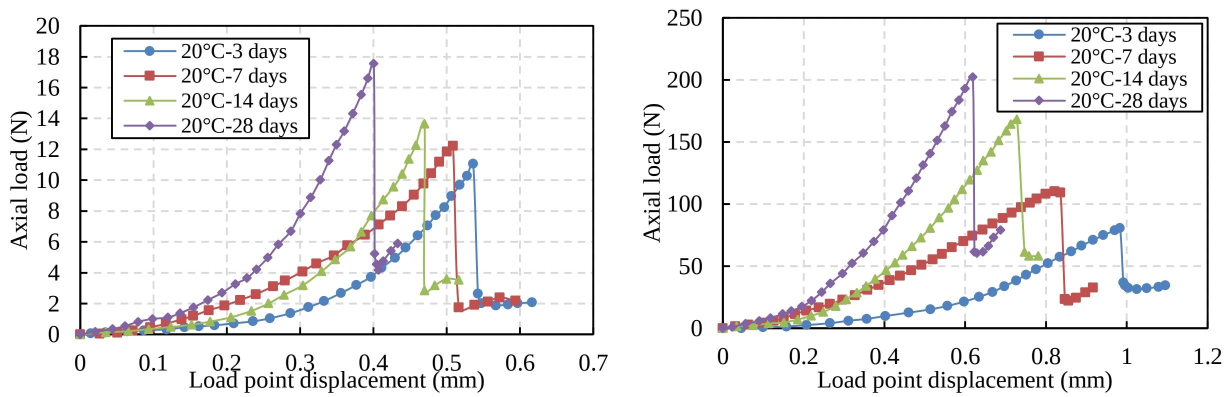

(a) Mode I (b) Mode II

Figure A-6 Loading-displacement curves of SCB test

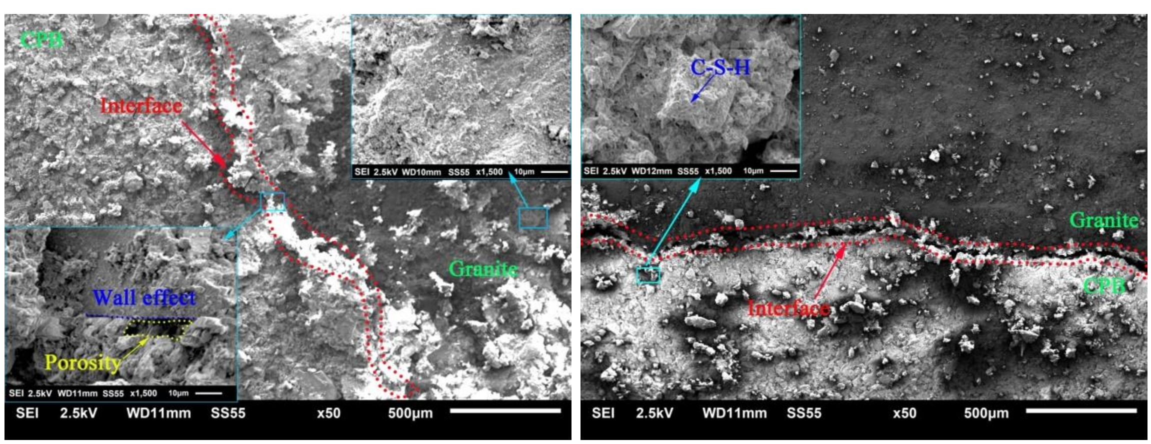

(a) Curing time: 3 days (b) Curing time: 7 days

Figure A-7 SEM images of the CPB-rock interface (cured at 20°C)

A.3.2 Temperature-dependent evolution of the peak load and the modes I & II fracture toughness of the CPB-rock interface

Some typical loading-displacement curves of the semi-circular samples under the three-point bending tests are shown in Figure A-8. Figure A-8(a) depicts the effect of temperature on the loading-displacement curves of the mode I samples, while Figure A-8(b) presents the evolution of axial load of the mode II samples with temperature (taking samples cured for 3 days as examples). The comparison between Figure A-8(a) and Figure A-8(b) shows that for the same curing conditions, the peak load of samples for the mode II fracture toughness measurement is obviously higher than that of samples for evaluating the mode I fracture toughness. In addition, the peak loads of samples used to calculate the modes I & II fracture toughness both increase with temperature. The increasing peak load with temperature is because of the temperature-induced acceleration of binder hydration. In other words, the cement hydration speeds up as temperature rises. Consequently, the quantity of C-S-H is increased significantly (Gani, 1997; Neville, 2011). This argument will be further discussed later. Figure A-9 displays the evolution of the modes I & II fracture toughness of interface samples cured at temperatures of 2°C, 20°C, 35°C. The values of the modes I & II fracture toughness rise with temperature, with the exception of samples cured at 35°C for 28 days, which will be explained in the following part as well.

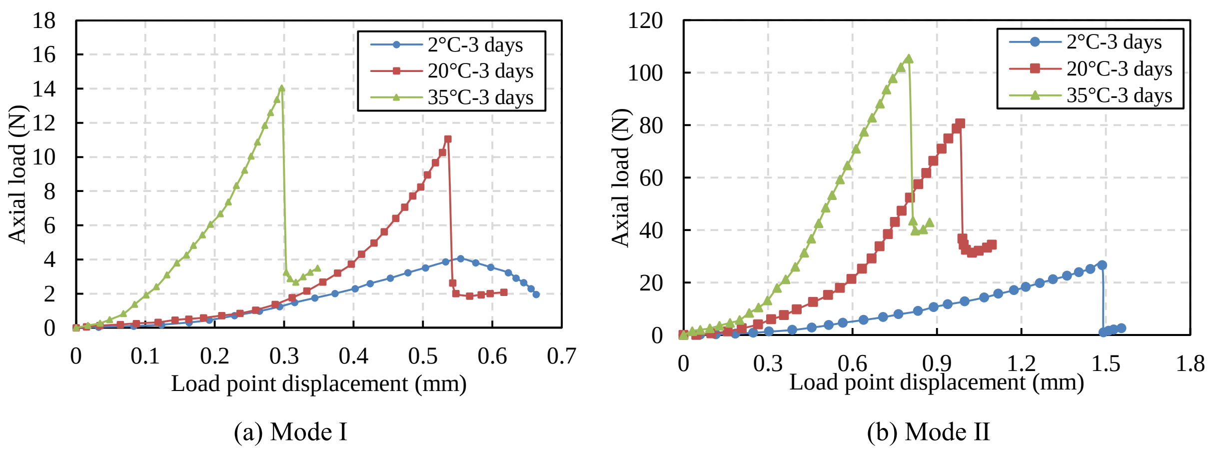

Figure A-8 Loading-displacement curves of SCB test

The modes I & II fracture toughness are founded to be positively associated with the increase in temperature (as shown in Figure A-9), excepting specimens cured at 35°C for 28 days. The increasing fracture toughness with temperature is mainly ascribed to two mechanisms: (i) higher rate and degree of binder hydration, as the temperature is increased, (ii) a higher degree of self-desiccation because of the increasing temperature.

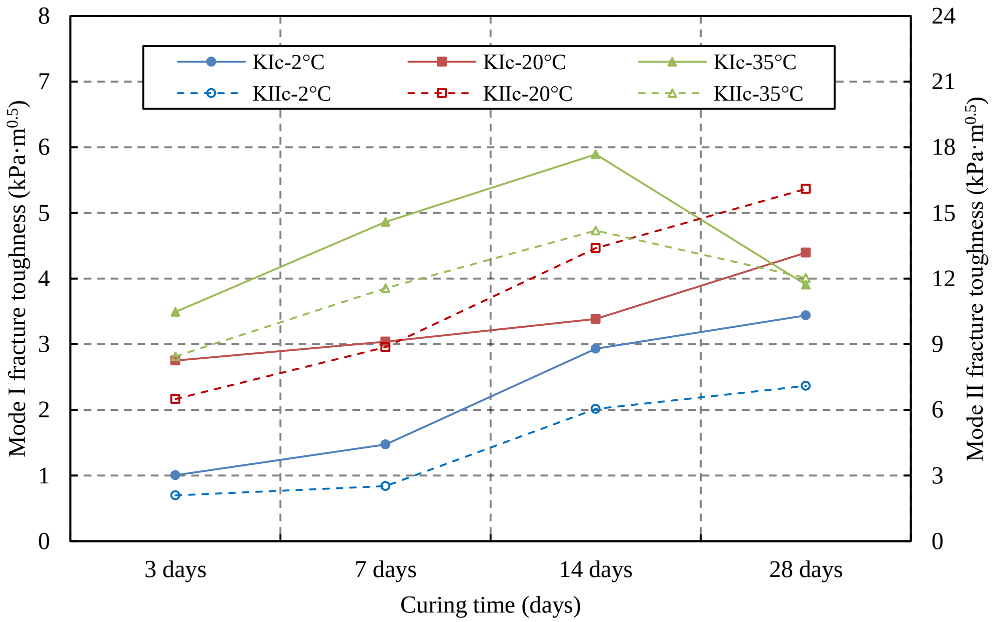

Figure A-9 Evolution of Modes I & II fracture toughness of samples cured at different temperatures

The chemical reaction (A-2) and (A-4), as introduced above, is sensitive to the temperature variation (Liu et al., 2019). As the temperature rises, the rate and degree of cement hydration improve, and consequently, the amount of C-S-H is significantly increased. The presence of C-S-H can improve the interaction force at the interface, and the modes I & II fracture toughness is then found to be increased with temperature. This also coincides with many studies on concrete (Richardson,1991; Neville, 2011). Concerning CPB, the increasing degree of binder hydration with temperature is demonstrated by the appearance of a number of cement hydration products, which can be concluded from the data of TG/DTG analyses. Figure A-10 demonstrates the outcomes of TG/DTG tests on CPB being cured at 20°C and 35°C for 7 days. The decreasing weight with temperature (up to 1000°C), as can be seen from Figure A-10, is caused by the dehydration and decomposition of the products generated by cement hydration (Sha et al., 1999; Pane and Hansen, 2005; Jiang et al., 2016). Specifically, the first obvious change in weight occurs at a temperature from 30°C~170°C, as a result of dehydration of C-S-H and gypsum. Nevertheless, the subsequent two peaks (at a temperature from 400°C~450°C and 640°C~700°C) are induced by the decomposition of calcium hydroxide (CH) and calcite respectively. The weight losses of the samples cured at 35°C at a temperature from 30°C~170°C and 400°C~450°C are both higher than those of the samples cured at 20°C. This indicates the amount of gypsum, C-S-H and CH in the samples cured at 35°C are larger than those cured at 20°C, which proves the beneficial effect of temperature on the improvement of the degree of cement hydration. In addition, the beneficial effect of temperature on the improvement of the rate of the binder hydration is attested by the monitoring results of EC values, as presented in Figure A-11. From the results, it is noticeable that all the EC curves of samples cured at different temperatures show a similar tendency. They all increase sharply and then followed by a slight decrease. The initial increase in EC value is because of the increasing concentration of ions, while the subsequent reduction is due to the decreasing concentration, as a result of the progression of cement hydration (Courard et al., 2014). However, for CPB cured at 2°C, EC value peaks at 4.26 mS/cm after being cured for 9.5 h. In contrast, the critical times for samples cured at higher temperature are much less (4.8 h (20°C) and 1.25 h (35°C), respectively). The shortest time required for sample cured at 35°C to reach the peak EC value proves the beneficial influence of higher temperature on the acceleration of binder hydration (Fang and Fall, 2018).

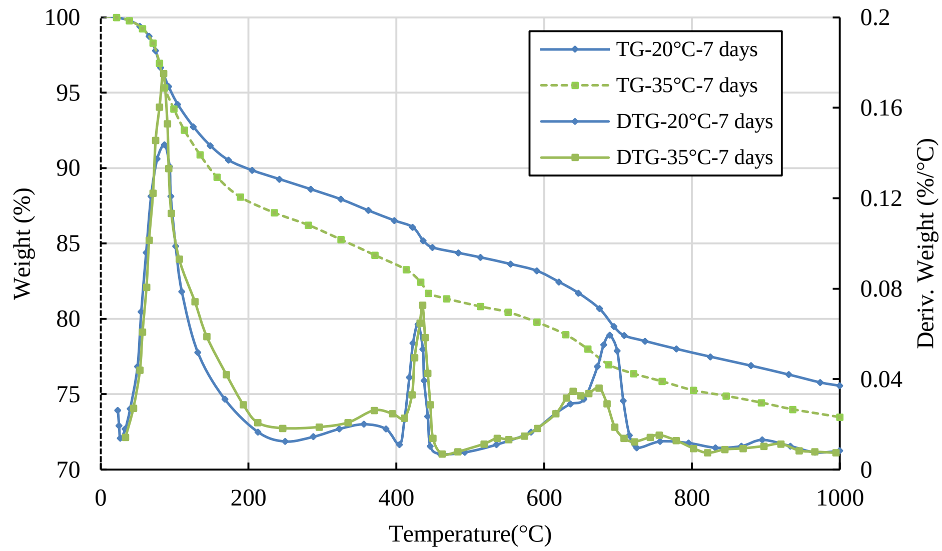

Figure A-10 Results of TG/DTG analyses on CPB cured at 20°C and 35°C for 7 days

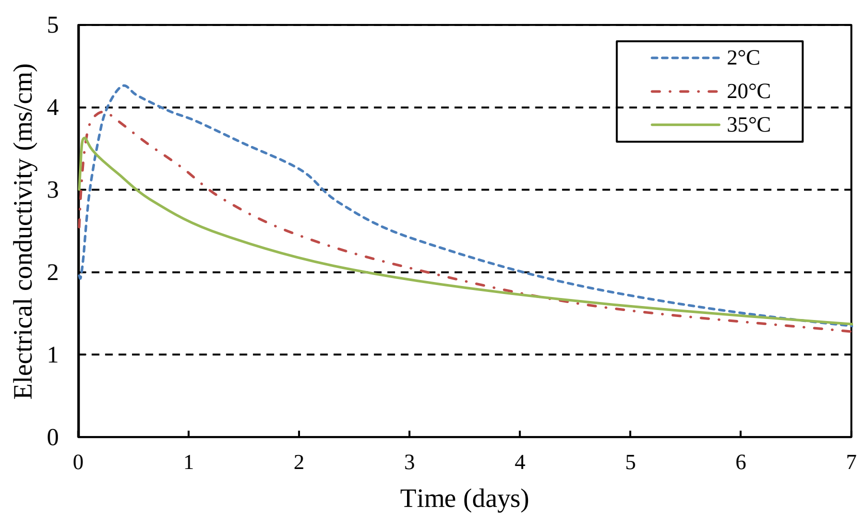

Figure A-11 Monitoring results of electrical conductivity in CPB cured at 2°C, 20°C and 35°C

Another factor contributing to a higher modes I & II fracture toughness with temperature is the increasing self-desiccation as the binder hydration gets more intense. As introduced above, a higher temperature can speed up the binder hydration. This, in turn, leads to more consumption of water, and consequently, the water content in CPB is fast decreased, thereby increasing the self-desiccation. Moreover, the temperature-induced tense self-desiccation then results in higher matrix suction in capillary pores, which also contributes to the increase in the modes I & II fracture toughness. This is in the same vein as the influence of the suction on the shear strength development of the soil-structure interface (Hossain and Yin, 2013; Borana et al., 2016). The increasing self-desiccation with temperature is attested by the evolution of volumetric water content (VWC) and matrix suction in CPB, the results of which are depicted in Figure A-12. The VWC in CPB cured at a temperature of 2°C is generally found to be the highest. Take samples cured for 3 days as an example, the VWC in CPB cured at 2°C, 20°C, 35°C is 0.53, 0.47 and 0.41, respectively. At the same time, the matrix suction increases from 54.4 kPa at 2°C to 232.6 kPa at 35°C.

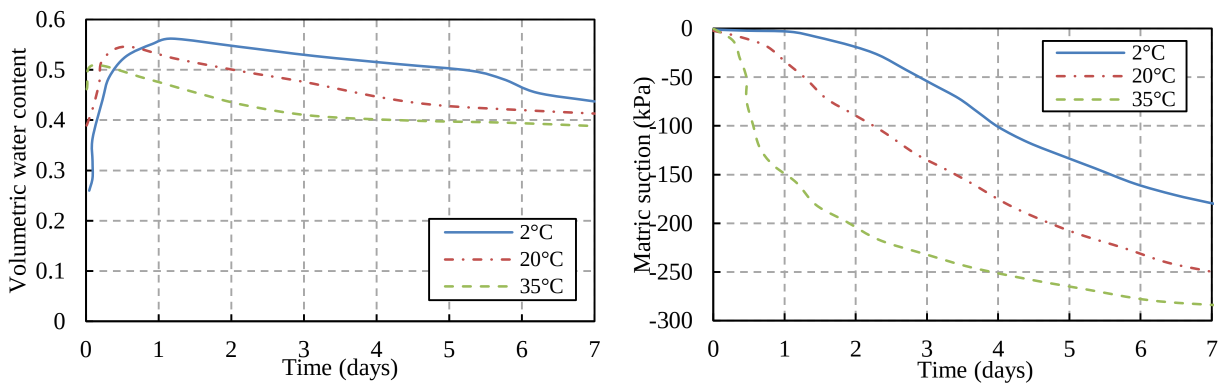

(a) Evolution of VWC

(b) Evolution of matrix suction

Figure A-12 Evolution of VWC and matrix suction in CPB cured at 2°C, 20°C and 35°C

However, the lower modes I & II fracture toughness of CPB-rock samples cured at 35°C for 28 days (compared with samples cured at 20°C) is caused by the crossover effect that is a common phenomenon in cementitious materials cured at a high temperature (Kjellsen et al., 1991; Escalante-Garcia and Sharp, 2001). Some previous studies have found that in terms of the uniaxial compressive strength (UCS), the optimum temperature for long-term concrete (produced with PCI) is 13°C (Klieger, 1958; Kjellsen and Detwiler, 1993). This means the magnitude of UCS will decrease with increasing temperature (higher than 13°C), and the decreasing tendency becomes pronounced with temperature. The occurrence of crossover effect is ascribed to the non-uniform distribution of C-S-H at the interface (Kjellsen et al., 1990). Specifically, higher temperature corresponds to tense binder hydration. Accordingly, the increasing amounts of cement hydration products with temperature will gather around the cement grains because of their low diffusivity. This will form a diffusion barrier and inhibit the generated C-S-H from migrating to a significant distance.

A.3.3 Chemically induced changes in the modes I & II fracture toughness

The loading-displacement curves of semi-circular samples with different sulphate contents are presented in Figure A-13, while the evolution of the modes I & II fracture toughness is shown in Figure A-14. Both the sulphate ions and time have significant effects on the peak load, as can be noticed in Figure A-13 and Figure A-14. However, the influence of sulphate ions on the modes I & II fracture toughness of CPB-rock interface varies with time. For example, for semi-circular samples cured for 7 days, the 5000 ppm sample has the highest modes I & II fracture toughness. In contrast, after being cured for 28 days, the 15000 ppm samples experience the highest modes I & II fracture toughness, followed by those with sulphate contents of 25000 ppm, 15000 ppm and 0 ppm. The change in the modes I & II fracture toughness of semi-circular samples (with various sulphate contents) with time is mainly due to the increasing amount of the cement hydration products, especially the amount of C-S-H, gypsum and ettringite, among which, C-S-H affects the joining forces among particles, while gypsum and ettringite can change its microstructure (refine or coarsen the microstructure, depending on the amount of gypsum and ettringite) (Neville, 2011; Fall et al., 2010; Pokharel and Fall, 2013). This argument will be explicitly discussed in the following section.

Before further discussion on the influence of sulphate ions on the microstructure at the interface, it is important to clarify the chemical reactions in sulphated CPB. After mixing sulphate ions with PCI and water, gypsum will be produced by the reaction of sulphate ions with calcium hydroxide (CH):

$$SO_4^{2-} + Ca(OH)_2 + 2H_2O \rightarrow CaSO_4 \cdot 2H_2O + 2OH^- \qquad \text{(A-5)}$$

The further reaction between the generated gypsum and tricalcium aluminate will generate ettringite, which is characterized as an expansive mineral (Li and Fall, 2016).

$$3CaSO_4 \cdot 2H_2O + 3CaO \cdot Al_2O_3 + 30H_2O \rightarrow 3CaO \cdot Al_2O_3 \cdot 3CaSO_4 \cdot 32H_2O \qquad \text{(A-6)}$$

The precipitation of gypsum and ettringite (generated by reactions (A-5) and (A-6)) facilitates the refinement of the capillary structure, thus increasing the contacting surface between CPB and granite. This will allow C-S-H to have more chance to get access to the interface, and then increase the modes I & II fracture toughness of CPB-rock interface.

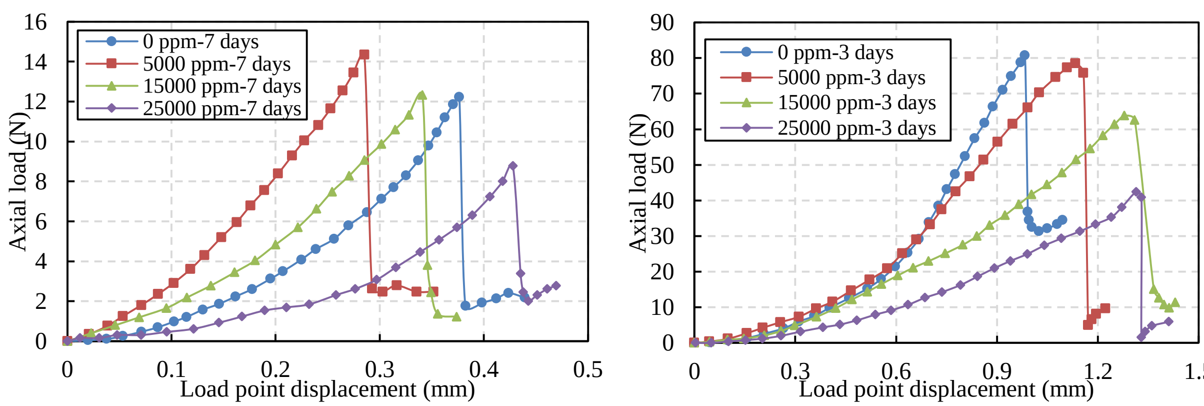

(a) Mode I

(b) Mode II

Figure A-13 Loading-displacement curve of SCB test

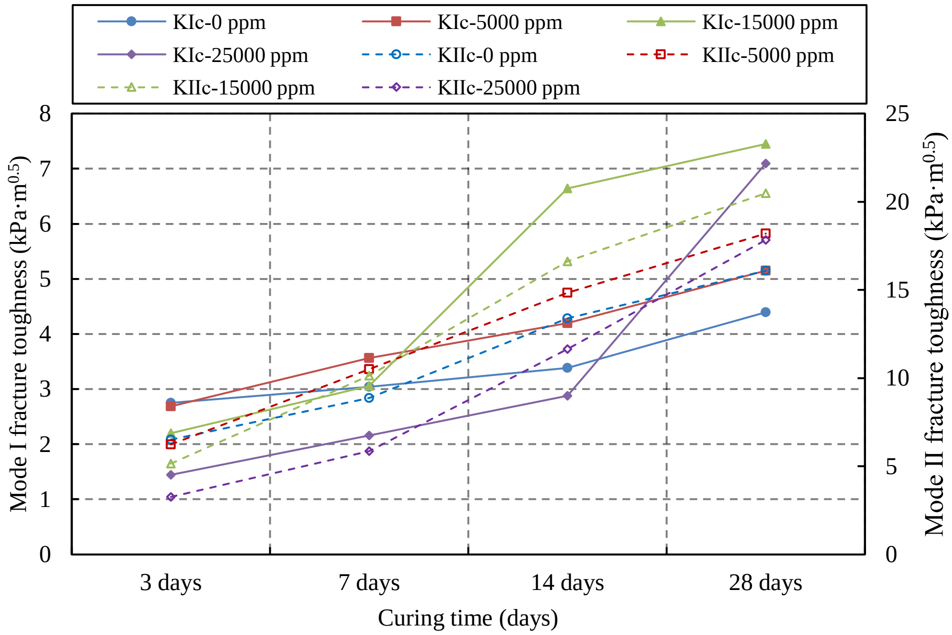

Figure A-14 Evolution of modes I & II fracture toughness of samples (with different sulphate contents)

The evolution of the modes I & II fracture toughness with sulphate contents shown in Figure A-14 indicates the nature and magnitude of the effects of the sulphate content on the modes I & II fracture toughness evolves with the age of the samples. The reasons contributing to the change in the modes I & II fracture toughness with sulphate contents are discussed below.

For differently sulphated semi-circular samples cured for 3 days, the modes I & II fracture toughness increases as the sulphate content reduces. This phenomenon also coincides with the effect of sulphate ions on the peak shear stress development of the interface (Fang and Fall, 2019). The reduction in the modes I & II fracture toughness is because of the retardation effect of sulphate ions on binder hydration. Specifically, the formation of ettringite generated by reaction (A-6) will cover the unhydrated cement particles. This will prevent the water from having access to C_3S and C_2S (Yilmaz and Fall, 2017), thereby leading to the inhibition effect on the binder hydration. Moreover, the inhibition effect becomes more pronounced with increasing sulphate contents. This conclusion is attested by the monitoring results of EC value, as shown in Figure A-15. From the results, the EC value in CPB without sulphate is found to firstly peak at 5.2 mS/cm, followed by CPB mixture with sulphate contents of 5000 ppm and 25000 ppm, with peak values of 4.9 mS/cm and 2.8 mS/cm, respectively. The decreasing peak value and longer time required for reaching the value all prove the retardation effect of sulphate on binder hydration.

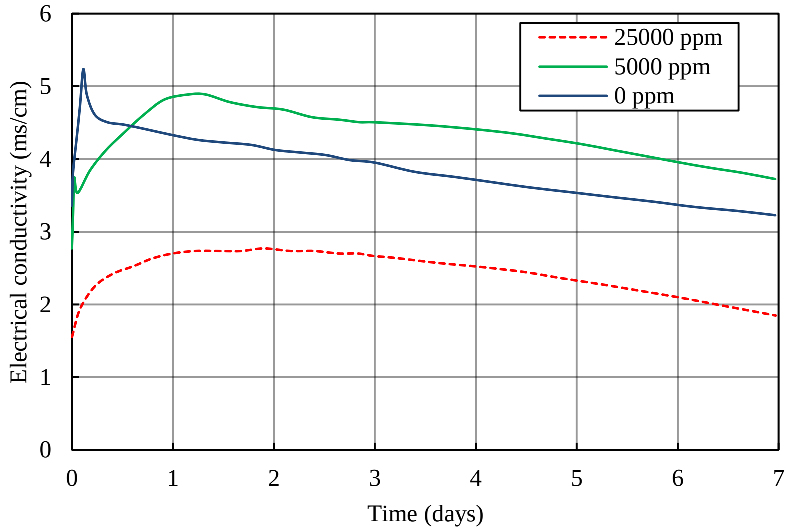

Figure A-15 Monitoring results of electrical conductivity in CPB with different sulphate contents

However, for samples cured for 7 days, the modes I & II fracture toughness of sulphate-free sample is lower than those of 5000 ppm samples. The adverse effect of sulphate ions on the magnitude of the modes I & II fracture toughness is because, with the ageing of samples, the inhibition influence of sulphate on the cement hydration becomes less obvious (with an exception of the sample with 25000 ppm sulphate content). Instead, the formation of a larger amount of expensive minerals (e.g., gypsum and ettringite) contributes to a finer capillary structure. This will increase the contacting area between CPB and granite. The C-S-H then has more possibility to get access to rock, thereby leading to a rise in the modes I & II fracture toughness. The refinement of the capillary structure by the precipitation of gypsum and ettringite has been demonstrated by the SEM analyses conducted by Fall et al. (2005). Moreover, for samples cured for 14 days, the refinement effect of expansive minerals on the capillary structure of differently sulphated CPB becomes pronounced with sulphate contents (for samples with sulphate contents smaller than 25000 ppm). The 15000 ppm sample has a higher modes I & II fracture toughness than that with a sulphate content of 5000 ppm. However, for 25000 ppm sample, the inhibition function of sulphate ions on the binder hydration still prevails (in comparison to the refinement effect of gypsum and ettringite on the pore structure at the interface).

After being cured for 28 days, the 15000 ppm interface sample has the highest modes I & II fracture toughness, while the samples without sulphate experience the lowest fracture toughness. The higher modes I & II fracture toughness of 5000 ppm sample (compared to 0 ppm sample) is due to the precipitation of expansive mineral, this is attested by the outcomes of MIP tests as shown in Figure A-16. It can be clearly seen that the porosity of the sample with no sulphate ions is larger than that of the 5000 ppm sample. However, the higher modes I & II fracture toughness of 25000 ppm sample (compared to sulphate-free sample) indicates there exists a competing effect between the factors that result in increase and decrease in these two kinds of fracture toughness. As described above, the growth in fracture toughness with sulphate content is because of the refinement of expansive minerals, while the descent is owing to the retardation of sulphate ions towards the binder hydration. The higher modes I & II fracture toughness of 25000 ppm sample means the beneficial effect of the refinement of pore structure counters the retardation effect of sulphate ions on binder hydration. In addition to the retardation effect, the lower modes I & II fracture toughness of 25000 ppm sample (compared to the sample with 15000 ppm sulphate content) is also ascribed to the sulphate adsorption by C-S-H (Li and Fall, 2016). The sulphate adsorption by C-S-H leads to the production of C-S-H gel (Bentur, 1976), which will decrease the binding force between CPB and rock. The phenomenon of sulphate being absorbed by C-S-H has been documented by many other studies as well (Jelenić et al., 1977; Barbarulo, 2002).

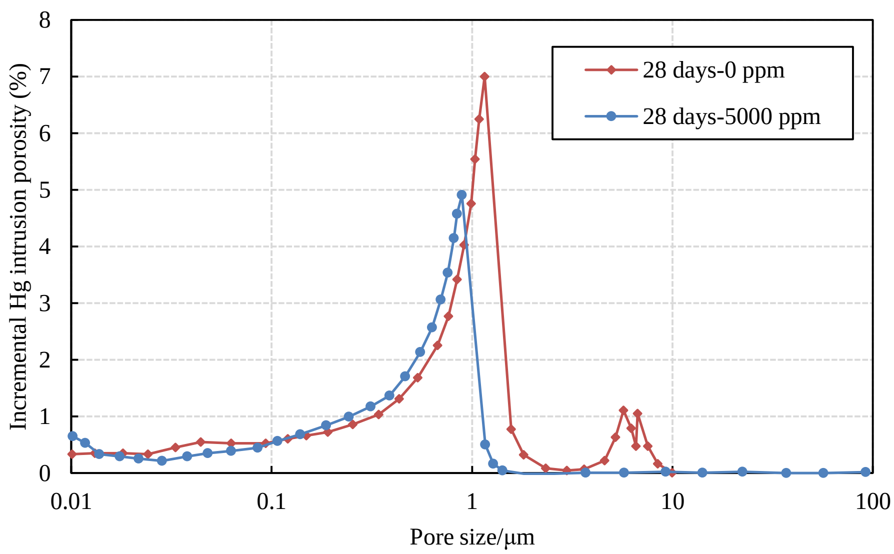

Figure A-16 Results of MIP test on samples with sulphate contents of 0 ppm and 5000 ppm cured for 28 days

A.4 Summary and conclusions

The evolution of the modes I & II fracture toughness of the CPB-rock interface (under various thermal and chemical conditions) was experimentally analyzed in this research. According to the results, the following conclusions are made:

- The load-displacement curves of SCB test and the modes I & II fracture toughness both change with curing time, temperature and sulphate content.
- The increasing peak load of the CPB-rock interface (both modes I & II samples) with time is due to the higher degree of binder hydration in CPB.
- Generally, the modes I & II fracture toughness increase with temperature (less than 35°C), except for the specimens cured for 28 days. The increasing modes I & II fracture toughness with temperature is owing to (i) temperature-induced acceleration of the binder hydration, and (ii)

beneficial effect of temperature on self-desiccation. The decreasing modes I & II fracture toughness of the specimens cured at 35°C for 28 days is ascribed to the crossover effect.

- The influence of sulphate ions on the evolution of modes I & II fracture toughness relies on the initial sulphate content and the curing time. For early ages sample (no longer than 3 days), the modes I & II fracture toughness decrease with sulphate content (because of the retardation effect of sulphate ions on binder hydration). For samples cured for 28 days, the modes I & II fracture toughness increase with sulphate content (with the exception of 25000 ppm sample). This is due to the increasing contacting area between CPB and granite, as a result of the refinement of pore structure by gypsum and ettringite. The lower modes I & II fracture toughness of the sample with 25000 ppm sulphate content (in comparison to 15000 ppm sample) is because of the sulphate being absorbed by C-S-H.

Acknowledgements

The authors would like to thank Dr. Saifen Zheng and Mr. Jean Claude Celestin for their advice and help.

A.5 References

Abrate S, Ferrero JF, Navarro P (2015) Cohesive zone modes and impact damage predictions for composite structures. Meccanica, 50(10):2587-2620.

Aliha MRM, Ayatollahi MR (2011) Mixed mode I/II brittle fracture evaluation of marble using SCB specimen. Proc. Eng. 10:311–318.

Ayatollahi M, Aliha M (2004) Fracture parameters for a cracked semi-circular specimen. Int. J. Rock. Mech. Min. Sci. 41:20-25.

Ayatollahi M, Aliha M (2006) On determination of mode II fracture toughness using semi-circular bend specimen. Int. J. Solids Struct. 43(17):5217-5227.

Ayatollahi M, Aliha M (2008) On the use of Brazilian disc specimen for calculating mixed mode I–II fracture toughness of rock materials. Eng. Fract. Mech. 75(16):4631-4641.

Barbarulo R (2002) Comportement des matériaux cimentaires: actions des sulfates et de la temperature. Ph.D. Dissertation, Université Laval, Canada.

Bentur A (1976) Effect of gypsum on the hydration and strength of C3S pastes. journal of the American Ceramic Society, 59(5-6):210-213.

Benzaazoua M, Fall M, Belem T (2004) A contribution to understanding the hardening process of cemented pastefill. Miner. Eng. 17(2):141-152.

Borana L, Yin JH, Singh DN, Shukla SK (2016) Interface Behavior from Suction-Controlled Direct Shear Test on Completely Decomposed Granitic Soil and Steel Surfaces. Int. J. Geomech. 16(6):D4016008.

Camanho PP, Davila CG, De Moura M (2003) Numerical simulation of mixed-mode progressive delamination in composite materials. J. Compos. Mater. 37(16):1415-1438.

Courard L, Michel F, Perkowicz S, Garbacz A (2014) Effects of limestone fillers on surface free energy and electrical conductivity of the interstitial solution of cement mixes. Cem. Concr. Compos. 45:111-116.

Dong W, Yang D, Zhou X, Kastiukas G, Zhang B (2017) Experimental and numerical investigations on fracture process zone of rock–concrete interface. Fatigue Fract. Eng. Mater. Struct. 40(5):820-835.

Ercikdi B, Kesimal A, Cihangir F, Deveci H, Alp, İ (2009) Cemented paste backfill of sulphide-rich tailings: Importance of binder type and dosage. Cem. Concr. Compos. 31(4):268-274.

Escalante-Garcia JI, Sharp JH (2001) The microstructure and mechanical properties of blended cements hydrated at various temperatures. Cem. Concr. Res. 31(5):695–702.

Fall M, Benzaazoua M, Ouellet S (2005) Experimental characterisation of the influence of mill tailings fineness and density on the quality of cemented paste backfill. Miner. Eng. 18(1):41-44.

Fall M, Célestin J, Pokharel M, Touré M (2010) A contribution to understanding the effects of curing temperature on the mechanical properties of mine cemented tailings backfill. Eng. Geol. 114(3):397-413.

Fang K, Fall M (2018) Effects of curing temperature on the shear behaviour of cemented paste backfill-rock interface. Int. J. Rock. Mech. Min. Sci. 112:184-192.
Fang K, Fall M (2019) Chemically induced changes in the shear behaviour of the interface between rock and tailings backfill undergoing cementation. Rock Mech. Rock Eng. 52(9):3047-3062.
Fang K, Fall M (2020) Shear Behavior of the Interface between Rock and Cemented Backfill: Effect of Curing Stress, Drainage Condition and Backfilling Rate. Rock Mech. Rock Eng. 53(1):325-336.
Gani MSJ (1997) Cement and Concrete, Chapman & Hall, London, UK.
Helinski M, Fahey M, Fourie A (2010) Behavior of cemented paste backfill in two mine stopes: Measurements and modeing. J. Geotech. Geoenviron. Eng. 137(2):171-182.
Hossain MA, Yin JH (2013) Unsaturated soil-cement interface behaviour in direct shear tests. Aust. Geomech. J. 48(3):141-153.
ISRM (2007) The complete ISRM suggested methods for rock characterization, testing and monitoring: 1974–2006. In: Ulusay R, Hudson JA (eds) Suggested methods prepared by the commission on testing methods. International Society for Rock Mechanics, Compilation Arranged by the ISRM Turkish National Group, Ankara, Turkey.
Jelenić I, Panović A, Halle R, Gaćeša T (1977) Effect of gypsum on the hydration and strength development of commercial Portland cements containing alkali sulfates. Cem. Concr. Res. 7:239-245.
Jiang HQ, Fall M, Cui L (2016) Yield stress of cemented paste backfill in sub-zero environments: experimental results. Miner. Eng. 92:141-150.
Kataoka M, Obara Y, Kuruppu M (2015) Estimation of fracture toughness of anisotropic rocks by semi-circular bend (SCB) tests under water vapor pressure. Rock Mech. Rock Eng. 48(4):1353-1367.
Kjellsen KO, Detwiler RJ, Gjorv OE (1991) Development of microstructures in plain cement pastes hydrated at different temperatures. Cem. Concr. Res. 21(1):179–189.
Kjellsen K, Detwiler R (1993) Later-age strength prediction by a modified maturity mode. ACI Mater. J. 90(3):220-227.
Kjellsen KO, Detwiler RJ, Gjorv OE (1990) Pore structure of plain cement pastes hydrated at different temperatures. Cem. Concr. Res. 20(6):927–933.
Klieger P (1958) Effect of mixing and curing temperature on concrete strength. Journal of the American Concrete Institute, 54:1063-1081.
Koupouli NJ, Belem T, Rivard P, Effenguet H (2016) Direct shear tests on cemented paste backfill–rock wall and cemented paste backfill–backfill interfaces. J. Rock Mech. Geotech. Eng. 8(4):472-479.
Kuruppu M, Obara Y, Ayatollahi M, Chong K, Funatsu T (2014) ISRM-suggested method for determining the mode I static fracture toughness using semi-circular bend specimen. Rock Mech. Rock Eng. 47(1):267-274.
Lanaro F, Sato T, Stephansson O (2009) Microcrack modeling of Brazilian tensile tests with the boundary element method. Int. J. Rock Mech. Min. Sci. 46:450–461.
Li S, Thouless M, Waas A, Schroeder J, Zavattieri P (2006) Mixed-mode cohesive-zone modes for fracture of an adhesively bonded polymer–matrix composite. Eng. Fract. Mech. 73(1):64-78.
Li WC, Fall M (2016) Sulphate effect on the early age strength and self-desiccation of cemented paste backfill. Constr. Build. Mater. 106:296-604.
Lim I, Johnston I, Choi S, Boland J (1994) Fracture testing of a soft rock with semi-circular specimens under three-point bending. Part 1—mode I. Paper presented at the International journal of rock mechanics and mining sciences & geomechanics abstracts.
Liu L, Zhu C, Qi C, Zhang B, Song KI (2019) A microstructural hydration mode for cemented paste backfill considering internal sulfate attacks. Constr. Build. Mater. 211:99-108.
Metha PK (1986) Concrete: Structure, Properties and Materials. Prentice-Hall Inc, Englewood Cliffs, N.J.
Nasir O, Fall M (2008) Shear behaviour of cemented pastefill-rock interfaces. Eng. Geol. 101(3):146-153.
Neville AM (2011) Properties of concrete, 5th Edition: Longman London.
Oliveira I, Cavalaro SHP, Aguado A (2013) New kinetic mode to quantify the internal sulfate attack in concrete. Cem. Concr. Res. 43:95–104.
Ouellet S, Bussière B, Mbonimpa M, Benzaazoua M, Aubertin M (2006) Reactivity and mineralogical evolution of an underground mine sulphidic cemented paste backfill. Miner. Eng. 19(5):407-419.
Pane I, Hansen W (2005) Investigation of blended cement hydration by isothermal calorimetry and thermal analysis. Cem. Concr. Res. 35(6):1155-1164.
Pokharel M, Fall M (2013) Combined influence of sulphate and temperature on the saturated hydraulic conductivity of hardened cemented paste backfill. Cem. Concr. Compos. 8:21-28.

Qi C, Fourie A (2019) Cemented paste backfill for mineral tailings management: Review and future perspectives. Miner. Eng. 144, 106025.
Reeder JR, Crews JH (1990) Mixed-mode bending method for delamination testing. AIAA Journal, 28(7):1270-1276.
Richardson DN (1991) Review of variables that influence measured concrete compressive strength. J. Mater. Civ. Eng. 3(2):95-112.
Scrivener KL, Crumbie AK, Laugesen P (2004) The interfacial transition zone (ITZ) between cement paste and aggregate in concrete. Interface Sci. 12(4):411-421.
Sha W, O'Neill E, Guo Z (1999) Differential scanning calorimetry study of ordinary Portland cement. Cem. Concr. Res. 29(9):1487-1489.
Tse R, Cruden DM (1979) Estimating Joint Roughness Coefficients. Int. J. Rock Mech. Min. Sci. 16(5):303–307.
Wong LNY, Guo TY, Lam WK, Ng JYH (2019) Experimental Study of Cracking Characteristics of Kowloon Granite Based on Three Mode I Fracture Toughness Methods. Rock Mech. Rock Eng. 1-19.
Yilmaz E, Fall M (2017) Paste tailings management. Springer International Publishing.
Yilmaz E, Kesimal A, Ercidi B (2004) Strength development of paste backfill simples at Long term using different binders. Proceedings of 8th symposium MineFill04, China.

Appendix B: Model parameters

B.1 Parameters used in section 5.2

Symbols	Value
α_{K1}	-3×10^{-14}
α_{K2}	8×10^{-10}
α_{K3}	-2×10^{-6}
α_{K4}	-0.0596
β_{K1}	7×10^{-13}
β_{K2}	-2×10^{-8}
β_{K3}	2×10^{-5}
β_{K4}	2.7104
λ_{K1}	-3×10^{-12}
λ_{K2}	1×10^{-7}
λ_{K3}	-1.4×10^{-3}
λ_{K4}	2.1231
d_1	14.11
d_2	1.1579
$\alpha_{\varphi1}$	2×10^{-14}
$\alpha_{\varphi2}$	-7×10^{-10}
$\alpha_{\varphi3}$	6×10^{-6}
$\alpha_{\varphi4}$	-1×10^{-15}
$\beta_{\varphi1}$	-5×10^{-13}
$\beta_{\varphi2}$	2×10^{-8}
$\beta_{\varphi3}$	-9×10^{-5}
$\beta_{\varphi4}$	0.4768
$\lambda_{\varphi1}$	-3×10^{-13}
$\lambda_{\varphi2}$	4×10^{-8}
$\lambda_{\varphi3}$	-1.1×10^{-3}
$\lambda_{\varphi4}$	8.9287
a_1	20.964
a_2	0.0194
α_{c1}	1×10^{-14}
α_{c2}	5×10^{-10}
α_{c3}	-4×10^{-6}
α_{c4}	-0.0119
β_{c1}	7×10^{-14}
β_{c2}	-7×10^{-9}
β_{c3}	1×10^{-4}
β_{c4}	0.6257
λ_{c1}	-3×10^{-13}
λ_{c2}	2×10^{-8}
λ_{c3}	-3×10^{-4}
λ_{c4}	1.1151
b_1	41.381
b_2	0.9188
$\alpha_{K_{\mathrm{I}c}1}$	-2×10^{-14}
$\alpha_{K_{\mathrm{I}c}2}$	9×10^{-10}
$\alpha_{K_{\mathrm{I}c}3}$	-9×10^{-6}
$\alpha_{K_{\mathrm{I}c}4}$	-8×10^{-4}
$\beta_{K_{\mathrm{I}c}1}$	6×10^{-13}
$\beta_{K_{\mathrm{I}c}2}$	-3×10^{-8}
$\beta_{K_{\mathrm{I}c}3}$	3×10^{-4}
$\beta_{K_{\mathrm{I}c}4}$	0.4054
$\lambda_{K_{\mathrm{I}c}1}$	-4×10^{-12}
$\lambda_{K_{\mathrm{I}c}2}$	1×10^{-7}
$\lambda_{K_{\mathrm{I}c}3}$	-9×10^{-4}
$\lambda_{K_{\mathrm{I}c}4}$	2.8227
$\alpha_{K_{\mathrm{II}c}1}$	-3×10^{-15}
$\alpha_{K_{\mathrm{II}c}2}$	1×10^{-10}
$\alpha_{K_{\mathrm{II}c}3}$	-9×10^{-7}
$\alpha_{K_{\mathrm{II}c}4}$	-0.008
$\beta_{K_{\mathrm{II}c}1}$	-4×10^{-14}
$\beta_{K_{\mathrm{II}c}2}$	-2×10^{-9}
$\beta_{K_{\mathrm{II}c}3}$	6×10^{-5}
$\beta_{K_{\mathrm{II}c}4}$	0.6957
$\lambda_{K_{\mathrm{II}c}1}$	3×10^{-13}
$\lambda_{K_{\mathrm{II}c}2}$	-2×10^{-9}
$\lambda_{K_{\mathrm{II}c}3}$	-1×10^{-4}
$\lambda_{K_{\mathrm{II}c}4}$	1.4025

B.2 Parameters used in section 5.3

Symbols	Value
α_{K1}	1.1227
α_{K2}	-24.651
α_{K3}	45.81
β_{K1}	-1.3625
β_{K2}	34.016
β_{K3}	-62.582
f_1	0.5627
f_2	-12.08
c_1	24.053
c_2	0.0003
$\alpha_{\varphi 1}$	-0.0018
$\alpha_{\varphi 2}$	0.0544
$\alpha_{\varphi 3}$	0.8984
$\beta_{\varphi 1}$	0.5309
$\beta_{\varphi 2}$	-4.7723
$\beta_{\varphi 3}$	7.4209
e_1	6.477
e_2	-2.0071
α_{c1}	0.0017
α_{c2}	-0.0935
α_{c3}	1.18
β_{c1}	-0.0048
β_{c2}	0.2309
β_{c3}	0.5573
m_1	0.9179
m_2	-2.815
$\alpha_{K_{\mathrm{I}c}1}$	0.0447
$\alpha_{K_{\mathrm{I}c}2}$	-0.8308
$\alpha_{K_{\mathrm{I}c}3}$	2.483
$\beta_{K_{\mathrm{I}c}1}$	-1.391
$\beta_{K_{\mathrm{I}c}2}$	33.553
$\beta_{K_{\mathrm{I}c}3}$	-61.543
n_1	1.837
n_2	-5.6333
$\alpha_{K_{\mathrm{II}c}1}$	0.0023
$\alpha_{K_{\mathrm{II}c}2}$	-0.1041
$\alpha_{K_{\mathrm{II}c}3}$	1.199
$\beta_{K_{\mathrm{II}c}1}$	-0.0027
$\beta_{K_{\mathrm{II}c}2}$	0.1308
$\beta_{K_{\mathrm{II}c}3}$	0.7491

Appendix C: Test set-up and equipment used in this study

Figure C-1 Direct shear test device

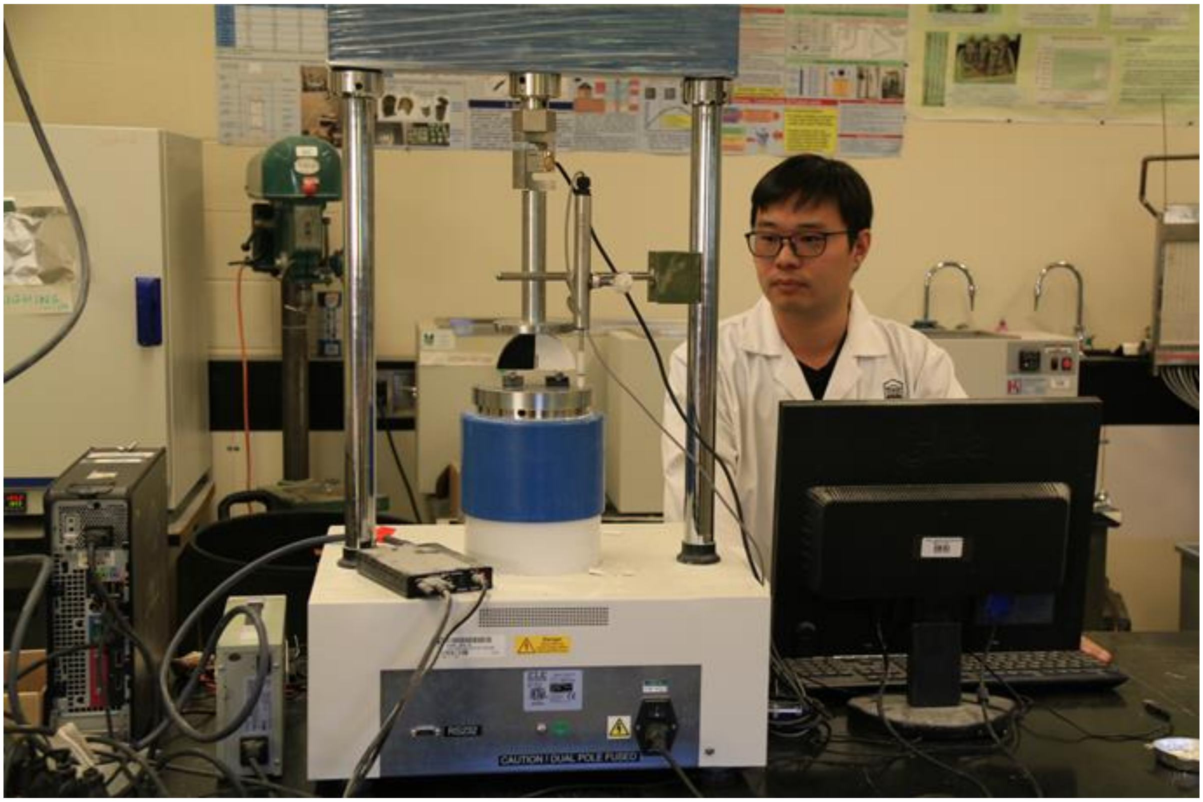

Figure C-2 Digital Tritest 50 device for SCB test

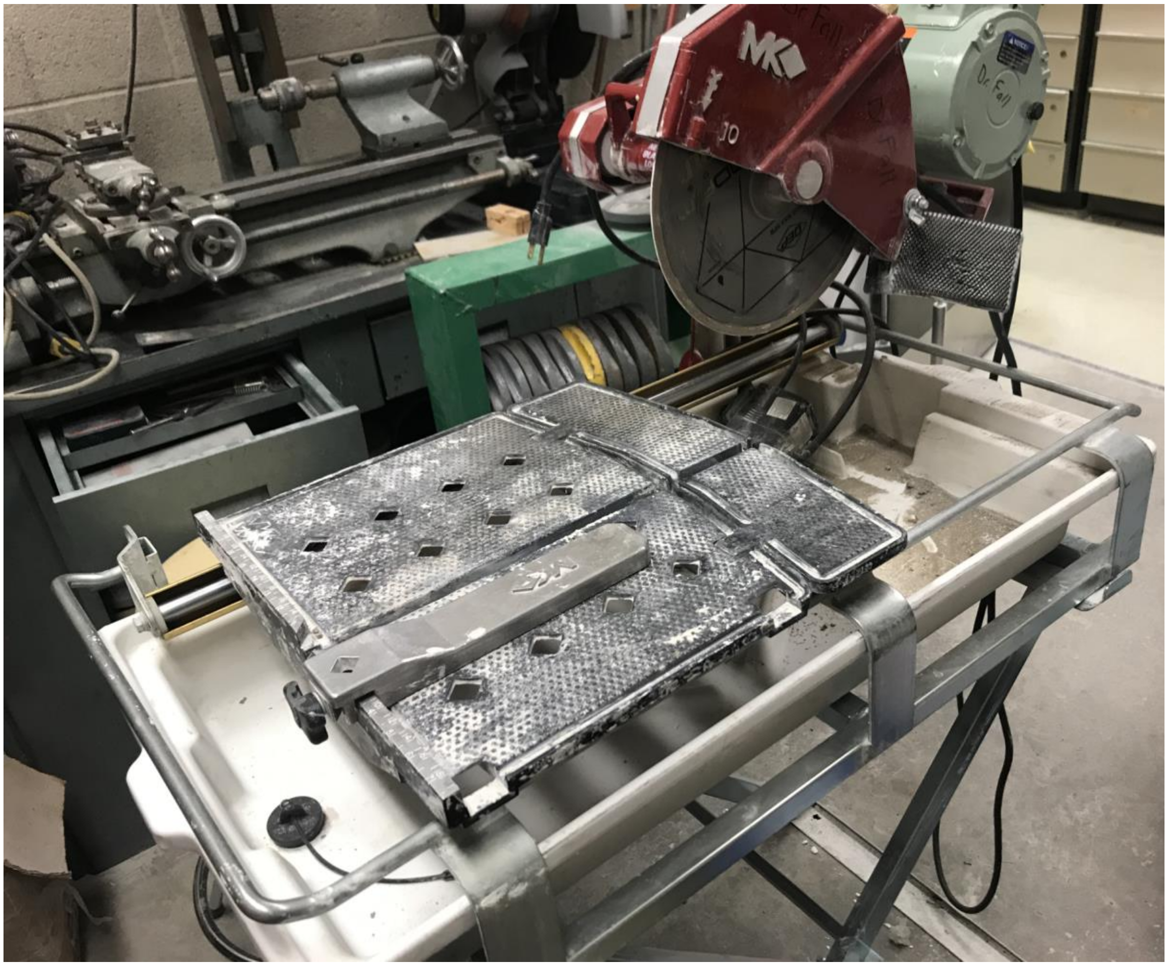

Figure C-3 Rock cutter

Figure C-4 Core cutter (DD 150-U) for obtaining rock disc

Figure C-5 Mixer for CPB preparation (Left one is for preparing small amount of CPB, right one is for preparing large volume of CPB)

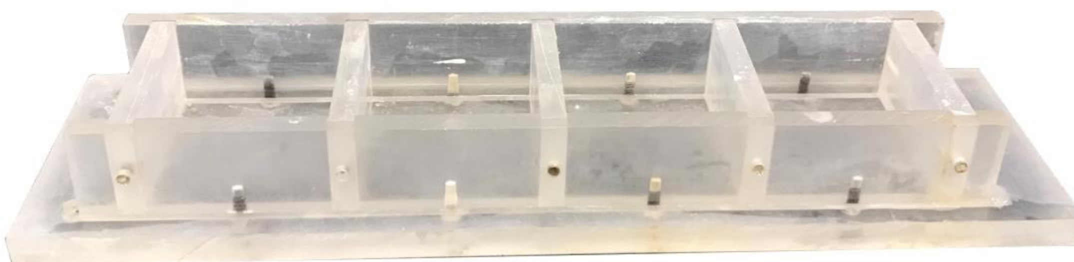

Figure C-6 Model for sample preparation

Figure C-7 uOttawa Backfill Curing System (Left one is for monitoring programs, right one is for curing interface sample)

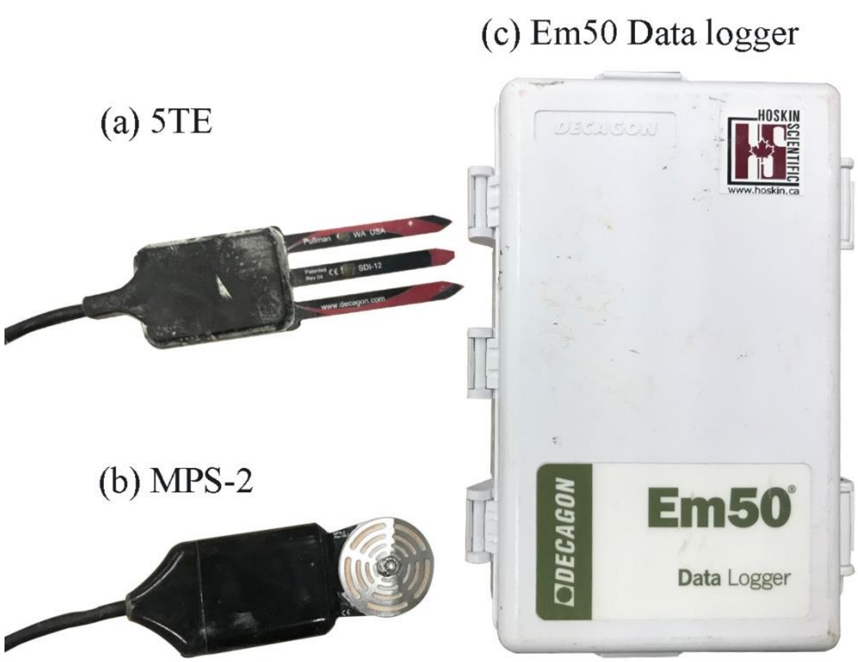

Figure C-8 Monitoring equipment (a) 5TE; (b) MPS-2; (C) Data logger

Figure C-9 Thermogravimetric analysis equipment (Q 5000 IR instrument)

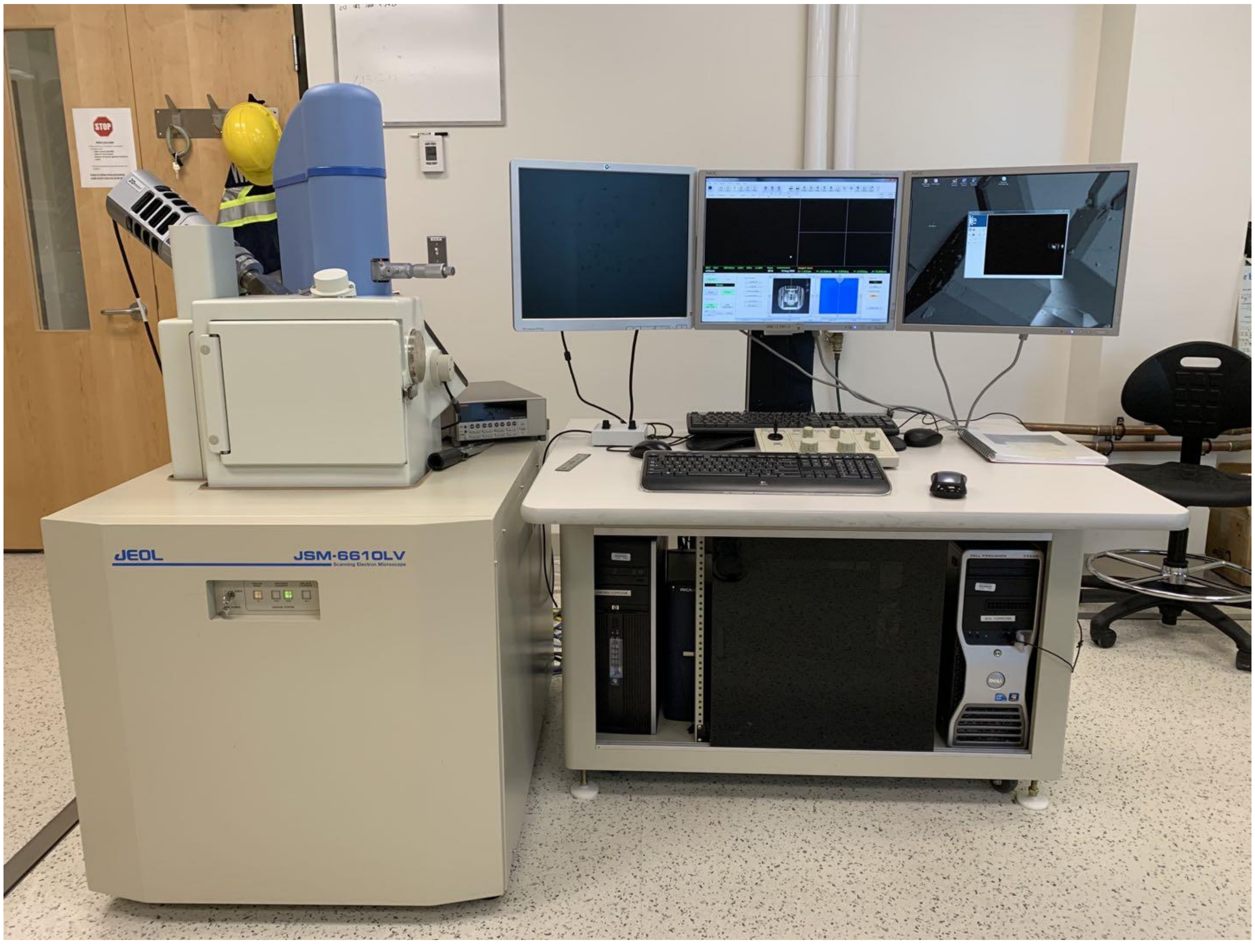

Figure C-10 Scanning electron microscope (SEM)

Figure C-11 X-ray diffraction (XRD, XDS-2000)

Figure C-12 Micromeritics AutoPore IV 9500 mercury porosimeter